

**THERMAL AND MECHANICAL PROPERTIES OF GYPSUM  
BOARDS AND THEIR INFLUENCES ON FIRE RESISTANCE OF  
GYPSUM BOARD BASED SYSTEMS**

A thesis submitted to the University of Manchester for the degree of

Doctor of Philosophy

in the Faculty of Engineering and Physical Sciences

**2011**

**IMA RAHMANIAN**

**School of Mechanical, Aerospace and Civil Engineering**

## LIST OF CONTENTS

<b>LIST OF FIGURES</b>	<b>7</b>
<b>LIST OF TABLES</b>	<b>16</b>
<b>NOMENCLATURE</b>	<b>17</b>
<b>ABSTRACT</b>	<b>19</b>
<b>DECLARATION</b>	<b>21</b>
<b>COPYRIGHT STATEMENT</b>	<b>22</b>
<b>ACKNOWLEDGEMENTS</b>	<b>23</b>
<b>CHAPTER 1. INTRODUCTION</b>	<b>24</b>
1.1    General Introduction .....	24
1.2    Research Significance and Objectives .....	26
1.3    Outline of the Thesis .....	27
<b>CHAPTER 2. LITERATURE REVIEW</b>	<b>29</b>
2.1    Introduction.....	29
2.2    Gypsum Board Assemblies .....	29
2.3    Fire Resistance.....	31
2.4    Thermo-Chemistry of Gypsum .....	32
2.5    Thermal Properties of Gypsum Plasterboard at Elevated Temperatures .....	34
2.5.1    Specific Heat.....	34
2.5.2    Density.....	36
2.5.3    Thermal Conductivity .....	37
2.5.4    Emissivity and Heat Transfer Coefficient .....	38
2.5.5    Ablation .....	40
2.6    Mechanical Properties of Gypsum Plasterboard at Elevated Temperatures .....	40
2.6.1    Thermal Expansion .....	40
2.6.2    Modulus of Elasticity and Strength .....	41
2.7    Previous Studies on the Behaviour of Gypsum Plasterboard in Fire 44	
2.7.1    The Effects of Thermal Properties of Gypsum .....	44

---

2.7.2	The Effect of Moisture Content .....	45
2.7.3	Cracks, Fissures and Fall-Off of Gypsum .....	46
2.7.4	Detailing of Gypsum Board Assembly .....	49
2.7.5	Standard Fires versus Real Fires.....	50
2.8	Summary and Originality of This Project.....	51
<b>CHAPTER 3. A METHOD OF EXTRACTING TEMPERATURE-DEPENDENT THERMAL PROPERTIES OF GYPSUM</b>		<b>53</b>
3.1	Introduction.....	53
3.2	One-Dimensional Finite Difference Formulation .....	54
3.2.1	Initial and Boundary Conditions.....	60
3.3	Validation of the Heat Conduction Model .....	61
3.3.1	Conduction with Constant Material Properties .....	61
3.3.2	Heat Conduction with Constant Material Properties and Convective Boundary Condition.....	64
3.3.3	Conduction with Temperature-Dependent Thermal Properties .....	66
3.4	Specific Heat and Density of Gypsum .....	67
3.5	Thermal Conductivity of Gypsum.....	70
3.6	Sensitivity Study .....	74
3.6.1	Mesh Size in the Heat Transfer Model.....	74
3.6.2	Specific Heat-Temperature Correlation .....	75
3.6.3	Thermal Conductivity-Temperature Correlation .....	82
3.7	A Method to Extract Controlling Parameters in Thermal Conductivity-Temperature Correlation .....	86
3.7.1	Thermal Conductivity of Dried Gypsum.....	87
3.7.2	Effective Pore Size .....	90
3.8	Proposed Methodology to Extract Thermal Properties of Gypsum.....	94
3.9	Conclusions.....	97
<b>CHAPTER 4. VALIDATION OF THE THERMAL CONDUCTIVITY MODEL THROUGH SMALL-SCALE HIGH TEMPERATURE TESTS</b>		<b>98</b>
4.1	Introduction.....	98
4.2	Experimental Set-Up .....	98
4.2.1	Thermocouple Layout .....	100

---

4.2.2	Specifications of the Kiln .....	101
4.2.3	Specifications of the Specimens.....	102
4.3	Fire Test Results and Discussions .....	104
4.4	Comparison of Numerical and Experimental Results.....	106
4.5	Conclusions.....	111
<b>CHAPTER 5. EXPERIMENTAL RESULTS OF TEMPERATURE-DEPENDENT MECHANICAL PROPERTIES OF GYPSUM</b>		<b>112</b>
5.1	Introduction.....	112
5.2	Dilatometer Tests .....	112
5.3	High Temperature Three-Point Bending Tests.....	115
5.3.1	Experimental Set-Up .....	115
5.3.2	Test Results and Discussions.....	118
5.3.3	Approximate Analysis of Stress-Strain Relationship of Gypsum at Elevated Temperatures .....	120
5.3.4	ABAQUS Modelling of the Three-Point Bending Tests .....	129
5.4	Gypsum Prism Compression Tests .....	132
5.5	Conclusions.....	133
<b>CHAPTER 6. MEDIUM-SCALE FIRE TESTS AND GYPSUM FALL-OFF IN FIRE</b>		<b>135</b>
6.1	Introduction.....	135
6.2	Experimental Set-Up .....	135
6.2.1	Experiments T1 and T2.....	137
6.2.2	Experiments T3 and T4.....	140
6.2.3	Experiments T5 and T6.....	141
6.3	Test Results and Discussions .....	142
6.4	Canadian Full-Scale Fire Tests .....	152
6.5	Conclusions.....	157
<b>CHAPTER 7. FINITE ELEMENT MODELLING OF STRUCTURAL PERFORMANCE OF GYPSUM BOARDS IN FIRE</b>		<b>158</b>
7.1	Introduction.....	158
7.2	Modelling Methodology .....	159
7.3	Thermal Analysis Using ABAQUS.....	161

---

7.3.1	Geometry .....	161
7.3.2	Material Properties .....	162
7.3.3	Mesh and Element Type .....	162
7.3.4	Initial and Boundary Conditions.....	163
7.3.5	Validation of Numerical Results for Thermal Analysis .....	164
7.4	Structural Analysis Using ABAQUS .....	170
7.4.1	Geometry .....	170
7.4.2	Material Models.....	170
7.4.2.1	Classic Metal Plasticity .....	171
7.4.2.2	Cast Iron Plasticity .....	172
7.4.2.3	Concrete Smeared Cracking .....	172
7.4.2.4	Damage for Traction-Separation Laws.....	173
7.4.3	Extended Finite Element Method .....	173
7.4.3.1	Current Limitations of the Numerical Analysis .....	177
7.4.3.2	Improving Convergence of Numerical Analysis .....	178
7.4.4	Thermal Expansion .....	180
7.4.5	Mesh and Element Type .....	181
7.4.6	Predefined Fields and Boundary Conditions.....	183
7.4.7	Validation of Numerical Simulation Models – Fireline Gypsum .....	184
7.4.7.1	Experiments T1F and T2F .....	185
7.4.7.2	Experiments T3F and T4F .....	189
7.4.7.3	Experiments T5F and T6F .....	193
7.4.7.4	Summary .....	197
7.4.8	Validation of Numerical Results for Stress Analysis – Wallboard Gypsum .....	199
7.4.8.1	Experiments T2W and T4W.....	199
7.4.8.2	Experiments T5W and T6W.....	204
7.4.8.3	Summary .....	208
7.4.9	Validation of Numerical Results for Stress Analysis – Canadian Tests.....	210
7.5	Conclusions.....	215

---

<b>CHAPTER 8. CRITICAL PARAMETERS IN STRUCTURAL BEHAVIOUR OF GYPSUM BOARDS IN FIRE</b>	<b>216</b>
8.1    Introduction.....	216
8.2    Detailing Parameters in Gypsum Board Wall Assemblies.....	217
8.3    Stud Spacing .....	217
8.4    Gypsum Board Attachment.....	221
8.5    Number of Gypsum Board Layers .....	222
8.6    Use of Insulation in the Wall Cavity .....	223
8.7    Thermal Shrinkage of Gypsum .....	225
8.8    Conclusions.....	226
<b>CHAPTER 9. CONCLUSIONS AND RECOMMENDATIONS FOR FUTURE RESEARCH</b>	<b>228</b>
9.1    Summary and Conclusions .....	228
9.2    Recommendations for Further Research .....	233
<b>REFERENCES</b>	<b>237</b>
<b>PUBLICATIONS</b>	<b>242</b>
<b>APPENDIX A. SMALL-SCALE HEAT TRANSFER TEST RESULTS</b>	<b>243</b>
<b>APPENDIX B. DETAILED DATA OF MECHANICAL TEST SAMPLES</b>	<b>246</b>
<b>APPENDIX C. OBSERVATIONS OF MEDIUM-SCALE FIRE TESTS</b>	<b>249</b>

## LIST OF FIGURES

Figure 1.1. Benefits of a reliable numerical model to predict fire resistance of gypsum board based systems .....	26
Figure 2.1. A typical gypsum board wall assembly .....	30
Figure 2.2. Time-temperature curves for standard fires according to BS476 (BSI, 1987) .....	32
Figure 2.3. Specific heat of gypsum according to various researchers (Thomas, 2002).....	35
Figure 2.4. Mass loss in gypsum with rising temperatures (Mehaffey et al., 1994).....	36
Figure 2.5. Thermal conductivity of gypsum versus temperature (Thomas, 2002).....	37
Figure 2.6. Contraction of gypsum as a function of temperature (Mehaffey et al., 1994).....	41
Figure 2.7. Modulus of elasticity and strength of gypsum measured up to 140°C (Bénichou and Sultan, 2000).....	42
Figure 2.8. Modulus of elasticity and bending strength of gypsum measured up to 400°C (Cramer et al., 2003) .....	43
Figure 2.9. Comparison of gypsum board fall-off temperature in wall and floor assemblies(Sultan, 2010) .....	48
Figure 3.1. Direction of heat flow in a wide panel.....	56
Figure 3.2. Finite Difference discretization for node <b>m</b> within the material.....	58
Figure 3.3. Finite Difference discretization for a boundary node.....	58
Figure 3.4. A panel with thickness <i>l</i> , both boundaries kept at zero temperature .....	62
Figure 3.5. Comparison of temperature distributions across the thickness of a 25mm example panel obtained by analytical method and Finite Difference method .....	63
Figure 3.6. Comparison of temperature development at the midpoint of a 25mm example panel obtained by analytical method and Finite Difference method .....	63
Figure 3.7. A panel with thickness <i>2L</i> , suddenly immersed into an ambient zero temperature. ....	64
Figure 3.8. Comparison between temperature distributions across the thickness of a 25mm example panel with convective boundary	

condition obtained by analytical method and Finite Difference method .....	65
Figure 3.9. Comparison between temperature developments at the surface of a 25mm example panel with convective boundary condition obtained by analytical method and Finite Difference method.....	66
Figure 3.10. Temperature development on the unexposed surface of a 25mm Fireline gypsum board by ABAQUS (Finite Element analysis) and Finite Difference method .....	67
Figure 3.11. Specific heat of gypsum as used in the analysis .....	69
Figure 3.12. Density of gypsum as used in the analysis (% of the original density).....	70
Figure 3.13. Thermal conductivity of gypsum, as reported by various researchers (Jones, 2001) .....	71
Figure 3.14. Effective thermal conductivity of gypsum as used in this study.....	73
Figure 3.15. Calculated temperatures on the unexposed surface of a 12.5mm Fireline gypsum board using different number of layers in the heat transfer analysis .....	75
Figure 3.16. Thermal properties of material using different temperature intervals for dehydration .....	77
Figure 3.17. Calculated temperatures on the unexposed surface using different temperature intervals for the two dehydration reactions .....	78
Figure 3.18. Thermal properties of material using different peak temperatures .....	80
Figure 3.19. Calculated temperatures on the unexposed surface using different peak temperatures.....	81
Figure 3.20. Thermal conductivity of gypsum using different drop temperatures (DT) .....	82
Figure 3.21. Calculated temperatures on the unexposed surface using different drop temperatures (DT) in thermal conductivity curve.....	83
Figure 3.22. Thermal conductivity of gypsum using different values for the minimum thermal conductivity (Min k) .....	84
Figure 3.23. Calculated temperatures on the unexposed surface using different values for minimum conductivity (Min k) in thermal conductivity-temperature curve .....	84
Figure 3.24. Thermal conductivity of gypsum using different effective void sizes ( $de$ ) .....	85
Figure 3.25. Calculated temperatures on the unexposed surface using different void sizes ( $de$ ) in thermal conductivity curve .....	86
Figure 3.26. Comparison between the effective thermal conductivity model for wallboard and Fireline gypsum boards with Hot Guarded Plate (HGP) test results .....	89

---

Figure 3.27. Calibration of the minimum thermal conductivity value (min k) against experimental results of temperature history on the unexposed surface of double layer of 9.5mm Wallboard gypsum panel (Test 10).....	90
Figure 3.28. Low magnification photograph of a sample gypsum board .....	91
Figure 3.29. Void size distribution of a sample gypsum board.....	91
Figure 3.30. Series and parallel arrangement of layers of uniform void size .....	93
Figure 3.31. Conceptual demonstration of temperature history properties used for calibration of thermal conductivity parameters.....	95
Figure 3.32. Proposed methodology for extracting the effective thermal conductivity of gypsum board products by calibrating two parameters: thermal conductivity of dried gypsum at 220°C and the effective pore size .....	96
Figure 4.1. Small-scale high temperature test set-up.....	100
Figure 4.2. Thermocouple layout for gypsum board specimens on plan and cross-section of single-layer and double-layer panels.....	101
Figure 4.3. Time-temperature curve for the kiln against standard cellulosic fire curve .....	102
Figure 4.4. Temperature recordings on the exposed and unexposed surfaces of a 12.5mm Fireline gypsum panel (Test 3) .....	104
Figure 4.5. Temperature recordings by the observer thermocouples in Test 1.....	105
Figure 4.6. Temperature recordings by the top observer thermocouples in Test 5, compared to thermocouple A1 at the centre of the unexposed side.....	105
Figure 4.7. Typical cracking observed in small-scale gypsum boards during high temperature tests .....	106
Figure 4.8. Temperature history for 12.5mm Fireline gypsum panel (Test 2) – thermal conductivity model based on calibrated dry gypsum value....	107
Figure 4.9. Temperature history for double layer of 12.5mm Fireline gypsum panel (Test 5) – thermal conductivity model based on calibrated dry gypsum value .....	108
Figure 4.10. Temperature history for 9.5mm Wallboard gypsum panel (Test 8) – thermal conductivity model based on calibrated dry gypsum value .....	108
Figure 4.11. Temperature history for double layer of 9.5mm Wallboard gypsum panel (Test 10) – thermal conductivity model based on calibrated dry gypsum value .....	109
Figure 4.12. Temperature history for 12.5mm Fireline gypsum panel (Test 1) – thermal conductivity model based on HGP test results at 20°C and 220°C .....	109

---

Figure 4.13. Temperature history for double layer of 12.5mm Fireline gypsum panel (Test 4) – thermal conductivity model based on HGP test results at 20°C and 220°C.....	110
Figure 4.14. Temperature history for 9.5mm Wallboard gypsum panel (Test 7) – thermal conductivity model based on HGP test results at 20°C and 220°C .....	110
Figure 4.15. Temperature history for double layer of 9.5mm Wallboard gypsum panel (Test 11) – thermal conductivity model based on HGP test results at 20°C and 220°C.....	111
Figure 5.1. The connecting rod dilatometer used for thermal expansion tests. ....	113
Figure 5.2. Dilatometer test results for Fireline gypsum board samples .....	114
Figure 5.3. Dilatometer test results for Wallboard gypsum board samples .....	114
Figure 5.4. Set-up of the three-point bending tests .....	117
Figure 5.5. Three-point bending test results for Fireline gypsum panels at 20°C to 400°C.....	118
Figure 5.6. Three-point bending test results for Fireline gypsum panels at 400°C to 800°C .....	119
Figure 5.7. Three-point bending test results for Wallboard gypsum panels at 20°C to 400°C .....	119
Figure 5.8. Bilinear stress-strain relationship .....	122
Figure 5.9. Typical load-deflection curve for a material with bilinear stress-strain relationship under three-point bending .....	123
Figure 5.10. Curvature change along the three-point bending specimen at the onset of failure .....	124
Figure 5.11. Stress and strain distributions across the thickness of the three-point bending specimen under the failure load .....	127
Figure 5.12. Bilinear stress-strain curves for Fireline gypsum at 400°C to 800°C ...	128
Figure 5.13. Comparison of load-deflection curves for Fireline gypsum at 400°C by theory and experiment .....	129
Figure 5.14. Comparison of load-deflection curves for Fireline gypsum at 500°C by theory and experiment .....	130
Figure 5.15. Comparison of load-deflection curves for Fireline gypsum at 600°C by theory and experiment .....	130
Figure 5.16. Comparison of load-deflection curves for Fireline gypsum at 700°C by theory and experiment .....	131
Figure 5.17. Comparison of load-deflection curves for Fireline gypsum at 800°C by theory and experiment .....	131
Figure 5.18. Comparison of bending and compressive strength of gypsum prisms at temperatures up to 180°C.....	133

---

Figure 6.1. Test arrangement of experiments T1 and T2 .....	138
Figure 6.2. The effect of the draw-wire transducer fixed on the plasterboard in test T1W .....	139
Figure 6.3. Test arrangement of experiments T3 and T4 .....	141
Figure 6.4. Test arrangement of experiments T5 and T6 .....	142
Figure 6.5. Temperature recordings for test T1F (12.5mm single-layer non-insulated Fireline gypsum) .....	144
Figure 6.6. Temperature recordings for test T2W (12.5mm single-layer insulated Wallboard gypsum) .....	145
Figure 6.7. Temperature recordings for test T2F (12.5mm single-layer insulated Fireline gypsum) .....	145
Figure 6.8. Temperature recordings for test T3F (12.5mm single-layer non-insulated Fireline gypsum) .....	146
Figure 6.9. Temperature recordings for test T4W (12.5mm single-layer insulated Wallboard gypsum) .....	146
Figure 6.10. Temperature recordings for test T4F (12.5mm single-layer insulated Fireline gypsum) .....	147
Figure 6.11. Temperature recordings for test T5W (25mm double-layer non-insulated Wallboard gypsum) .....	147
Figure 6.12. Temperature recordings for test T5F (25mm double-layer non-insulated Fireline gypsum) .....	148
Figure 6.13. Temperature recordings for test T6W (25mm double-layer insulated Wallboard gypsum) .....	148
Figure 6.14. Temperature recordings for test T6F (25mm double-layer insulated Fireline gypsum) .....	149
Figure 6.15. Deflection recordings of tests T1F, T2W, T2F and T3F - Solid lines: draw-wire transducers, dashed lines: laser sensors - Negative values indicate deflecting towards the furnace .....	150
Figure 6.16. Deflection recordings of tests T4W, T4F, T5W and T5F - Solid lines: draw-wire transducers, dashed lines: laser sensors - Negative values indicate deflecting towards the furnace .....	151
Figure 6.17. Deflection recordings of tests T6W and T6F - Solid lines: draw-wire transducers, dashed lines: laser sensors - Negative values indicate deflecting towards the furnace .....	152
Figure 6.18. Test arrangement for full-scale wall assembly F-07 (Sultan and Lougheed, 2002).....	153
Figure 6.19. Test arrangement for full-scale wall assembly F-09 (Sultan and Lougheed, 2002).....	154

Figure 6.20. Test arrangement for full-scale wall assemblies UW-8V and UW-9V (Bwalya et al., 2007).....	155
Figure 6.21. Wide vertical cracks on the unexposed gypsum board in test UW-8V.....	156
Figure 6.22. Temperature history on the back of the exposed board in test UW-9V.....	156
Figure 7.1. Boundary conditions for out-of-plane deflection of the gypsum board in (a) and out (b) of the furnace .....	160
Figure 7.2. Geometry of the heat transfer model .....	161
Figure 7.3. Temperature predictions on the exposed and unexposed surfaces of a 12.5mm layer of Fireline gypsum board using different number of elements through the thickness of the board .....	163
Figure 7.4. Temperature history for Test T1F (12.5mm single-layer non-insulated Fireline gypsum) .....	165
Figure 7.5. Temperature history for Test T2F (12.5mm single-layer insulated Fireline gypsum) .....	165
Figure 7.6. Temperature history for Test T3F (12.5mm single-layer non-insulated Fireline gypsum) .....	166
Figure 7.7. Temperature history for Test T4F (12.5mm single-layer insulated Fireline gypsum) .....	166
Figure 7.8. Temperature history for Test T5F (25mm double-layer non-insulated Fireline gypsum) .....	167
Figure 7.9. Temperature history for Test T6F (25mm double-layer insulated Fireline gypsum) .....	167
Figure 7.10. Temperature history for Test T2W (12.5mm single-layer insulated Wallboard gypsum) .....	168
Figure 7.11. Temperature history for Test T4W (12.5mm single-layer insulated Wallboard gypsum) .....	168
Figure 7.12. Temperature history for Test T5W (12.5mm double-layer non-insulated Wallboard gypsum) .....	169
Figure 7.13. Temperature history for Test T6W (12.5mm double-layer insulated Wallboard gypsum) .....	169
Figure 7.14. Defining failure in classic metal plasticity material model by introducing a sudden drop in the stress-strain relationship.....	171
Figure 7.15. Typical linear (a) and nonlinear (b) traction-separation response .....	175
Figure 7.16. Sensitivity of the simulation results of the deflection at the mid-span of test T1F to different values of the displacement at failure ( $\delta_{max}$ ) .....	176

Figure 7.17. Comparison between the total strain energy and the total viscous dissipation energy in test T1F .....	177
Figure 7.18. Comparison of numerical results for the mid-span deflection in test T1F, using thermal shrinkage data from dilatometer tests with different heating rates .....	181
Figure 7.19. Deflection at the mid-span of Fireline gypsum board in test T1F, predicted by numerical analysis using different mesh sizes.....	182
Figure 7.20. Support condition for the gypsum board in tests T1, T2, T5 and T6 ...	183
Figure 7.21. Boundary conditions, defined at the highlighted nodes and line on the half board in tests T1, T2, T5 and T6.....	183
Figure 7.22. Schematic boundary conditions imposed on the gypsum board from the steel studs in tests T3 and T4 .....	184
Figure 7.23. Boundary conditions, defined at the highlighted positions on the half board in tests T3 and T4.....	184
Figure 7.24. ABAQUS stress distribution results in the direction of the length of the beam for test T1F at different times during heating. Compressive stresses are shown in grey .....	186
Figure 7.25. Comparison between numerical and experimental results for the deflection at the mid-span of the gypsum board in test T1F.....	186
Figure 7.26. Large deformation of the board close to the edge in test T1F .....	187
Figure 7.27. Crack pattern for test T2F as predicted by ABAQUS just before the test is terminated .....	188
Figure 7.28. Comparison between numerical and experimental results for the deflection at the mid-span of the board in test T2F .....	188
Figure 7.29. Comparison between numerical results for the deflection at the mid-span of the beam in test T3F, considering fully-rigid or pin supports and the experimental results .....	189
Figure 7.30. Schematic view of the semi-rigid support provided to the gypsum board by the studs in tests T3 and T4 .....	191
Figure 7.31. Comparison between numerical results of the deflection at the mid-span of the gypsum board in test T3F using the semi-rigid support model and the experimental results .....	191
Figure 7.32. Distribution of the maximum principal stresses on the gypsum board in test T3F just before the test is terminated .....	192
Figure 7.33. Distribution of the maximum principal stresses on the gypsum board in test T4F just before the test is terminated .....	192
Figure 7.34. Comparison between numerical and experimental results of the deflection at the mid-span of the board in test T4F .....	193
Figure 7.35. Temperature history for the exposed board in Test T5F.....	194

Figure 7.36. Deflection of the exposed gypsum board in test T5F at 10, 30 and 55 minutes.....	194
Figure 7.37. Comparison between numerical and experimental results of the deflection at the mid-span of the unexposed gypsum board in test T5F .....	195
Figure 7.38. Temperature history for the exposed board in Test T6F.....	196
Figure 7.39. Distribution of maximum principal stresses on the exposed beam in test T6F just after the crack cuts through the thickness of the board. ....	196
Figure 7.40. Comparison between numerical and experimental results of the deflection at the mid-span of the unexposed board in test T6F. ....	197
Figure 7.41. Distribution of maximum principal stresses on the beam in test T2W just after the cracks cut through the thickness of the board .....	199
Figure 7.42. Temperature history for the Wallboard gypsum in Test T2W .....	200
Figure 7.43. Buckling of the middle stud into the furnace at 24 minutes in test T2W .....	201
Figure 7.44. Comparison between numerical and experimental results for the deflection at the mid-span of the gypsum board in test T2W .....	201
Figure 7.45. Deflection of the gypsum board in test T4W at 5, 10 and 16 minutes (deflections are 5 times magnified) .....	202
Figure 7.46. Temperature history for the Wallboard gypsum in Test T4W .....	203
Figure 7.47. Comparison between numerical and experimental results for the deflection at the mid-span of the gypsum board in test T4W .....	203
Figure 7.48. Deflection of the exposed gypsum board in test T5W at 7, 14 and 20 minutes (deflections are 5 times magnified) .....	204
Figure 7.49. Cracks opening all along the gypsum board in test T5W soon after the first crack completes its progress through the thickness. (The image is presented out of scale to improve visual clarity of the cracks).....	205
Figure 7.50. Temperature history between the two layers of the boards in test T5W .....	205
Figure 7.51. Comparison between numerical and experimental results for the deflection at the mid-span of the unexposed board in test T5W.....	206
Figure 7.52. Distribution of maximum principal stresses on the exposed beam in test T6W just after a crack cuts through the thickness of the board .....	207
Figure 7.53. Temperature history between the two layers of the boards in test T5W .....	207
Figure 7.54. Comparison between numerical and experimental results for the deflection at the mid-span of the unexposed board in test T6W.....	208

---

Figure 7.55. Schematic boundary conditions used for modelling Canadian test UW-8V.....	210
Figure 7.56. Temperature history on the back of the exposed board in test F-07.....	211
Figure 7.57. Distribution of maximum principal stresses on the exposed board in test F-07 just after a crack cuts through the thickness of the board .....	211
Figure 7.58. Temperature history on the back of the exposed board in test F-09.....	212
Figure 7.59. Distribution of maximum principal stresses on the exposed board in test F-09 just after cracks cut through the thickness of the board...213	
Figure 7.60. Deflection of the gypsum board in tests UW-8V and UW-9V at 5, 10 and 15 minutes (deflections are 5 times magnified) .....	214
Figure 7.61. Temperature history on the back of the exposed board in test UW-8V .....	214
Figure 8.1. Schematic gypsum board model for structural analysis.....	218
Figure 8.2. Temperature history calculated through thermal analysis in ABAQUS for a 12.5mm gypsum board exposed to standard fire on one side and ambient temperature on the other.....	219
Figure 8.3. Simulation results for the deflection at the mid-span of gypsum board with 600mm span and 12.5mm thickness.....	220
Figure 8.4. Incomplete formation of through-thickness cracks in gypsum board with 600mm span and 12.5mm thickness after 150 minutes of fire exposure.....	221
Figure 8.5. Schematic drawing of a gypsum board fixed to a steel stud by two screws at its edge .....	222
Figure 8.6. Temperature history for 12.5mm exposed gypsum board in single-layer and double-layer assembly .....	223
Figure 8.7. Temperature history for 12.5mm gypsum board with and without insulation .....	224
Figure 8.8. Thermal shrinkage of an improved gypsum board product (hypothetical) as compared to thermal shrinkage of Fireline gypsum board.....	225
Figure A.1. Temperature recordings on the exposed and unexposed surfaces of gypsum panels in Tests 1 to 4 .....	243
Figure A.2. Temperature recordings on the exposed and unexposed surfaces of gypsum panels in Tests 5 to 8 .....	244
Figure A.3. Temperature recordings on the exposed and unexposed surfaces of gypsum panels in Tests 9 to 12 .....	245

---

## LIST OF TABLES

Table 2.1. Fall-off temperatures of gypsum board Type X (Sultan, 2008).....	47
Table 3.1. Calculating thermal conductivity of dried Fireline and Wallboard gypsum boards.....	88
Table 3.2. Arranging gypsum in various layers, each with a uniform void size .....	92
Table 3.3. Effective pore size for series and parallel arrangement of layers at different temperatures .....	93
Table 4.1. Specifications of gypsum board specimens (British-Gypsum, 2009) .....	99
Table 4.2. Measured moisture content of the specimens.....	103
Table 5.1. Dilatometer gypsum board samples .....	113
Table 5.2. Mechanical properties of Wallboard gypsum panels at different temperatures.....	121
Table 5.3. Mechanical properties of Fireline gypsum panels at 20°C to 300°C.....	121
Table 6.1. Specifications of the medium-scale fire tests on gypsum board wall assemblies .....	137
Table 6.2. Observation report for test T2W.....	143
Table 7.1. Comparison between experimental and numerical results for single-layer Fireline gypsum board wall assemblies.....	198
Table 7.2. Comparison between experimental and numerical results for double-layer Fireline gypsum board wall assemblies. ....	198
Table 7.3. Comparison between experimental and numerical results for single-layer Wallboard gypsum wall assemblies .....	209
Table 7.4. Comparison between experimental and numerical results for double-layer Wallboard gypsum wall assemblies.....	209
Table B.1. Sample data for dilatometer tests .....	246
Table B.2. Sample data for three-point bending tests.....	247
Table B.3. Sample data for gypsum prism compression tests .....	248
Table C.1. Observation report for test T2F, part 1.....	249
Table C.2. Observation report for test T2F, part 2.....	250
Table C.3. Observation report for test T5W, part 1 .....	251
Table C.4. Observation report for test T5W, part 2 .....	252

## NOMENCLATURE

Symbol	Definition
$b$	Width
$c$	Specific heat
$d$	Depth
$d_e$	Effective diameter
$D$	Deflection
$e_d$	Dehydration water content (percentage by total weight)
$e_{free}$	Free water content (percentage by total weight)
$E$	Effective emissivity
$E_a$	Elastic modulus of steel at 20°C
$E_f$	Flexural modulus of elasticity
$f_1, f_2$	Correction factors
$F_0$	Fourier number as defined in the text
$h(T)$	Convection heat transfer coefficient
$I$	Moment of inertia of section
$k(T)$	Thermal conductivity
$k^*$	Effective thermal conductivity
$k_g$	Effective thermal conductivity of gas
$k_s$	Thermal conductivity of solid
$K_{R1}, K_{R2}$	Reduction factors
$L$	Length
$L_c$	Characteristic length
$m$	Slope of load deflection curve
$P$	Load
$\dot{q}$	Heat generated per unit volume
$Q$	Heat
$R_s$	Bending rigidity provided by studs
$t$	Time

$T$	Temperature
$T_0$	Initial temperature
$T_{bc}$	Boundary temperature
$T_\infty$	Gas temperature
$x, y, z$	Cartesian coordinates

<b>Symbol</b>	<b>Definition</b>
$\Delta$	Deflection
$\delta_c$	Displacement at which crack initiates
$\delta_{max}$	Element displacement at failure
$\delta(x)$	Deflection of beam at $x$
$\varepsilon$	Emissivity / porosity (as stated in the text)
$\varepsilon_f$	Strain in outer fibres of beam (mm/mm)
$\varepsilon_u$	Strain corresponding to the ultimate strength
$\theta(x)$	Slope of deflected beam
$\rho$	Density
$\sigma$	Stefan-Boltzmann constant ( $5.67 \times 10^{-8} \text{ W/m}^2\text{K}^4$ )
$\sigma_f$	Stress in outer fibres of beam
$\varphi$	Geometric “view factor”
$\varphi(x)$	Section curvature

## **ABSTRACT**

Gypsum board assemblies are now widely used in buildings, as fire resistant walls or ceilings, to provide passive fire protection. The fire resistance of such systems is fundamentally due to the desirable thermal properties of gypsum. Yet there is wide variability in reported values of thermal properties of gypsum at high temperatures and a lack of understanding of its integrity in fire. To evaluate the fire protection performance of gypsum board assemblies, it is essential to quantify its thermal properties and obtain information on its mechanical properties at high temperatures. Gypsum boards shrink and crack at high temperatures, and this leads to collapse of parts of the gypsum boards in fire. Fall-off of gypsum in fire affects the fire resistance of the assembly considerably, and cannot be overlooked when evaluating the fire resistance of gypsum board assemblies.

The current research proposes a model to define the temperature-dependent thermal properties of gypsum boards at high temperatures. Thermal conductivity of gypsum is considered as the most influential parameter in conduction of heat through gypsum, and a hybrid numerical-experimental method is presented for extracting thermal conductivity of various gypsum board products at elevated temperatures. This method incorporates a validated one-dimensional Finite Difference heat conduction program and high temperature test results on small samples of gypsum boards.

Moreover, high temperature mechanical tests have been performed on different gypsum board products; thermal shrinkage, strength and stress-strain relationships of gypsum products at elevated temperatures are extracted for use in numerical mechanical analysis.

To simulate the structural performance of gypsum boards in fire, a two-dimensional Finite Element model has been developed in ABAQUS. This model successfully predicts the complete opening of a through-thickness crack in gypsum, and is validated against medium-scale fire tests designed and conducted as part of this research. Gypsum fall-off in fire is a complex phenomenon; however, it is believed

that delaying the formation of through-thickness cracking will delay falling off of gypsum in fire, and hence improve the fire resistance of gypsum board assemblies. Finally, a study has been performed on the effects of various detailing parameters in gypsum board wall assemblies, and recommendations are offered for improving the fire resistance of such systems.

## **DECLARATION**

No portion of the work referred to in the thesis has been submitted in support of an application for another degree or qualification of this or any other university or other institute of learning.

## COPYRIGHT STATEMENT

- i. The author of this thesis (including any appendices and/or schedules to this thesis) owns certain copyright or related rights in it (the “Copyright”) and s/he has given The University of Manchester certain rights to use such Copyright, including for administrative purposes.
- ii. Copies of this thesis, either in full or in extracts and whether in hard or electronic copy, may be made **only** in accordance with the Copyright, Designs and Patents Act 1988 (as amended) and regulations issued under it or, where appropriate, in accordance with licensing agreements which the University has from time to time. This page must form part of any such copies made.
- iii. The ownership of certain Copyright, patents, designs, trade marks and other intellectual property (the “Intellectual Property”) and any reproductions of copyright works in the thesis, for example graphs and tables (“Reproductions”), which may be described in this thesis, may not be owned by the author and may be owned by third parties. Such Intellectual Property and Reproductions cannot and must not be made available for use without the prior written permission of the owner(s) of the relevant Intellectual Property and/or Reproductions.
- iv. Further information on the conditions under which disclosure, publication and commercialisation of this thesis, the Copyright and any Intellectual Property and/or Reproductions described in it may take place is available in the University IP Policy (see <http://www.campus.manchester.ac.uk/medialibrary/policies/intellectual-property.pdf>), in any relevant Thesis restriction declarations deposited in the University Library, The University Library’s regulations (see <http://www.manchester.ac.uk/library/aboutus/regulations>) and in The University’s policy on presentation of Theses.

## **ACKNOWLEDGEMENTS**

I wish to express my deeply-felt gratitude to my supervisor Prof. Yong C. Wang whose absolute care and support, encouragement, patience, thoughtful guidance and professionalism has inspired me at every single step, and has made the completion of this project possible.

I would also like to thank the sponsoring company, British Gypsum, for their financial support, and Drs. Kane Ironside and Jan Rideout for their industrial supervision and technical support. The technical assistance by the laboratory staff at the University of Manchester, and also at British Gypsum, is greatly appreciated.

I am indebted to my many colleagues for providing a stimulating and fun environment in which to learn and grow, academically and otherwise.

My sincere thanks also go to my parents and my family of whom no words can do justice to, for their unconditional love and support throughout my entire life and study.

Finally, my greatest thanks and devotions to my beloved husband whose endless support and patience fed me all the way through.

## **CHAPTER 1. Introduction**

### **1.1 General Introduction**

Designing structures against fire attack is constantly attracting more importance and investment on a global scale. Uncontrolled fires can cause huge number of injuries, fatalities and economic loss. Hence, providing a system to control fires is of great significance in engineering practice. Different measures currently used to control a fire can be divided into two general categories of active and passive fire protection. Active measures essentially attempt to extinguish a fire (e.g. water sprinklers, deluges and sprays), whereas passive measures impede the spread of fire or minimise the consequences of a fire. Passive fire protection to a building can be provided by the structure itself, coating or partitions. One common practice in passive fire protection is compartmentalization of a building using fire-resistant barriers, so that in the case of fire in one compartment, it is not spread to the adjacent areas, the impact of fire is limited, and occupants can safely evacuate the building.

Gypsum board based systems are among those now widely used, as walls or ceilings, for such purposes. Gypsum plasterboards are mainly utilized as lining material in light-weight construction, which is an efficient and cost effective method of providing flexible partitioning assemblies in commercial and residential buildings. The thickness of the gypsum board lining and the configuration of the framing can be flexibly changed to meet specified fire performance requirements. The use of such systems is increasing every day and there is a demand for more research on their properties and behaviour.

Most structural elements lose their ability to sustain loads in temperatures between 450°C and 800°C. Besides, release of smoke, toxic gas and excessive heat or possible explosions are some of the many hazards caused by fire. Therefore, evaluating the response of the fire-resistant barriers during fire is of great concern in safety and reliability assessments in building industry.

To evaluate their fire resistance, building regulations in the UK require construction components to undergo standard fire tests. BS 476-part 20 (BSI, 1987) defines standard fire testing procedures, as well as insulation, integrity and stability criteria to be satisfied by an element of building construction. However, evaluating fire resistance of many construction elements, including gypsum board assemblies, is a very complicated process involving many variables, such as the growth and duration of fires, variations of material properties, temperature distribution in the system, interactions between building elements and the effects of structural loads on the stability of the system. Although standard fire tests provide useful means to simplify the fire resistance evaluation and classify building elements, the outcome cannot be generalized and exploited in the absence of a reliable analytical procedure.

The low cost and efficiency that can be provided by numerical modelling of the behaviour of gypsum board systems in elevated temperatures has led many researchers in recent years to focus their studies on development of analytical methods (to supplement fire testing) for optimal design of gypsum board systems. Moreover, with the advent of performance-based codes and design options, numerical models that can simulate the fire resistance performance of gypsum board assemblies are gaining paramount importance. However, development of fire resistance models faces numerous challenges, many of which remain unsolved despite the recent endeavours. The chief objective of this study is, therefore, to develop a numerical method that facilitates fire resistance prediction of gypsum board based systems.

## 1.2 Research Significance and Objectives

In the highly competitive market of gypsum board systems, it is essential for leading manufacturers to constantly develop new products by using new materials and new systems. The current method for evaluating fire resistance of new products, exercised by the sponsoring company, British Gypsum, is iterative design requiring full-scale fire tests, which is both expensive and time-consuming. Whilst full-scale fire testing according to regulatory standards will still be necessary for final accreditation purpose, much of this may be avoided by developing a predictive model to calculate gypsum board system fire resistance time. Figure 1.1 demonstrates how benefits of such predictive model can give the sponsoring company a genuine competitive edge.

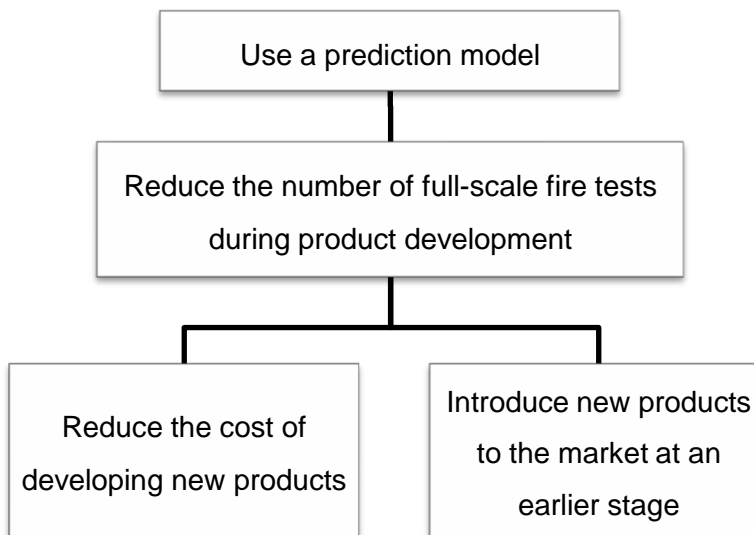


**Figure 1.1.** Benefits of a reliable numerical model to predict fire resistance of gypsum board based systems

Therefore, the main objective of this research work is to:

- Develop a model that simulates thermal and structural behaviour of gypsum boards in standard fire conditions
- Evaluate the numerical model through experimental verifications.

Developing a reliable fire resistance model requires reliable data on the thermal and mechanical properties of gypsum boards, as well as a verified numerical method that can simulate the thermal and structural performance of gypsum at elevated temperatures. Hence, the key issues addressed in this research are:

- Extracting temperature-dependent thermal properties of gypsum
- Extracting temperature-dependent mechanical properties of gypsum
- Simulating structural failure of gypsum at elevated temperatures

Although thermal properties of gypsum have been studied in the literature, there is a lack of consistency in the reported values of thermal properties of gypsum at high temperatures. So there is a need to establish a procedure to evaluate thermal properties of new gypsum board products based on fundamental understanding of heat transfer and experimental validations. Mechanical properties of gypsum at high temperatures are almost non-existent in the literature. Hence, providing reliable data on the mechanical properties of gypsum is of great significance. Also non-existent in the literature is a structural model to predict the performance of gypsum in fire. Gypsum provides the main fire resistance protection of gypsum board assemblies; however, it loses strength at high temperatures and falls off in fire. Therefore, it is essential to study the structural performance of gypsum at elevated temperatures and predict its failure in fire conditions.

### **1.3 Outline of the Thesis**

The following outlines the contents of this thesis:

Chapter 1 gives a general introduction to the research project and highlights its objectives.

Chapter 2 looks into gypsum board assemblies and the basics of fire resistance. It reviews related literature on thermal and mechanical properties of gypsum and the behaviour of gypsum board systems in fire conditions.

Chapter 3 introduces a procedure for extracting temperature-dependent thermal properties of gypsum at high temperatures, incorporating a one-dimensional Finite Difference heat transfer model and experimental calibrations.

Chapter 4 presents the results of small-scale heat transfer tests on gypsum board specimens. The results are used to validate the methodology proposed in Chapter 3 for extracting thermal properties of gypsum.

Chapter 5 provides the results of mechanical properties of gypsum at high temperatures extracted through experiments and original theoretical models.

Chapter 6 presents the results of medium-scale fire tests performed on gypsum board wall assemblies and reports on observations of gypsum fall-off in fire.

Chapter 7 outlines the features of two-dimensional Finite Element modelling of gypsum using ABAQUS that predicts temperature developments through gypsum, and simulates its structural performance in fire. The model is validated against experimental results provided in Chapter 6, and successfully predicts formation of cracks in gypsum.

Chapter 8 is devoted to the study of the effects of detailing parameters in wall assemblies utilizing the Finite Element model proposed in Chapter 7. Various detailing parameters are considered and their influence on the structural fire performance of gypsum boards is reported.

Finally, Chapter 9 summarizes the discussions, draws conclusions from the research carried out and offers recommendations for future research studies.

## CHAPTER 2. Literature Review

### 2.1 Introduction

Gypsum board assemblies are probably the most common practice in providing passive fire resistance in a variety of constructions. Evaluating fire resistance of such assemblies has therefore been of interest to many researchers. Gypsum boards are the main fire resistant components of these systems. Although much research has been conducted to quantify their properties, many uncertainties still remain. This chapter starts with a general introduction to gypsum board assemblies and standard fire tests, followed by a review of the thermal and mechanical properties of gypsum board at high temperatures reported in the literature. Also reviewed are studies that address the performance of gypsum board assemblies in fire condition. Finally, gaps in knowledge are identified, and some conclusions are presented on the literature reviewed.

### 2.2 Gypsum Board Assemblies

Gypsum plasterboards are mainly used as sheet material lining in light-weight constructions, namely Light Steel Framing (LSF) and Light Timber Framing (LTF). A typical wall assembly of drywall construction is shown in Figure 2.1. Such walling systems consist of steel studs or wood studs with one or two layers of gypsum boards fixed to each side of the studs. The cavity between the boards are filled with insulation layers or left empty. The insulation materials commonly used in the cavity are glass fibre, rock wool and cellulose fibre insulation.

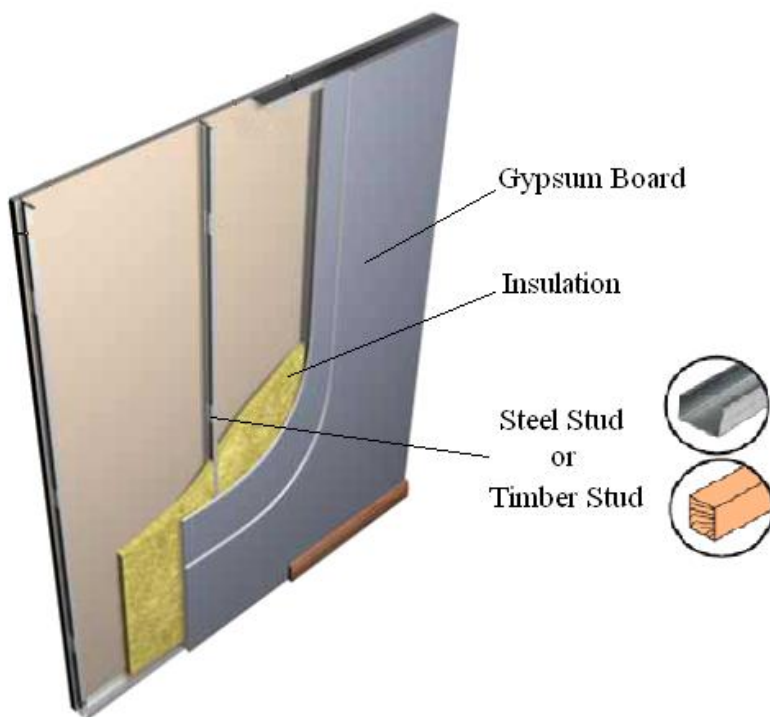


**Figure 2.1.** A typical gypsum board wall assembly

Each board is composed of a non-combustible gypsum core with paper-laminated surfaces which provide tensile strength to the lining. Gypsum contains chemically bound water and a small amount of free water, which play a key role in the performance of the assembly at elevated temperatures. During a fire, when gypsum board is heated up to about 100°C, a great amount of heat is absorbed to drive off the water. This process delays the development of temperature rise through gypsum until the entire board is dehydrated. Gypsum also has a very low thermal conductivity which enables the unexposed surface of a gypsum board to remain at low temperatures and provide a reasonably cheap and lightweight fire resistant barrier to be used in compartmentalisation of a wide range of residential and commercial buildings.

Based on composition and performance, gypsum boards are classified into different types. The two types of interest in this study are regular and fire-rated gypsum boards. The gypsum core in gypsum boards, defined as regular (or standard) gypsum, provides the main fire resistance. In fire-rated boards, the gypsum core is enhanced with special additives to improve the natural fire resistance of gypsum.

Considerable variations in fire performance of gypsum boards have been observed based on the type and the formulation of the core of the board, which differs from one manufacturer to another.

### 2.3 Fire Resistance

To specify fire resistance of a system, building codes and regulations rely on standard fire test procedures. Fire resistance is then defined as the duration for which a fire protection system can withstand a standard fire test until it reaches failure criteria. Failure is by loss of either fire separating function or load bearing function and categorized as insulation (excessive temperature rise on the unexposed surface), integrity (fire spread through fissures and openings) and stability (structural collapse) criteria.

In a standard fire test, the elements of interest are subjected to increasing temperatures governed by a specified temperature-time relationship. BS476 (BSI, 1987) provides two types of time-temperature curves for a standard fire:

- 1) Cellulosic fire (Standard fire):

$$T = 345 \log_{10}(8t + 1) + 20$$

- 2) Hydrocarbon fire (proposed in ISO/DIS 834):

$$T = 1100(1 - 0.325 e^{-0.1667t} - 0.204e^{-1.417t} - 0.471e^{-15.833t})$$

where

$T$  is the fire temperature (in °C);

$t$  is the time (in min) up to a maximum of 360 min.

It should be noted that the standard fire curves are attempts to classify construction elements, but they do not represent fire scenarios in the real world. In general building uses, the cellulosic fire condition is applied. Hydrocarbon fires are more likely to occur in petrochemical industry. The two fire curves are plotted in Figure 2.2. As can be seen from the plots, hydrocarbon fire has a steep initial temperature rise to 1100°C, simulating fast reaction of hydrocarbons.

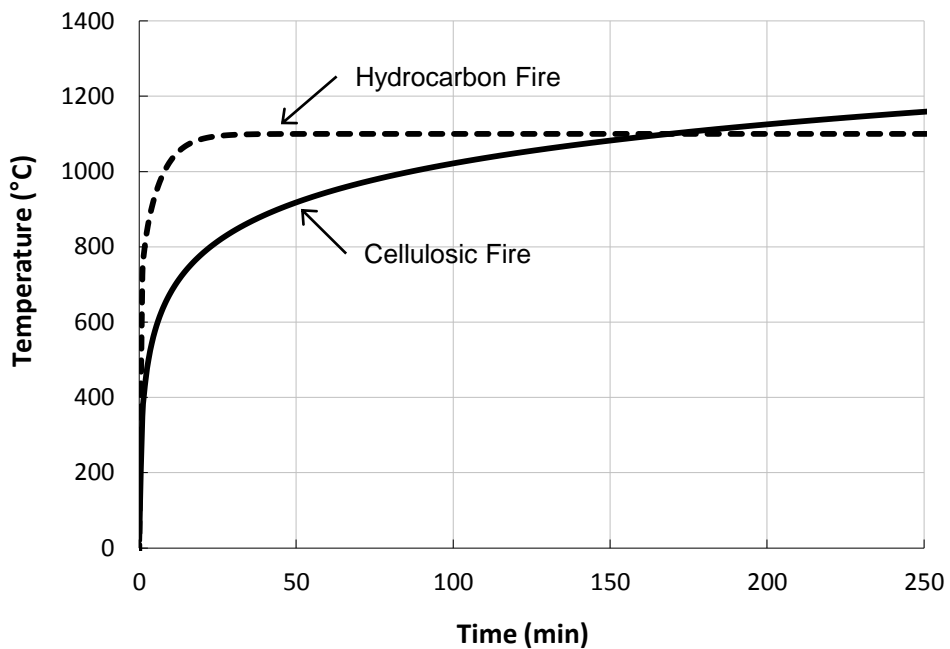
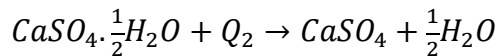
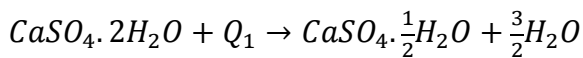


**Figure 2.2.** Time-temperature curves for standard fires according to BS476 (BSI, 1987)

## 2.4 Thermo-Chemistry of Gypsum

Pure gypsum ( $\text{CaSO}_4 \cdot 2\text{H}_2\text{O}$  - calcium sulphate dihydrate) is a crystalline mineral, composed of calcium sulphate and approximately 21% (by weight) chemically bound water of crystallisation (Mehaffey et al., 1994). In addition, gypsum contains free water of about 3% at ambient conditions. The amount of the equilibrium moisture content depends on ambient temperature and relative humidity (Thomas, 2002). The composition of gypsum core varies from one manufacturer to another; however, when used as lining in drywall construction, it usually contains some additives such as glass fibre and vermiculite in small quantities, so as to improve the integrity and performance of the system at elevated temperatures.

Being a hydroscopic material (i.e. containing water), calcium sulphate dihydrate undergoes chemical decomposition reactions when heated, and the water of crystallisation is driven off in two stages. This process is called calcination which results in shrinkage of the material and its loss of strength:



During the first reaction, gypsum dehydrates to calcium sulphate hemihydrate (or Plaster of Paris) and 75% of the chemically combined water is released. With further increase in the temperature, the remainder 25% of the chemically bound water is also removed and calcium sulphate anhydrite is left.

The crystal structure for the hemihydrate and anhydrite can be in two forms:  $\alpha$  and  $\beta$ .  $\beta$  is a lower energy form and has larger crystals. Accordingly, the reaction heat for producing form  $\beta$  is smaller; less heat is absorbed by gypsum and thus less heat is mitigated from the fire condition. Therefore, to cut down the discussion and be on the safe side, we consider form  $\beta$  further in this study.

Several research studies (Bénichou and Sultan, 2005, Bakhtiary et al., 2000) indicate that the first dehydration reaction starts at a temperature in the region of 100°C and is completed by about 150°C; however this range can be altered by the rate of heating (Mehaffey et al., 1994). The energy required for the first dehydration reaction,  $Q_1$ , is 100 kJ per kg of gypsum (Weast et al., 1989). The water released then requires more energy to evaporate based on the latent heat of evaporation of water (2.26MJ/kg).

The heat of the second reaction is 50 kJ per kg of gypsum, excluding the energy required to evaporate the dissociated water. The temperature at which the second dehydration reaction occurs varies according to different researchers. Andersson and Jansson (1987) suggest a temperature of about 210°C, Groves (1958) suggests 300°C and Sultan (1996) reports it at about 700°C. Some variations of this value can be due to the different heating rates and measuring techniques. However, Ghazi Wakili et al. (2007) suggest that the peak in the specific curve around 700-800°C corresponds to the decomposition of calcium carbonate and magnesium carbonate content of gypsum boards and their quantities can be deducted from thermogravimetric analysis. They show that the first and second dehydration reactions occur closely and conclude before 250°C. Recent tests using differential thermal analyses by other researchers also confirm that the second dehydration reaction

takes place around 200°C (Bakhtiary et al., 2000, Elbeyli and Pişkin, 2004), and this value is adopted for this study.

## 2.5 Thermal Properties of Gypsum Plasterboard at Elevated Temperatures

In order to develop heat transfer models of gypsum board assemblies and evaluate their fire resistance, it is necessary to quantify the thermal properties of gypsum at elevated temperatures. These properties are often difficult to measure given the transient effects. The measuring techniques can also affect the results. Moreover, the water content of gypsum highly affects its properties at high temperature. The dissociation, evaporation and subsequent condensation of the chemical water content of gypsum significantly influence the thermal conductivity and specific heat of gypsum. The following sections report on thermal properties of gypsum boards in literature as measured or used by other researchers in numerical heat transfer simulation.

### 2.5.1 Specific Heat

The specific heat of gypsum at different temperatures has been investigated by several researchers (Figure 2.3). As expected, the specific heat of gypsum experiences two peaks corresponding to the two phases of water dissociation. Some researchers have also reported a third peak, which corresponds to the decomposition of the carbonates in gypsum as suggested by Ghazi Wakili and Hugi (2009). The results from different studies agree well on the first peak to occur at about 100°C. However, there is inconsistency on the temperature at which the second peak is observed as well as the value of the peaks.

Harmathy (1988) reports a peak of 7.32 kJ/kg.°C at 100°C and although he does not give measurements over 630°C, his results shows a peak of 2 kJ/kg.°C at this temperature. Andersson and Jansson (1987) provide peak values of 52.2 kJ/kg.°C and 19.2 kJ/kg.°C at 110°C and 210°C, respectively. Mehaffey et al. (1994) first conditioned the specimens at 40°C for 24 hours in an attempt to drive off free moisture and then used a differential scanning calorimeter at two scanning rates of

$2^{\circ}\text{C}/\text{min}$  and  $20^{\circ}\text{C}/\text{min}$ . The results showed a peak of  $29 \text{ kJ/kg.}^{\circ}\text{C}$  at  $95^{\circ}\text{C}$  when the slower scanning rate was used, and a peak of  $14 \text{ kJ/kg.}^{\circ}\text{C}$  at  $140^{\circ}\text{C}$  when the faster scanning rate was employed, while the area under both peaks was about  $500 \text{ kJ/kg}$  corresponding closely to the heat required for the first reaction and evaporation of the water released ( $100 + 0.75 \times 0.21 \times 2260 = 456 \text{ kJ per kg of gypsum}$ ). In their heat transfer model they used a peak of  $49.95 \text{ kJ/kg.}^{\circ}\text{C}$  between  $100^{\circ}\text{C}$  and  $120^{\circ}\text{C}$ . Mehaffey et al. measured specific heat up to  $200^{\circ}\text{C}$  and no second peak was observed. Sultan (1996) reports the first peak of  $18.5 \text{ kJ/kg.}^{\circ}\text{C}$  occurring at  $125^{\circ}\text{C}$  and the second peak of  $3.07 \text{ kJ/kg.}^{\circ}\text{C}$  at  $670^{\circ}\text{C}$ . As mentioned earlier, Ghazi Wakili and Hugi (2009) suggest that the peak observed by Sultan around  $700^{\circ}\text{C}$  corresponds to decomposition of carbonate contents of gypsum, and the heat of the second dehydration was hidden in the large peak observed as a result of the first dehydration reaction.

The specific heat at ambient temperature is the base value when no reaction occurs. This base value is reported to be  $0.88 \text{ kJ/kg.}^{\circ}\text{C}$  by Harmathy,  $0.95 \text{ kJ/kg.}^{\circ}\text{C}$  by Mehaffey et al. and taken as  $0.7 \text{ kJ/kg.}^{\circ}\text{C}$  by Andersson and Jansson. In this research, the base value is  $0.95 \text{ kJ/kg.}^{\circ}\text{C}$ , based on Mehaffey et al.'s work which is widely adopted by other researchers too.

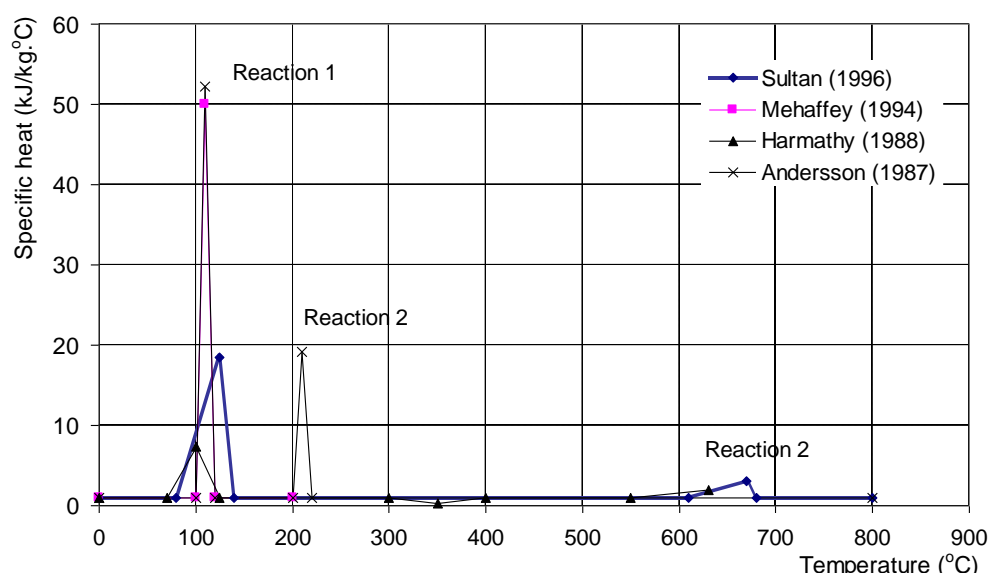


**Figure 2.3.** Specific heat of gypsum according to various researchers (Thomas, 2002)

### 2.5.2 Density

Mehaffey et al. (1994) used thermo-gravimetric analysis (TGA) at a scanning rate of 20°C/min to determine the changes in mass of 10-30 mg specimens of gypsum with temperature (specimens were of fire-rated gypsum type called Type X). The result is demonstrated in Figure 2.4. As can be seen, between 100°C and 160°C about 17.5% of the initial mass is lost, which indicates the first dehydration reaction and the release of water of crystallization ( $0.75 \times 21\% = 15.75\%$ ) as well as the evaporation of the free water (less than 3%). They also noticed a mass loss at 650°C which corresponds to the decomposition of carbonates in gypsum according to Ghazi Wakili and Hugi (2009). Bénichou and Sultan (2001) report similar results using the same measurement methods.

Mehaffey et al. (1994) report the initial density of the 15.9mm Type X gypsum board as 648 kg/m<sup>3</sup>. However, the density of the gypsum core of different gypsum boards at ambient condition varies from type to type and also from different manufacturers. A study by Thomas et al. (Thomas et al., 2005) on a large number of Type X gypsum board samples shows that the density of 12.5mm and 15.8mm boards varies largely both within and between manufacturers. The mean value of the densities in their study ranges from 687 kg/m<sup>3</sup> to 811 kg/m<sup>3</sup>.

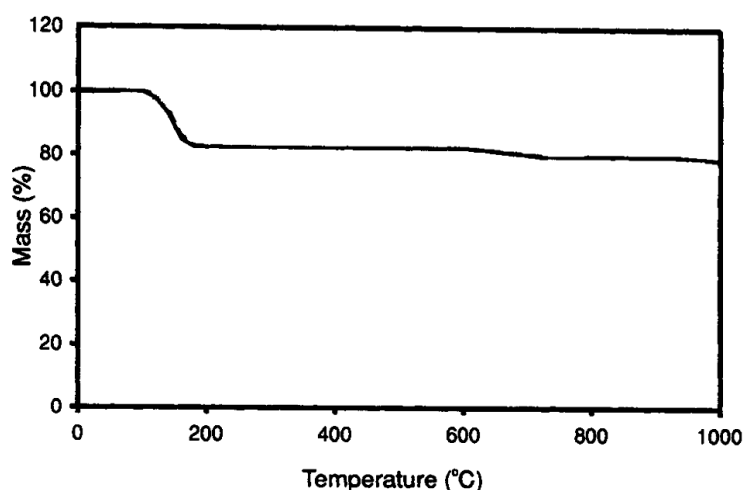


**Figure 2.4.** Mass loss in gypsum with rising temperatures (Mehaffey et al., 1994)

### 2.5.3 Thermal Conductivity

There are complications involved in measuring thermal conductivity of gypsum due to the effects of moisture and radiation in the pores. Gypsum from different sources or manufacturers varies in microstructure, and the methods employed to measure its thermal conductivity also differ. As a result the values reported by different studies vary widely, especially at temperatures above 500°C; nevertheless, they follow a similar trend. Figure 2.5 shows thermal conductivity of gypsum versus temperature given by a few studies. The symbols represent measured values and the lines represent modified curves used in heat transfer models to provide good calibration between numerical and experimental results.

Andersson and Jansson (1987) used the Transient Hot Strip (THS) method which measures the resistance of a metal strip embedded in the material and derives the thermal conductivity of the material. Their results for thermal conductivity of gypsum is quite isolated compared to others.

Harmathy (1988) used a variable state scanning technique with relatively small temperature gradients. His results are very much in agreement with Mehaffey's who used the TC-31 thermal conductivity meter (Mehaffey et al., 1994).

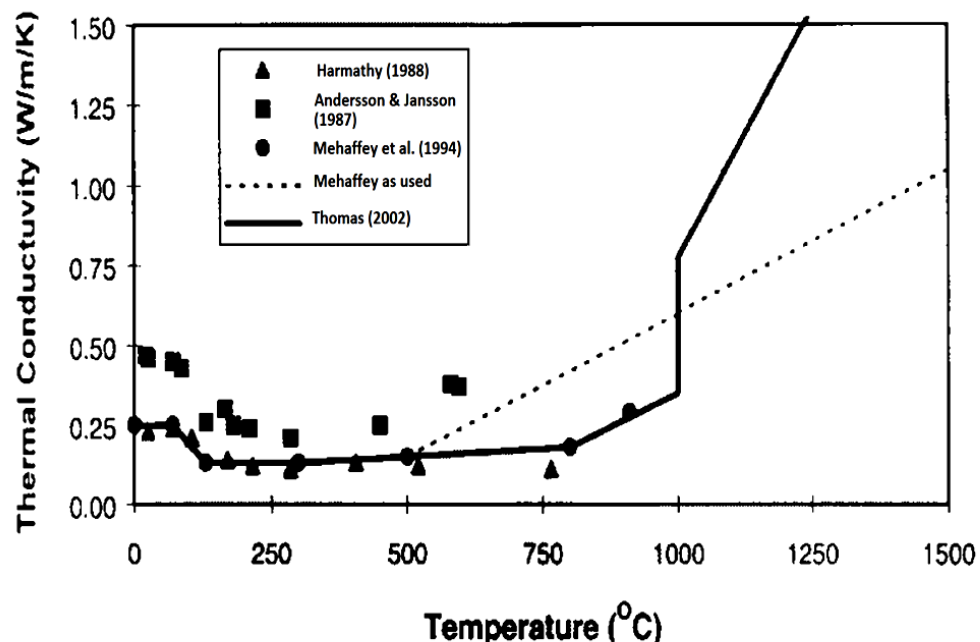


**Figure 2.5.** Thermal conductivity of gypsum versus temperature (Thomas, 2002)

Thomas (2002) mentions that the significant increase in thermal conductivity of gypsum at temperatures above 800°C is to allow for the opening of cracks and ablation of gypsum, since the testing method used by Mehaffey et al prevents the cracks from opening up in the board. It can also cover accelerated radiations in the voids at high temperatures.

The aforementioned various small-scale test methods to measure thermal conductivity can give an indication of the variation of thermal conductivity of gypsum. However, it can be difficult to obtain precise values for a specific product due to the complications of accounting for water movement in gypsum, radiation in voids and cracks in gypsum.

Despite the diversity of data provided by different researchers, they all agree that thermal conductivity does not change noticeably before the first dehydration reaction starts. This can be explained by considering two simultaneous effects: 1) thermal conductivity at a certain moisture content increases with temperature rise (Parrott and Stuckes, 1975), 2) Overall moisture content of gypsum decreases with temperature rise. Accounting for these two effects, Wang (1995) concludes that the thermal conductivity of gypsum increases only slightly with temperature, while losing its water. So it is not unreasonable to assume that the thermal conductivity remains constant before the first dehydration reaction takes place. Furthermore, all data point out a sharp reduction in the thermal conductivity of gypsum at around the temperature of water evaporation. Therefore, the main uncertainty in the thermal conductivity of gypsum appears to be its variations after water evaporation and at higher temperatures. This will be further addressed in CHAPTER 3.

#### **2.5.4 Emissivity and Heat Transfer Coefficient**

To simulate heat transfer in convection and radiation modes, researchers have adopted different values for emissivity and heat transfer coefficient.

Mehaffey et al. (1994) took the emissivity of gypsum (on all sides), cavity and furnace as 0.9. For the heat transfer coefficient they adopted 25 W/m<sup>2</sup>.°C and 9 W/m<sup>2</sup>.°C at the exposed and unexposed surfaces, respectively.

Sultan (1996) recommended some exponential functions for the heat transfer coefficients and suggested a value of 0.8 for the combined emissivity of the gypsum board and the furnace walls lined with ceramic fibre insulation blanket. Combined or effective emissivity is the resultant emissivity with the assumption of infinite parallel plates in this case, which is calculated by:

$$\varepsilon = \frac{1}{\frac{1}{\varepsilon_f} + \frac{1}{\varepsilon_s} - 1}$$

where  $\varepsilon_f$  is the equivalent emissivity of flames, gases and walls in furnace and  $\varepsilon_s$  is the emissivity of the surface of the specimen.

Gerlich et al. (Gerlich et al., 1996) used values of 0.8, for the resultant emissivity at the fire exposed surface of gypsum, and 0.6 at the other surfaces.

Wang (Wang, 1995) assumed that the emissivity of the furnace is 0.9 at the beginning of the test and linearly decreases to 0.15, while the convective heat transfer coefficient declines from 60 W/m<sup>2</sup>.°C at the beginning of the test to 2 W/m<sup>2</sup>.°C at 1000°C. He explains that the declining trend of emissivity is consistent with the emissivity of gas, insulating brick and ceramic fibre linings. The decline in the convective heat transfer coefficient is based on the high fire turbulence at the initial stages of the test, due to rapid increase in the temperature. He noted that the surface emissivity of unexposed gypsum is that of the liner paper manufactured from long fibre pulp. However, the paper facings on the exposed side are consumed after a temperature of approximately 300°C. Therefore he took the emissivity of gypsum as 0.8 and 0.4 at the unexposed and exposed sides, respectively.

It should be noted that the heat transfer coefficients are furnace dependent and contain a high degree of uncertainty. When calibrating the thermal conductivity of gypsum, it is important to eliminate the impact of such uncertainties; this can be done by using the measured surface temperatures of gypsum, as adopted in this research.

### 2.5.5 Ablation

Given sufficient time under heat, some materials undergo physical and chemical changes, which results in bonding reduction of the material and removal of successive thin layers from its surface. This process is referred to as ablation. With rising temperatures the exposed surface of gypsum loses water and turns into calcium sulphate anhydrite, which falls off the unaltered substrate. As heat penetrates through the thickness, more material transforms to anhydrite powder and consecutive layers are shed. Using glass fibre reinforcements in fire-rated boards delays the ablation of the exposed surface. Thomas (2002) observed ablation at about 700°C for normal gypsum boards and 1000°C for fibre reinforced boards. It is also worth noting that ablation is of greater importance for thin boards compared to thick ones, as a larger proportion of the material is shed off.

Including ablation in numerical analysis by reducing the thickness of the material usually adds unnecessary complexity to the model. Hence, often it is accounted for by modifying the thermal conductivity at high temperatures. Nevertheless, since ablation occurs at very high temperatures, its effects are insignificant.

## 2.6 Mechanical Properties of Gypsum Plasterboard at Elevated Temperatures

To facilitate prediction of failure of gypsum in fire, it is essential that mechanical properties of gypsum boards are quantified. Yet, since gypsum is rarely used as a structural member, its mechanical properties at elevated temperatures are not well known. There have been some studies to measure thermal expansion of gypsum, as this is usually considered as thermal property of the material. However, when it comes to strength and modulus of elasticity of different gypsum boards in fire, very little data is available. The following sections review the limited literature available.

### 2.6.1 Thermal Expansion

Figure 2.6 shows the shrinkage of gypsum board and gypsum core against temperature according to NRCC (National Research Council of Canada). When subjected to high temperatures, gypsum core experiences significant shrinkage. In

addition, at the temperature range of about 200-350°C the paper laminates on the sides of gypsum core burn off. Thus the thickness of the board (gypsum and paper) is reduced, too. This significant reduction (shrinkage) needs to be considered when modelling the structure, since it eventually causes the formation of cracks as well as the opening of the joints. Both of these effects can also hugely influence the heat transfer through the system.

Vermiculite, a natural mineral, is commonly used as an additive to the gypsum core to mitigate the effect of shrinkage. Vermiculite expands with the application of heat, partly offsets the contraction of gypsum and therefore enhances the performance of the system in fire. Glass fibre is also a reinforcing agent which bridges shrinkage cracks and attempts to sustain the integrity of gypsum board during calcination (Gerlich, 1995).

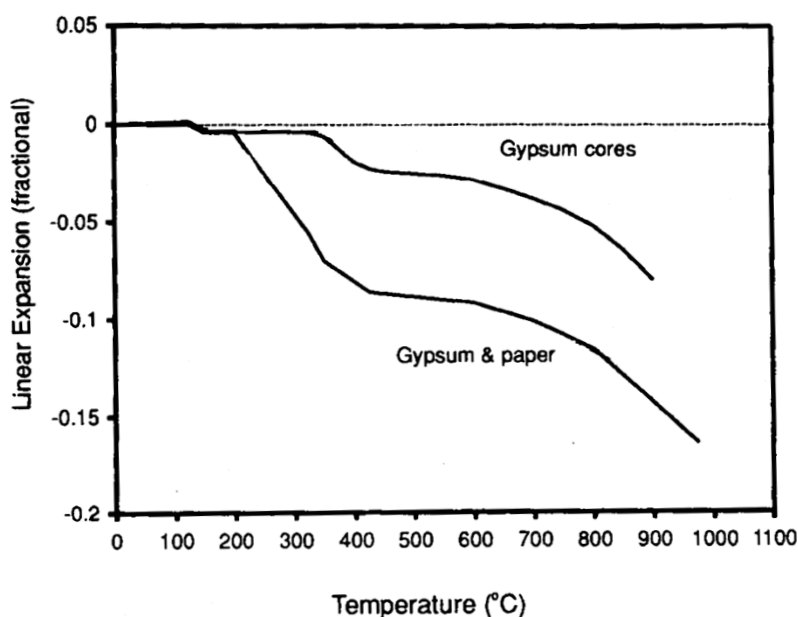


**Figure 2.6.** Contraction of gypsum as a function of temperature (Mehaffey et al., 1994)

### 2.6.2 Modulus of Elasticity and Strength

The knowledge of strength and elastic modulus of gypsum at high temperatures is very limited. Thomas, (1997) as cited in Bénichou and Sultan (2000), reported on some of the data found in the literature for modulus of elasticity and strength of

gypsum up to 140°C . As shown in Figure 2.7, the results suggest that strength and stiffness of gypsum reduce to zero by 120°C.

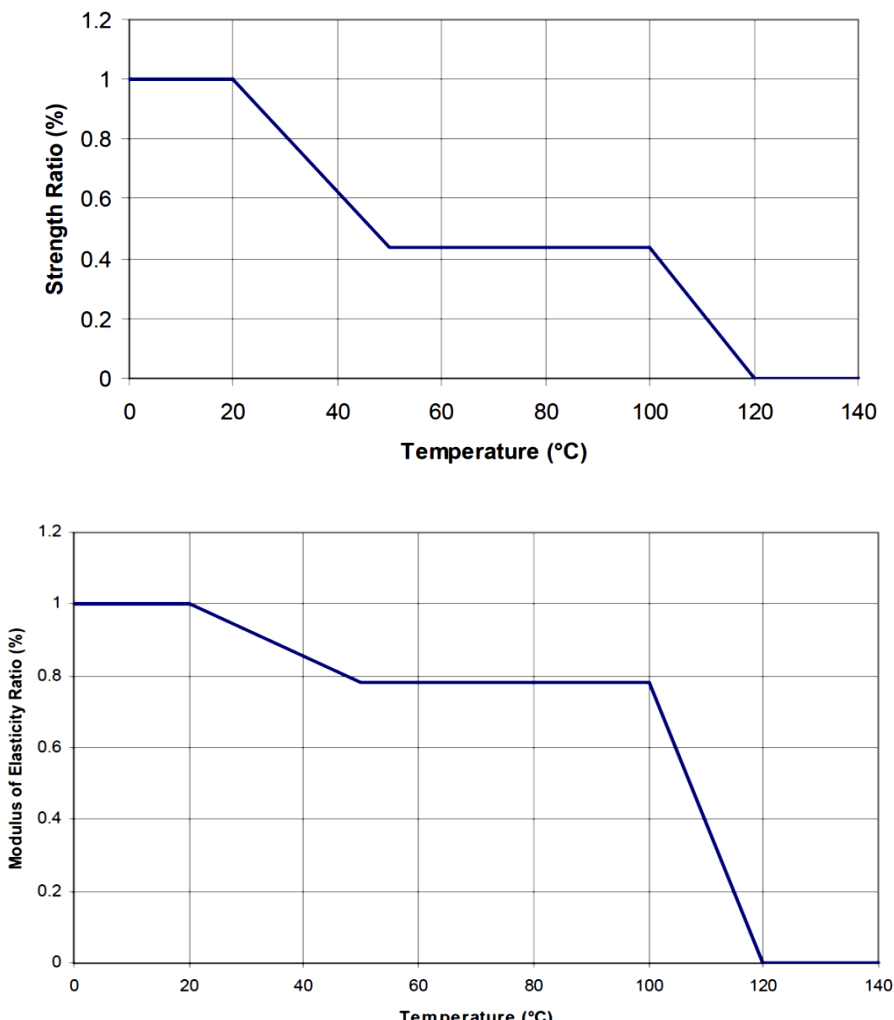


**Figure 2.7.** Modulus of elasticity and strength of gypsum measured up to 140°C (Bénichou and Sultan, 2000)

In a more recent study Cramer et al. (2003) investigated the effect of temperature on the bending strength and modulus of elasticity of gypsum. They measured these properties for 15.9mm thick fire-rated Type X gypsum samples (177.8mm by 50.8mm) by performing three-point bending tests on specimens that were soaked for 60 minutes at 23°C, 100°C, 200°C, 300°C and 400°C. The specimens were cut from gypsum board in two directions: along the length and from the width of the panels. The results are depicted in Figure 2.8. Gypsum appears to reserve minimal strength and stiffness by 400°C. The stiffness and bending strength of the gypsum

board samples cut along the panels are shown to be greater than those of the samples cut from the short direction of the panels. Cramer et al. propose that the difference is due to the machine direction and cross direction properties of the face paper on gypsum samples. When paper burns away by 300°C, its strengthening influence gradually disappears. The values of bending strength and modulus of elasticity of gypsum at ambient temperature are reported in the range of 2.0 to 4.0 MPa and 1.7 to 2.5 GPA, respectively.

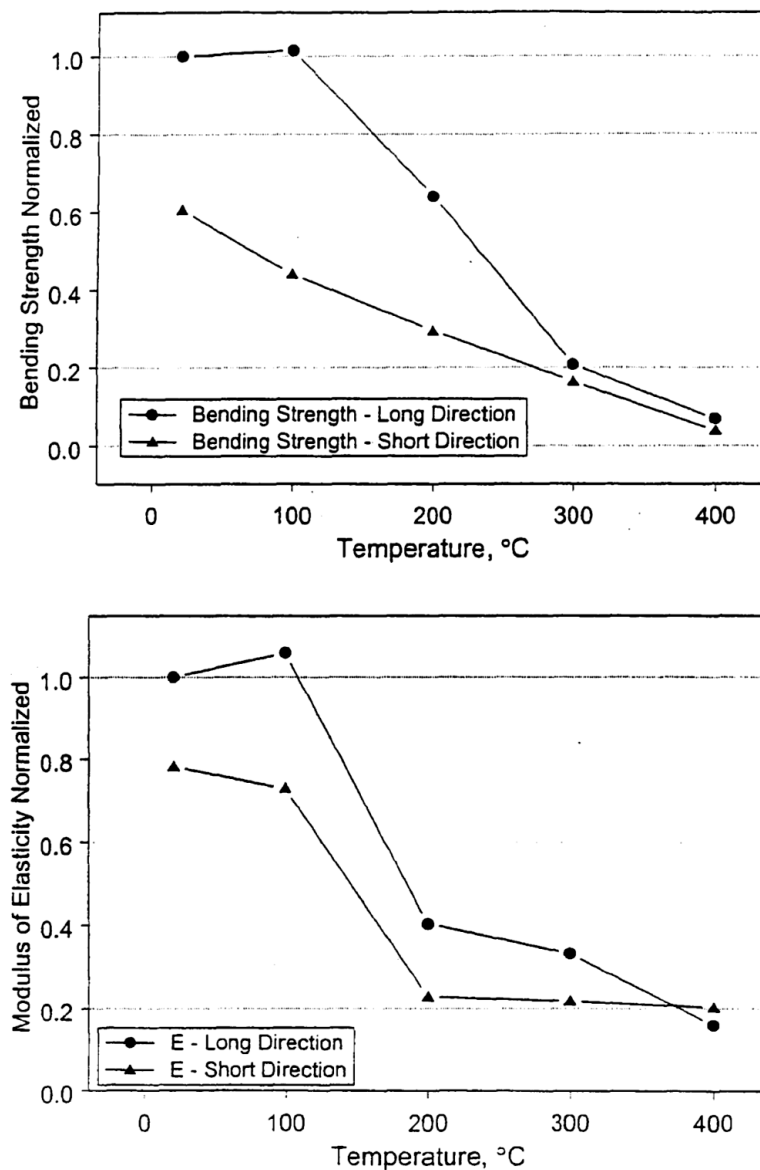


**Figure 2.8.** Modulus of elasticity and bending strength of gypsum measured up to 400°C  
(Cramer et al., 2003)

## **2.7 Previous Studies on the Behaviour of Gypsum Plasterboard in Fire**

Having discussed the properties of gypsum, this section provides a description on some of the literature on the behaviour of gypsum board assemblies at elevated temperatures.

Some research works primarily focus on the experimental methods, while most others are devoted to numerical modelling of the behaviour of gypsum board systems in fire. The majority of these research studies are concerned only with heat transfer in gypsum board systems. An example of such models is the two-dimensional computer model developed by Takeda and Mehaffey (1998, Takeda, 2003) for predicting heat transfer through un-insulated wood-stud walls protected by gypsum boards. Most numerical models incorporate finite element analysis for heat transfer predictions. Nevertheless, apart from the accuracy of the numerical methods used, there are some other important elements that need to be addressed when studying gypsum plaster boards. The main issues regarding the prediction of fire resistance of gypsum board assemblies can be summarised as the following:

- Thermal properties of gypsum to be used in the simulation
- The effect of moisture content on thermal properties
- The effect of cracks, fissures and fall-off of gypsum
- The effect of detailing of the assembly
- The extent to which the standard time-temperature relationships represent real fire scenarios, especially when performance-based design is concerned

A variety of previous studies are reviewed and categorized according to the above aspects.

### **2.7.1 The Effects of Thermal Properties of Gypsum**

Some key research works on thermal properties of gypsum were mentioned in section 2.5. Many researchers have used calibrated values of thermal properties to match experimental results. Nonetheless, it is worth mentioning the numerical

parametric study by Wullschleger and Ghazi Wakili (2008) who investigated the influence of different deviations of material properties on the prediction of thermal behaviour of gypsum plaster board. Their results showed that a variation of  $\pm 50\text{kJ/kg}$  in the enthalpy for dehydration of gypsum (enthalpy is defined as the integral of the product of specific heat, density and volume over a temperature interval) had a small effect on the temperature development in gypsum, with alterations of about  $\pm 10^\circ\text{C}$ . Similar temperature alterations were obtained for variations of  $\pm 10^\circ\text{C}$  in the temperature range of the peak in specific heat. Further sensitivity study using the numerical model developed by the author has been performed as part of the current research work, and is presented in CHAPTER 3.

### **2.7.2 The Effect of Moisture Content**

Being a hydroscopic material, gypsum's thermal behaviour is very much affected by its moisture content. The main influence is the delay in heat transfer through gypsum due to dissociation and evaporation of water or crystallization. A great amount of energy is absorbed for detachment of the chemically bond water, its evaporation, movement of moisture and possible cycles of condensation-evaporation due to fluctuations in pore pressure. To address such effect precisely one must carry out a combined heat and mass transfer, which makes the analysis rather complicated. A simpler approach has been to use modified thermal properties of gypsum (specific heat in particular) in a heat-transfer-only analysis to allow for the effects of moisture. This modification was first considered as an additional specific heat at temperature regions when dehydration and evaporation of water occurs. The additional value, as suggested by Mehaffey et al. (1994) and later completed by Thomas (2002), takes into account the heat of dehydration reaction and evaporation of water.

Wang (1995) developed a one-dimensional finite difference method to determine transient temperature distribution through gypsum panels and concluded that the effect of moisture movement cannot be neglected. He suggested a factor of 1.8 (rather than 1.33) to be applied to the specific heat of gypsum, which correlated well with experimental results from a number of furnace tests of gypsum boards

exposed to the standard fire. This was later confirmed by Ang and Wang (2004), who theoretically studied the effect of moisture movement in thermal behaviour of gypsum boards at elevated temperatures. They used a combined heat and mass transfer analysis as well as a numerical parametric study and concluded that the additional specific heat value can be altered by the heating rate of natural fires and permeability of gypsum boards. The method proposed by Ang and Wang has been adopted for this study, and is explained further in CHAPTER 3.

### **2.7.3 Cracks, Fissures and Fall-Off of Gypsum**

As gypsum shrinks in fire, cracks and fissures start to form within the board, and certain configuration of wide cracks and opened joints leads to fall-off of sections of gypsum board in fire. Both cracks and fall-off of gypsum increases the heat transfer rate through the assembly, but these effects are generally ignored in heat transfer modelling due to their complexity.

There are very limited research studies which have looked into predicting cracks and fall-off of gypsum boards at elevated temperatures. The first study (to the knowledge of the author) to confirm cracking of gypsum in fire by numerical analysis is published by Axenenko and Thrope (1996). They showed, with a short over-simplified strength analysis, that normal stresses within gypsum board (with built-in edges) exceed the tensile strength of the material by two orders of magnitudes soon after gypsum dehydrates. They used mechanical properties of gypsum and glass fibre at ambient temperature as proposed by Ali and Singh (1975). Axenenko and Thrope concluded that this level of normal stresses results in the formation of numerous micro-cracks in the dehydrated part of the board, and hence no load-bearing capacity can be expected of the dehydrated gypsum. However, they did not comment on the effects of these micro-cracks on the overall performance of gypsum boards as insulating sheets.

In an attempt to establish a temperature criterion for the fall-off of gypsum board, Roy-Poirier and Sultan (2007) studied several tests performed by the National Research Council of Canada on gypsum board floor assemblies exposed to standard

fires (Sultan et al., 1998, Sultan et al., 2005). The tests included eighty floor assemblies, 4.8 m long by 3.9 m wide, constructed with solid wood joists, wood I-joists, steel C-joists and wood trusses; protected with one or two layers of fire-rated Type X gypsum board and with and without insulation in the floor cavity. In 72 floor assemblies, resilient channels, spaced either 203 mm, 406 mm, or 610 mm, were used for acoustical purposes and attached perpendicular to either the joists or trusses to support the gypsum board ceiling finish. All floor assemblies were under superimposed loads depending on the components of the assembly.

Roy-Poirier and Sultan (2007) employed a few approaches to determine gypsum board fall-off temperatures in the floor assemblies. They concluded that the most efficient approach was to study the temperature history of the thermocouples at the back face of gypsum board layers. They observed that very close to the time of the fall-off of gypsum, there is a sudden and significant increase of often about 300°C over a period of a minute in the temperature history of the back of that gypsum layer. Roy-Poirier and Sultan suggested that the sudden temperature rise observed actually correspond to the increase in temperature caused by the fall-off of the gypsum board layer; the fallen board piece allowing heat to penetrate rapidly into the next layer of the assembly. Table 2.1 gives a summary of the average fall-off temperatures for different assemblies based on this criterion.

Assembly Characteristics		Fall-Off Temperature ± Standard Deviation (°C)		
Insulation	Screw Spacing (mm)	Single Layer Assembly	Double Layer Assembly	
			Face Layer	Base Layer
<i>No Insulation</i>	406	460 ± 20	620 ± 50	430 ± 90
	610	***	510 ± 50	330 ± 40
<i>Insulation against Gypsum Board Layers</i>	406	680 ± 50	680 ± 40	620 ± 40
	610	***	640 ± 40	480 ± 40
<i>Sprayed-on Insulation</i>	406	670 ± 40	***	***
	610	***	600 ± 40	380 ± 30

**Table 2.1.** Fall-off temperatures of gypsum board Type X (Sultan, 2008)

In another study, Sultan (2010) compared fall-off temperatures in forty-one full-scale wall assemblies with those of the floor assemblies (see Figure 2.9).

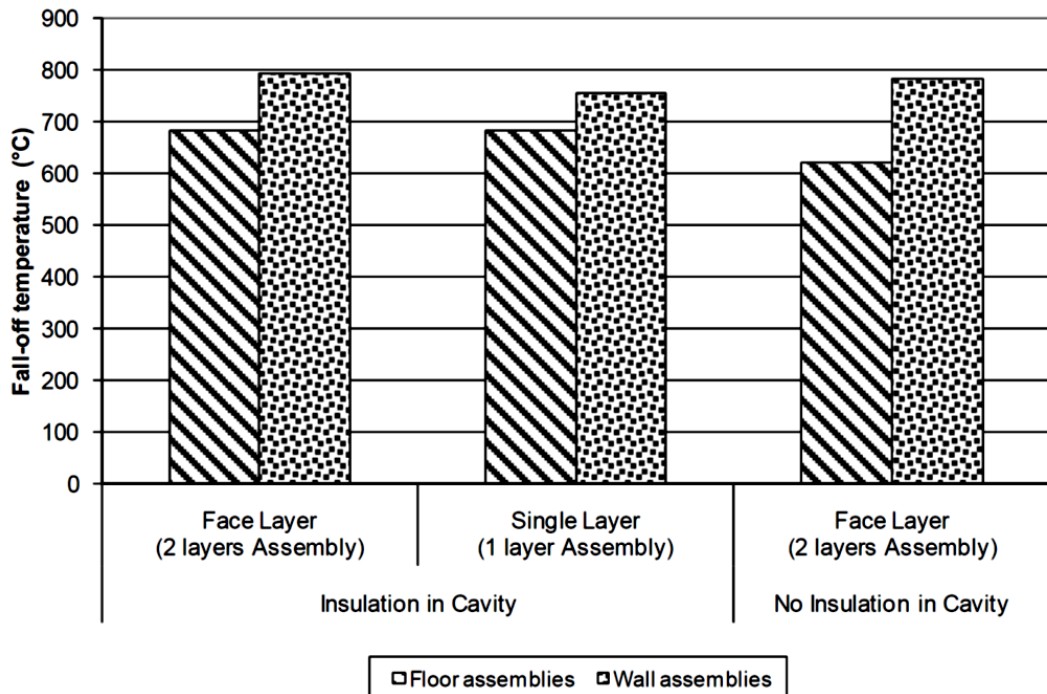


**Figure 2.9.** Comparison of gypsum board fall-off temperature in wall and floor assemblies(Sultan, 2010)

Clearly, there is no fixed temperature at which gypsum falls off. Observations also confirm that non-insulated assemblies experience fall-off at lower temperatures, which suggests that gypsum fall-off depends on the temperature profile through the thickness of the board, and not temperature alone. Moreover, fall-off temperatures for floor assemblies with wider screw spacing are lower. This is explained by the higher stress in the vicinity of the wider spaced screws due to higher loads per screw. As expected, Sultan observed that screw spacing is less important for wall assemblies. Overall, observations suggest that the temperature and stress distribution through gypsum affects its failure and a more in-depth study is required to predict falling-off or cracking of gypsum boards. Temperature alone cannot be an efficient criterion. This study aims to provide more insight into this

gap in knowledge. A numerical method is proposed in CHAPTER 7 for predicting the formation of discrete cracks in gypsum boards.

#### **2.7.4 Detailing of Gypsum Board Assembly**

Although the thermal behaviour of gypsum is generally controlled by its thermal properties, detailing of gypsum board assemblies can affect the fire resistance performance of such systems. A number of experimental studies have been performed on gypsum board assemblies to investigate the effects of a variety of detailing parameters on the fire resistance of gypsum assemblies.

Sultan and Bénichou (2003), for example, conducted 23 full-scale fire tests on floor assemblies exposed to standard fires. They explored the effects of the gypsum board attachment to the studs (e.g. screw spacing from board edges), insulation installation and their types, joist spacing and resilient channel spacing. Their results confirmed that the assemblies with screws located further away from gypsum board edges (38 mm versus 10 mm) provide higher fire resistance. For wood-I joist floor assemblies, wider joist spacing and narrower resilient channel spacing resulted in a higher fire resisting performance, while for steel-I joist assemblies, the effect of joist spacing was not significant. The narrower resilient channel spacing results in more screws fixed on gypsum, and hence there is less stress concentration per screw. Therefore cracking and falling-off of gypsum occurs later during fire, and fire resistance is improved. The slight improvement in the fire resistance of the assemblies with wider wood joist spacing is due to the increased convective cooling within the larger floor cavity created by the joists. This effect is negligible in steel joist assemblies. Sultan and Bénichou also studied the effect of load on the floor assemblies and found that increase in the structural load decreases their fire resistance.

Another study by Kodur et al. (2001) investigated the behaviour of load-bearing wood-stud shear walls in fire and observed that the installation of a plywood shear membrane increases the fire resistance of the assembly. They also concluded that

the assemblies with rock fibre or cellulose fibre insulation provided more fire resistance in comparison with assemblies with glass fibre insulation.

Bwalya (Bwalya, 2005) studied the effect of the orientation of gypsum boards (parallel or perpendicular) against the studs. His study showed that the fire resistance of parallel orientation was slightly less than perpendicular orientation. However, the wood studs in parallel wall assemblies experienced a greater extent of charring than the studs in perpendicular walls.

Fire resistance of a wall or floor assembly is highly dependent on the performance of gypsum boards in the assembly. Different parameters of detailing can affect the failure time of the gypsum boards, and hence influence the overall fire resistance of the system. A numerical model that can predict the failure of the gypsum boards, based on the detailing of the assembly, would significantly reduce the need for conducting numerous full-scale experiments that attempt to shed light on the influence of a vast variety of possible construction detailing of gypsum board assemblies. The research in this thesis aspires to provide such a model that facilitates the prediction of gypsum failure in fire.

### **2.7.5 Standard Fires versus Real Fires**

The standard fire curves suggested by codes, such as BS 476 (BSI, 1987), ISO 834 (ISO, 1992) or ASTM E119 (ASTM, 1988), are means which enable the comparison and categorisation of different construction systems; however, they are not reliable for predicting the real performance of gypsum board assemblies. Therefore, in line with the general tendency towards performance-based design in fire engineering practice, some researchers have addressed the performance of gypsum board systems exposed to real fires.

Jones (2001) conducted full-scale compartment testing and confirmed that temperatures within a compartment can go far beyond those of standard curves, when subjected to typical residential fire scenarios. He employed SAFIR, a finite element programme, to predict the thermal behaviour of different gypsum board assemblies exposed to a range of non-standard fires. The results were verified by

several full and pilot scale fire tests. His study showed that the temperature predictions by finite element analysis for moderate fires were in good agreement with the temperature development within the specimens; however temperature results for severe fires were much different from those of the tested assemblies.

Frangi et al. (2008) also tested a gypsum board assembly with a non-standard fire exposure more severe than the standard fire, and showed that the thermal behaviour of the gypsum board was affected considerably by the fire exposure. In order to achieve conformable results, they calibrated the thermal conductivity of gypsum used in finite element thermal analysis.

In this study, the standard fire curve is adopted for all analyses. However, the method proposed for extracting the thermal conductivity of gypsum, includes calibration with experimental results, which should allow for adopting the material properties to the fire exposure scenario simply by performing small-scale fire test.

## **2.8 Summary and Originality of This Project**

This chapter has provided a review of relevant literature on fire resistance of gypsum board assemblies, focusing on properties of gypsum and its failure in fire condition. There exist a large number of studies on thermal properties of gypsum, each considering some aspects of the problem, which verifies the breadth of the matter and the ongoing demand for more accurate and efficient approaches.

It is clear that there are large discrepancies in results of thermal properties of gypsum from different investigators and there is a need to develop a method to help manufacturers to extract relevant specific thermal properties of their specific gypsum products. These thermal properties can then be implemented in numerical models to generate results to evaluate the effectiveness of different new products before committing great resources to expensive full-scale fire testing, which is the current practice. Evidently, the closer the thermal properties of gypsum (used in numerical analysis) to their actual values, the better the agreement between numerical and experimental results. However, it is almost impossible, or in other words, too complicated to include all the details of the behaviour of a material or

its properties in a model. Therefore, the pragmatic approach to be adopted in this research is to consider some key elements of the properties and behaviours and modify them so that the predicted response of the model conforms to the actual performance of the system. The adopted key thermal properties of gypsum in this research will be the specific heat and thermal conductivity. The thermal conductivity of gypsum will be the main parameter to be calibrated against experimental results, because the values of specific heat of gypsum can be obtained with good accuracy compared to its thermal conductivity.

The other key issue addressed in this project is failure of gypsum in fire. Given its complexity, not much literature is available on this subject, and this project can be considered as a pioneer in proposing a numerical method for predicting failure of gypsum. Investigating gypsum failure requires its mechanical properties to be quantified at high temperatures. Again, such data is almost non-existent in the literature. It should be noted that gypsum fall-off in fire is what significantly affects the fire resistance of gypsum board assemblies. Fall-off of gypsum occurs as a result of openings of cracks. Certain layouts of cracks and opened joints will lead to a section of gypsum board falling off. Therefore, the current project addresses this phenomenon and proposes a numerical method for predicting the formation of discrete cracks in gypsum when exposed to fire.

## **CHAPTER 3. A Method of Extracting Temperature-Dependent Thermal Properties of Gypsum**

### **3.1 Introduction**

Evidently, to predict the fire resistance of gypsum boards, it is essential to quantify the thermal properties of gypsum. Yet gypsum thermal property values reported in the literature spread widely and to date there is no unified model to help guide the development of a consistent thermal property model for gypsum. This chapter presents the development of such a model.

The main thermal properties of gypsum addressed in this research study are specific heat, density and thermal conductivity, which are highly affected by its water content. Even though gypsum undergoes chemical reactions as outlined in the previous chapter, for heat transfer analysis purpose, these chemical reactions may be considered instantaneous upon reaching a certain temperature. Therefore, the thermal properties of gypsum may be considered temperature dependent only. Furthermore, Gypsum contains a large amount of water, so calculating temperatures in gypsum should combine both heat and mass transfer. However, the results of a previous study by Ang and Wang (2004) suggest that for calculating temperature purposes, heat transfer only analysis may be used provided the effect of mass transfer (water movement) is incorporated in the specific heat of gypsum. This approach is adopted here and is further discussed in section 3.4.

Analytical methods are employed to model thermal properties of gypsum at different temperatures, with a special attention to thermal conductivity. Theoretically, it is possible to conduct heat conductivity tests at high temperatures. However, for the high temperatures concerned, these tests will be very difficult.

Most thermal conductivity tests are limited below 250°C. Therefore, this research will develop an alternative method. This method is based on the assumption that a theoretical model of thermal conductivity of gypsum may be derived (section 3.5) with the input of a small number of key parameters. This theoretical model is then used to predict the temperature response of a series of high-temperature tests on small scale gypsum plasterboards with different thicknesses. The input parameters that give consistently accurate predictions of the high temperature tests are accepted as the properties of the gypsum for prediction of its thermal conductivity. For this purpose, a one-dimensional numerical heat transfer model is developed to predict temperature development through gypsum board. This chapter will present the 1-D heat transfer model, its validation, the derivation of the theoretical model for thermal conductivity, and the sensitivity of gypsum temperature predictions to uncertainties in the thermal conductivity model. CHAPTER 4 will present the small scale high temperature test results and validation of the thermal conductivity-temperature model.

### **3.2 One-Dimensional Finite Difference Formulation**

To model the transient heat transfer through a gypsum panel, a computer program has been developed and implemented in the familiar environment of Microsoft Excel using VBA, and is based on one-dimensional Finite Difference formulations. The following describes the basis of the modelling method.

Assuming a homogenous and isotropic material, the general three-dimensional transient heat-conduction equation (based on Fourier's law of conduction) in Cartesian coordinates is (Holman, 2002):

$$\frac{\partial}{\partial x} \left( k \frac{\partial T}{\partial x} \right) + \frac{\partial}{\partial y} \left( k \frac{\partial T}{\partial y} \right) + \frac{\partial}{\partial z} \left( k \frac{\partial T}{\partial z} \right) + \dot{q} = \rho c \frac{\partial T}{\partial t} \quad (3.1)$$

where

$T(x, y, z, t)$  is temperature (°C);

$k(T)$  is thermal conductivity (W/m.°C);

$\dot{q}$  is heat generated per unit volume (W/m<sup>3</sup>);

$\rho$  is material density ( $\text{kg}/\text{m}^3$ );

$c$  is specific heat of material ( $\text{J}/\text{kg}\cdot^\circ\text{C}$ );

$t$  is time (sec);

$x, y, z$  are Cartesian coordinates.

The left hand side of Eq. (3.1) corresponds to net heat conduction and heat generation, while the right hand side represents the accumulated internal energy. Calculation of heat flow is based on the solution of this differential equation. Due to complexity of many geometric shapes and boundary conditions of practical interest, analytical solutions to Eq. (3.1) are not always possible. The Finite Difference Method (FDM) is a relatively simple technique which can provide approximate numerical solutions to many practical cases. FDM replaces the differential expressions in Eq. (3.1) with approximately equivalent partial difference quotients. Two approaches can be taken to transform the partial differential equation into a finite difference equation (Croft and Lilley, 1977):

- i) Mathematical replacement approach
- ii) Physical heat balance approach

The two techniques often result in the same finite difference equations. However, the heat balance technique might be better suited to irregular boundaries with convective heat loss (Croft and Lilley, 1977) and therefore is adopted in this study. In this approach one includes a control volume around each grid point and locally applies direct approximations to the energy balance principles to this volume. In other words, the method considers the heat flow into and out of the cell for a particular time-step and determines the temperature change of the cell based on its mass and specific heat.

The resultant finite difference equations can be either explicit or implicit. In the implicit approach a set of simultaneous equations has to be solved at each step in time. Although the solution process is relatively complex, it allows for the use of larger time intervals. In the explicit approach, on the other hand, the temperature of a volume cell at a time step is computed directly based on the temperatures of

the adjacent cells in the last time step, leading to a very simple scheme of computation. However, the time interval required can sometimes be inconveniently small.

Given the simplicity and effectiveness the explicit approach in finite difference method provides, it was found suitable and adopted for the purpose of this study. Although the time intervals required in this method are small, it does not cause any further complications to the computations, since small time steps are already necessary in fire resistance analysis due to rapid changes of temperature in fire conditions.

Considering a wide panel (Figure 3.1) whose thickness is small compared to its other two dimensions, away from the edges the problem will reduce to a one dimensional heat transfer analysis, i.e. heat flows in the direction perpendicular to the panel. Hence, the governing Eq. (3.1) with no heat generation reduces to:

$$\frac{\partial}{\partial x} \left( k(T) \frac{\partial T(x, t)}{\partial x} \right) = \rho c \frac{\partial T(x, t)}{\partial t} \quad (3.2)$$

where  $t > 0$  and  $0 \leq x \leq L$ ,  $L$  being the thickness of the panel.

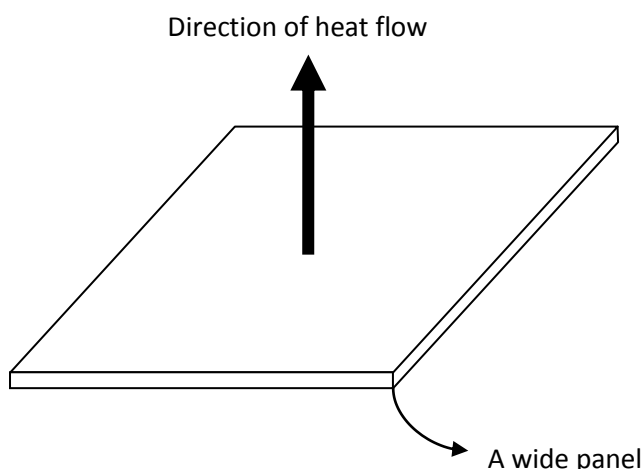


**Figure 3.1.** Direction of heat flow in a wide panel

The initial condition is:

$$T_0 = T(x) \quad \text{at} \quad t = 0, \quad 0 \leq x \leq L$$

where  $T(x)$  is the known distribution of temperature through the thickness.

The boundary conditions used in this study are of two types:

- i) Prescribed temperatures are given at the surface of the solid ( $x = 0$  or  $x = L$ ):

$$T = T_{bc}(t) \quad t > 0$$

where  $T_{bc}(t)$  is the known temperature of the boundary surface.

- ii) The surfaces of the solid exchange heat with a gas by convection and radiation:

$$k(T) \frac{\partial T}{\partial x} = h(T)(T_\infty - T_{bc}) + \varphi E \sigma [(T_\infty + 273)^4 - (T_{bc} + 273)^4] \quad (3.3)$$

where

$h(T)$  is the convection heat transfer coefficient ( $\text{W}/\text{m}^2 \cdot ^\circ\text{C}$ );

$T_\infty$  is the gas temperature ( $^\circ\text{C}$ );

$T_{bc}$  is the boundary temperature ( $^\circ\text{C}$ );

$\varphi$  is a geometric “view factor”;

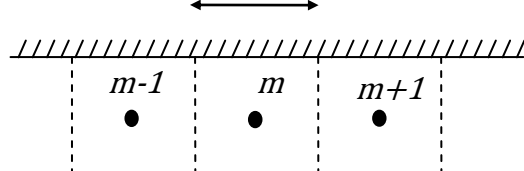
$E$  is the effective emissivity; and

$\sigma$  is the Stefan-Boltzmann constant ( $5.67 \times 10^{-8} \text{ W}/\text{m}^2 \cdot \text{K}^4$ ).

The left hand side of Eq. (3.3) is the heat conducted into the solid, while the right hand represents the heat convected (first term) and radiated (second term) from the ambient environment.

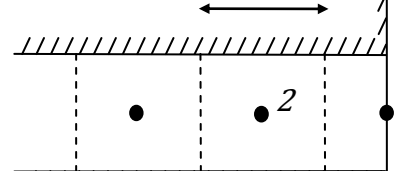
Now the partial differential equations need to be transformed into explicit finite difference equations. There are two typical nodes for which finite difference equations need to be derived: an internal node within the material and a boundary node.

$$\Delta x$$



*Direction of heat flow*

$$\Delta x$$



$$T_\infty$$

*Direction of heat flow*

**Figure 3.2.** Finite Difference discretization for node **m** within the material

**Figure 3.3.** Finite Difference discretization for a boundary node

i) For a typical node **m** within the material (Figure 3.2):

According to the energy balance principle:

*Rate of change in*

*internal energy of cell m = Heat conducted into cell m – Heat conducted out of cell m*

*cell m*

Therefore:

$$\frac{(\rho \Delta x)c(T'_m - T_m)}{\Delta t} = \frac{k_{m,m-1}(T_{m-1} - T_m)}{\Delta x} - \frac{k_{m,m+1}(T_m - T_{m+1})}{\Delta x} \quad (3.4)$$

where  $T'_m$  is the temperature of **m** in the subsequent time step and  $k_{i,j}$  is the thermal conductivity at the average temperature of cells *i* and *j*:

$$k_{i,j} = k \left( \frac{T_i + T_j}{2} \right)$$

Introducing Fourier number ( $F_0$ ) and rearranging Eq. (3.4) will yield:

$$T'_m = F_0 \left[ \frac{2(k_{m-1,m}T_{m-1} + k_{m+1,m}T_{m+1})}{k_{m-1,m} + k_{m+1,m}} + T_m \left( \frac{1}{F_0} - 2 \right) \right] \quad (3.5)$$

where  $F_0$  is defined as:

$$F_0 = \frac{(k_{m-1,m} + k_{m+1,m})\Delta t}{2\rho c(\Delta x)^2}$$

It should be noted that in Eq. (3.4), the heat transferred *at a given instant in time* is equated with the rate of energy accumulated in the cell *over a period of time*. Because the internal energy change is not a linear function of time, the time step of the analysis should be chosen small enough so as to achieve the desirable accuracy in the calculation.

In Eq. (3.5), the coefficients of  $T_{m-1}$  and  $T_{m+1}$  are inherently positive. But the coefficient of  $T_m$ , which is  $\left(\frac{1}{F_0} - 2\right)$ , can become negative if  $\Delta t$  is chosen large enough. This would be physically unreasonable, because it would mean that the higher the temperature of cell  $m$  is now, the lower it will be after the time interval  $\Delta t$  (Dusinberre, 1962). Therefore, numerical stability criterion for the finite difference equation requires:

$$\frac{1}{F_0} - 2 \geq 0$$

$$\rightarrow F_0 \leq 0.5$$

and  $\Delta t$  should be chosen small enough to satisfy the following numerical stability criterion:

$$\Delta t \leq \frac{\rho c(\Delta x)^2}{(k_{m-1,m} + k_{m+1,m})}$$

**ii)** For a boundary node (Figure 3.3) subjected to the boundary condition defined by Eq. (3.3):

If node 1 is the boundary node and node 2 is the adjacent node to the boundary, the heat balance equation will be:

$$\frac{\rho c \Delta x (T'_1 - T_1)}{2\Delta t} = \frac{k_1(T_2 - T_1)}{\Delta x} - h(T_1 - T_\infty) - \varphi E \sigma [(T_1 + 273)^4 - (T_\infty + 273)^4] \quad (3.6)$$

If  $F'_0$  is:

$$F'_0 = \frac{k_1 \Delta t}{\rho c (\Delta x)^2}$$

Eq. (3.6) can be rearranged as:

$$T'_1 = 2F'_0 \left[ T_2 + \frac{h \Delta x}{k_1} T_\infty + \left( \frac{1}{2F'_0} - 1 - \frac{h \Delta x}{k_1} \right) T_1 \right] + \varphi E \sigma [(T_\infty + 273)^4 - (T_1 + 273)^4] \frac{2\Delta t}{\rho c \Delta x} \quad (3.7)$$

Numerical stability criterion for Eq. (3.7) results from the notion that the coefficient of  $T_1$  should be positive:

$$2F'_0 \left( \frac{1}{2F'_0} - 1 - \frac{h \Delta x}{k_1} \right) - \varphi E \sigma \frac{(T_1 + 273)^4}{T_1} \frac{2\Delta t}{\rho c \Delta x} \geq 0$$

Therefore numerical stability limits the time step to:

$$\Delta t \leq \frac{0.5 \rho c (\Delta x)^2}{k_1} \left[ 1 + \frac{h \Delta x}{k_1} + \frac{\varphi E \sigma \Delta x}{k_1} \cdot \frac{(T_1 + 273)^4}{T_1} \right]^{-1}$$

### 3.2.1 Initial and Boundary Conditions

The initial temperature of gypsum board is assumed to be uniform throughout the board and equal to the temperature of the room before the fire test is started.

The surface of gypsum plasterboards is laminated by paper with emissivity of 0.8-0.9 as reported in reference (Ozisik, 1985). Thus, the unexposed surface emissivity

of the board is taken as 0.7 and the view factor equals unity. The convective heat transfer coefficient on the unexposed side is taken as  $4 \text{ W/m}^2 \cdot ^\circ\text{C}$  as advised by Wang (2002) and close to the value used by other researchers (Mehaffey et al., 1994).

On the exposed side of the board, however, the heat transfer coefficients are furnace dependent and contain a high degree of uncertainty. Therefore, the numerical heat transfer procedure outlined above will use the recorded temperatures on the exposed surface of the gypsum samples as input data, so as to eliminate the uncertainty related to quantification of the fire boundary condition.

### **3.3 Validation of the Heat Conduction Model**

Three different comparisons have been undertaken to validate the accuracy of the Finite Difference modelling:

- i) Verification for conductive heat transfer with constant thermal conductivity through a panel against an exact analytical solution;
- ii) Verification for conduction in a panel with convective boundary condition against an exact analytical solution;
- iii) Verification for conductive heat transfer with temperature-dependent material properties against independent numerical simulations using the general finite element package ABAQUS.

#### **3.3.1 Conduction with Constant Material Properties**

Consider one-dimensional heat transfer through a panel with thickness  $l$  and constant thermal conductivity  $k$ . The initial temperature of the panel is uniform and denoted by  $T_0$  (Figure 3.4). If both surfaces of the panel are suddenly changed to zero temperature ( $0^\circ\text{C}$ ), temperature development through the thickness of the panel at time  $t$  can be calculated by (Carslaw and Jaeger, 1959):

$$T = \frac{4T_0}{\pi} \sum_{n=0}^{\infty} \frac{1}{(2n+1)} e^{-\alpha(2n+1)^2 \pi^2 t/l^2} \sin \frac{(2n+1)\pi x}{l} \quad (3.8)$$

Where  $\alpha = \frac{k}{\rho c}$ ,  $\rho$  is the density of the material and  $c$  is its specific heat.

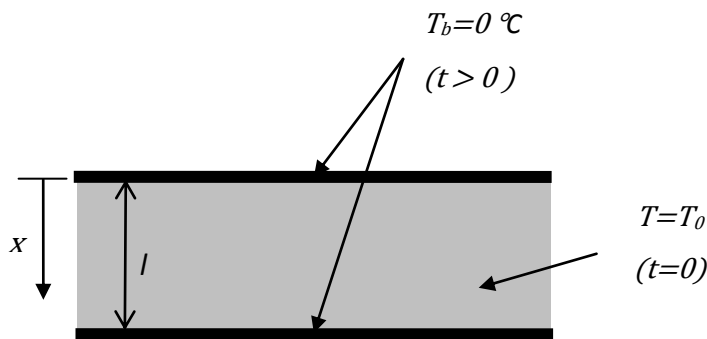


**Figure 3.4.** A panel with thickness  $l$ , both boundaries kept at zero temperature

An example problem of the above case has been analysed with the following properties:

$$l = 25 \text{ mm}, \quad k = 0.25 \text{ W/m.}^\circ\text{C}, \quad \rho = 680 \text{ kg/m}^3$$

$$c = 950 \text{ J/kg.}^\circ\text{C}, \quad T_0 = 20^\circ\text{C}$$

The temperature development of this example is obtained using both the analytical method, i.e. Eq. (3.8) and the Finite Difference (FD) method. The results are compared in Figures 3.5 and 3.6.

The thickness of the panel is divided into 6 elements, temperatures are calculated for the nodes representing each element (5 internal nodes and 2 boundary nodes) and the time step for FD analysis is 5 seconds. For calculation purposes, the infinite series in Eq. (3.8) has been limited to only 12 members. It is evident from the comparison demonstrated in Figures 3.5 and 3.6 that Finite Difference method can provide very accurate results for heat transfer analysis in solids with constant thermal properties despite its simple approach.

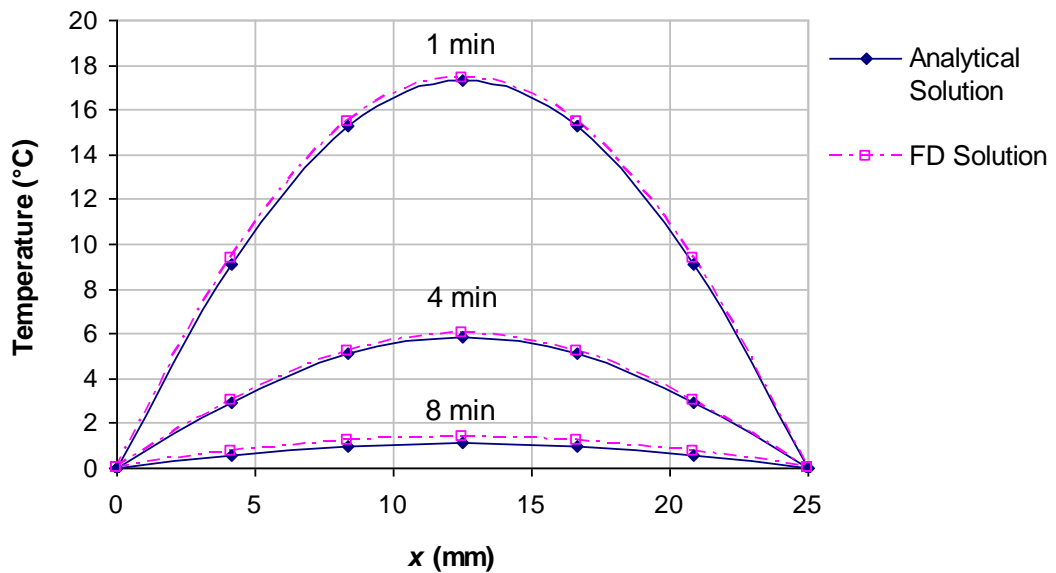


**Figure 3.5.** Comparison of temperature distributions across the thickness of a 25mm example panel obtained by analytical method and Finite Difference method

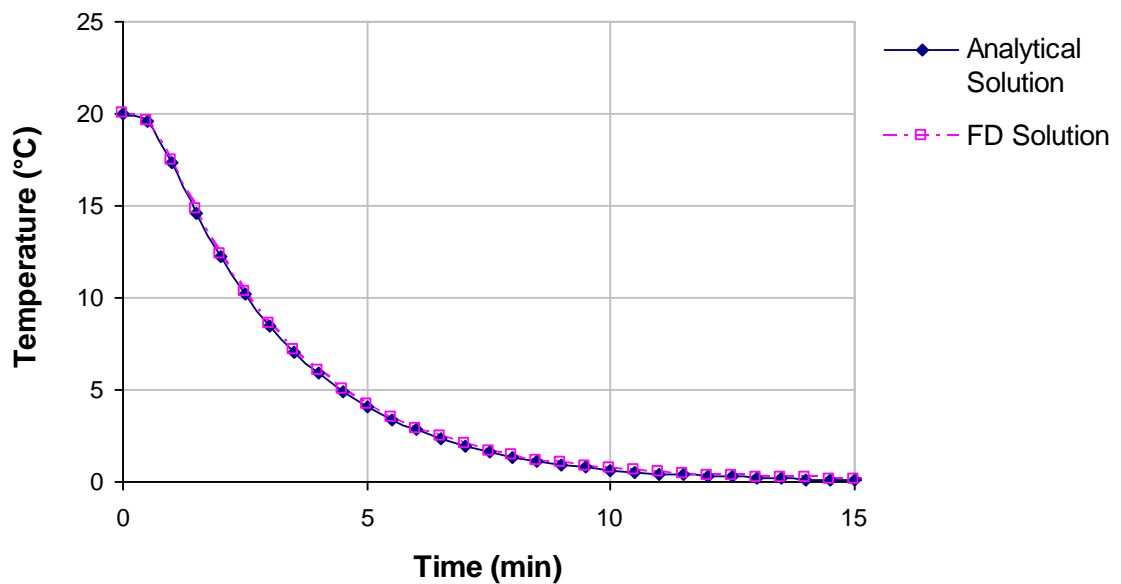


**Figure 3.6.** Comparison of temperature development at the midpoint of a 25mm example panel obtained by analytical method and Finite Difference method

### 3.3.2 Heat Conduction with Constant Material Properties and Convective Boundary Condition

Verification is also made for a problem where convective boundary conditions exist. Consider the one-dimensional heat transfer through a panel with thickness of  $2L$  and constant thermal conductivity of  $k$  shown in Figure 3.7. The initial temperature of the panel is  $T_0$ . The panel is suddenly taken to an ambient temperature of  $T_\infty$  and the convective heat transfer coefficient at the surfaces of the panel is  $h$ . If  $\theta = T - T_\infty$ , the temperature development across the thickness of the panel at time  $t$  can be calculated by (Harmathy, 1988):

$$\frac{\theta}{\theta_0} = 2 \sum_{n=1}^{\infty} \frac{\sin \lambda_n}{\lambda_n + \sin \lambda_n \cos \lambda_n} \cdot e^{-\lambda_n^2 \alpha t / L^2} \cos \frac{\lambda_n x}{L} \quad (3.9)$$

where  $\alpha = \frac{k}{\rho c}$  and  $\lambda_n$  are roots of the equation:  $\lambda_n \tan \lambda_n = \frac{hL}{k}$

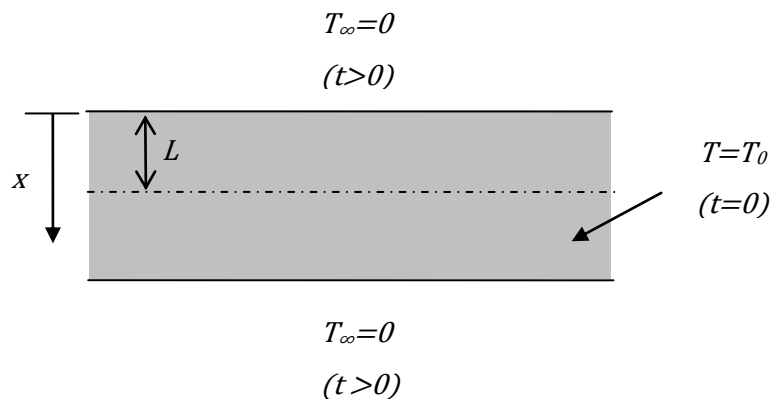


**Figure 3.7.** A panel with thickness  $2L$ , suddenly immersed into an ambient zero temperature.

The example problem analysed has the following properties:

$$L = 12.5 \text{ mm} , \quad k = 0.25 \text{ W/m}\cdot\text{°C}, \quad h = 10 \text{ W/m}^2\cdot\text{°C}, \quad c = 950 \text{ J/kg}\cdot\text{°C}$$

$$\rho = 700 \text{ kg/m}^3, \quad T_0 = 20 \text{ °C}, \quad T_\infty = 0 \text{ °C}$$

The first 20 roots of  $\lambda_n$  are used in Eq. (3.9). The time step in FD analysis is 5 seconds and the thickness of the panel is represented by 7 nodes. The results are compared in Figures 3.8 and 3.9 . Again results from the Finite Difference method are in perfect agreement with the analytical results.

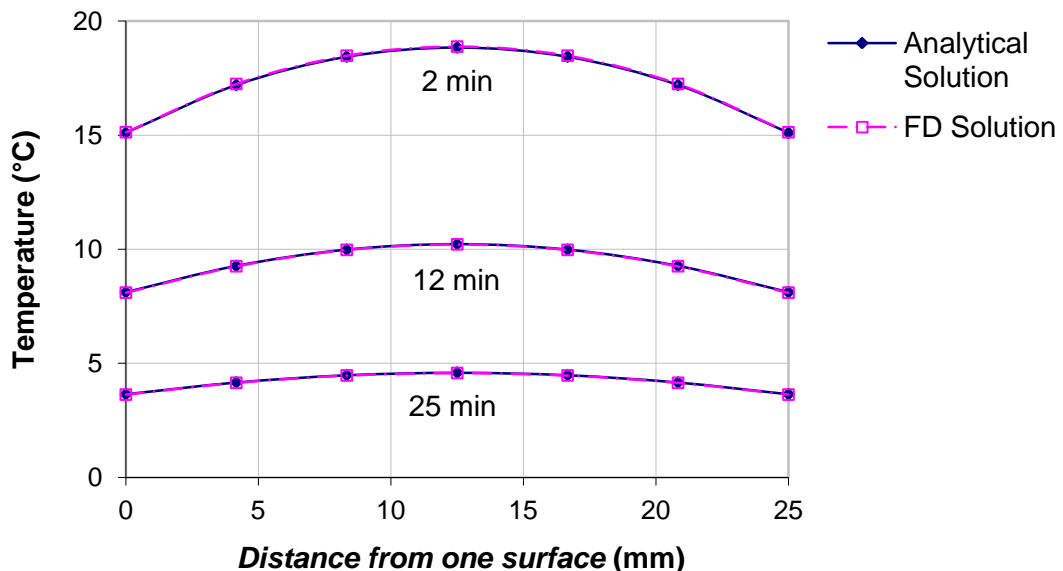


**Figure 3.8.** Comparison between temperature distributions across the thickness of a 25mm example panel with convective boundary condition obtained by analytical method and Finite Difference method

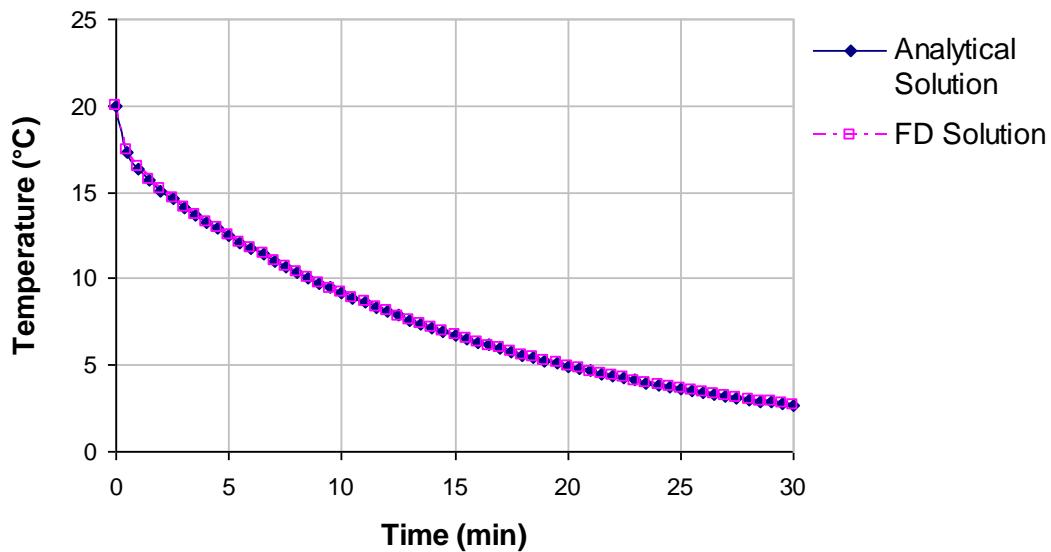


**Figure 3.9.** Comparison between temperature developments at the surface of a 25mm example panel with convective boundary condition obtained by analytical method and Finite Difference method

### 3.3.3 Conduction with Temperature-Dependent Thermal Properties

Thermal properties of building materials (e.g. gypsum) are often temperature-dependant. Since exact analytical solutions for heat transfer through these materials are not available, another numerical method, Finite Element analysis, is employed for validation of the FD analysis.

The example panel considered is a 25mm Fireline gypsum board initially at 25°C. The temperature-dependent thermal properties of the board are modelled as explained in sections 3.4 and 3.5, with density of 770 kg/m<sup>3</sup> at ambient temperature. One surface of the panel is exposed to high temperatures and the other side faces the ambient temperature of 25°C. Figure 3.10 illustrates the temperature curve applied on the exposed surface of the panel and compares the temperature predictions of the unexposed side by the proposed FD analysis and by Finite Element analysis using the commercial software package, ABAQUS (2010). The validity of FD formulations is confirmed yet again.

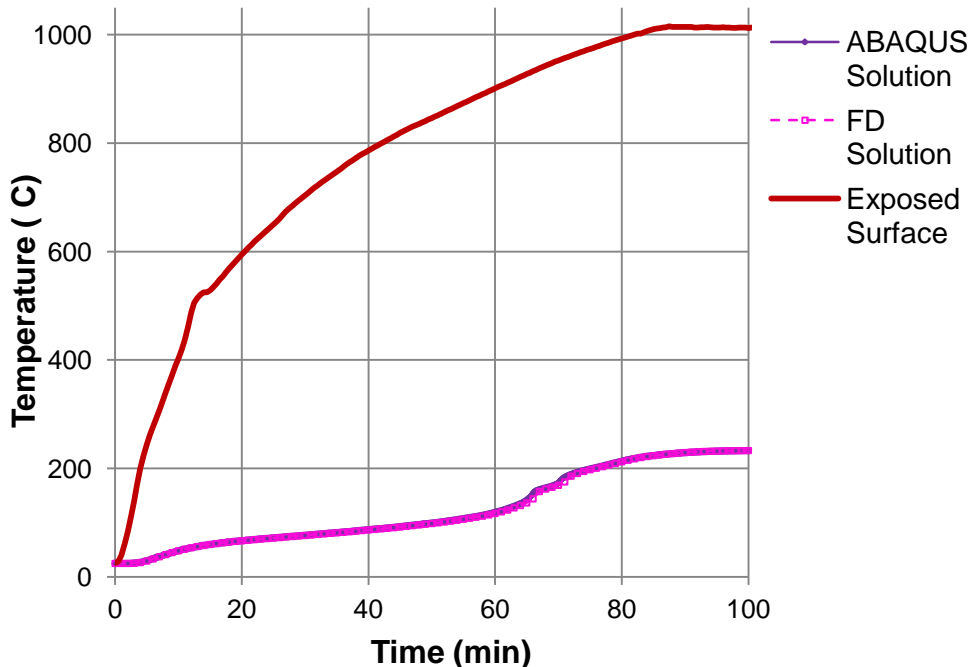


**Figure 3.10.** Temperature development on the unexposed surface of a 25mm Fireline gypsum board by ABAQUS (Finite Element analysis) and Finite Difference method

The validation of Finite Difference formulations proves that although the explicit Finite Difference method is a relatively simple algorithm, yet it can provide very accurate results as compared to analytical methods or other complicated numerical ones.

### 3.4 Specific Heat and Density of Gypsum

The specific heat of gypsum at room temperature is assumed to be 950 J/kg. $^{\circ}$ C as reported by Mehaffey et al. (1994), which is the base value for the specific heat-temperature correlation of gypsum; however this correlation experiences two peaks corresponding to the two dehydration reactions of gypsum as shown in Figure 3.11. To allow for a heat transfer only analysis to be sufficiently accurate, these peaks should represent not only the energy consumed to dissociate and evaporate water, but also include the effects of water movement and re-condensation in cooler regions of gypsum (Ang and Wang, 2004). Gypsum also contains free water of about 3% as equilibrium moisture content at ambient

conditions (Gerlich, 1995), depending on the ambient temperature and relative humidity. Evaporation of this free water can be accounted for in the first peak.

The additional specific heat at each dehydration reaction can be expressed by (Ang and Wang, 2004):

$$\Delta c = \frac{2.26 \times 10^6}{\Delta T} (e_d f_1 + e_{free}) f_2 \quad (\text{J/kg.}^\circ\text{C}) \quad (3.10)$$

where

$\Delta c$  is the average additional specific heat;

$e_d$  is the dehydration water content (percentage by total weight);

$e_{free}$  is the free water content (percentage by total weight);

$\Delta T$  is the temperature interval; and

$f_1, f_2$  are correction factors to account for heat of reactions and effects of water movement

Knowing the heat of reactions (CHAPTER 2, section 2.4),  $f_1$  is easily obtained as 1.28 and 1.42 for the first and second dehydration peaks, respectively. According to Ang and Wang (2004),  $f_2 = 1.4$  for the standard fire condition.

The temperature intervals for the first and second dehydration reactions are assumed to be 95 -155°C and 180 -220°C, respectively and a triangular distribution of the additional specific heat is used over the temperature intervals. The results of the sensitivity study (section 3.6.2) indicate that temperature predictions through gypsum are insensitive to variations in these values.

An additional peak in specific heat-temperature correlation has been reported by some researchers around 700°C, corresponding to the decomposition of calcium carbonate and magnesium carbonate content of gypsum boards (Ghazi Wakili and Hugi, 2009). The percentage of these ingredients is negligible in gypsum boards produced by British Gypsum and its effects on specific heat are ignored here.

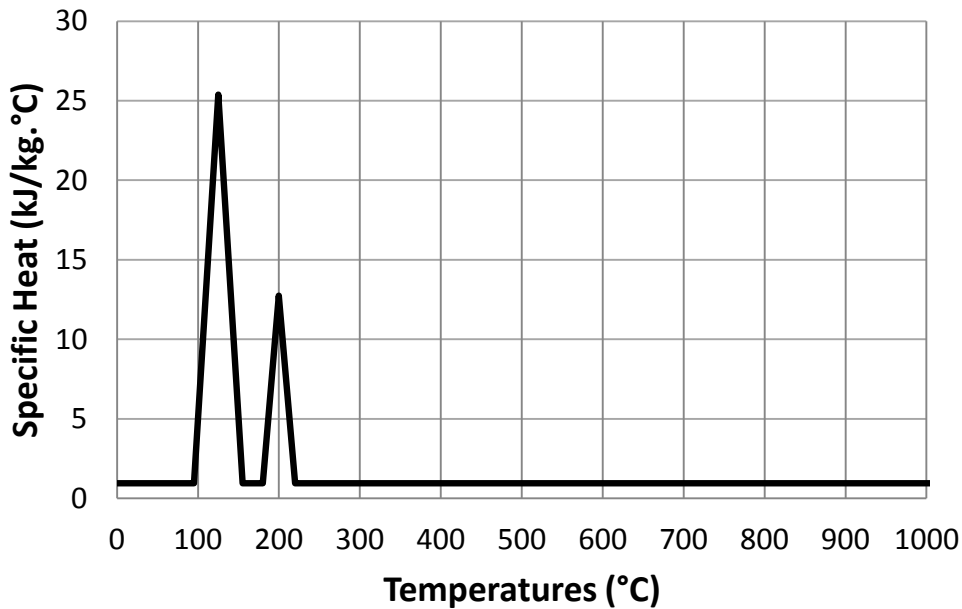


**Figure 3.11.** Specific heat of gypsum as used in the analysis

The density of gypsum is also affected by the evaporation of water and undergoes a two-step reduction with temperature increase. Figure 3.12 shows the density used in the modelling as a percentage of the original density of gypsum at ambient temperature. The first reduction of density corresponds to the loss of free water and 75% of the chemically bound water, which amounts to about 19% of the total mass. The second reduction in density corresponds to the second dehydration reaction. The total mass loss of gypsum by 220°C is taken as 24% of the original value.

Gypsum also undergoes volume change when exposed to rising temperatures, which is insignificant below 900°C (see section 5.2); therefore the effect of this volume change on density is not included during heat transfer analysis and the relative change in density is taken equal to that in mass.

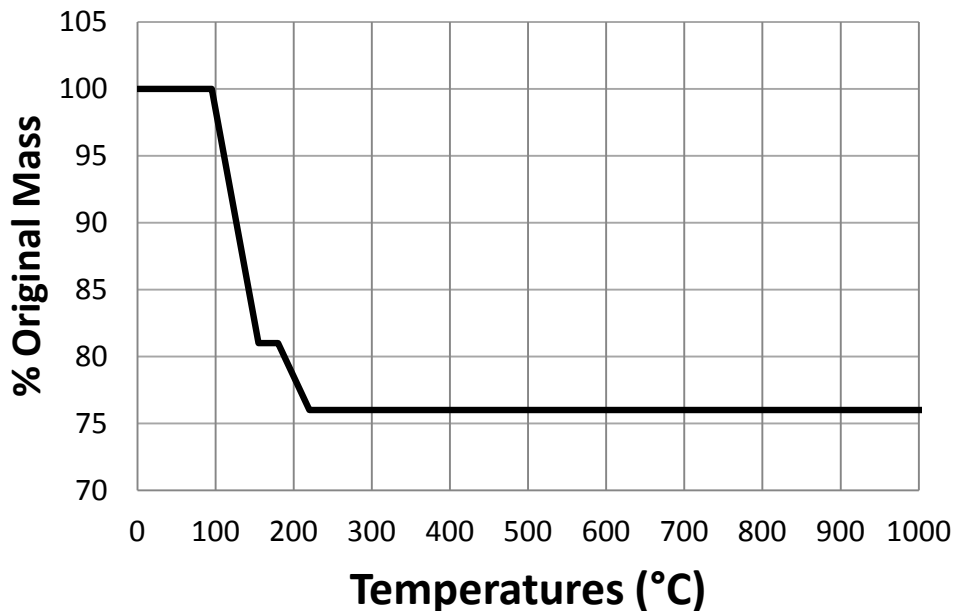


**Figure 3.12.** Density of gypsum as used in the analysis (% of the original density)

### 3.5 Thermal Conductivity of Gypsum

Among the three thermal properties required for heat transfer analysis, namely density, specific heat and thermal conductivity, the value of thermal conductivity reported in literature shows the largest scatter from different sources as demonstrated in Figure 3.13. These values are based on ad-hoc tests by the different authors. Some are true measured values of conductivity and some represent an effective thermal conductivity adopted to account for other complex behaviour such as mass transfer or ablation and cracks in gypsum. Nevertheless, there has been no fundamental theory to help develop a more consistent approach to obtaining thermal conductivity values. Given the effects of porosity, non-homogeneity, moisture and non-linear temperature distribution in gypsum under heating, direct measurement of thermal conductivity of gypsum is time-consuming and highly impractical at high temperatures. Direct measurement also would require a large number of tests at high temperatures and it would be difficult to extrapolate the test results. A different approach is necessary; one which is based on a fundamental understanding of gypsum and does not require the

determination of many variables. In addition, these variables should have clear physical meaning.

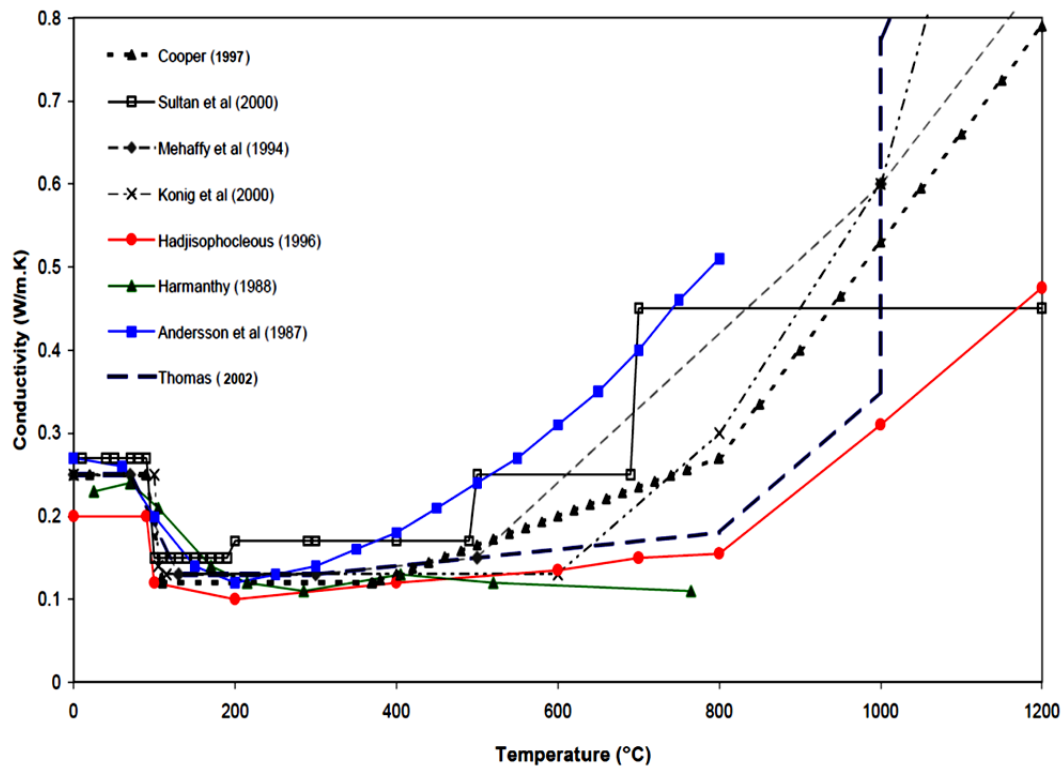


**Figure 3.13.** Thermal conductivity of gypsum, as reported by various researchers (Jones, 2001)

Since gypsum is a porous material, heat transfer through gypsum is a combination of all three modes. Therefore the effective thermal conductivity of gypsum should include the effects of conduction through the solid, as well as convection and radiation through the pores. This effective thermal conductivity can be affected by many factors such as temperature, density, moisture content and porosity of the material. Moreover, when used in gypsum boards, the composition of the gypsum core varies from one manufacturer to another and it usually contains some additives in small quantities. Such sensitivity contributes to the diverse data reported in literature.

Despite the diversity of reported data, there are some common trends in the relationship of thermal conductivity with temperature. Based on experimental measurements by many researchers (Thomas, 2002, Wang, 1995), thermal conductivity of gypsum before dehydration does not seem to change considerably; however, when the dehydration process starts, thermal conductivity of gypsum drops significantly. This can be explained by higher porosity due to the evaporation of the combined water.

After the two dehydration reactions are concluded, there is even less consistency in the value of measured (or used) thermal conductivity by different research studies, yet almost all concur that the thermal conductivity of dried gypsum increases with temperature. This increase in thermal conductivity of dried gypsum is primarily a result of radiation within voids in gypsum.

Assuming the dehydrated gypsum is made of solid substrate and uniformly distributed spherical pores, the effective thermal conductivity of gypsum when all the water content is evaporated, may be calculated using the following equation (Yuan, 2009):

$$k^* = k_s \frac{k_g \varepsilon^{\frac{2}{3}} + \left(1 - \varepsilon^{\frac{2}{3}}\right) k_s}{k_g \left(\varepsilon^{\frac{2}{3}} - \varepsilon\right) + \left(1 - \varepsilon^{\frac{2}{3}} + \varepsilon\right) k_s} \quad (3.11)$$

where

$k^*$  is the effective thermal conductivity of gypsum;

$k_g$  is the effective thermal conductivity of the gas within the pores, accounting for all three modes of heat transfer in the pores;

$k_s$  is the thermal conductivity of the solid;

$\varepsilon$  is the porosity of the material (the ratio of the volume of the voids to the overall volume)

Since the size of the pores in gypsum is very small (not larger than 5mm), natural convection of gas in the pores can be neglected (Burns and Tien, 1979, Yu et al., 2006). Therefore, based on the assumption of spherical pores, the effective thermal conductivity of the gas is (Yuan, 2009):

$$k_g = 4.815 \times 10^{-4} T^{0.717} + \frac{2}{3} \times 4d_e \sigma T^3 \quad (3.12)$$

where  $T$  is the absolute temperature and  $d_e$  is the effective diameter of the pores.

Hence, the effective thermal conductivity-temperature relationship of gypsum can be expressed in three parts, as demonstrated in Figure 3.14 for the two types of gypsum boards used in this study:

- i) Constant thermal conductivity up to 95°C before water evaporation, equal to that at ambient temperature reported by the manufacturer (British-Gypsum, 2009)
- ii) Linear reduction of thermal conductivity till 220°C due to evaporation of water;
- iii) Non-linear increase in thermal conductivity based on Eqs. (3.11) and (3.12).

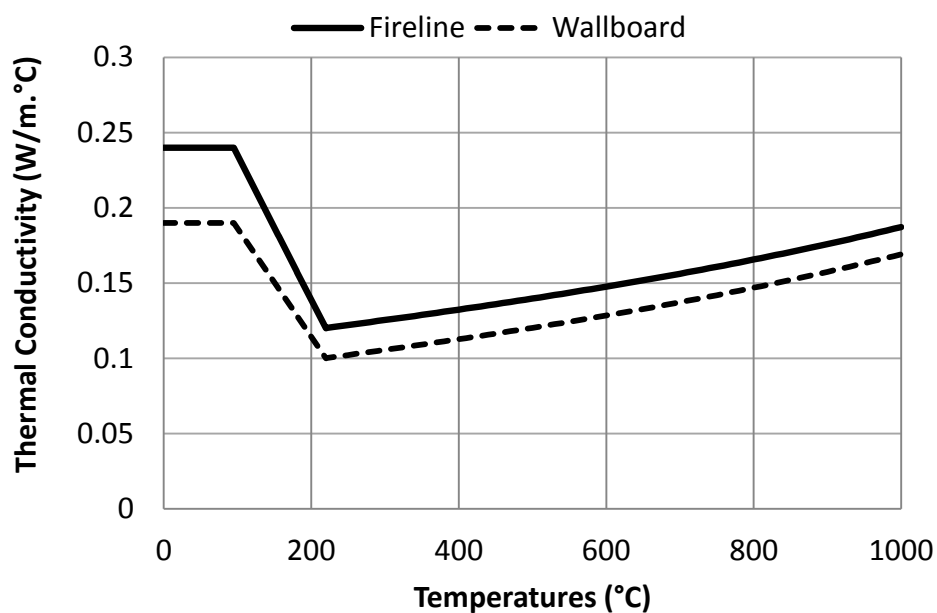


**Figure 3.14.** Effective thermal conductivity of gypsum as used in this study

### **3.6 Sensitivity Study**

The accuracy of the modelling results is the direct outcome of the quality of the material properties, boundary conditions and the heat transfer model applied. Having demonstrated that the heat transfer model is sufficiently accurate (section 3.3), a numerical parameter study is performed to examine the influence of different material properties. All cases discussed here are for a 12.5mm Fireline gypsum board. The exposed boundary conditions are the exposed surface temperature-time curves directly obtained from test measurements. Parameters not mentioned in the discussion are kept equal to those given in previous sections.

#### **3.6.1 Mesh Size in the Heat Transfer Model**

With the heat transfer model and the time-step size being of good accuracy (sections 3.2 and 3.3), the optimal mesh size should be set to produce results with the most possible precision and the least computation cost. Figure 3.15 compares the results of heat transfer analysis for different mesh sizes (or number of layers in the direction of heat flow). Six appears to be an optimal number of layers, corresponding to the mesh size of about 2mm, which will be used in further analysis.

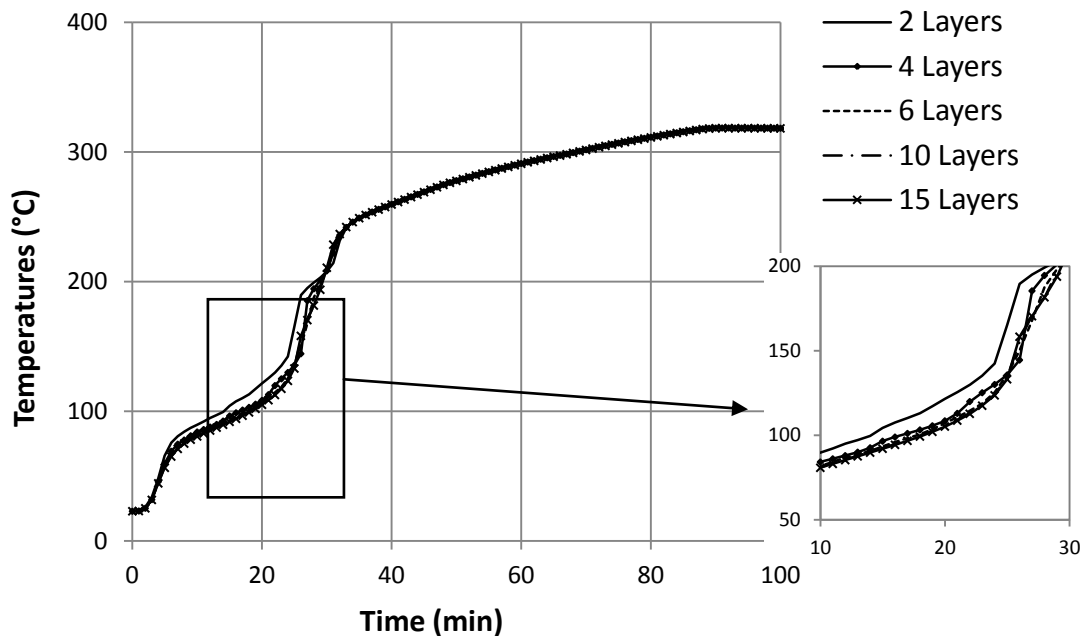


**Figure 3.15.** Calculated temperatures on the unexposed surface of a 12.5mm Fireline gypsum board using different number of layers in the heat transfer analysis

### 3.6.2 Specific Heat-Temperature Correlation

There is no absolute certainty about the starting temperature and the length of the temperature interval during which the gypsum dehydration reactions take place. Therefore a study has been performed on the influences of different widths of the two peaks in the specific heat curve (Figure 3.11); and the mean temperature at which the peaks take place.

The values in Figure 3.11 were obtained by using a temperature interval of 60°C (from 95°C to 155°C) and 40°C (from 180°C to 220°C) for the first and second reactions, respectively. In this sensitivity study, the following five alternative cases have been studied:

Case 1: First peak width=40°C , Second peak width=20°C

Case 2: First peak width=50°C , Second peak width=30°C

Case 3: First peak width=60°C , Second peak width=40°C

Case 4: First peak width=70°C , Second peak width=50°C

Case 5: First peak width=80°C , Second peak width=60°C

The total energy of the peaks were kept constant, hence the peak heights were changed accordingly. The revised temperature intervals were also used to obtain the thermal conductivity and density-temperature curves as shown in Figure 3.16.

Using the finite difference analysis explained earlier, the temperature histories for the five different cases of temperature intervals are compared in Figure 3.17. Clearly, the changes in the temperature intervals of the two dehydration reactions do not noticeably affect the temperatures of gypsum in fire.

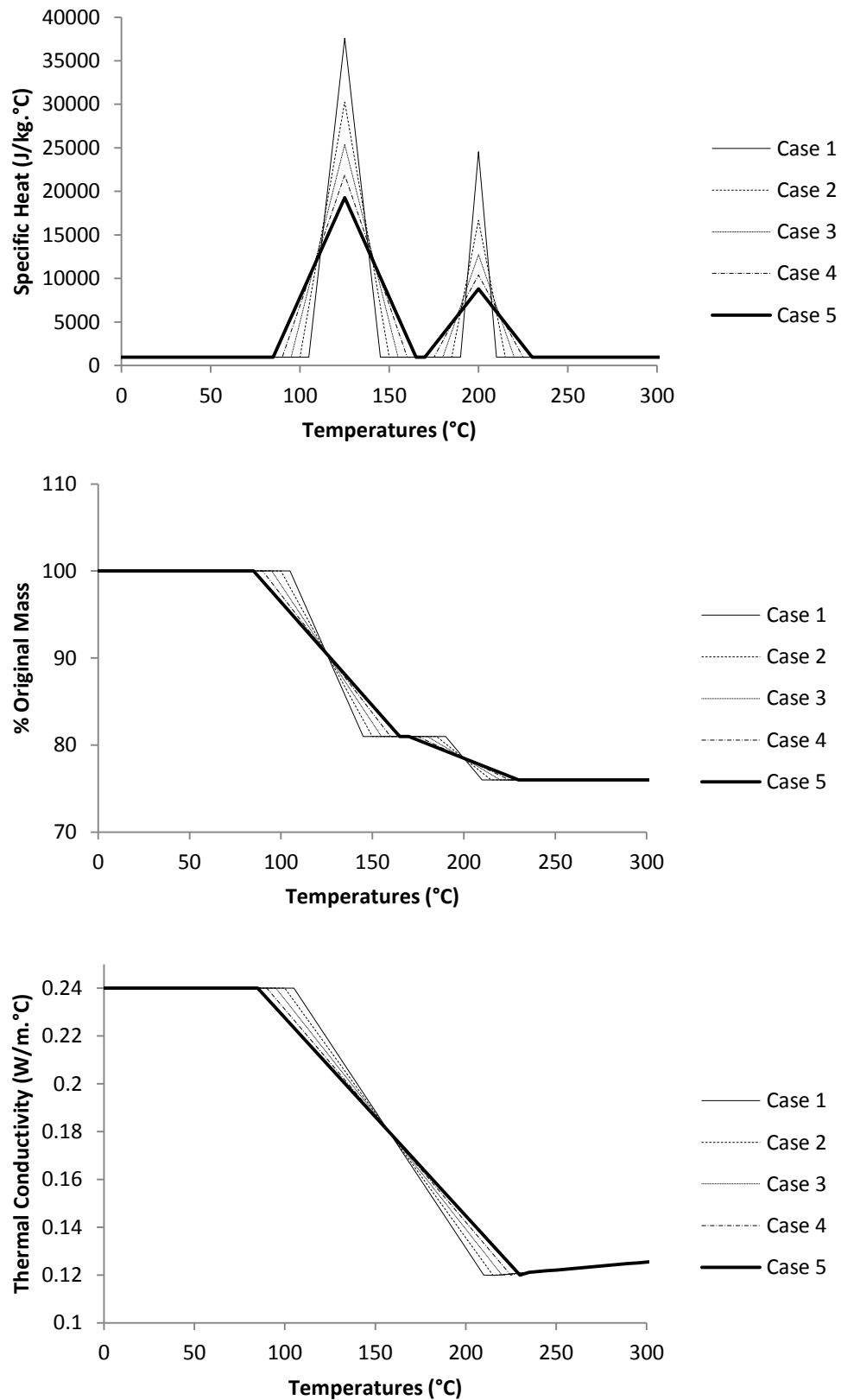


**Figure 3.16.** Thermal properties of material using different temperature intervals for dehydration

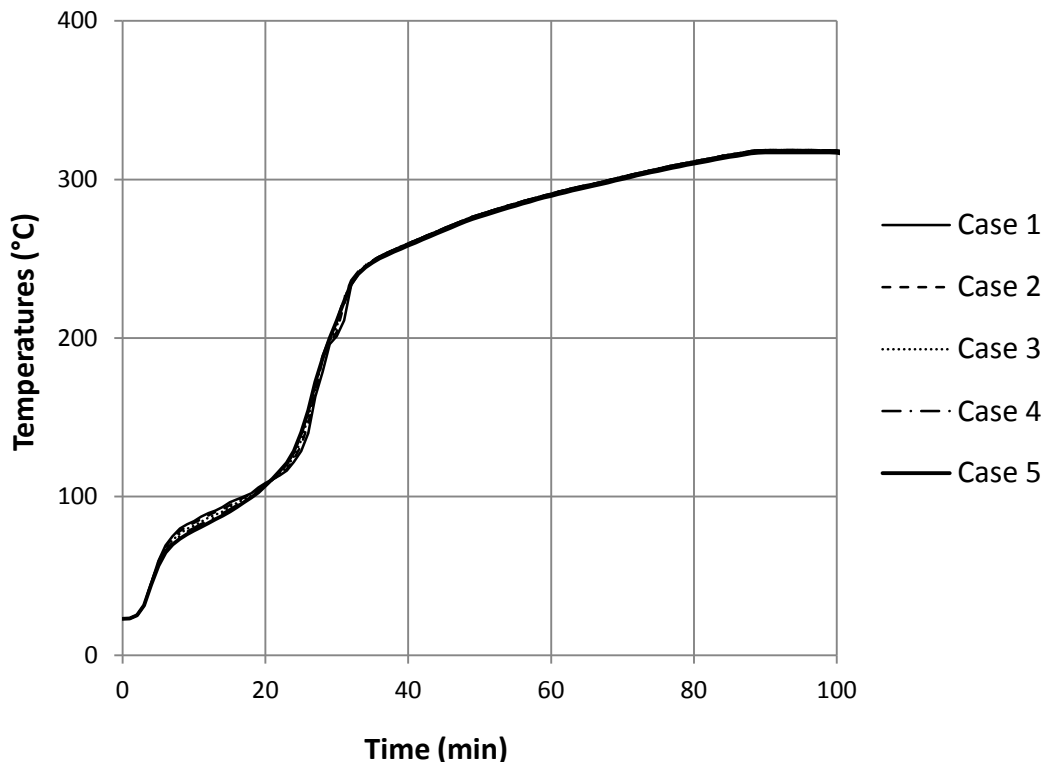


**Figure 3.17.** Calculated temperatures on the unexposed surface using different temperature intervals for the two dehydration reactions

The temperatures of the two peaks may also shift depending on the temperature increase rate of the heating regime. To simulate this effect, the first and second peaks were taken to occur at 125°C and 200°C, respectively. In the sensitivity study, the following variations of the peak temperatures have been considered:

Case i: First peak temperature=105°C , Second peak temperature=180°C

Case ii: First peak temperature=115°C , Second peak temperature=190°C

Case iii: First peak temperature=125°C , Second peak temperature=200°C

Case iv: First peak temperature=135°C , Second peak temperature=210°C

Case v: First peak temperature=145°C , Second peak temperature=220°C

Again, the thermal conductivity and density-temperature curves have been changed accordingly, as shown in Figure 3.18. The results of heat transfer analysis are illustrated in Figure 3.19.

Shifting the temperature at which the peaks occur, obviously affects the temperature history of the unexposed surface. The most considerable effect is observed before the sudden rise of the temperature of the unexposed surface. Although noticeable, this effect is not of great practical concern because it happens below the critical temperature rise ( $140^{\circ}\text{C}$ ) for the insulation criterion of fire resistance, as explained below. Beyond 40 minutes, the temperature development is barely influenced.

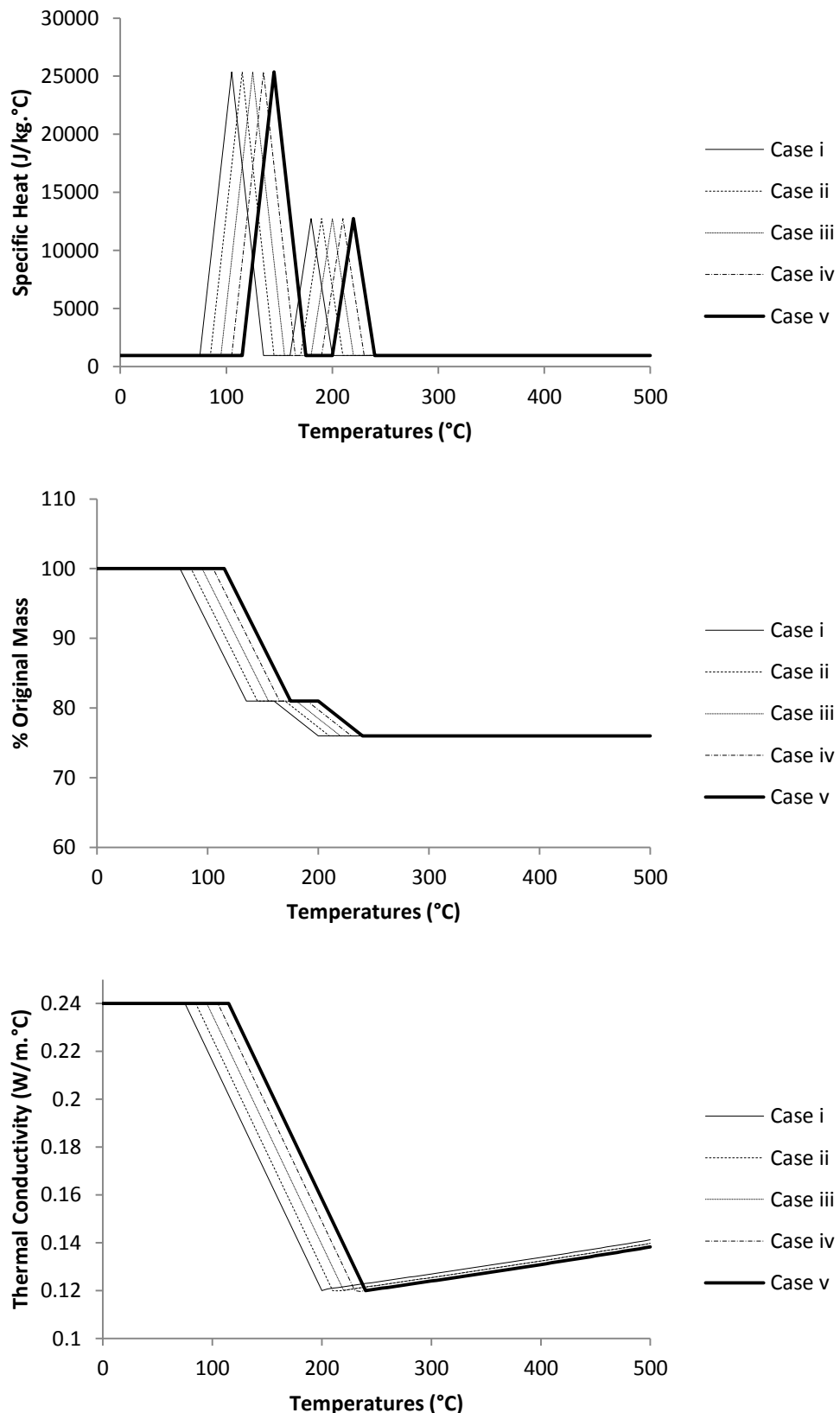


**Figure 3.18.** Thermal properties of material using different peak temperatures

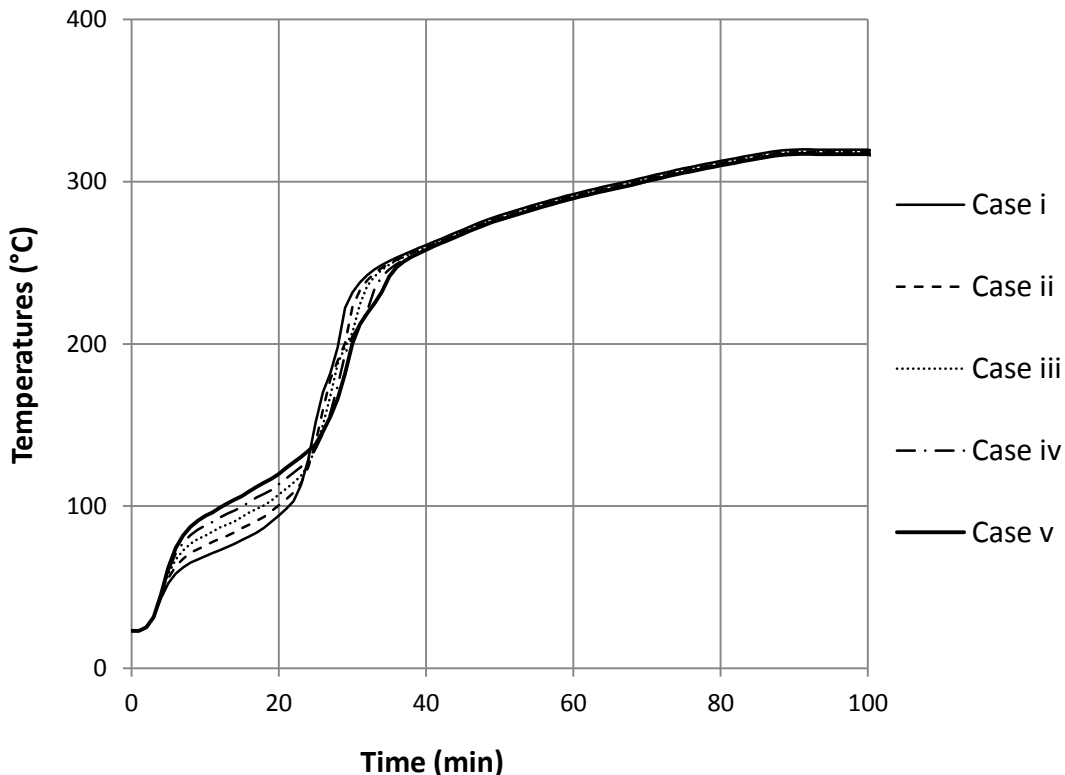


**Figure 3.19.** Calculated temperatures on the unexposed surface using different peak temperatures

The British Standard (BSI, 1987) defines two criteria for insulation failure: One is that the mean temperature of the thermocouples on the unexposed side of the panel does not exceed 140°C above its initial value. The other criterion is that the temperature recorded at any position on the unexposed side does not increase more than 180°C above its initial temperature. The influence of shifting the peak temperature is mainly observed before the temperature of the unexposed side reaches 150°C (from the initial temperature of about 25°C); hence it is not of practical concern when modeling the fire performance of a gypsum board sample. The predicted failure time difference in the case studied, is less than one minute for 10°C shift in peak temperature.

### 3.6.3 Thermal Conductivity-Temperature Correlation

As shown in Figure 3.13, the thermal conductivity of gypsum experiences a sharp drop after evaporation of the water. The following studies have been conducted to assess the degree of accuracy required for the temperature at which the thermal conductivity is at the minimum (dried gypsum) and the minimum value of thermal conductivity.

The first parameter is referred to as drop temperature (DT) in this study (Figures 3.20 and 3.21). It is assumed that the reduction of thermal conductivity due to evaporation of water is a linear one, starting with the first reaction at 95°C and stopping by the end of the second reaction at 220°C. The approach adopted is to examine whether this linear trend provides sufficient accuracy or a possible two-step reduction (similar to that for the density curve) would be preferable. Figure 3.21 shows the results for five different drop temperatures in thermal conductivity (other properties are kept unchanged). Temperature predictions are hardly influenced by the different drop temperatures, confirming that the simple linear reduction of thermal conductivity between 95°C-220°C is a reasonable, yet simple assumption.

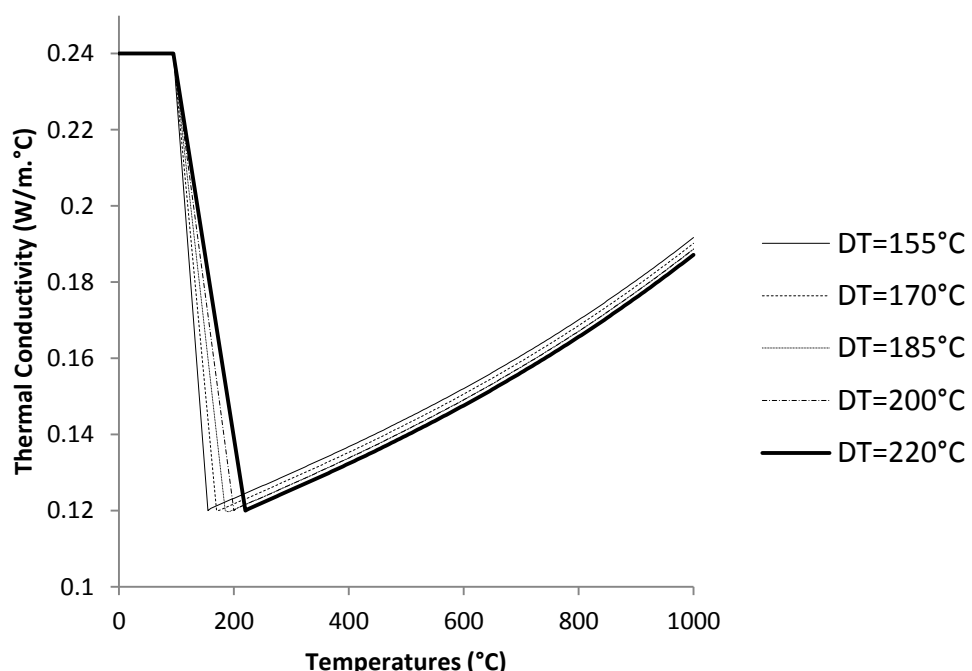


**Figure 3.20.** Thermal conductivity of gypsum using different drop temperatures (DT)

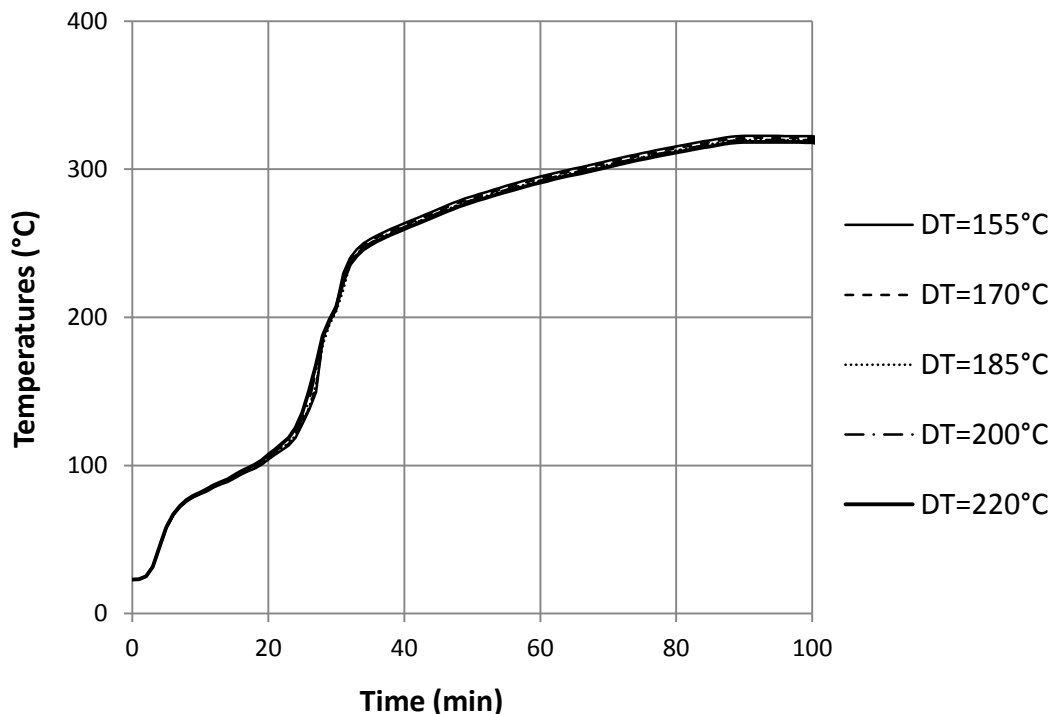


**Figure 3.21.** Calculated temperatures on the unexposed surface using different drop temperatures (DT) in thermal conductivity curve

The second parameter is the minimum value of thermal conductivity ("Min k" in Figures 3.22 and 3.23). This value can change with different gypsum board types and manufacturers. Five variations are studied (Figure 3.22) and the temperature results are compared in Figure 3.23.

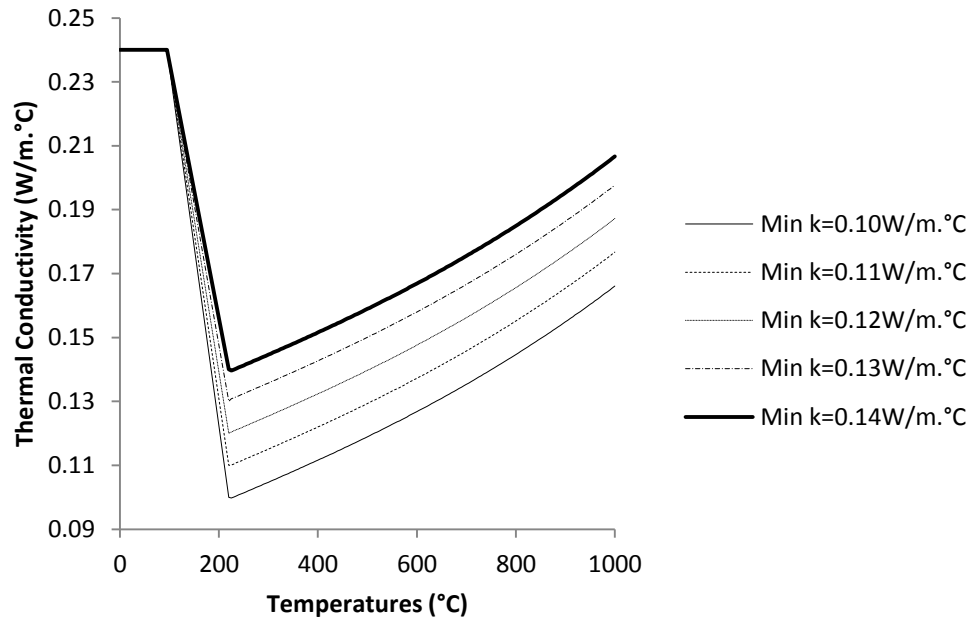


**Figure 3.22.** Thermal conductivity of gypsum using different values for the minimum thermal conductivity (Min k)

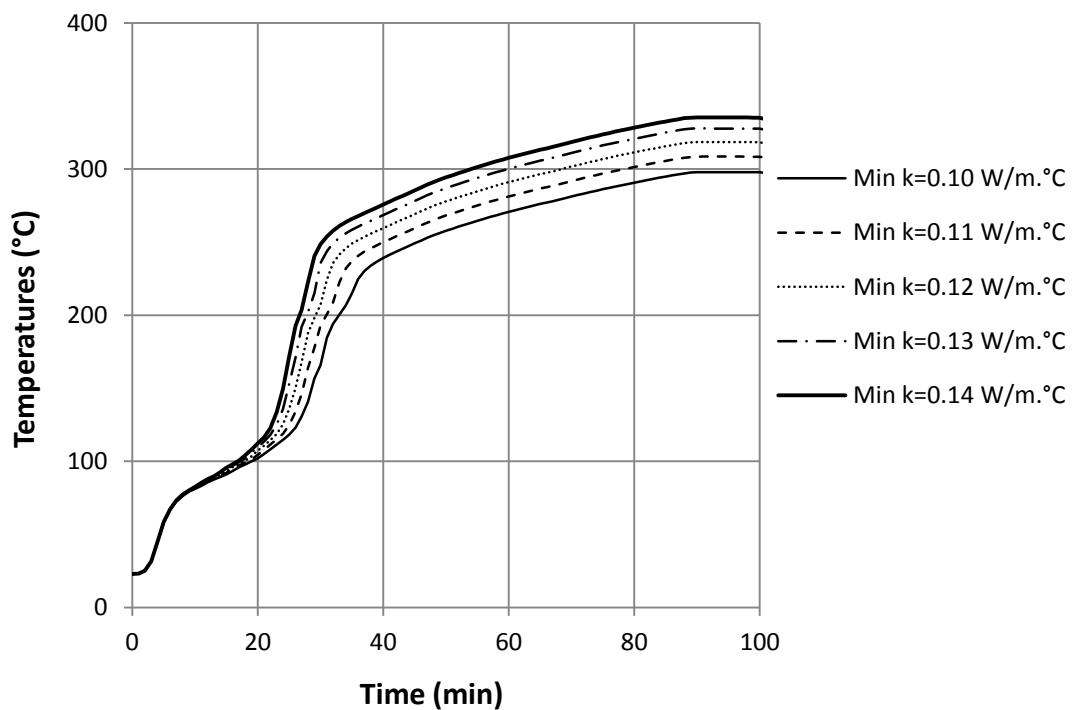


**Figure 3.23.** Calculated temperatures on the unexposed surface using different values for minimum conductivity (Min k) in thermal conductivity-temperature curve

Variations in the minimum conductivity value considerably affect the temperature development in gypsum. The higher the minimum conductivity, the shorter the temperature plateau on the unexposed surface of gypsum board, hence the earlier the insulation failure and the more rapidly the temperature development by time.

The third parameter studied is the effective void size ( $d_e$ ) used in the final part of thermal conductivity curve (3.12). This effective void size is found to be 0.12mm for a gypsum sample studied in section 3.7.2. However, it can easily be calibrated to account for crack formations and its influence on temperature development. The results of the variations of this parameter (Figure 3.24) are shown in Figure 3.25. As expected, the influence of the void size is mainly observed after the dehydration of gypsum. In other words, the length of the plateau in temperature development on the unexposed surface is not changed noticeably, but after this plateau the temperature rises considerably higher for models with larger void sizes.

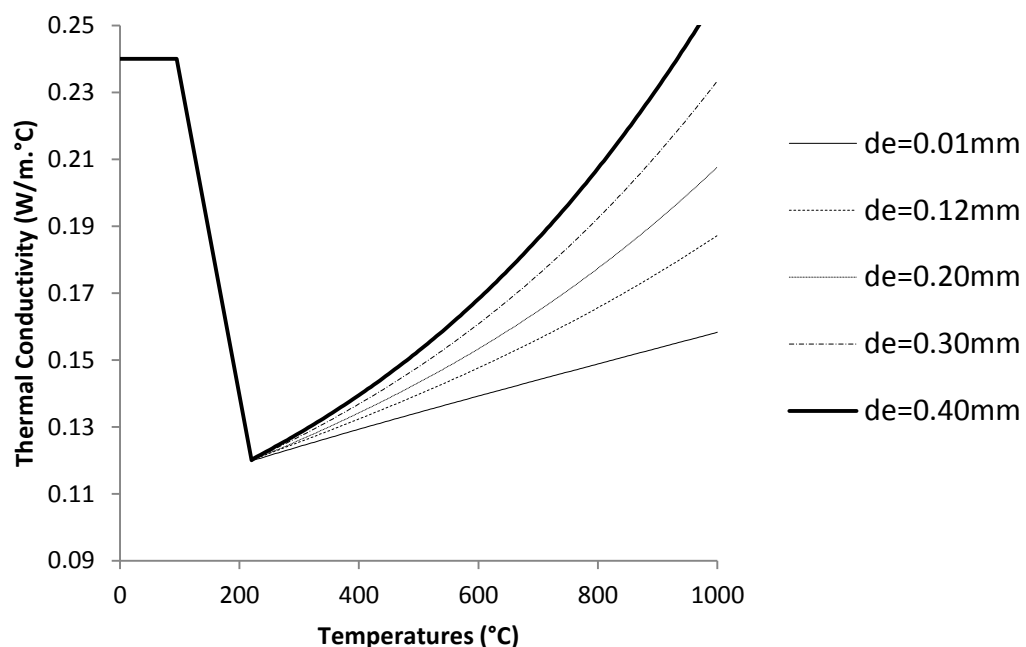


**Figure 3.24.** Thermal conductivity of gypsum using different effective void sizes ( $d_e$ )

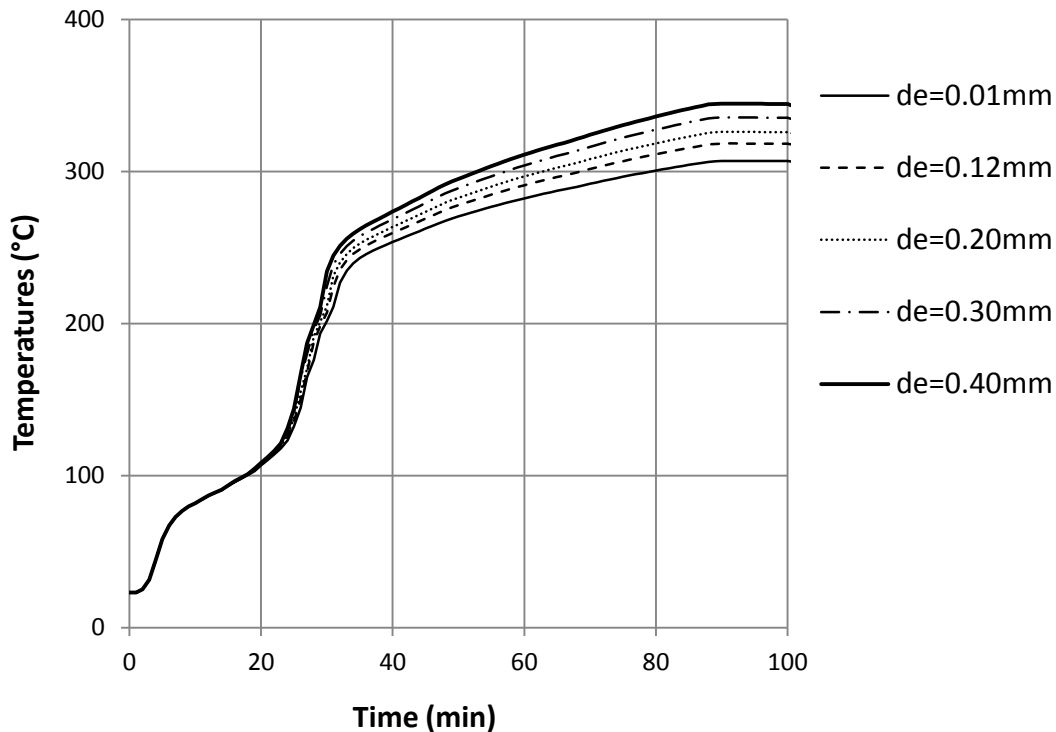


**Figure 3.25.** Calculated temperatures on the unexposed surface using different void sizes ( $d_e$ ) in thermal conductivity curve

### 3.7 A Method to Extract Controlling Parameters in Thermal Conductivity-Temperature Correlation

With the proposed three-part thermal conductivity-temperature correlation (Figure 3.14), there are three parameters to be determined for any gypsum board product: Thermal conductivity of gypsum at room temperature; thermal conductivity of dried gypsum and effective void size. The first value can be easily measured by readily available thermal probes and is usually reported by the manufacturers. The latter two can either be determined through direct measurements or by calibration against high temperature experimental results.

### **3.7.1 Thermal Conductivity of Dried Gypsum**

The value of thermal conductivity of gypsum after all its water content (both free and bound water) is evaporated is at its lowest (at 220°C). Knowing the volume of free water (about 2% of the total volume) and chemically bound water ( $\frac{28}{74}$  of the volume of solid gypsum) and using Eq. (3.11), the theoretical value of thermal conductivity of dried porous gypsum board can be calculated. Calculations for the two types of available British Gypsum boards (Fireline and Wallboard) are summarized in Table 3.1.

The thermal conductivity of dried gypsum board (the minimum conductivity) calculated this way is much higher than the measured thermal conductivity values reported by other researchers, which results in much higher temperatures on the unexposed side of gypsum when compared with experimental results from the small-scale fire tests (CHAPTER 4); i.e. the length of the temperature plateau on the unexposed surface is shorter.

This suggests that the effect of free water is greater than simply its higher thermal conductivity than air. This phenomenon has been reported in the literature (G.N. Dulnev 1989, Jakob, 1949), but there has not been any study (to the knowledge of the author) to explain or to clearly quantify this effect. Other factors such as the change in crystal structure of gypsum from calcium sulphate di-hydrate to anhydrite could also affect its thermal conductivity.

Gypsum board type	Units	Fireline gypsum board	Wallboard gypsum board
Density	kg/m <sup>3</sup>	770	623
Initial thermal conductivity (British-Gypsum, 2009)	W/m°C	0.24	0.19
Thermal conductivity of air at 20°C (Eq. (3.12))	W/m°C	0.028	0.028
Initial porosity (based on density of gypsum rock, 2320 kg/m <sup>3</sup> )	-	0.67	0.73
Using Eqs. (3.11) and (3.12) ↓			
Thermal conductivity of the solid gypsum with free water	W/m°C	0.83	0.81
Thermal conductivity of water at 20°C (Weast et al., 1989)	W/m°C	0.61	0.61
Ratio of the volume of free water to the non-gas volume of the board (3% × 2320/1000)	-	0.07	0.07
Using Eq. (3.11) ↓			
Thermal conductivity of solid gypsum without free water	W/m°C	0.85	0.82
Thermal conductivity of water at 95°C (Weast et al., 1989)	W/m°C	0.68	0.68
Ratio of the volume of chemically bound water to the volume of solid gypsum (based on molecular volume = 28/74)	-	0.38	0.38
Using Eq. (3.11) ↓			
Thermal conductivity of solid dried gypsum	W/m°C	0.96	0.92
Thermal conductivity of air at 220°C (Eq. (3.12))	W/m°C	0.043	0.043
Overall Porosity (initial porosity plus the volume of the voids appeared after the evaporation of both free and bound water)		0.81	0.85
Using Eq. (3.11) ↓			
Thermal conductivity of porous dried gypsum board	W/m°C	0.17	0.14

**Table 3.1.** Calculating thermal conductivity of dried Fireline and Wallboard gypsum boards

Due to this uncertainty, this research proposes that the thermal conductivity of dried gypsum be obtained by direct measurement using the Hot Guarded Plate tests (HGP). Tests have been performed on both Wallboard and Fireline gypsum boards. Two  $100 \times 100 \times 12.5\text{mm}$  samples of each type were heated from  $20^\circ\text{C}$  to  $250^\circ\text{C}$  and thermal conductivity was measured at certain temperatures (Figure 3.26). The HGP test confirms that the thermal conductivity stays fairly unchanged before dehydration process and then drops to its minimum at  $220^\circ\text{C}$ .

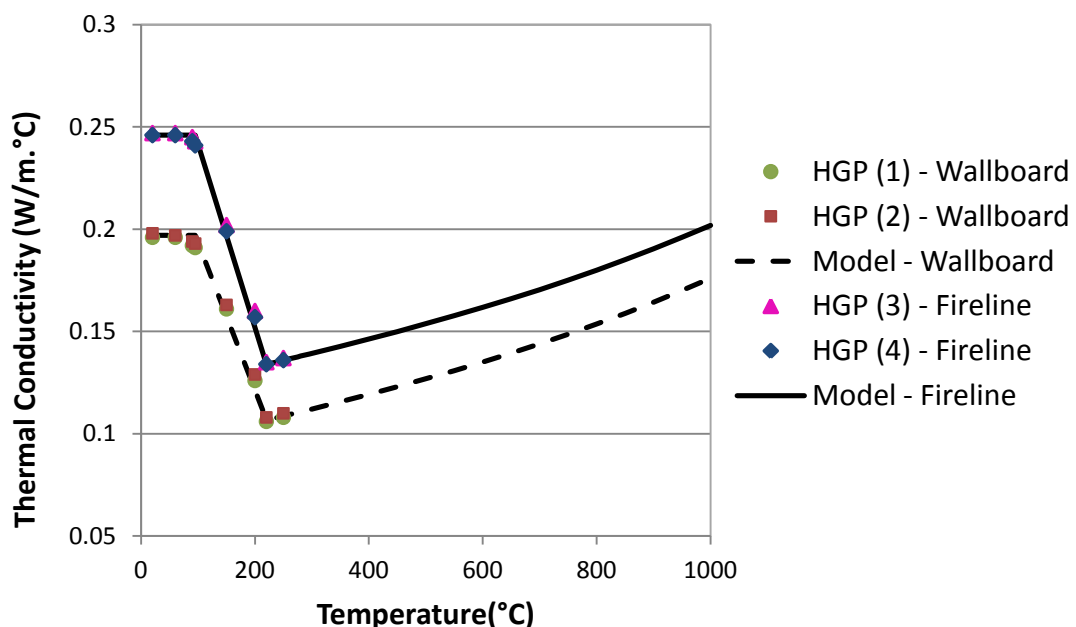


**Figure 3.26.** Comparison between the effective thermal conductivity model for wallboard and Fireline gypsum boards with Hot Guarded Plate (HGP) test results

Nevertheless, should the methods and instruments to measure thermal conductivity at this high temperature not be easily available, the minimum conductivity can be calibrated against heat transfer test results so that on the unexposed surface, the same temperature plateau as the experimental results is achieved by numerical analysis. Figure 3.27 shows an example of this calibration for double layer of 9.5mm Wallboard gypsum panel. From the results of this research, the calibrated value of thermal conductivity of dried gypsum is  $0.1 \text{ W/m}^\circ\text{C}$  for the

Wallboard gypsum boards. The same process was used to give a value of 0.12 W/m°C for Fireline gypsum boards.

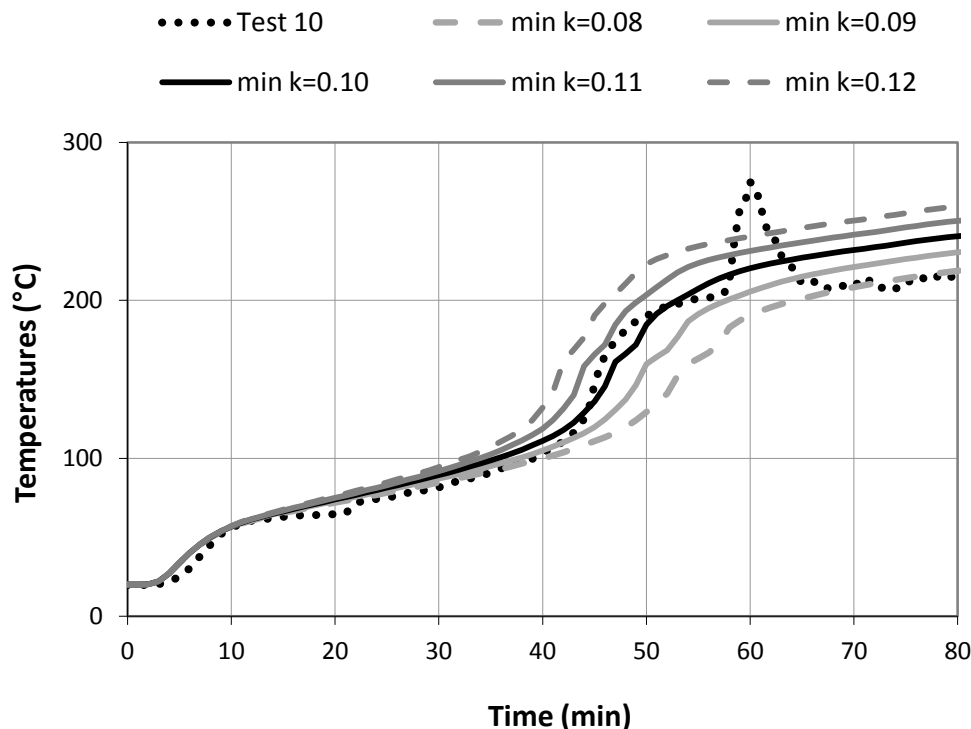


**Figure 3.27.** Calibration of the minimum thermal conductivity value (min k) against experimental results of temperature history on the unexposed surface of double layer of 9.5mm Wallboard gypsum panel (Test 10)

### 3.7.2 Effective Pore Size

To examine the size of the pores in gypsum boards, microscopic photographs of gypsum have been studied. Figure 3.28 shows a typical photograph and Figure 3.29 provides the void size distribution in that sample.

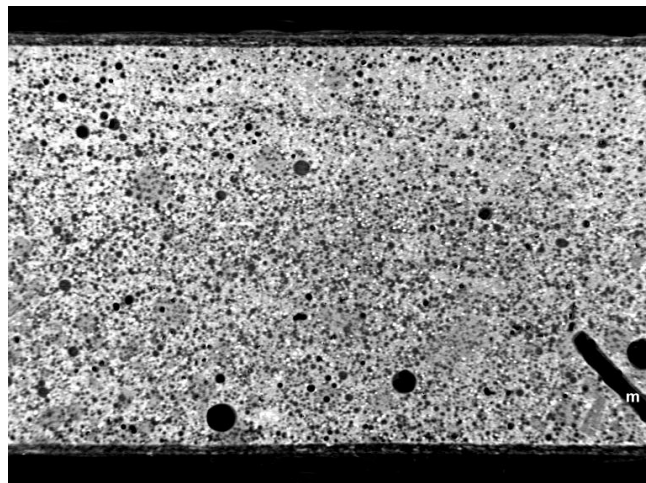


**Figure 3.28.** Low magnification photograph of a sample gypsum board

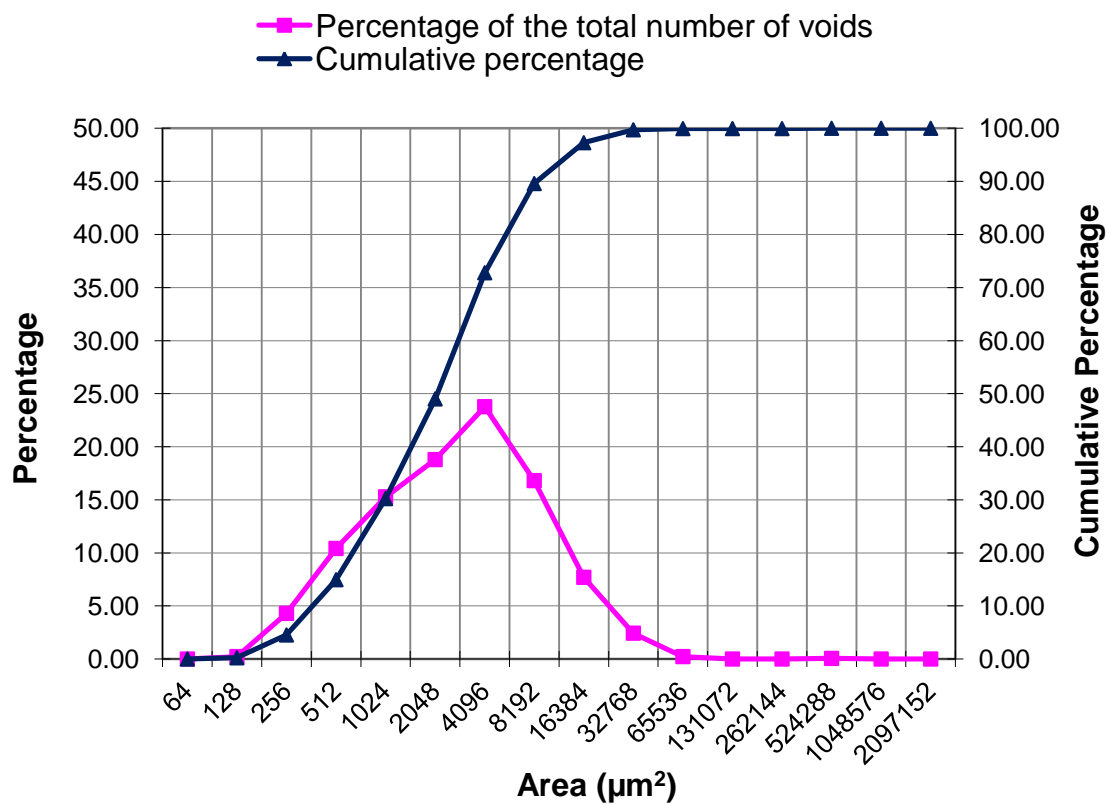


**Figure 3.29.** Void size distribution of a sample gypsum board

As expected, the pores in gypsum are not of a uniform size, but there are a range of void sizes with different frequencies. The effective pore size used in Eq. (3.12) is the size of uniform pores in a hypothetical gypsum board, which would result in the same thermal conductivity as that of real gypsum with various sizes of pores. To find this effective pore size, gypsum can be assumed to consist of various layers, each with a uniform pore size and consistent porosity (72% in this sample). Table 3.2 shows the details of such layers.

Layer	Void Diameter ( $\mu\text{m}$ )	Void Area ( $\mu\text{m}^2$ )	Number of Voids	Total Void Area ( $\mu\text{m}^2$ )	Total Area of the Layer ( $\mu\text{m}^2$ )	Thickness or width (when the other dimension equals unit, $\mu\text{m}$ )
1	18	256	4	1101	1529	1529
2	26	512	10	5332	7405	7405
3	36	1024	15	15647	21732	21732
4	51	2048	19	38480	53444	53444
5	72	4096	24	97358	135220	135220
6	102	8192	17	137692	191240	191240
7	144	16384	8	126102	175142	175142
8	204	32768	2	79741	110751	110751
Overall						696462

**Table 3.2.** Arranging gypsum in various layers, each with a uniform void size

The thermal conductivity of each layer can be determined using Eqs. (3.11) and (3.12). The overall conductivity depends on the arrangement of these layers against the heat flow. The two extreme cases are series and parallel arrangements of the thermal resistance of all the layers in the direction of heat flow (Figure 3.30), which would result in the minimum and maximum overall thermal conductivity, respectively. The effective pore size can then be worked out using the overall thermal conductivity and again Eqs. (3.11) and (3.12).

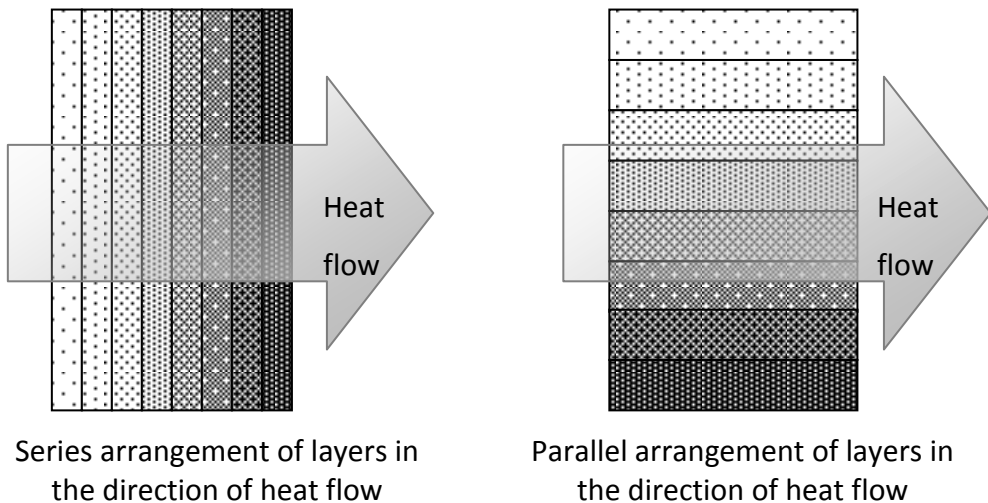


**Figure 3.30.** Series and parallel arrangement of layers of uniform void size

Table 3.3 shows the resultant pore sizes for the series and parallel arrangements of layers at different temperatures. Since there is negligible difference between the upper and lower bound values, the effective pore size can reasonably be taken as 0.12mm.

Temperature (°C)	20	100	200	300	400	500	600	700	800	900	1000
Effective pore size for <b>series</b> arrangement (μm)	116	116	116	116	116	116	116	115	115	115	114
Effective pore size for <b>parallel</b> arrangement (μm)	116	116	116	116	116	116	116	116	116	116	116

**Table 3.3.** Effective pore size for series and parallel arrangement of layers at different temperatures

Should such photographic study not be feasible, one can use the Finite Difference method to calibrate the effective pore size against high temperature test results so that the temperatures on the unexposed side after the sudden rise closely matches the experimental results. In this study a constant effective void size throughout the

test is deemed satisfactory; however if need be, it can be assumed to vary to account for the effects of ablation and cracks in gypsum at high temperatures.

### **3.8 Proposed Methodology to Extract Thermal Properties of Gypsum**

The main thermal properties of gypsum to be used in a heat transfer analysis to predict temperature development in gypsum are thermal conductivity, specific heat and density of gypsum, all of which are temperature dependent and directly affected by the two dehydration reactions of gypsum during the course of heating.

The first dehydration reaction is assumed to start at 95°C and end by 155°C, while the second dehydration reaction starts at 180°C and concludes by 220°C. The prediction of insulation failure of gypsum in fire is hardly sensitive to the temperature ranges at which the dehydration reactions occur, as long as they are close to the temperatures suggested above.

The density of gypsum can be modelled as proposed in Figure 3.12. The density-temperature correlation starts with the density of gypsum at ambient temperature and experiences two linear drops corresponding to the two dehydration reactions.

The specific heat of gypsum can be modelled as proposed in Figure 3.11. The base of the specific heat-temperature correlation is the specific heat of gypsum at ambient temperature. The peak values are calculated using Eq. (3.10), which accounts for the heat of reactions and the latent heat of evaporated water, as well as water mass transfer during heating.

The effective thermal conductivity-temperature correlation can be modelled as proposed in Figure 3.14. The first section in this correlation equals the thermal conductivity of gypsum at ambient temperature. The linear reduction in thermal conductivity starts by the first dehydration reaction and continues till the second dehydration reaction is concluded. Then it increases nonlinearly based on Eqs. (3.11) and (3.12), which account for radiation through voids in dried gypsum. The thermal conductivity of dried gypsum at 220°C and the equivalent void size in gypsum are the two most important parameters, which can be measured directly or through calibration with easily accessible small-scale high temperature test results.

Examples of such tests are presented in CHAPTER 4 and the calibration methodology is demonstrated in Figures 3.31 and 3.32.

The thermal conductivity of dried gypsum at 220°C can be directly measured provided high temperature measurement techniques (e.g. HGP) are accessible, otherwise the calibration procedure summarised in the first part of Figure 3.32 can be adopted to determine this minimum value of thermal conductivity of gypsum. The equivalent void size may be determined by carrying out an analysis of thermal conductivity based on microscopic pictures of gypsum. This process has been described in section 3.7.2. For the products studied in this research, the equivalent void size is 0.12 mm. Should such information not be available, the second part of Figure 3.32 may be used to find the equivalent void size.

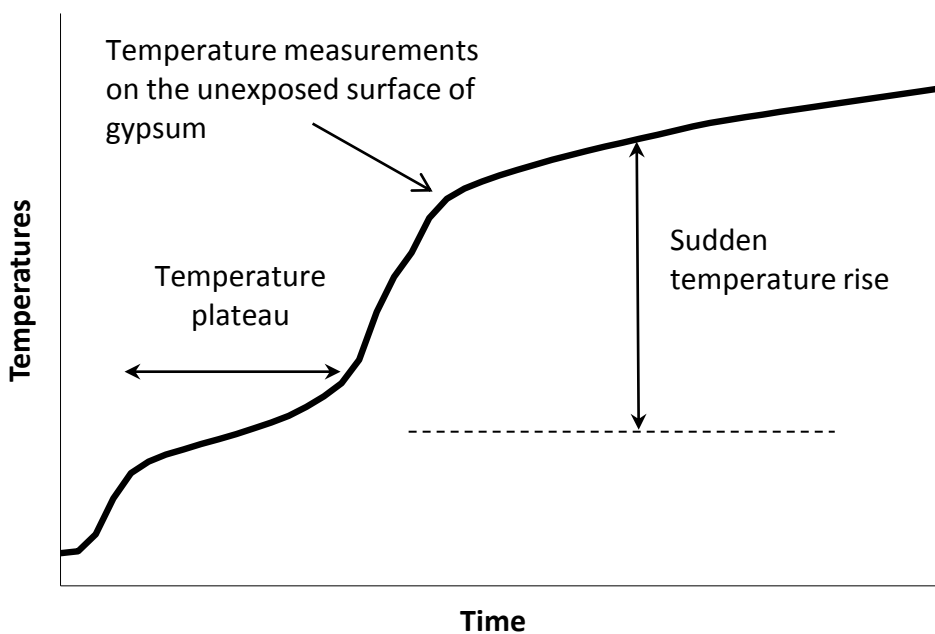


**Figure 3.31.** Conceptual demonstration of temperature history properties used for calibration of thermal conductivity parameters

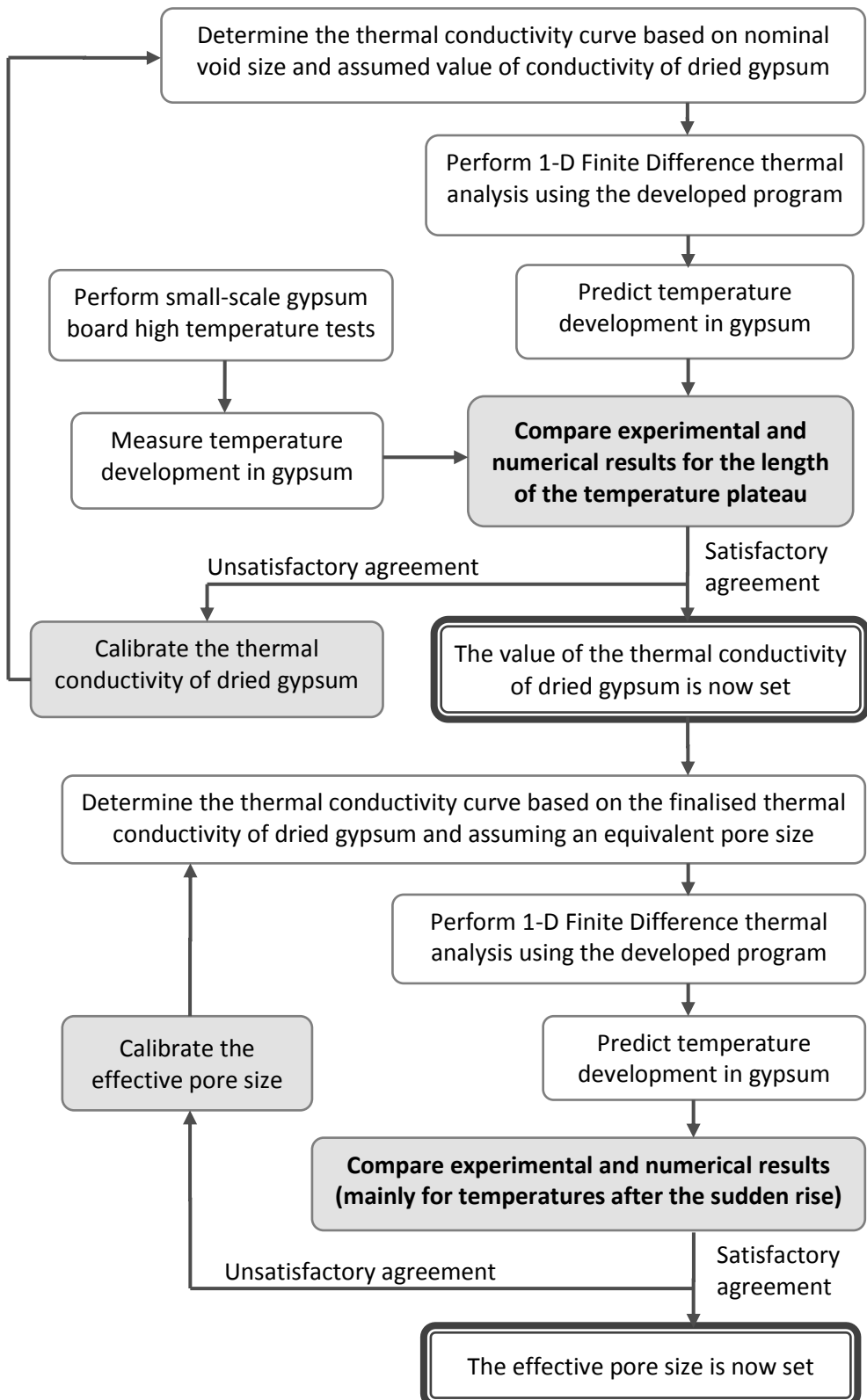


**Figure 3.32.** Proposed methodology for extracting the effective thermal conductivity of gypsum board products by calibrating two parameters: thermal conductivity of dried gypsum at 220°C and the effective pore size

### **3.9 Conclusions**

This chapter has presented an effective model to determine the thermal properties of various gypsum board products. A one-dimensional heat transfer analysis scheme has been developed and models for thermal properties of gypsum boards have been proposed to be used for predicting temperature development in gypsum. Among the thermal properties, the thermal conductivity and its variation have the most significant effect on temperature developments in gypsum. A combined numerical and experimental approach has been developed to extract the thermal conductivity. In this approach, gypsum is treated as a porous material consisting of solid and pores and the effects of radiation at high temperatures are taken into consideration. Therefore the thermal conductivity–temperature relationship of gypsum is described as a function of two variables: reduction in thermal conductivity from its value at ambient temperature due to dehydration, and effective spherical void size. Quantification of these two parameters is realized through a hybrid experimental–numerical method. The proposed model employs the validated one-dimensional finite difference heat conduction program and high temperature test results on small samples of gypsum boards. Through a clearly defined trial and error procedure, the water evaporation related drop in thermal conductivity value and void size that give the best agreement between numerical prediction and high temperature tests can be obtained to quantify the gypsum thermal conductivity – temperature relationship. The next chapter provides the details of such small-scale high temperature tests and confirms the efficiency of the proposed methodology that can be easily utilised to aid manufacturers to develop their products without having to conduct numerous large-scale fire tests.

## **CHAPTER 4. Validation of the Thermal Conductivity Model through Small-Scale High Temperature Tests**

### **4.1 Introduction**

Several small scale high temperature experiments have been performed on gypsum board samples. The results of these high-temperature tests are used to validate the proposed methodology for extracting the effective thermal properties of gypsum to be used in heat transfer analysis. Test results are also used to calibrate the small number of input data for determining the thermal conductivity of gypsum. This chapter provides the details of the experiments, the set-up and the results obtained. Also presented is the comparison of the results from the numerical analysis using the one-dimensional Finite Difference model and the experiments.

### **4.2 Experimental Set-Up**

The specimens tested were gypsum board panels of two different types; *Gyproc Fireline* plasterboard (12.5mm) and *Gyproc Wallboard* plasterboard (9.5mm and 12.5mm), both *British Gypsum* products. A total number of 12 specimens were tested as detailed in Table 4.1. All specimens were with approximate dimensions of 400 × 400mm.

Test No	Plaster board Type	Layers	Total Thickness (mm)	Density (kg/m <sup>3</sup> )	Initial Thermal Conductivity (W/m.°C)
1	Gyproc Fireline	Single	12.5	770	0.24
2	Gyproc Fireline	Single	12.5	770	0.24
3	Gyproc Fireline	Single	12.5	770	0.24
4	Gyproc Fireline	Double	25	770	0.24
5	Gyproc Fireline	Double	25	770	0.24
6	Gyproc Fireline	Double	25	770	0.24
7	Gyproc Wallboard	Single	9.5	641	0.19
8	Gyproc Wallboard	Single	9.5	641	0.19
9	Gyproc Wallboard	Single	12.5	623	0.19
10	Gyproc Wallboard	Double	19	641	0.19
11	Gyproc Wallboard	Double	19	641	0.19
12	Gyproc Wallboard	Double	25	623	0.19

**Table 4.1.** Specifications of gypsum board specimens (British-Gypsum, 2009)

Each specimen was placed horizontally on top of an electric kiln (Figure 4.1) as the source of heat, so that one side of the panel was subjected to kiln temperature and the other side faced up to the room temperature (19-25°C). There was a 280 × 265mm opening on the top lid of the kiln, which allowed the lower side of the panel to be exposed to elevated temperatures. A 30mm layer of glass wool (with the same opening size as the kiln lid) was laid under the specimen to insulate the contact surface of the top lid and the plasterboard. The specimens were kept in place at the corners with 2kg weights and were heated up to about 1100°C with approximate standard time-temperature curve (the exact standard fire curve was not achievable with the available kiln). Figure 4.1 shows the experiment set-up.

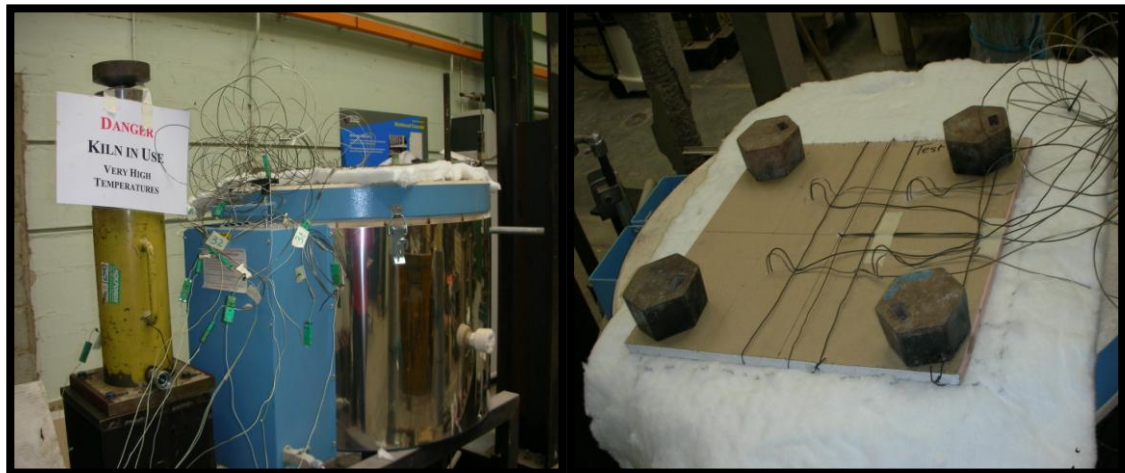


**Figure 4.1.** Small-scale high temperature test set-up

#### **4.2.1 Thermocouple Layout**

The heat transfer through the experimental gypsum board panels may be assumed to be one-dimensional, perpendicular to the panel's face. Therefore, to investigate temperature development through gypsum and to minimise the edge effects, the centre point of the panel was chosen as the reference. Temperatures of the centre point were recorded both on the exposed and the unexposed surfaces of the panel.

To inspect how reasonable the one-dimensional heat transfer assumption is, eight more thermocouples (later referred to as observers) were located at four corners of a  $150 \times 150\text{mm}$  square, shown as 1-8 in Figure 4.2. Based on the one-dimensional heat transfer assumption, temperature histories of the four observer thermocouples on each side should be very similar and also very close to the temperatures recorded at the centre.

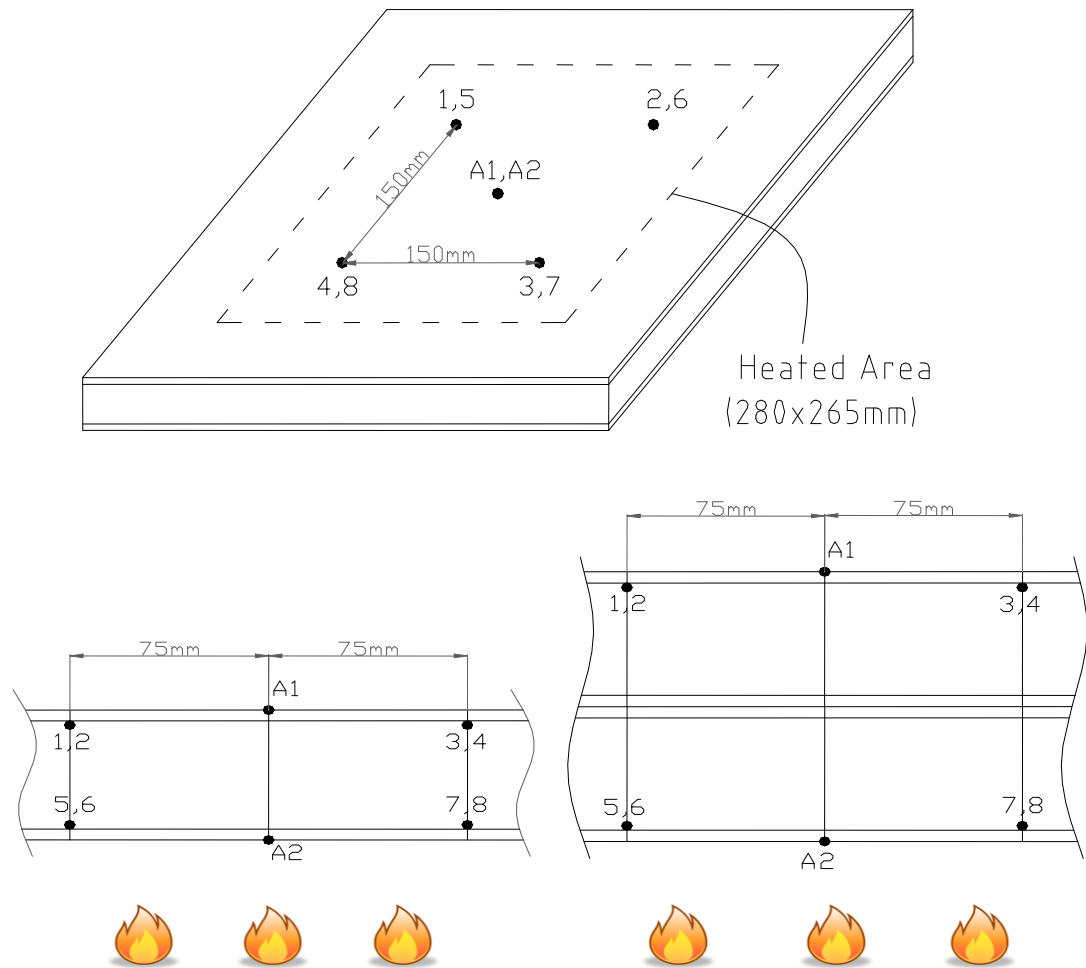


**Figure 4.2.** Thermocouple layout for gypsum board specimens on plan and cross-section of single-layer and double-layer panels

All Thermocouples were of Type K, which are the most commonly used general purpose thermocouples. A data logger was used to read the temperature data from the thermocouples every 30 seconds and the data were recorded by a computer connected to the logger.

#### 4.2.2 Specifications of the Kiln

A Harrier Top Loading Electric Kiln was used as the source of heat for all twelve experiments. High temperature coiled heating elements were fitted in the inner wall of the kiln and a microprocessor control system was used to control the temperature of the kiln, which allowed the user to define the firing curves by five

data points. However, the capacity of the kiln (the maximum possible heating rate) did not meet the requirements of a standard cellulosic fire test introduced in BS476 (1987). Therefore, the system was set such that the firing curve was as close to the standard fire curve as possible. Figure 4.3 shows the heating curve achieved in the kiln as compared to a standard fire.

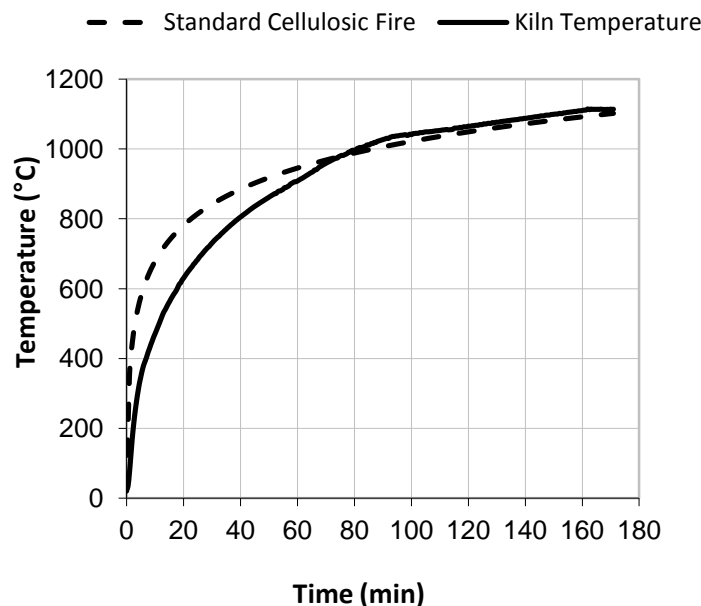


**Figure 4.3.** Time-temperature curve for the kiln against standard cellulosic fire curve

#### 4.2.3 Specifications of the Specimens

As mentioned earlier, two types of gypsum boards were used; *Gyproc Wallboard*, which is a standard board product and is suitable for most applications where normal fire, structural and acoustic levels are required; and *Gyproc Fireline*, which is a plasterboard with glass fibre reinforcement and other additives in the core and is used to give increased fire protection. The density and thermal conductivity of the boards, according to the product data sheet provided by the manufacturer, are reported in Table 4.1.

To measure the moisture content of the gypsum boards, the following procedure was followed: Three 150 × 150mm samples of *Gyproc Wallboard* and three 150 × 150mm samples of *Gyproc Fireline* were prepared for testing. To measure

the amount of free water in the specimens, they were kept at 50°C for 48 hours and their weight loss was recorded. Then the temperature was raised to 150°C and maintained for 4 days. Since the first dehydration reaction occurs at about 100°C, the weight loss at this stage should correspond to the release of three quarter of the chemically bound water. The results for weight loss of the specimens are presented in Table 4.2. Note that the weight loss at each heating stage is expressed as percentage of the initial weight of the samples before they were placed in the oven.

Plasterboard type	<i>Gyproc Fireline</i>			<i>Gyproc Wallboard</i>		
Sample No	1	2	3	4	5	6
Initial Weight (gr)	228.81	226.05	251.32	144.43	141.52	143.55
Weight loss after 2 days in 50°C (% of initial weight)	0.6	0.6	0.6	0.9	0.9	0.9
Excess weight loss after 4 days in 150°C (% of initial weight)	18.6	18.6	18.6	18.5	18.3	18.1

**Table 4.2.** Measured moisture content of the specimens

The first heating at 50°C was assumed to remove most of the free moisture in the boards. The results would suggest that the gypsum board samples contained less than 1% free water, which is not in the range expected (3 to 8% as reported in the literature). Apparently, this heating temperature was too low to drive off the free water. In fact, the recordings of the second weight loss at 150°C may be used to confirm that not all the free moisture had been removed in the first stage. In the first dehydration reaction, only  $0.75 \times 21 = 15.75$  percent of the weight should be driven off as water. But all the recordings at 150°C are more than 18%, with the average being about 18.6% for the Fireline gypsum and 18.3% for the Wallboard gypsum. The differences of 18.6-15.75 (2.85) and 18.3-15.75 (2.55) should be taken as free water. Together with the free water lost at 50°C (0.6% and 0.9% respectively), the total free water would have been about 3.45% for both products.

In later calculations, it is assumed that the free water is 3.5% by weight and the chemically bound water is 21% by weight.

### 4.3 Fire Test Results and Discussions

Twelve small-scale fire tests were performed in total. The temperature histories recorded at the centre of each specimen on the exposed and unexposed sides of the panel (thermocouples A1 and A2 in Figure 4.2) are presented in Appendix A. The result for Test 3 is plotted in Figure 4.4 as an example. The temperature plateau on the unexposed surface of the panel expectedly shows the effect of chemically bound water in gypsum. Evidently, the thicker the gypsum board, the longer the delay in heat transfer and the better the fire resistance of the panel.

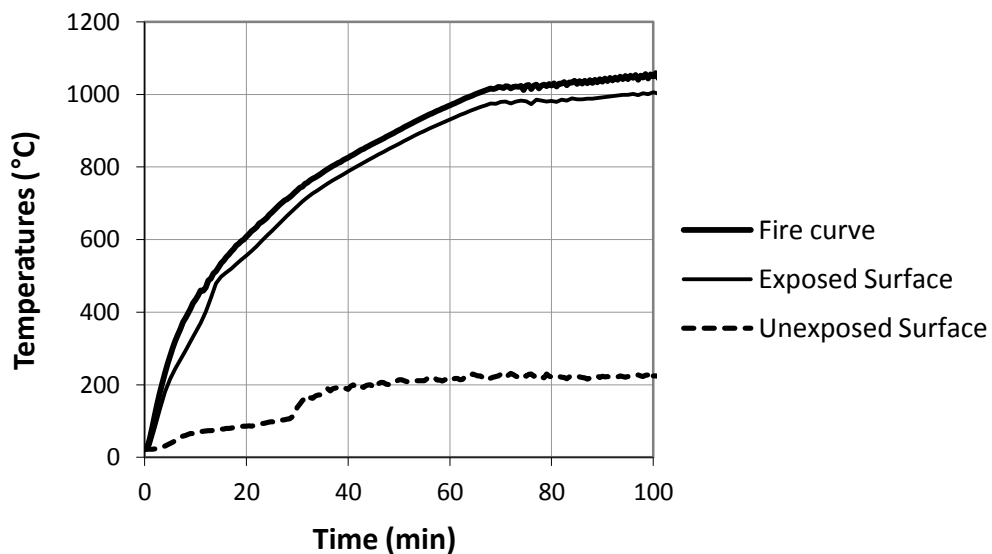


**Figure 4.4.** Temperature recordings on the exposed and unexposed surfaces of a 12.5mm Fireline gypsum panel (Test 3)

Also recorded are the temperature histories of the observer thermocouples in each test. The top observers were placed very close to the unexposed surface and bottom observers were placed very close to the exposed surface as explained earlier. The intention was to assess the assumption of one-directional heat transfer in the specimens. Some typical results of these recordings are shown in Figures 4.5

and 4.6. It is observed that the temperature histories of each set of four thermocouples on the two sides of the panel are very similar and also close to the temperature history of the centre of the board. This confirms that the flow of heat in the specimens is dominated in one dimension and that is across the thickness of the panels.

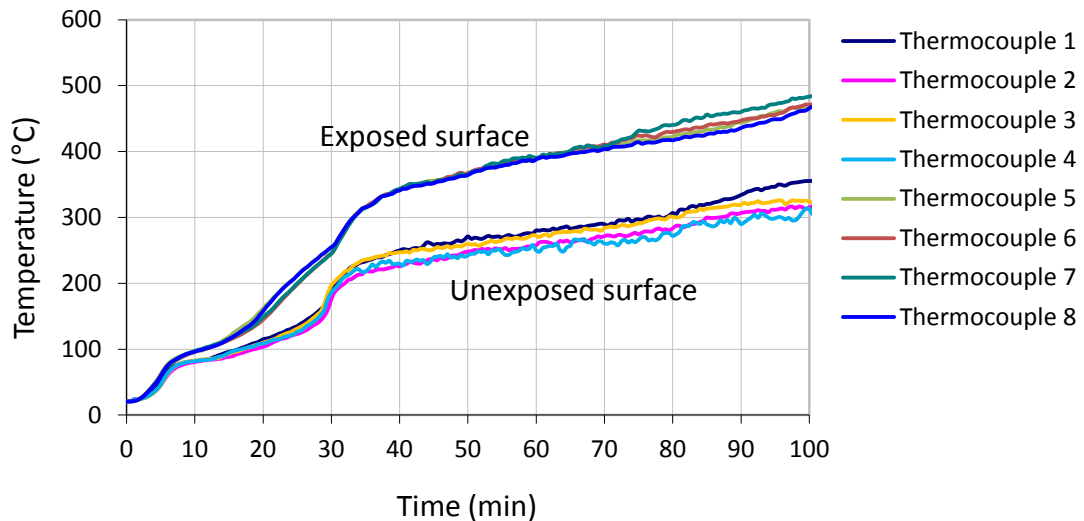


**Figure 4.5.** Temperature recordings by the observer thermocouples in Test 1

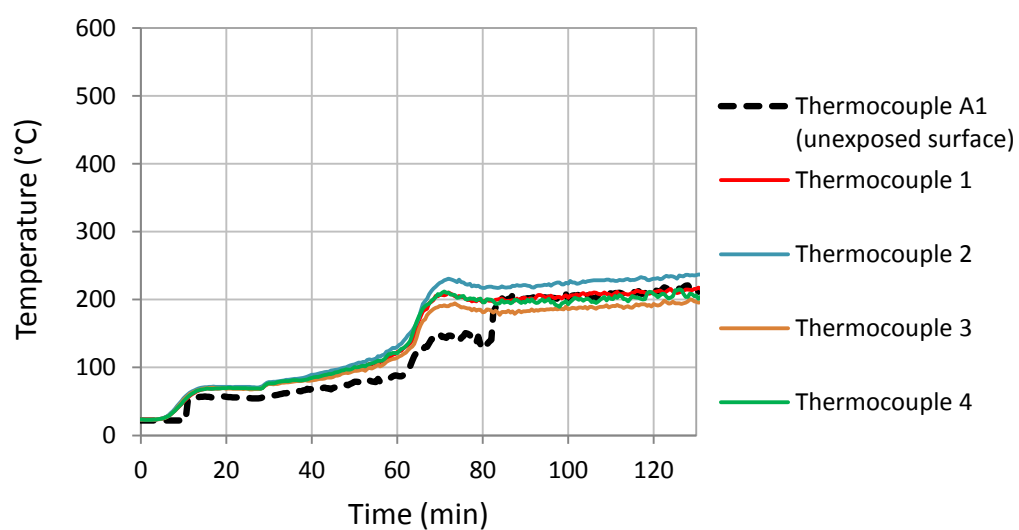


**Figure 4.6.** Temperature recordings by the top observer thermocouples in Test 5, compared to thermocouple A1 at the centre of the unexposed side

It should be noted that during these small-scale tests, gypsum boards experienced cracking of a size comparable to those observed in large scale tests (see Figure 4.7). Therefore, the thermal properties of gypsum obtained from these small scale samples may be considered to be applicable to more realistic scale panels.

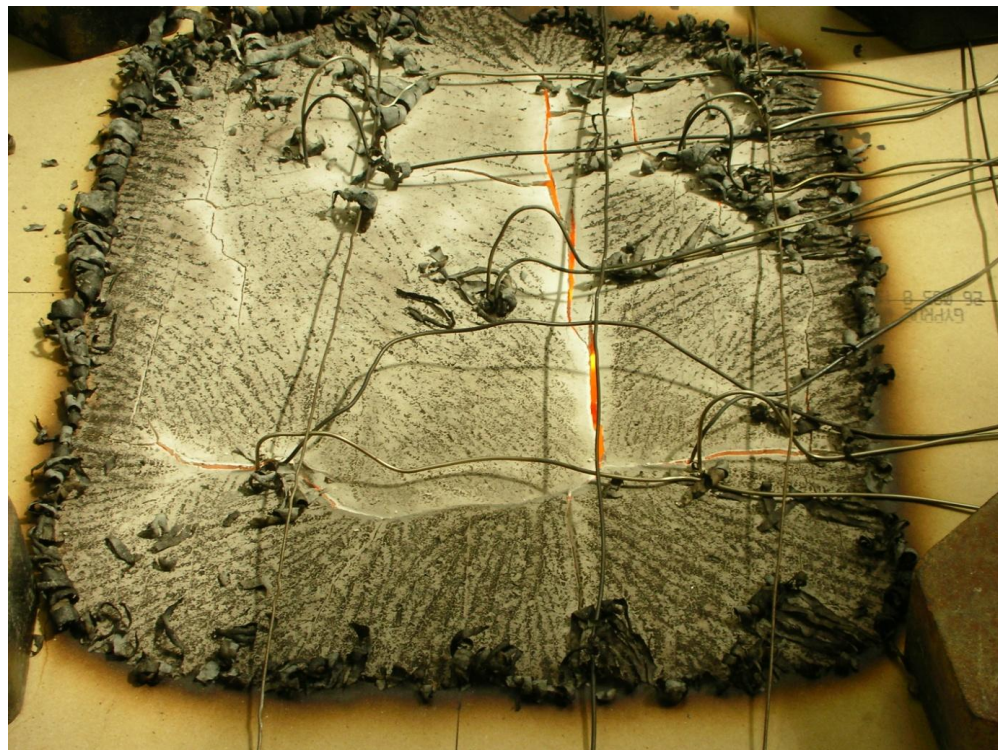


**Figure 4.7.** Typical cracking observed in small-scale gypsum boards during high temperature tests

#### **4.4 Comparison of Numerical and Experimental Results**

In Figures 4.8 to 4.15, the temperature histories measured from selected tests are compared with the temperatures calculated by the one-dimensional Finite Difference heat transfer program using the extracted material thermal properties, as explained in CHAPTER 3. Also plotted in these figures are the numerical results utilizing thermal conductivity of gypsum as used by Mehaffey *et al* (1994), where other thermal properties are kept identical.

The thermal conductivity of gypsum in Figures 4.8 to 4.11 is modelled using the calibrated values for minimum thermal conductivity (Figure 3.14). In Figures 4.12 to 4.15 the thermal conductivity is obtained based on HGP measurements of thermal conductivity at room temperature and at 220°C (Figure 3.26). Using either the calibrated or measured minimum thermal conductivity values at 220°C give very similar results, confirming the suitability of the proposed thermal conductivity extraction method as detailed in 3.32. The unexposed surface temperature was predicted with good accuracy throughout the entire testing period, giving confidence in the pore size (0.12mm) used. Furthermore, the results demonstrate a considerable improvement in the prediction of temperature development through gypsum when using the new thermal conductivity model described in CHAPTER 3 compared to the popular thermal conductivity relationship of Mehaffey et al (1994).

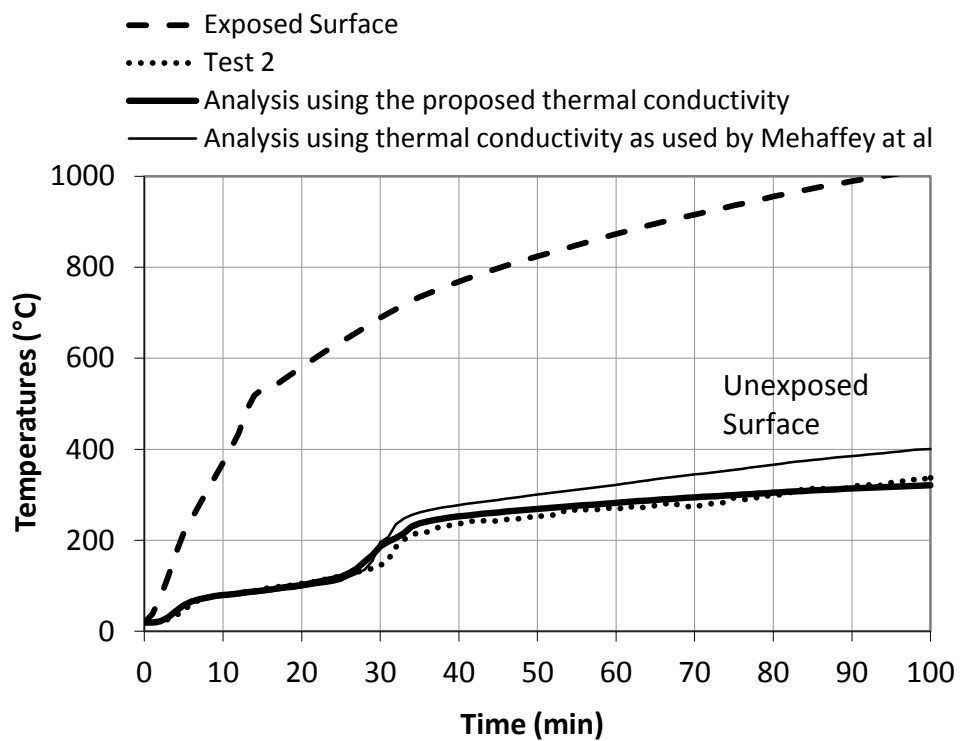


**Figure 4.8.** Temperature history for 12.5mm Fireline gypsum panel (Test 2) – thermal conductivity model based on calibrated dry gypsum value

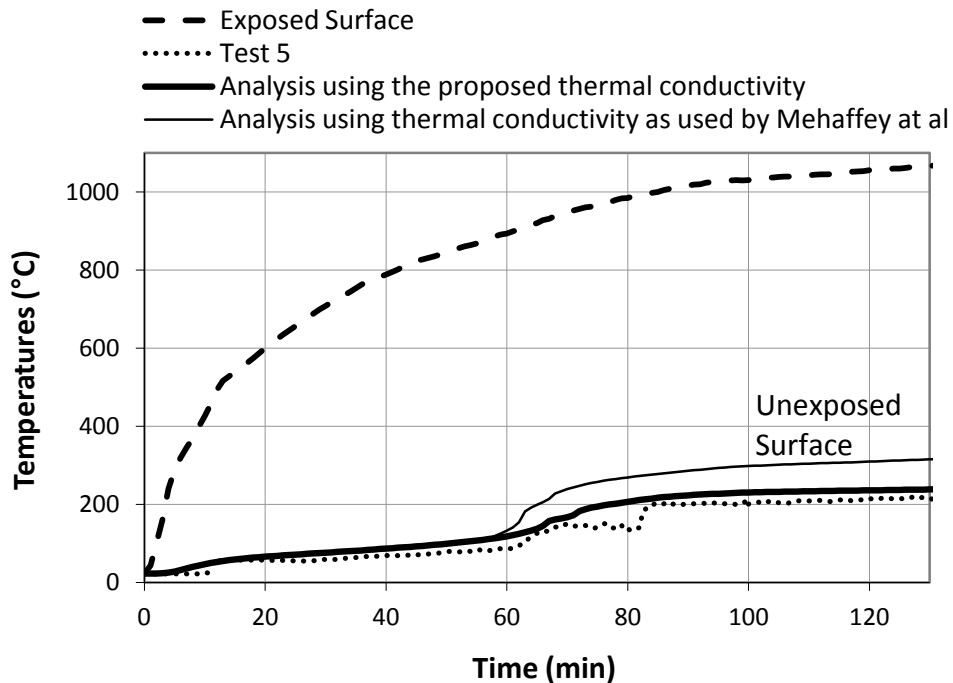


**Figure 4.9.** Temperature history for double layer of 12.5mm Fireline gypsum panel (Test 5)  
– thermal conductivity model based on calibrated dry gypsum value

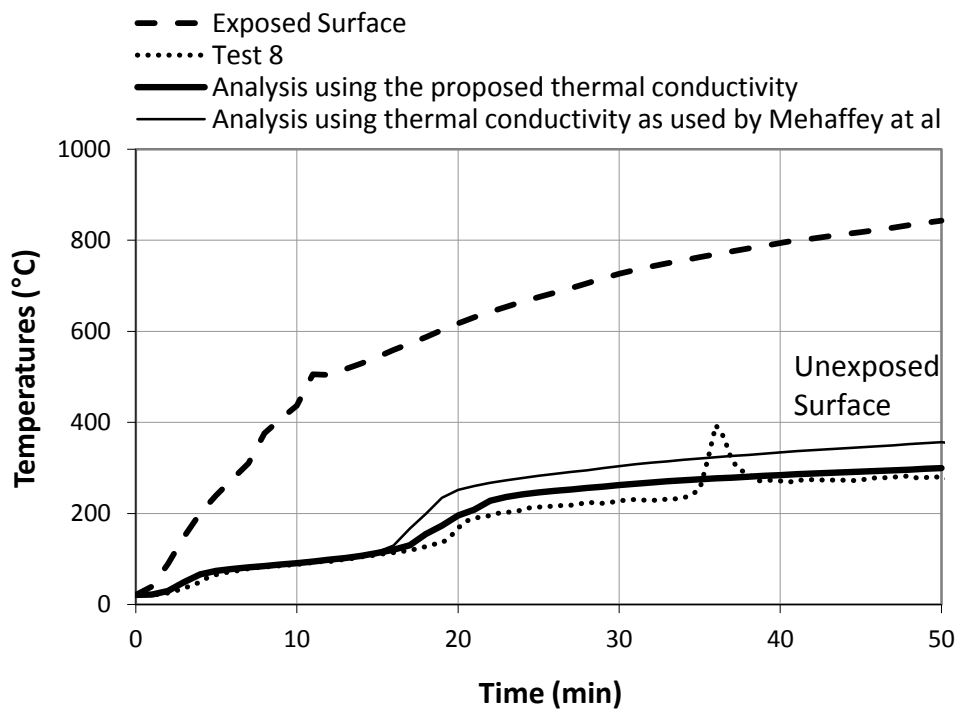


**Figure 4.10.** Temperature history for 9.5mm Wallboard gypsum panel (Test 8) – thermal conductivity model based on calibrated dry gypsum value

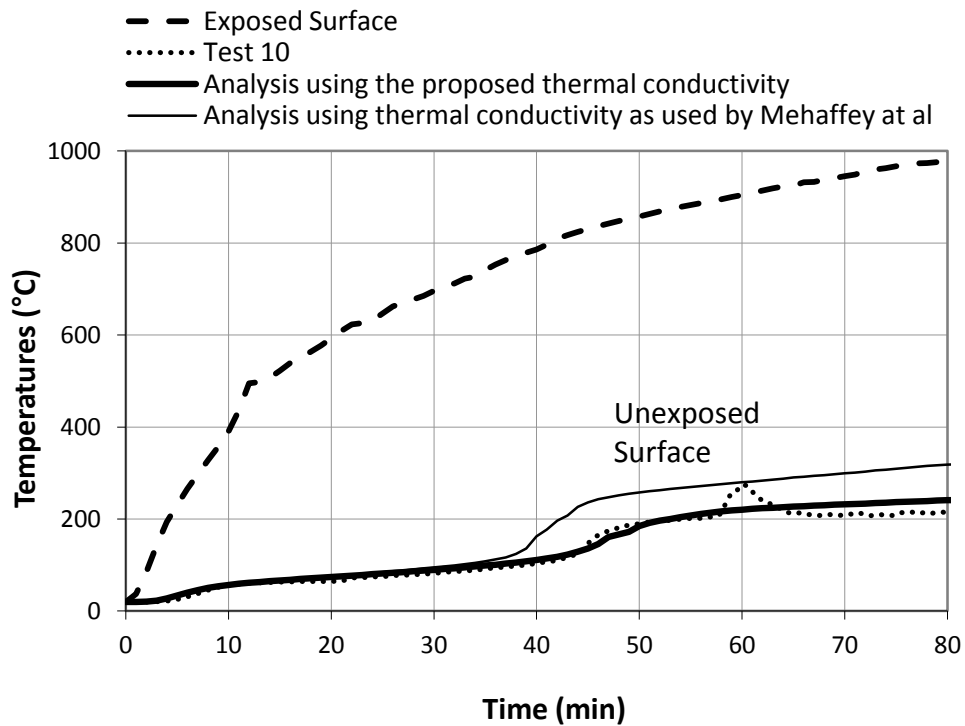


**Figure 4.11.** Temperature history for double layer of 9.5mm Wallboard gypsum panel (Test 10) – thermal conductivity model based on calibrated dry gypsum value

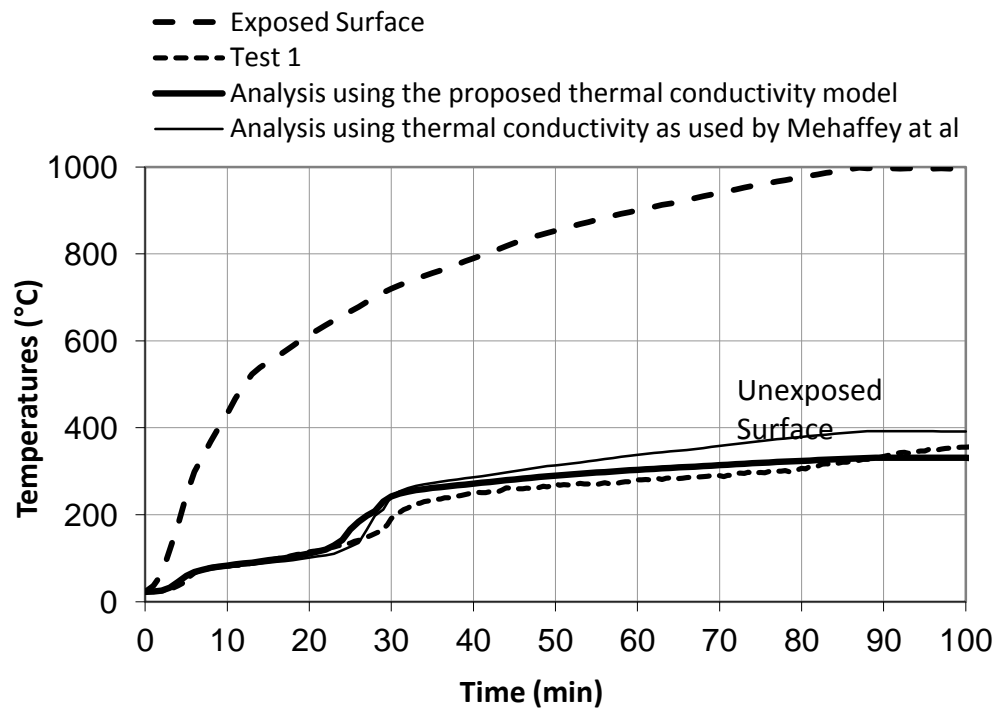


**Figure 4.12.** Temperature history for 12.5mm Fireline gypsum panel (Test 1) – thermal conductivity model based on HGP test results at 20°C and 220°C

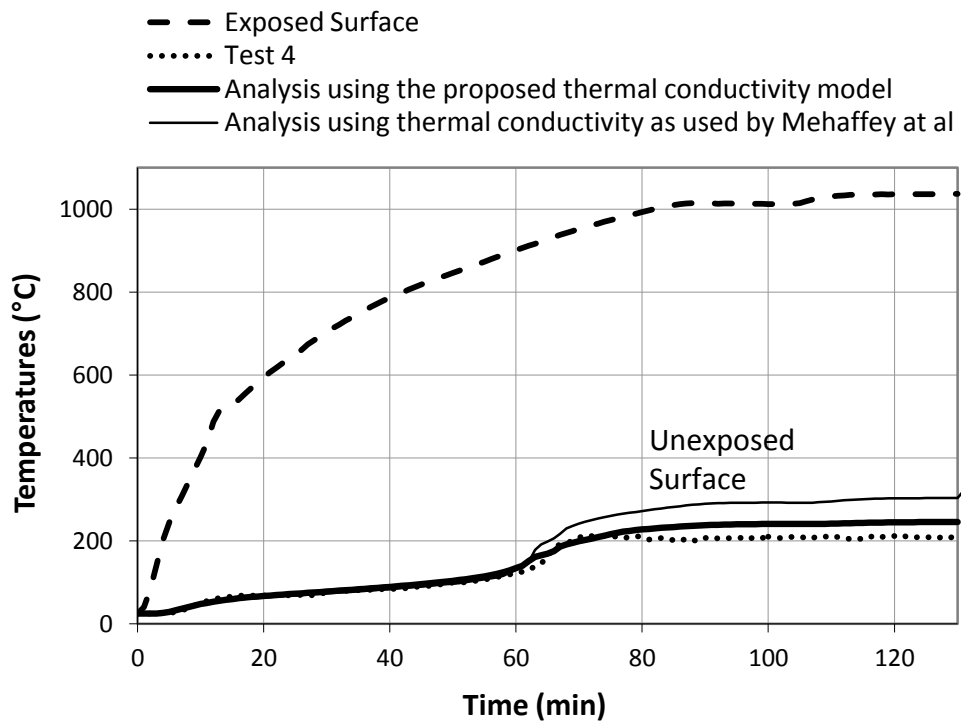


**Figure 4.13.** Temperature history for double layer of 12.5mm Fireline gypsum panel (Test 4)

– thermal conductivity model based on HGP test results at 20°C and 220°C

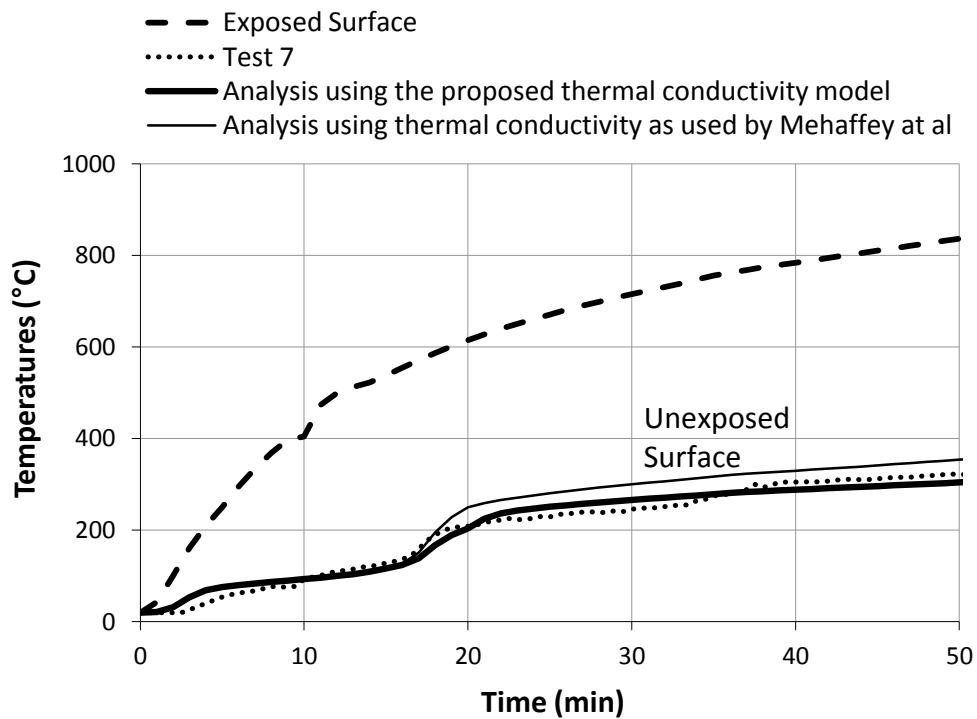


**Figure 4.14.** Temperature history for 9.5mm Wallboard gypsum panel (Test 7) – thermal conductivity model based on HGP test results at 20°C and 220°C

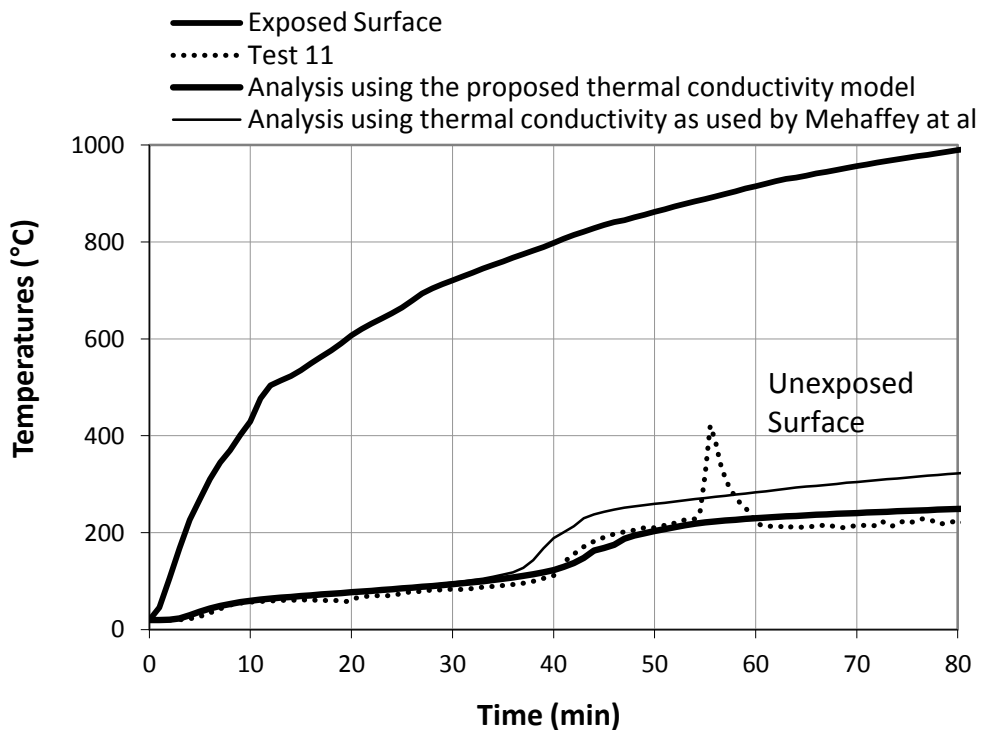


**Figure 4.15.** Temperature history for double layer of 9.5mm Wallboard gypsum panel (Test 11) – thermal conductivity model based on HGP test results at 20°C and 220°C

#### 4.5 Conclusions

A number of small-scale high temperature tests have been performed on two types of gypsum board products to provide experimental data for validation of the extraction method for thermal properties, primarily thermal conductivity of gypsum. It is confirmed that using the thermal property models of gypsum and the calibration method proposed in the previous chapter, the one-dimensional Finite Difference heat transfer program can predict gypsum temperatures in close agreement with the experimental results. Compared to the results obtained using the thermal conductivity values of gypsum by other established research studies, there was considerable improvement in the accuracy of the gypsum board temperature prediction results.

## **CHAPTER 5. Experimental Results of Temperature- Dependent Mechanical Properties of Gypsum**

### **5.1 Introduction**

Gypsum board fall-out in fire causes reduction in fire resistance of gypsum plasterboard wall assemblies by increasing the construction temperatures, and it is an important issue to be addressed in prediction methods. In order to facilitate the prediction of gypsum board fall-out in fire, the temperature-dependent mechanical properties of gypsum should be quantified.

Since there is very little data available on the mechanical properties of gypsum at elevated temperatures, a limited amount of elevated temperature mechanical property tests have been carried out, and this chapter reports on the obtained results. These tests were performed on different types of gypsum boards, and the measured results include coefficients of thermal expansion and shrinkage, mechanical strength and stress-strain relationships at various temperatures up to 800°C. This chapter will also present a proposed mechanical property model for later use in numerical modelling (CHAPTER 7).

### **5.2 Dilatometer Tests**

To measure the thermal expansion and shrinkage of the two types of British Gypsum board, Fireline and Wallboard, fourteen dilatometer tests were performed at British Gypsum's facility. Samples were 10 × 10 × 25mm and heated up to 1000°C with two heating rates of 5°C/min and 50°C/min as summarised in Table 5.1. All samples, except EL1 and EL2, were prepared in the lab using formulations of

the two board types and dried overnight at 40°C before testing. Samples EL1 and EL2 were made using British Gypsum's main plant mix of Fireline gypsum. Further details of the samples are reported in Appendix B.

Board type	Fireline Gypsum		Wallboard gypsum	
Heating rate	5 °C/min	50 °C/min	5 °C/min	50 °C/min
Samples	F1, F2, F3, EL1	F4, F5, F6, EL2	W1, W2, W3	W4, W5, W6

**Table 5.1.** Dilatometer gypsum board samples

The dilatometer used is a connecting rod dilatometer, where the samples are placed inside the furnace and a connecting rod transfers the thermal expansion of the samples to a strain gauge that measures the movements (Figure 5.1). The furnace used could not be programmed for variable heating rates; hence the aforementioned constant ones were chosen to examine the effects of heating rate on thermal expansion and shrinkage of the gypsum boards. Figures 5.2 and 5.3 present the dilatometer test results for Fireline and Wallboard gypsum boards, respectively.



**Figure 5.1.** The connecting rod dilatometer used for thermal expansion tests.

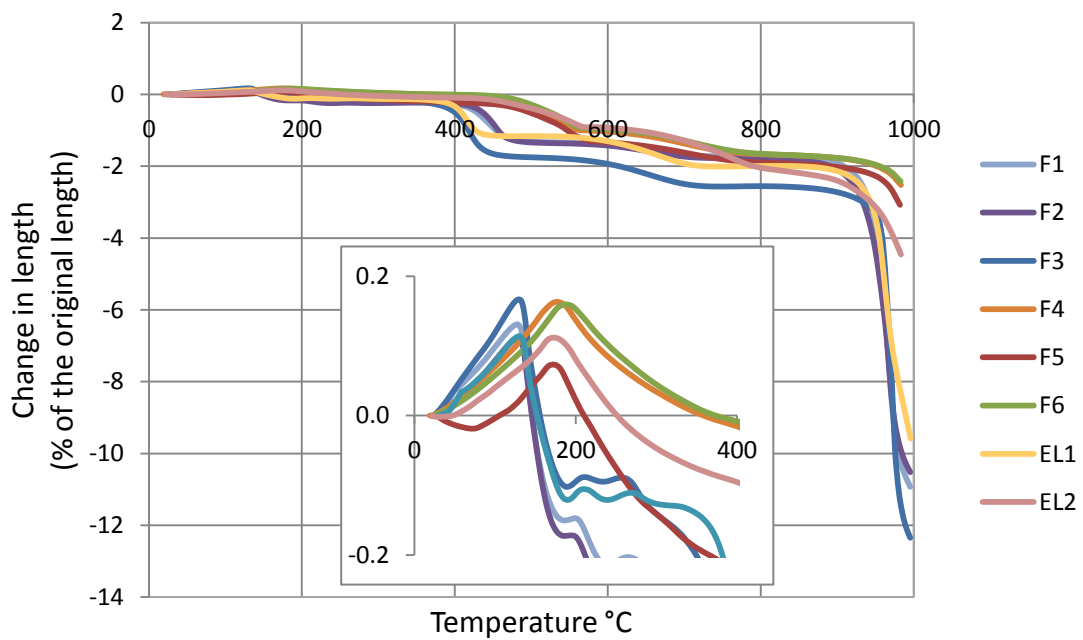


**Figure 5.2.** Dilatometer test results for Fireline gypsum board samples

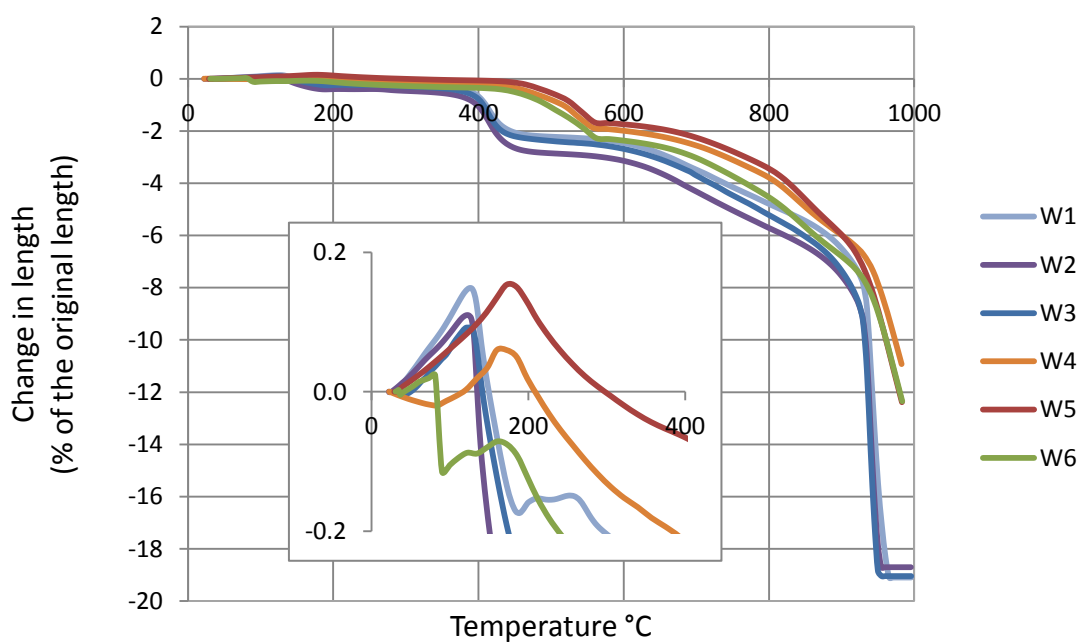


**Figure 5.3.** Dilatometer test results for Wallboard gypsum board samples

As can be observed from the results, gypsum expands slightly until 200°C and then shrinks with further temperature rise (negative expansion in the test results). There is a sudden increase in the shrinkage rate at just above 400°C for samples with the lower heating rate, and at 500°C for samples with the higher heating rate. The dilatometer test results for lab made Fireline gypsum and plant samples show no significant difference.

A comparison of the results for the Wallboard (Figure 5.3) and Fireline (Figure 5.2) gypsum boards highlights a considerably higher shrinkage rate above 600°C for the Wallboard gypsum.

### **5.3 High Temperature Three-Point Bending Tests**

Performing direct tensile tests on gypsum at high temperatures involves a number of complications, not only because tensile test machines with a furnace that provides heating for high temperatures are not easily available, but also due to the very brittle nature of gypsum, especially at high temperatures. Hence three-point bending tests were adopted to provide an alternative for determining the stress-strain relationship of gypsum at various temperatures.

#### **5.3.1 Experimental Set-Up**

The specimens tested were 300 × 100 × 12.5mm boards of Fireline and Wallboard gypsum. The samples were prepared in the British Gypsum lab using the two British Gypsum mix formulations. The wet gypsum was cast in metal moulds (no paper liner) and dried over night at 40°C before testing. Further details of the samples are included in Appendix B.

The three-point Bending tests were performed at nine different temperatures: 20°C (room temperature), 80°C, 180°C, 300°C, 400°C, 500°C, 600°C, 700°C and 800°C. Temperatures of 80°C and 180°C were chosen assuming that the former is before the first dehydration reaction and the latter is after the first but before the second dehydration reaction.

The bending test rig was placed inside an electric kiln, mounted on fire bricks. Figure 5.4 shows the experiment set-up. The specimens were positioned on the two parallel supports with rounded tips of a radius of 6mm and centred 200mm apart. Loading was applied by adding weights on a lightweight loading pan outside the kiln, hung from a 6mm steel rod that sat on the gypsum board at mid-span. Vertical displacement of the mid-span was measured using a transducer. To protect the transducer from heat, it was hung over the kiln and it measured the displacement of a ceramic rod which sat on the 6mm steel loading rod to transfer the displacement of test specimen at mid-span. The opening in the lid of the kiln was covered by a 50mm insulation board. The ceramic rod passed through a fitted hole in the insulation board, while it was allowed to move freely in the vertical direction. The loading arrangement weighed about 200g before any weights were added on the load pan.

Type K thermocouples were attached to the gypsum board on the surface and inside the thickness (approximately halfway through) outside the bending span to measure the temperature rise in the gypsum specimen. The specimen was heated with the maximum heating rate possible up to the selected temperature and was kept at that temperature for an hour to ensure that a steady-state condition was achieved. Loading was then applied steadily until failure (when the gypsum board could not carry any more loads and broke). The average loading rate of the tests were in the range of 2 to 20 N/min with a mean of about 7N/min.

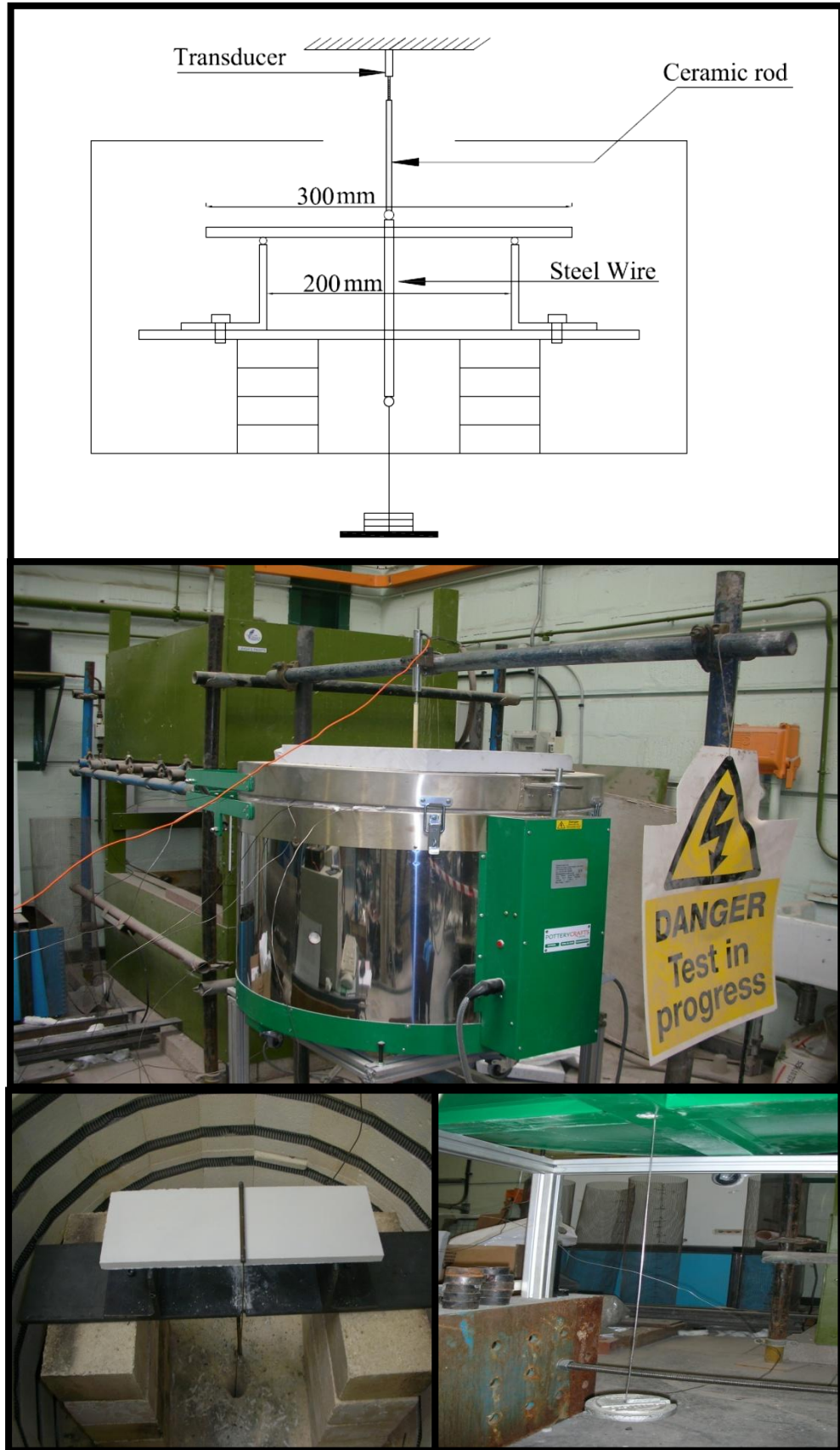


**Figure 5.4.** Set-up of the three-point bending tests

### 5.3.2 Test Results and Discussions

A total of 30 bending tests have been performed on gypsum board specimens. Tests at each steady-state temperature were repeated twice and proved to be fairly reproducible, especially up to 500°C. The load-deflection results are demonstrated in Figures 5.5 to 5.7. The results include an initial load that accounts for both the weight of the loading arrangement (2N) and the self-weight of the gypsum boards within the span. In later analysis, the uniformly distributed self-weight of the specimens are approximated by an equivalent point-load at the mid-span that results in the same deflection as the distributed load. This value amounts to about 1N.

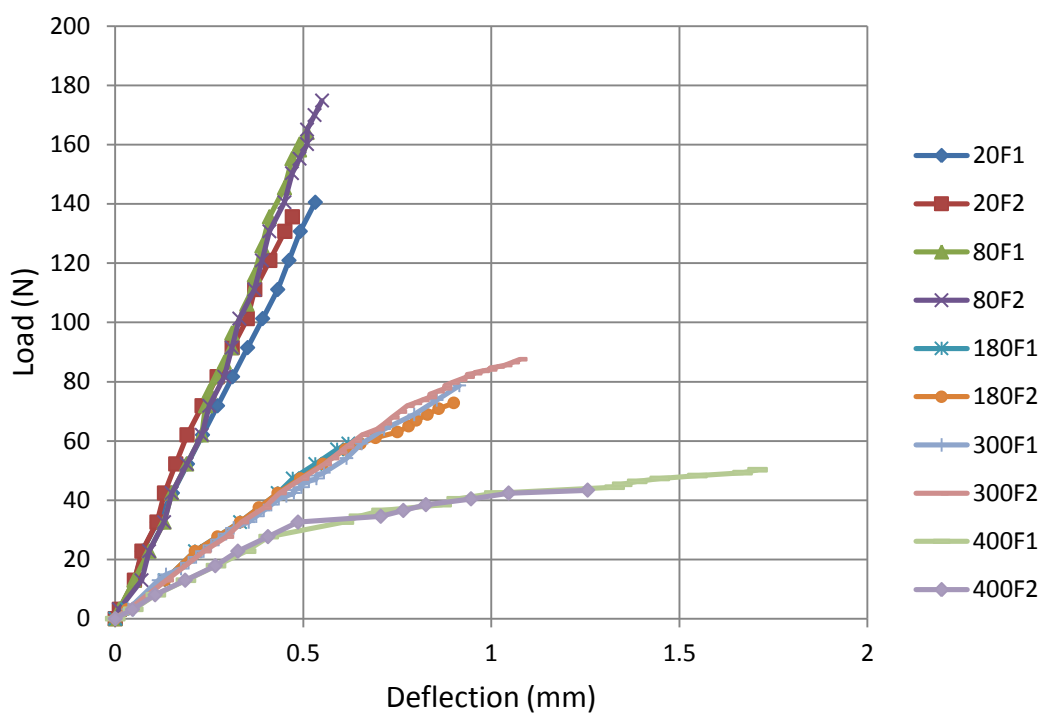


**Figure 5.5.** Three-point bending test results for Fireline gypsum panels at 20°C to 400°C

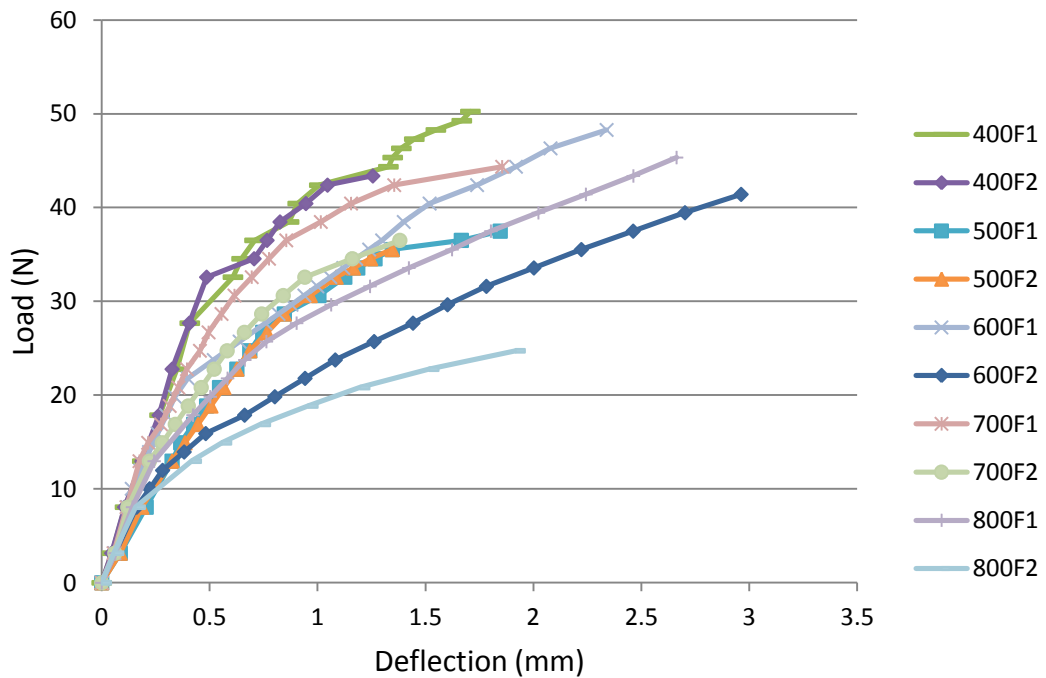


**Figure 5.6.** Three-point bending test results for Fireline gypsum panels at 400°C to 800°C

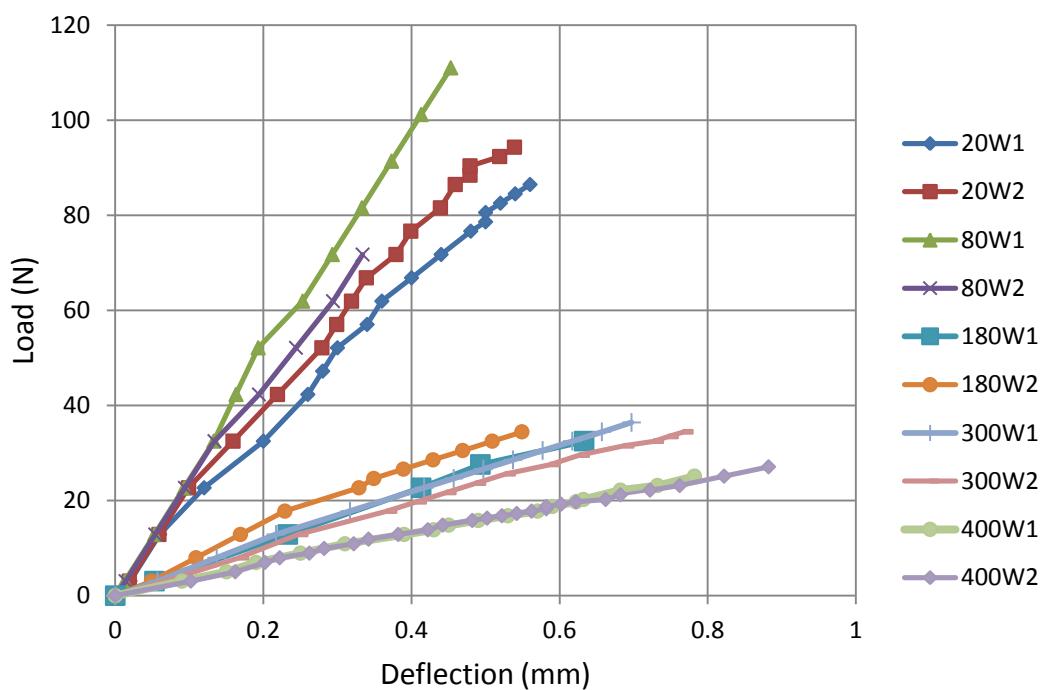


**Figure 5.7.** Three-point bending test results for Wallboard gypsum panels at 20°C to 400°C

Observation of the test specimens suggests tensile failure in all cases, i.e. when the test specimen failed to carry more load above the maximum, there were wide cracks on the tension side (the lower part) of the test specimen near the centre.

The stress-strain behaviour of both gypsum board types up to 300°C can be well defined by a linear relationship. Although the strength and stiffness of both gypsum board types increase slightly when heated from room temperature to 80°C, they drop considerably with further temperature rise, due to water evaporation and calcination of gypsum.

The linear load-deflection behaviour continues for Wallboard gypsum up to about 470°C. For Fireline boards, the stress-strain relationship becomes evidently nonlinear at higher temperatures (Figure 5.6). The nonlinear behaviour of Fireline gypsum above 300°C is a direct result of the glass fibre reinforcement that holds the board together in tension, resulting in increased ductility and flexural strength of the gypsum substrate.

### **5.3.3 Approximate Analysis of Stress-Strain Relationship of Gypsum at Elevated Temperatures**

Where experimental load-deflection curves are linear, the modulus of elasticity, flexural stress and strain can be calculated using simple beam theory for the test set-up (Al Nageim et al., 2003) to give:

$$\sigma_f = \frac{3PL}{2bd^2} \quad , \quad \varepsilon_f = \frac{6Dd}{L^2} \quad , \quad E_f = \frac{L^3m}{4bd^3}$$

where

$\sigma_f$  is stress in outer fibres at midpoint, (MPa)

$\varepsilon_f$  is strain in outer fibres at midpoint, (mm/mm)

$E_f$  is flexural modulus of elasticity,(MPa)

$P$  is load at a given point on the load deflection curve, (N)

$L$  is support span, (mm)

$b$  is width of test panel, (mm)

$d$  is depth of test panel, (mm)

*D* is the deflection of the centre of the beam, (mm)

*m* is the slope of the load deflection curve, (N/mm)

The above mechanical properties of all Wallboard panels can therefore be calculated easily, and the results are summarized in Table 5.2.

Temperature (°C)	20	80	180	300	400
Failure Load (N)	90.4	101.2	36.9	35.9	26.1
Maximum Deflection (mm)	0.52	0.44	0.62	0.73	0.83
Slope of Load-Deflection Curve (N/mm)	174.4	231.4	59.9	49.5	31.9
Elastic Modulus (MPa)	1573	1964	518	575	394
Stress at Failure (MPa)	1.607	1.728	0.643	0.751	0.568
Strain at Failure	0.001022	0.000879	0.001240	0.001306	0.001444

**Table 5.2.** Mechanical properties of Wallboard gypsum panels at different temperatures

The modulus of elasticity, flexural stress and strain of Fireline panels up to 300°C can also be calculated using the same linear beam theory and the results are presented in Table 5.3.

Temperature (°C)	20	80	180	300
Failure Load (N)	140.5	171.4	67.9	86.1
Maximum Deflection (mm)	0.50	0.55	0.70	0.97
Slope of Load-Deflection Curve (N/mm)	279.3	313.3	97.6	88.8
Elastic Modulus (MPa)	2378	2797	875	792
Stress at Failure (MPa)	2.401	3.014	1.198	1.513
Strain at Failure	0.001010	0.001078	0.001369	0.001909

**Table 5.3.** Mechanical properties of Fireline gypsum panels at 20°C to 300°C

The nonlinear behaviour of Fireline gypsum boards above 300°C cannot be quantified by using linear elastic beam theory and determination of their mechanical properties becomes more complicated. The load-deflection curves suggest that a bilinear stress-strain relationship may be sufficient for defining the mechanical behaviour at these elevated temperatures. Based on this assumption, the following procedure may be used to determine the stress-strain relationship.

Assuming the stress-strain relationship is as shown in Figure 5.8 , the consequent load-deflection curve at the mid-point of the beam under the three-point bending test will be similar to the curve illustrated in Figure 5.9.. Note that there are four variables in the stress-strain relationship that need to be determined, namely  $\sigma_0$ ,  $\sigma_1$ ,  $\varepsilon_0$  and  $\varepsilon_1$ .

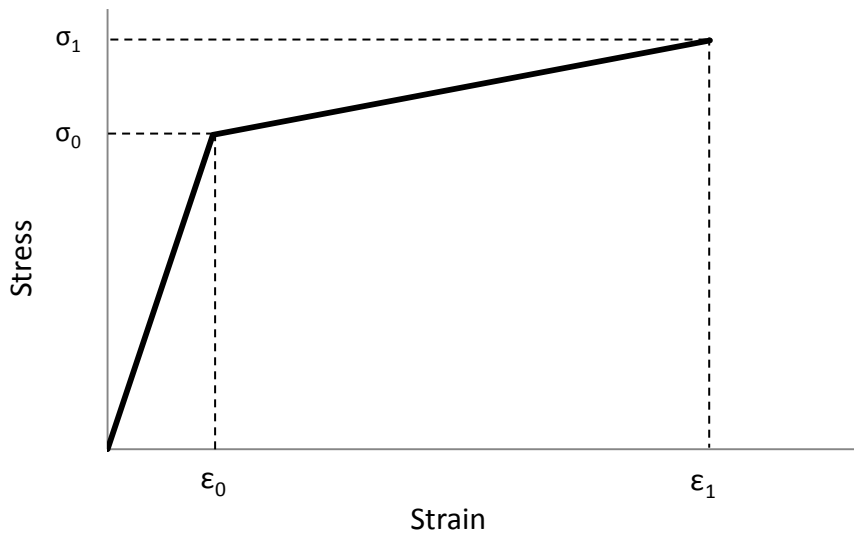


**Figure 5.8.** Bilinear stress-strain relationship

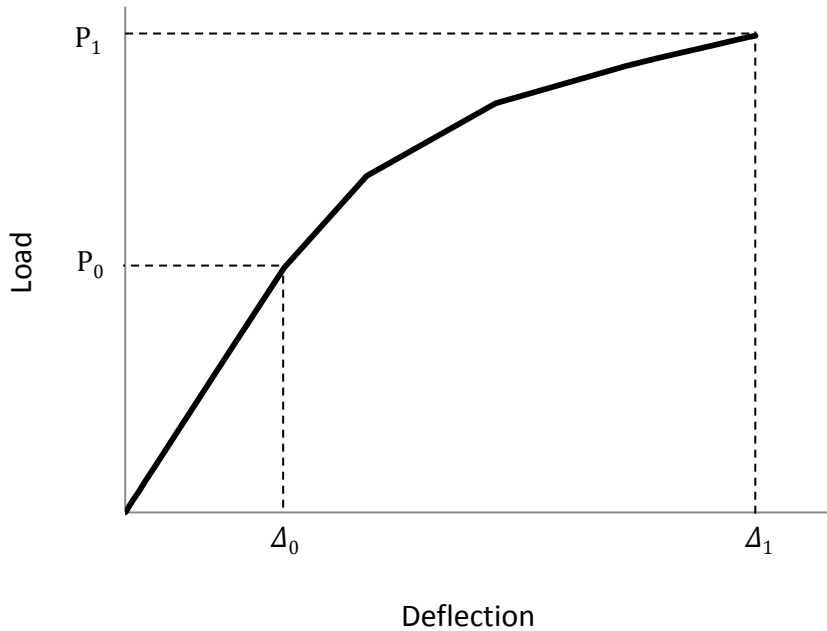


**Figure 5.9.** Typical load-deflection curve for a material with bilinear stress-strain relationship under three-point bending

The initial linear part of the load-deflection curve corresponds to the linear elastic response of the beam, i.e. when no point along the beam has reached the yield stress,  $\sigma_0$ . Therefore  $P_0$  in Figure 5.9 is the load at which the outer surfaces of the mid-point section just reach the stress  $\sigma_0$ , and hence, the linear elastic beam theory can be applied to determine  $\sigma_0$  and  $\varepsilon_0$ :

$$\sigma_0 = \frac{3P_0L}{2bd^2} , \quad \varepsilon_0 = \frac{6\Delta_0d}{L^2} \quad (5.1)$$

where all the parameters are as defined earlier in this chapter.

After the initial yield, the stresses near the centre of the beam exceed the elastic range. However, not all sections along the beam have reached their yield stress; sections near the supports are still under the elastic stress range. Assuming the elastic zone is between  $x = 0$  to  $x = x_0$ , where  $x$  is the coordinate along the beam from the supports, the internal bending moment at  $x = x_0$  is:

$$M_{x_0} = \sigma_0 \left( \frac{bd^2}{6} \right)$$

Knowing that the applied bending moment on the beam increases linearly from the support to the midpoint,  $x_0$  can be calculated using the following expression:

$$x_0 = \frac{M_{x_0}}{\left(\frac{P_1 L}{4}\right)} \left(\frac{L}{2}\right) = \frac{bd^2 \sigma_0}{3P_1}$$

The deflection curve of the beam can be determined through double integration of the curvature curve, assuming that deflections are small. The curvature of the beam at any section is defined as:

$$\varphi = \frac{2\varepsilon_{max}}{d}$$

where  $\varphi$  is the section curvature and  $\varepsilon_{max}$  is the maximum strain in the section at the outer surfaces.

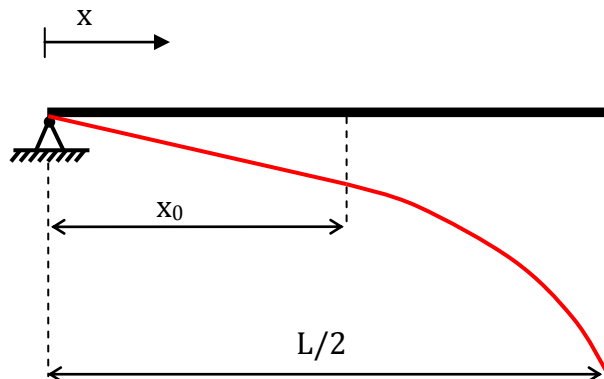


**Figure 5.10.** Curvature change along the three-point bending specimen at the onset of failure

Consider half of the three-point bending beam in Figure 5.10, the curvature of the beam increases linearly from  $x = 0$  to  $x = x_0$ , but nonlinearly from  $x = x_0$  to  $x = L/2$  due to the effects of plastic deformations. This unknown nonlinear change in curvature within the centre zone of the beam can be approximated by a linear or parabolic relationship. A parabolic relationship seems to be more realistic, since the curvature should increase even more rapidly towards the centre of the beam.

Based on a parabolic change in curvature distribution, the change in curvature along the beam can be expressed as:

$$\varphi(x) = \begin{cases} \frac{2\varepsilon_0}{dx_0}x & 0 \leq x \leq x_0 \\ a_1(x - x_0)^2 + a_2(x - x_0) + a_3 & x_0 < x \leq \frac{L}{2} \end{cases}$$

Note that there are three variables in the expression of  $\varphi$  that need to be determined, namely  $a_1$ ,  $a_2$  and  $a_3$ . The three input conditions necessary for the determination of the three unknowns are: continuity at  $x = x_0$  (curvature and its derivative), and the measured deflection at  $x = \frac{L}{2}$ . Assuming that the parabolic curvature curve is continuous and tangential to the linear part at  $x = x_0$ , and knowing the curvature at mid-point in terms of the material strain limit  $\varepsilon_1$ , these variables can be determined as shown below:

$$\varphi(x_0) = \frac{2\varepsilon_0}{d} \Rightarrow a_3 = \frac{2\varepsilon_0}{d}$$

$$\varphi'(x_0) = \frac{2\varepsilon_0}{dx_0} \Rightarrow a_2 = \frac{2\varepsilon_0}{dx_0}$$

$$\varphi\left(\frac{L}{2}\right) = \frac{2\varepsilon_1}{d} \Rightarrow a_1 = \frac{2\left[\varepsilon_1 - \varepsilon_0 - \frac{\varepsilon_0}{x_0}\left(\frac{L}{2} - x_0\right)\right]}{d\left(\frac{L}{2} - x_0\right)^2}$$

Single integration of the curvature yields the slope of the beam,  $\theta(x)$ , as expressed below:

$$\theta(x) = \begin{cases} \frac{\varepsilon_0}{dx_0}x^2 + C_1 & 0 \leq x \leq x_0 \\ \frac{2}{d}\left[\frac{\varepsilon_1 - \frac{\varepsilon_0 L}{2x_0}}{3\left(\frac{L}{2} - x_0\right)^2}(x - x_0)^3 + \frac{\varepsilon_0}{2x_0}x^2\right] + C_2 & x_0 < x \leq \frac{L}{2} \end{cases}$$

where  $C_1$  and  $C_2$  are constants of integration. Continuity of the slope at  $x = x_0$  requires that  $C_1 = C_2$  and symmetry requires the slope at the midpoint of the beam to be zero, hence:

$$C_2 = \frac{1}{12d} \left[ 4\varepsilon_1(2x_0 - L) - \varepsilon_0 \left( 4L + \frac{L^2}{x_0} \right) \right]$$

In turn, integration of the slope curve yields the deflection of the beam,  $\delta(x)$ , as expressed below:

$$\delta(x) = \begin{cases} \frac{\varepsilon_0}{3dx_0}x^3 + C_1x + C_3 & 0 \leq x \leq x_0 \\ \frac{2}{d} \left[ \frac{\varepsilon_1 - \frac{\varepsilon_0 L}{2x_0}}{12 \left( \frac{L}{2} - x_0 \right)^2} (x - x_0)^4 + \frac{\varepsilon_0}{6x_0}x^3 \right] + C_2x + C_4 & x_0 < x \leq \frac{L}{2} \end{cases} \quad (5.2)$$

where  $C_3$  and  $C_4$  are constants of integration.  $C_3$  can be determined applying the boundary condition at the support:

$$\delta(0) = 0 \quad \Rightarrow \quad C_3 = 0$$

and continuity of the deflection curve at  $x = x_0$  requires that  $C_4 = 0$ .

Finally, substituting the measured deflection of the midpoint ( $\Delta_1$ ) into Eq. (5.2) for the deflection of the beam and rearranging it will yield the following expression for the maximum strain:

$$\varepsilon_1 = \frac{24\Delta_1 d + \varepsilon_0 \left[ \frac{L^3}{2x_0} + 2x_0 L + 2L^2 \right]}{4x_0^2 + 4x_0 L - 3L^2} \quad (5.3)$$

For calculation of the limit stress, consider the midpoint section of the three-point bending specimen just before failure. Assuming that plane sections remain plane after bending, the stress and strain distributions across the thickness of the section at the mid-point of the beam are shown in Figure 5.11.

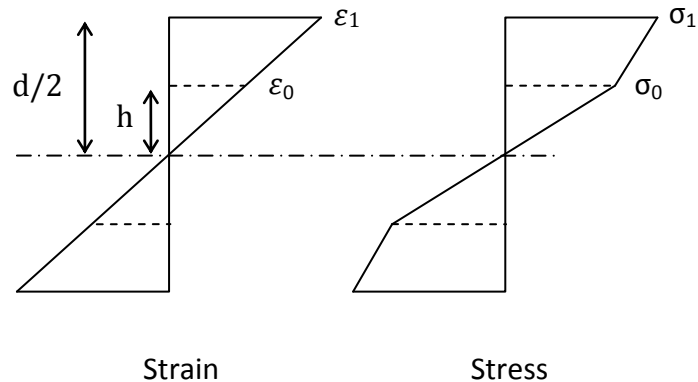


**Figure 5.11.** Stress and strain distributions across the thickness of the three-point bending specimen under the failure load

Static equilibrium requires the applied bending moment at the mid-point to be equal to the resisting moment at this section:

$$\frac{PL}{4} = 2b \left[ \left( \frac{\sigma_0 h}{2} \right) \left( \frac{2h}{3} \right) + \sigma_0 \left( \frac{d}{2} - h \right) \left( \frac{d+2h}{4} \right) + (\sigma_1 - \sigma_0) \left( \frac{d-2h}{4} \right) \left( \frac{d+h}{3} \right) \right]$$

$$\text{where } h = \left( \frac{\varepsilon_0}{\varepsilon_1} \right) \frac{d}{2}$$

The solution to the above equation gives  $\sigma_1$  as:

$$\sigma_1 = \frac{\frac{3PL}{bd^2} - \sigma_0 \left( 1 + \frac{\varepsilon_0}{\varepsilon_1} \right)}{2 - \frac{\varepsilon_0}{\varepsilon_1} - \frac{\varepsilon_0^2}{\varepsilon_1^2}} \quad (5.4)$$

Therefore, using Eqs. (5.1) to (5.4), the bilinear strain-stress relationship of Fireline gypsum at temperatures above 300°C can be derived based on the three-point bending experimental load-deflection curves. The extracted stress-strain curves are presented in Figure 5.12.

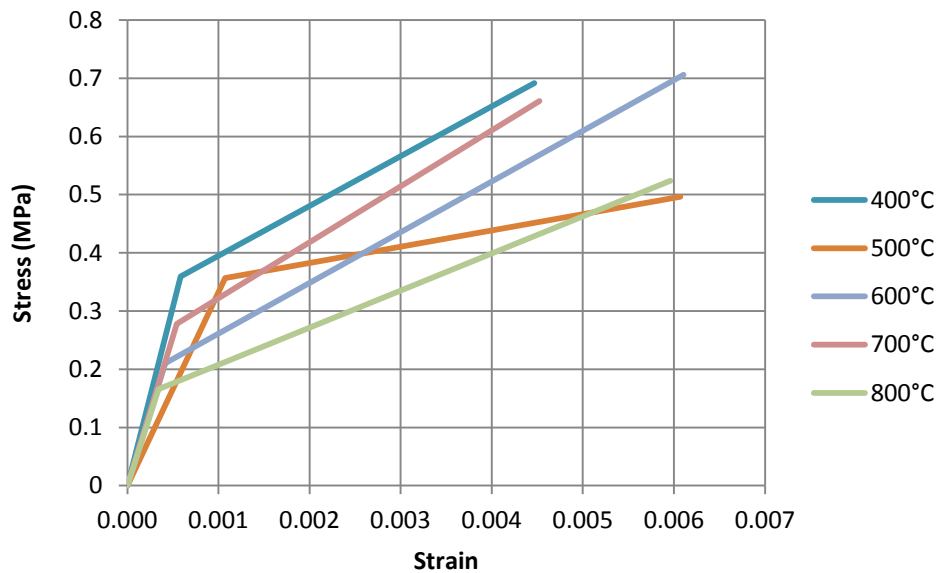


**Figure 5.12.** Bilinear stress-strain curves for Fireline gypsum at 400°C to 800°C

It can be observed that the stiffness of gypsum continues the decreasing trend up to 500°C, but interestingly, both the elastic and plastic stiffness increase from 500°C to 600°C and remain approximately unchanged up to 800°C. This increase in stiffness, although small, can be explained by the behaviour of glass fibres in Fireline gypsum. The glass fibres used in the plasterboards are E-glass, which has a softening (melting) point of about 1300°C. The glass transition temperature is around 550°C, and at temperatures around this value, chemical changes such as incorporation of more Ca-ions (from the surrounding gypsum) will start and will act as a catalyst for further transformations. Glass filaments (about 15 µm in diameter) have a very high surface to volume ratio. This means that conversion of the filaments to other shapes and/or to other substances (silicates, oxides) happen very rapidly, especially at temperatures around 600-800°C. The changed composition of the filaments acts as glue for the anhydrite sintering structure, exhibiting as increased stiffness at temperatures above 500°C.

### 5.3.4 ABAQUS Modelling of the Three-Point Bending Tests

In the previous section, the stress-strain curves for Fireline gypsum above 300°C, were extracted from the results of three-point bending tests based on bilinear stress-strain relationship and an assumed curvature distribution. To check the validity of these assumptions, the same three-point bending tests have been modelled using ABAQUS with the extracted stress-strain relationships. A simply supported beam model was built using beam elements of 2mm size and a point load was applied at the midpoint of the beam. The average dimensions of the test specimens and the extracted stress-strain curves were input into the model and the load-deflection curves were predicted using ABAQUS. The numerical results are compared with the experimental load-deflection curves in Figures 5.13 to 5.17. There is excellent agreement between the numerical and experimental results, confirming the validity of the theoretical technique proposed in the section 5.3.3.

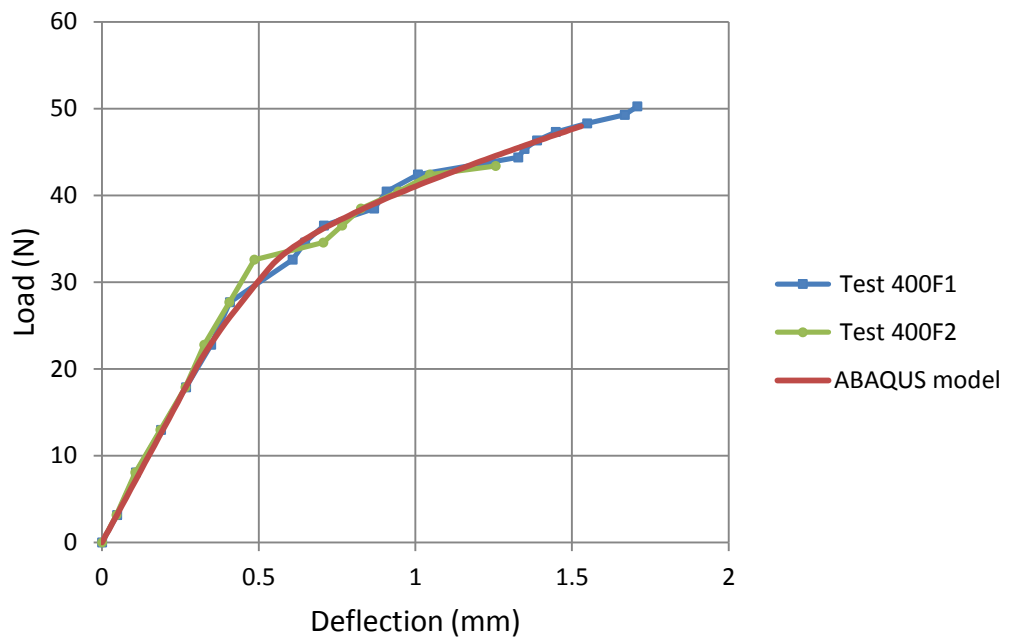


**Figure 5.13.** Comparison of load-deflection curves for Fireline gypsum at 400°C by theory and experiment

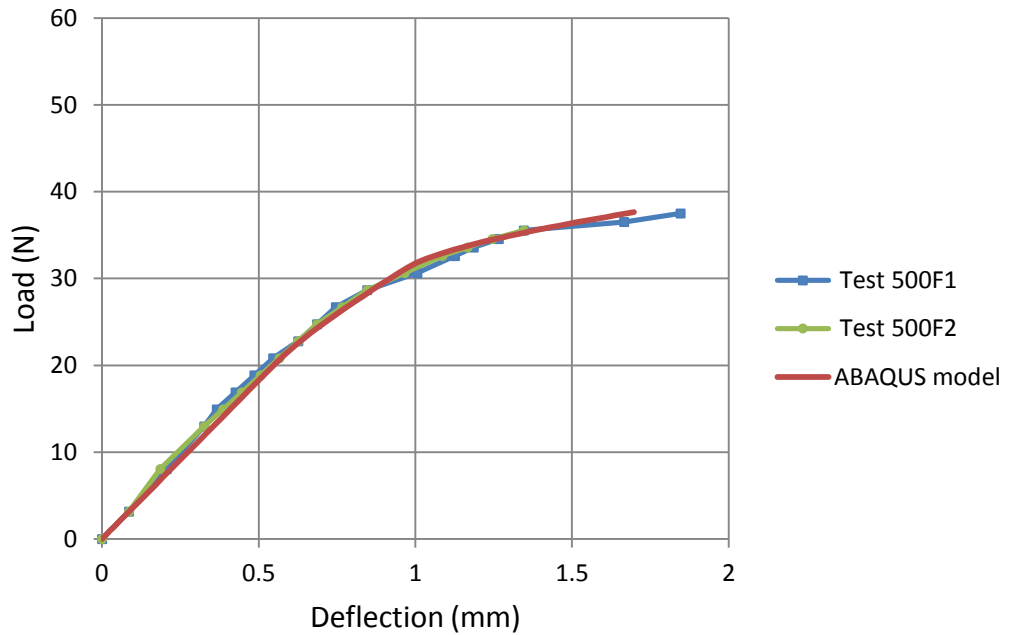


**Figure 5.14.** Comparison of load-deflection curves for Fireline gypsum at 500°C by theory and experiment

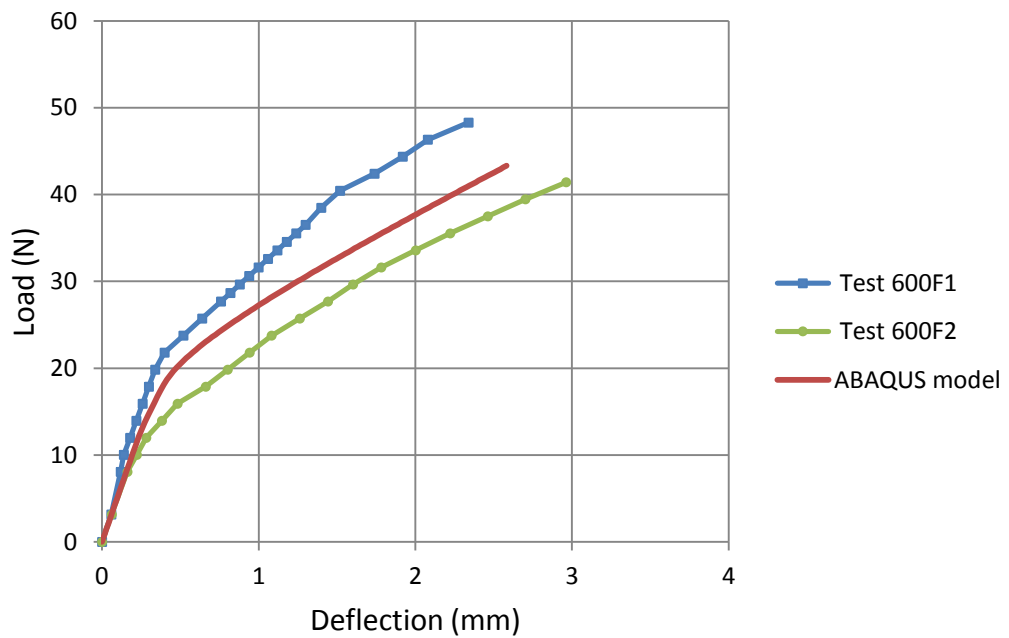


**Figure 5.15.** Comparison of load-deflection curves for Fireline gypsum at 600°C by theory and experiment

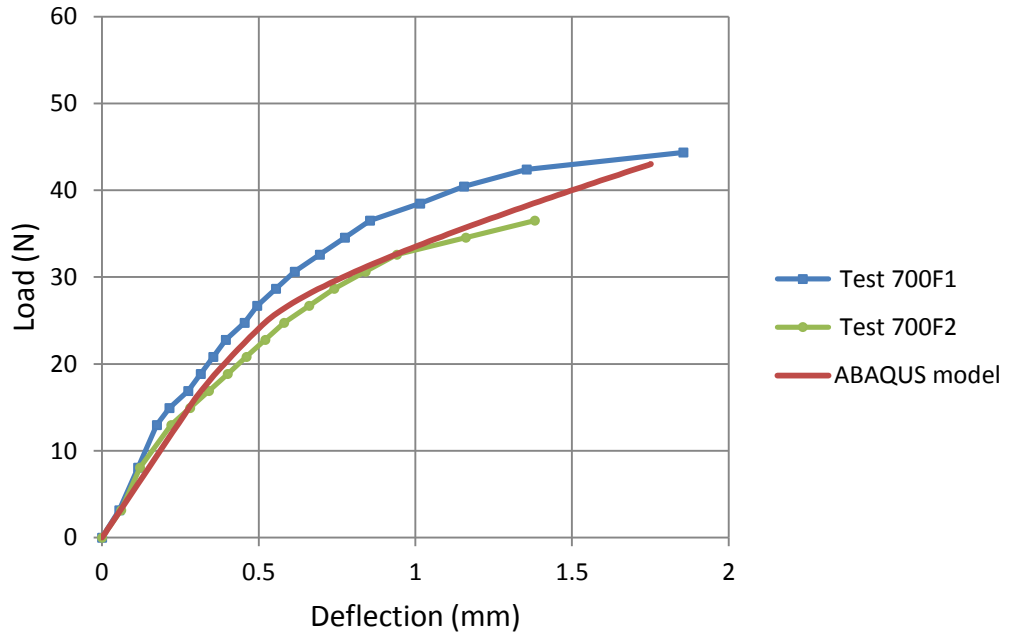


**Figure 5.16.** Comparison of load-deflection curves for Fireline gypsum at 700°C by theory and experiment

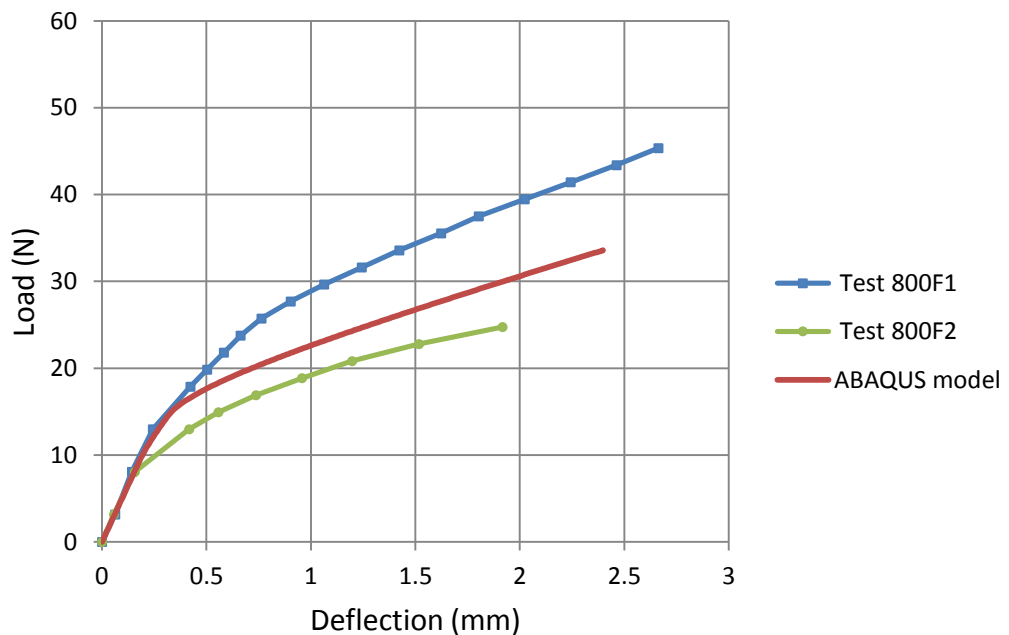


**Figure 5.17.** Comparison of load-deflection curves for Fireline gypsum at 800°C by theory and experiment

#### **5.4 Gypsum Prism Compression Tests**

Due to unavailability of a compression test apparatus that can operate at elevated temperatures, an alternative approach was adopted. Gypsum prisms of  $20 \times 20 \times 100\text{mm}$  were prepared in the British Gypsum lab using Wallboard gypsum composition. The prisms were heated for an hour at different temperatures and then cooled down in the kiln. Loading was applied when the prisms were cooled down to room temperatures. Three-point bending tests were also performed on identical gypsum prisms using the same method of heating to enable direct comparison of the compression and flexural strength. Detailed data of the prisms are provided in Appendix B. Figure 5.18 summarises the results.

It is evident that both the bending and compressive strengths of gypsum drop considerably after the first dehydration reaction has taken place, confirming the results from the three-point bending tests of the boards. It should be noted that comparison of the flexural strength from the prism tests and the three-point bending tests on gypsum boards is erroneous for a number of reasons: firstly, the density of the gypsum prisms are about 35% higher than that of the gypsum boards; secondly, the heating method is different for the two tests and finally, the effect of shear on the bending strength of gypsum prisms is considerable given the shorter span of the prisms as compared to their thickness. Nevertheless, the direct comparison between the flexural and compressive strengths of gypsum prisms confirms that gypsum is much stronger in compression than in tension. In the numerical investigations to be reported in CHAPTER 7, it will be conservatively assumed that the tensile and compressive strength of gypsum are the same.

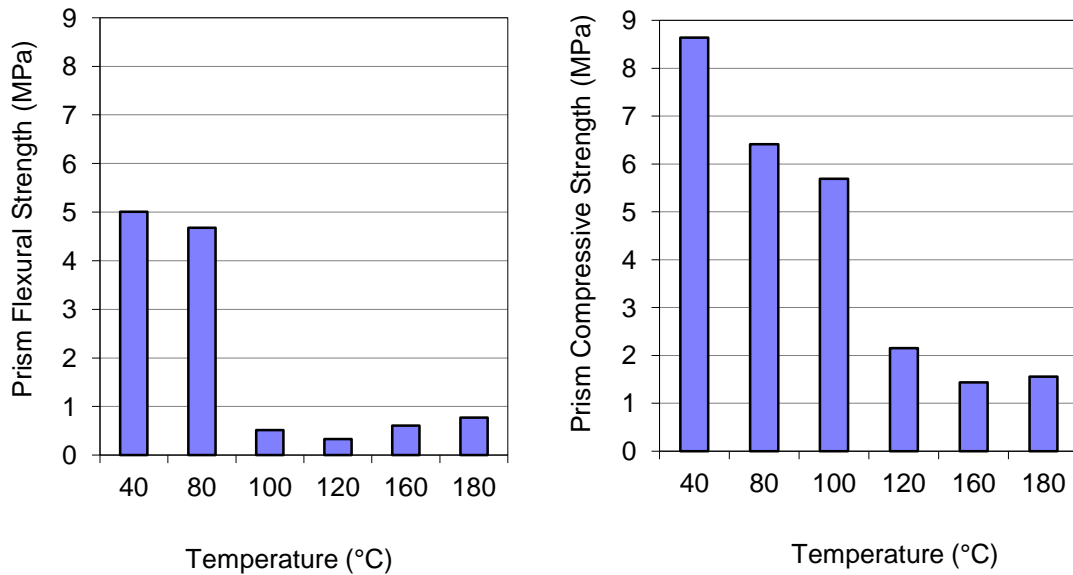


**Figure 5.18.** Comparison of bending and compressive strength of gypsum prisms at temperatures up to 180°C.

## 5.5 Conclusions

This chapter reports the results of a series of mechanical tests performed on different types of gypsum boards to extract their thermal expansion and shrinkage, mechanical strength and stress-strain relationship at various temperatures up to 800°C.

Dilatometer tests were used to measure the thermal expansion and shrinkage. The results show that both glass fibre-reinforced and standard gypsum boards mainly shrink when exposed to high temperatures. A simple three-point bending test set-up was used to measure the load-deflection relationships of gypsum at high temperatures, from which the stress-strain relationships of gypsum at different temperatures were derived based on assumptions of the stress-strain relationship shape (linear to 300°C and bilinear at higher temperatures for Fireline gypsum, linear to 500°C for Wallboard gypsum) and curvature distribution along the beam. The extracted stress-strain relationships are summarised in Tables 5.2 and 5.3 and Figure 5.12. ABAQUS simulations of the three-point bending tests using the indirectly extracted stress-strain relationships show that these stress-strain

relationships can be used to give accurate predictions of the measured load-deflection curves.

A limited number of compression tests were also performed and the results indicate that the compression strength of gypsum was much greater than its tensile strength.

The quantified mechanical properties will be used in finite element simulations to develop thorough understanding of the structural behaviour of gypsum at high temperatures, particularly to predict the formation of cracks.

## **CHAPTER 6. Medium-Scale Fire Tests and Gypsum Fall-Off in Fire**

### **6.1 Introduction**

Insulation and integrity of gypsum board assemblies are significantly affected by gypsum falling off in fire. In order to investigate this phenomenon, some medium-scale fire tests have been designed and performed for Wallboard and Fireline gypsum boards. This chapter provides the details of the tests and reports on the observation of any gypsum falling off. Also presented in detail are some Canadian tests performed on wall assemblies of different arrangements. The results of the tests presented here are used in CHAPTER 7 to validate the proposed numerical analysis.

### **6.2 Experimental Set-Up**

A total of 12 medium-scale fire tests have been performed on 1000x1000mm non-loaded wall assemblies, lined with Fireline or Wallboard gypsum. The assemblies were exposed to furnace temperature on one side and to ambient temperature of 19-25°C on the other. Furnace temperature was controlled to follow the standard cellulosic fire curve introduced in BS476 (BSI, 1987). The pressure of the furnace was set to be controlled at  $16.2 \pm 2$  Pa relative to the atmosphere pressure. A video camera was positioned to the room side of the assemblies to record the tests as observed from the unexposed side. A small window in the opposing furnace wall allowed a limited view of the exposed side of the assembly. Observations of the exposed side were taken every 10-15 minutes. Some examples of such observations are presented in Appendix C.

The tests were performed at The Building Test Centre in East Leake. The metal components of the tests (manufactured from galvanised mild steel) and the plasterboards were supplied by British Gypsum (British-Gypsum, 2009). Six test arrangements (T1 to T6) were designed to include the effects of different boundary conditions and temperature profiles across the thickness of the wall assemblies:

- Boundary condition: In tests T1, T2, T5 and T6 (shown in Figures 6.1 and 6.4), the boards were extended over two spans of studs and were screwed to the studs. The screws were spaced at 300mm. While in tests T3 and T4 (Figure 6.3), the boards were slotted in between the studs with no screw fixings.
- Insulation: In tests T2, T4 and T6, three layers of 25mm Isover APR (supplied by The Building Test Centre) were fitted at the back of the gypsum boards to provide insulation.
- Plasterboard layers: The wall assemblies in tests T1 to T4 were lined with a single layer of plasterboard, whereas the assemblies in tests T5 and T6 included two layers of plasterboard.

The above arrangements were repeated for both Wallboard and Fireline gypsum, cut from 2400 (long) x 1200 (wide) boards. The boards were positioned vertically in all tests, i.e. the machine direction of the face paper of the boards was vertical. Table 6.1 summarises the specification of the twelve tests. Further details of the test arrangements are provided in the following sections.

Test No.	Plasterboard type	No. of plasterboard layers	Insulation	No. of spans	Screw fixing of the boards to the studs
T1W	Wallboard	1	None	2	Yes
T1F	Fireline	1	None	2	Yes
T2W	Wallboard	1	75mm Isover APR	2	Yes
T2F	Fireline	1	75mm Isover APR	2	Yes
T3W	Wallboard	1	None	1	No
T3F	Fireline	1	None	1	No
T4W	Wallboard	1	75mm Isover APR	1	No
T4F	Fireline	1	75mm Isover APR	1	No
T5W	Wallboard	2	None	2	Yes
T5F	Fireline	2	None	2	Yes
T6W	Wallboard	2	75mm Isover APR	2	Yes
T6F	Fireline	2	75mm Isover APR	2	Yes

**Table 6.1.** Specifications of the medium-scale fire tests on gypsum board wall assemblies

### 6.2.1 Experiments T1 and T2

Figure 6.1 shows the wall assemblies in tests T1 and T2, and the positions of the thermocouples and the transducers. In each test, the specimen was constructed in a concrete lined restraint frame that formed one of the vertical walls of the furnace. 0.5mm thick Gypframe 72C50 Channel was fixed to the head and base of the test frame using 60mm fire resistant fixings at 300mm centres, leaving a 25mm gap at each end. 25mm thick Rockwool Firebatt was positioned vertically at each end of the test frame to create two free ends of the test specimen. Gypframe 70S50 'C' studs were positioned at each end of the channel and one centrally within the test frame. The framework was clad with a single layer of 12.5mm Gyproc Fireline or Gyproc Wallboard on the fire side, leaving the studs uncovered on the non-fire side.

The board was fixed to all studs at 300mm centres using Gyproc drywall screws, and all screw heads were sealed with Gyproc Joint Filler. In test T2, three layers of 25mm Isover APR was fitted between the studs on the non-fire side.

### Tests T1

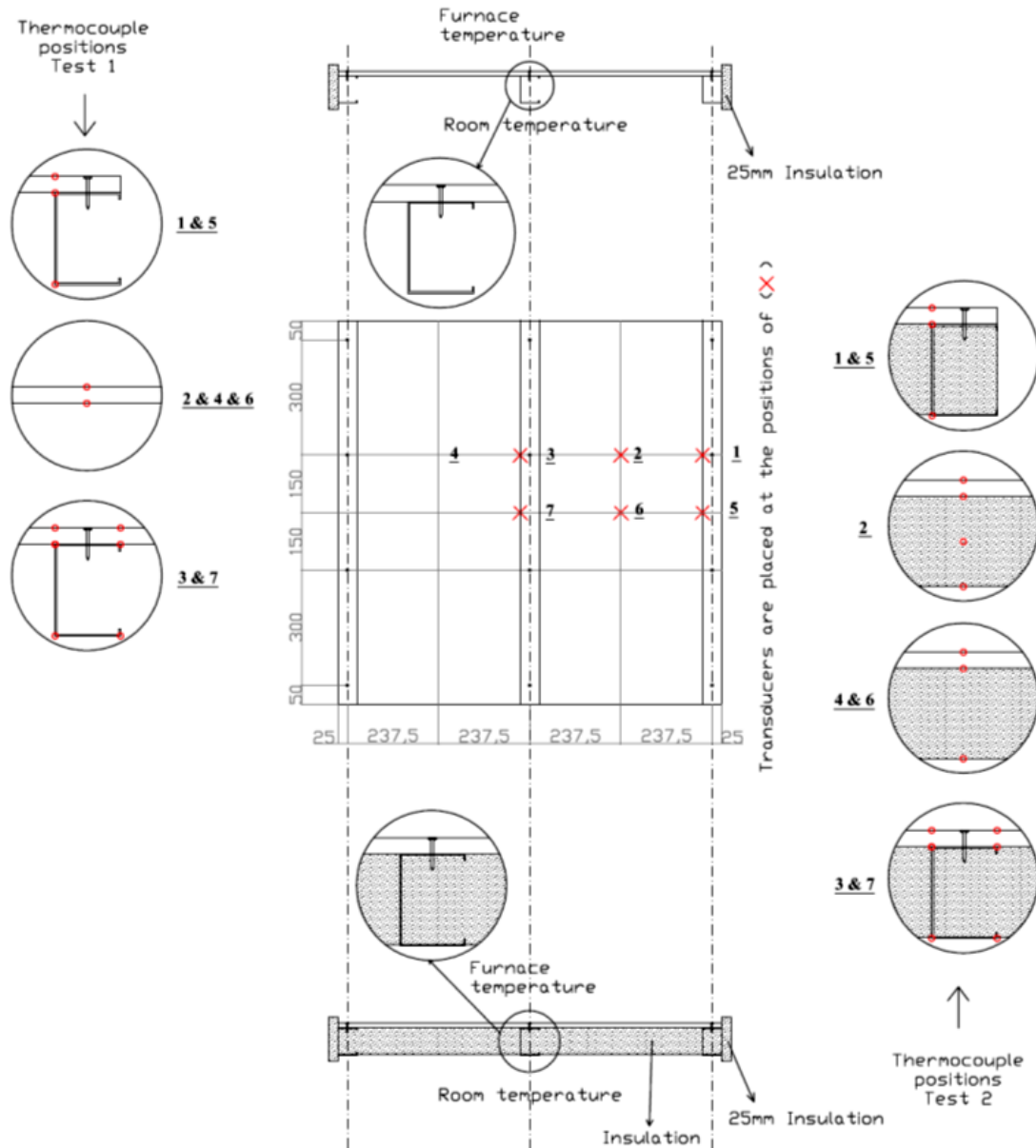


**Figure 6.1.** Test arrangement of experiments T1 and T2

Positions 1, 3, 5 and 7 marked in 6.1 show the position of the draw-wire linear transducers that measured the deflection of the studs. At positions 2 and 6, the deflection of the board was measured using laser sensors. The drawing force applied by the transducers was found to be too great for the boards and affected the behaviour of the assembly. Figure 6.2 shows a snapshot of the unexposed side of the assembly in test T1W. The right hand side of the board is cracked widely and pulled significantly out of the furnace due to the force applied by the transducers. The left hand side, on the other hand, does not show the same behaviour. Tests T1W and T3W were discarded for this reason. It was then decided to use laser sensors to measure the deflection of the boards at all positions. In the experiments with insulation, a small hole was made in the insulation at positions 2 and 6 to enable measuring the deflection of the board rather than that of the insulation.



**Figure 6.2.** The effect of the draw-wire transducer fixed on the plasterboard in test T1W

### **6.2.2 Experiments T3 and T4**

The arrangement of the wall assemblies in tests T3 and T4 is shown in Figure 6.3. Gypframe GA1 steel angle was fixed to the perimeter on the fire side of the test frame using 35mm Huss screws at 300mm centres. Two Gypframe 60I70 'I' studs were positioned at 200mm centres from each end of the test frame. A single layer of 12.5mm plasterboard was positioned within the cavity formed between the Gypframe GA1 steel angle and Gypframe 60I70 'I' studs. Gypframe GA1 steel angle was fixed to the studs on the non-fire side of the test frame to secure the plasterboard panels using three 25mm Gyproc Jack Point Drywall screws. The slot formed between the steel angle and the studs was about 2mm wider than the thickness of the plasterboard so that the panels were allowed to move easily when shrinking. There was no screw fixing on the plasterboard panels. In test T4, three layers of 25mm Isover APR was fitted between the studs on the non-fire side.

Similar to tests T1 and T2, the deflection of the board was measured using laser sensors, and the deflection of the steel studs were measured using draw-wire transducers.

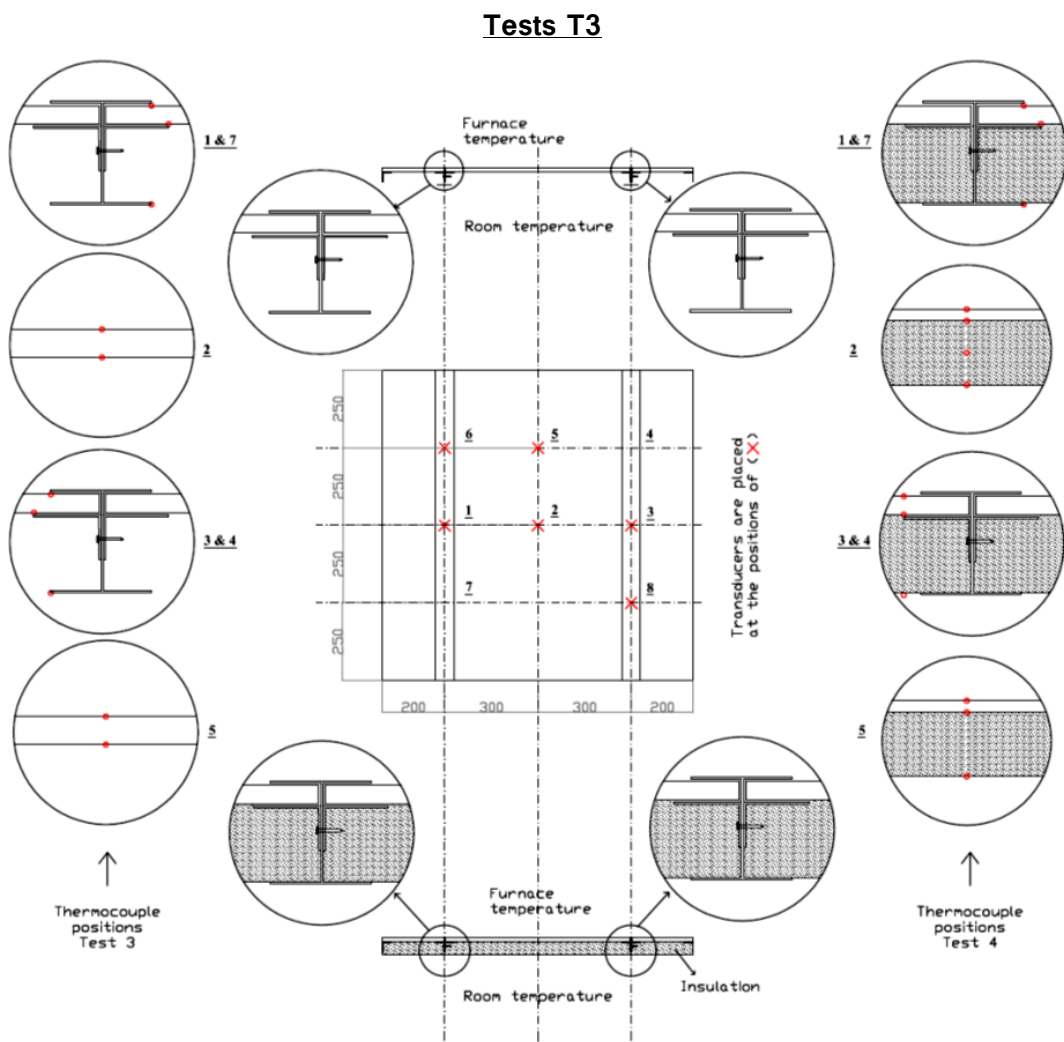


**Figure 6.3.** Test arrangement of experiments T3 and T4

### 6.2.3 Experiments T5 and T6

The construction of experiments T5 and T6 was similar to that of tests T1 and T2, respectively, except that two layers of plasterboard was used to clad the framework. Figure 6.4 illustrates the arrangement of tests T5 and T6.

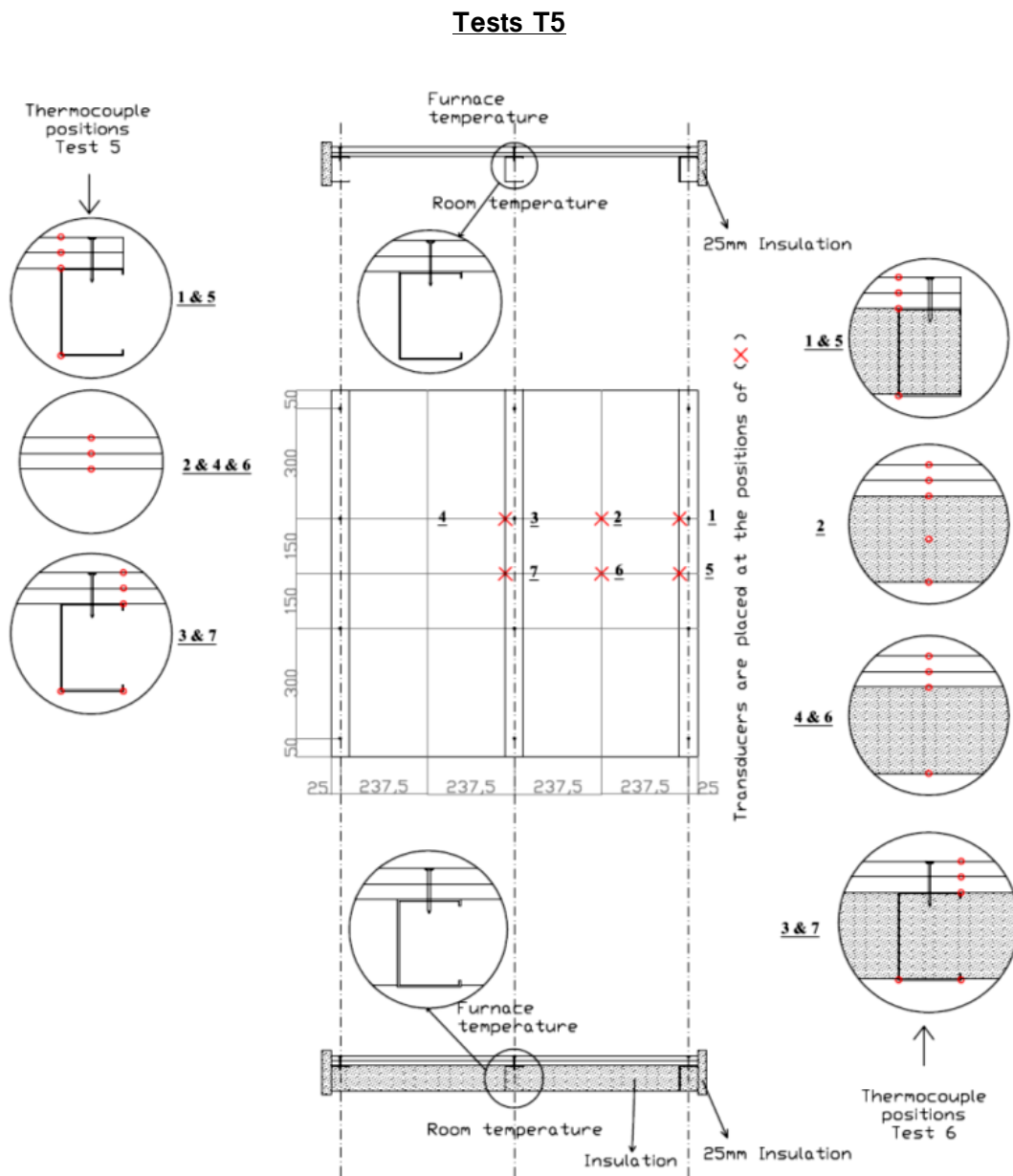


**Figure 6.4.** Test arrangement of experiments T5 and T6

### 6.3 Test Results and Discussions

Temperature measurements were taken at different positions in the plane of the wall assemblies and also across the thickness of the walls. As explained in previous sections, temperature was recorded at the exposed and unexposed sides of

gypsum, in between gypsum layers (in double-layer tests), on the unexposed flange of the studs, in the middle of the insulation and at the unexposed face of insulation (in insulated wall assemblies). Representative results are plotted in Figures 6.5 to 6.14.

Temperature measurements on the back of the exposed gypsum layer in some tests experiences a sudden increase of more than 100°C per minute (e.g. Figure 6.11), which is often linked with formation of discrete cracks in the exposed gypsum board. The wide cracks are either observed from the furnace window (e.g. see observation report for test T2W in Table 6.2 ) or predicted by numerical analysis. This phenomenon is further discussed in the CHAPTER 7.

Time		Observations <i>All observations refer to the exposed face unless otherwise stated.</i>
hours	mins	
0	0	Test started.
0	11	<p><b>Face papers charred.</b></p> <p><i>Unexposed face</i> Smoke issued from the head of the specimen.</p>
0	18	<p><i>Unexposed face</i> The temperature rise of thermocouple no.49, positioned at 650mm height on the centre stud, exceeded 180 °C.</p>
0	20	<p>Cracking visible horizontally and vertically to the boards.</p> <p><i>Unexposed face</i> Tearing to the insulation at the top right hand corner. Tearing to the insulation at the base of the specimen at the centre.</p>
0	24	<p><i>Unexposed face</i> The gap at the centre of the specimen at approximately 150mm height exceeded 6mm x 150mm (6mm gap gauge).</p>
0	25	<p><i>Unexposed face</i> The gap in the centre of the specimen at approximately 150mm height exceeded 25mm (25mm gap gauge). The centre stud had bent into the furnace.</p>
0	26	<b>TEST TERMINATED</b> at the request of the laboratory.

**Table 6.2.** Observation report for test T2W

Falling off of Fireline gypsum board was reported for the exposed boards in tests T5F and T6F at 210 and 180 minutes of the respective tests. A section of the Wallboard in experiment T4W was reported to have fallen off at 30 minute of the test, and approximately 50% of the exposed Wallboard in test T5W was observed falling 40 minutes into the fire test.

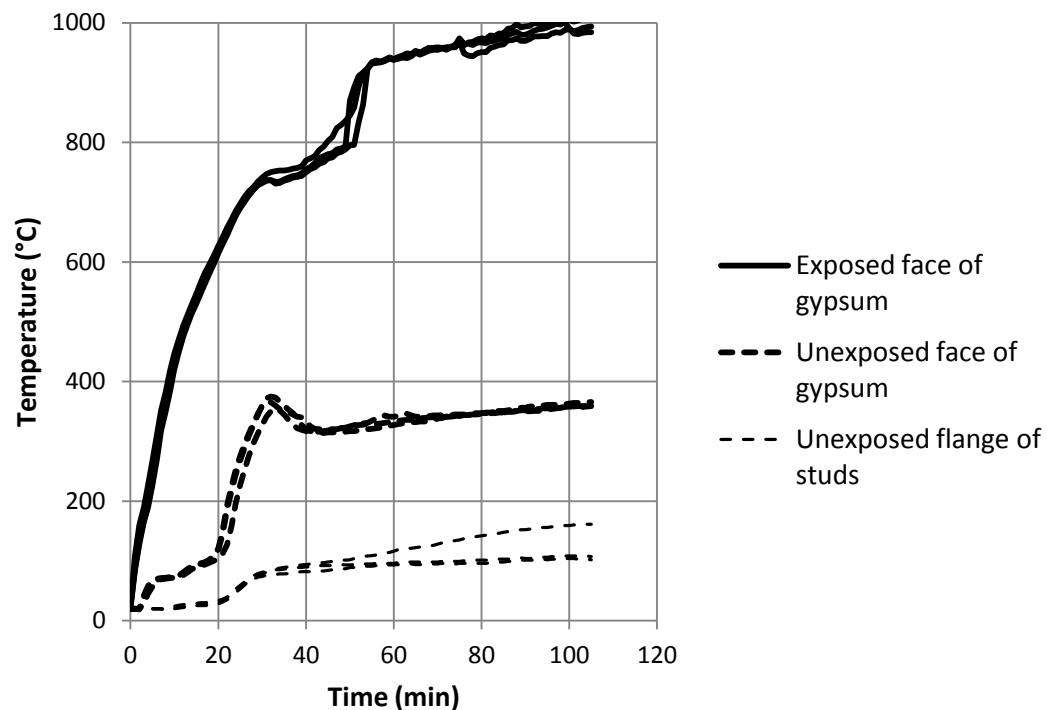


**Figure 6.5.** Temperature recordings for test T1F (12.5mm single-layer non-insulated Fireline gypsum)

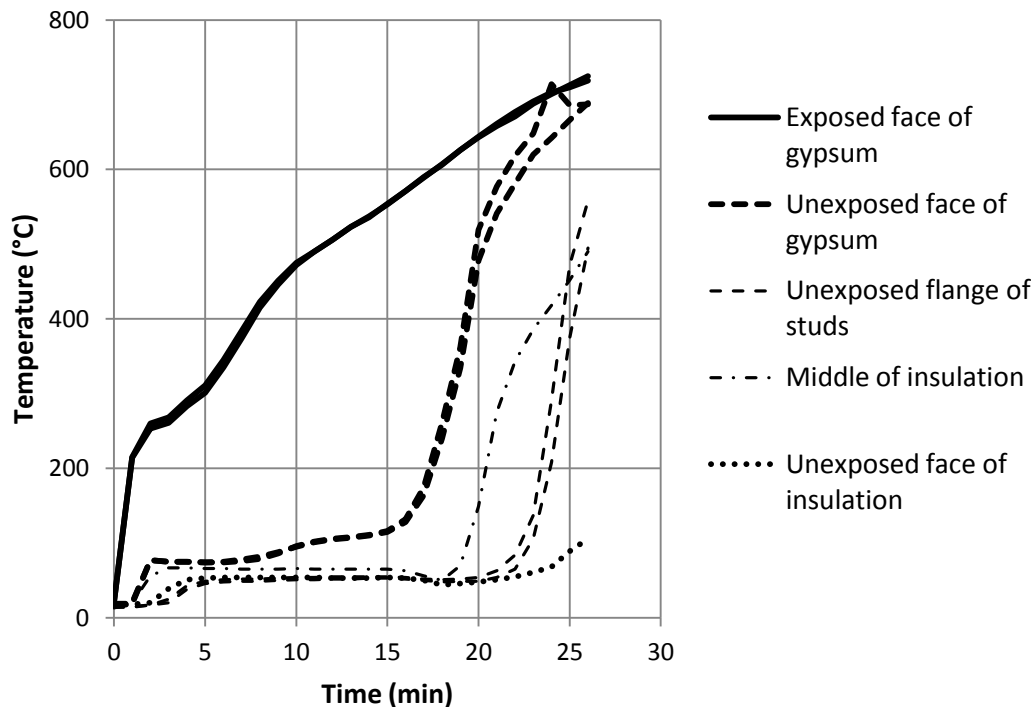


**Figure 6.6.** Temperature recordings for test T2W (12.5mm single-layer insulated Wallboard gypsum)

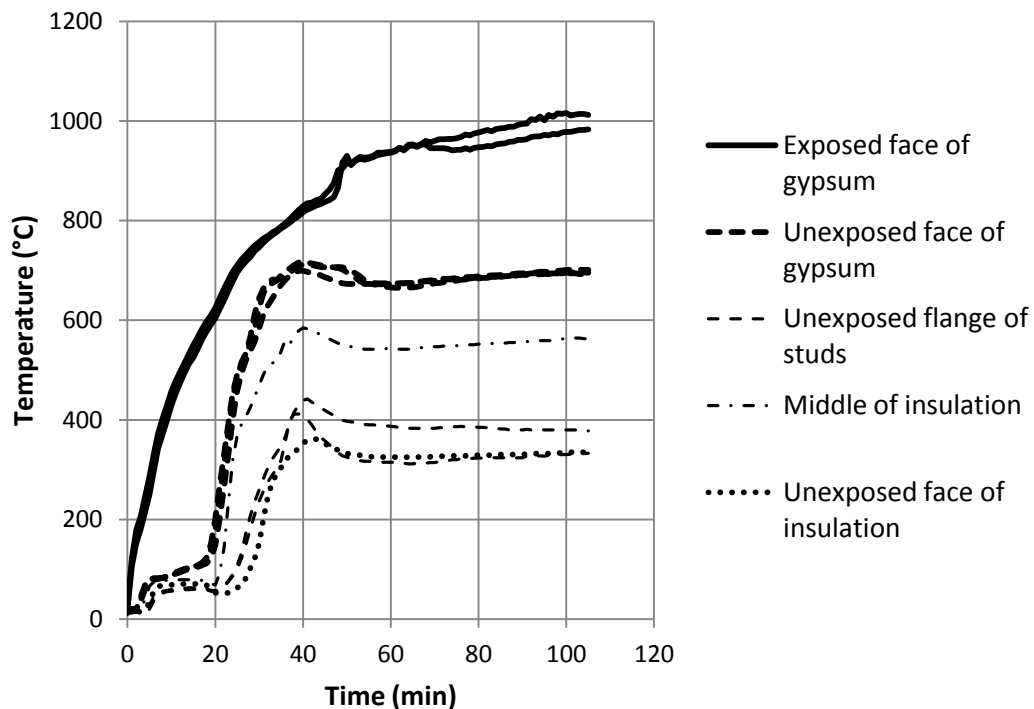


**Figure 6.7.** Temperature recordings for test T2F (12.5mm single-layer insulated Fireline gypsum)

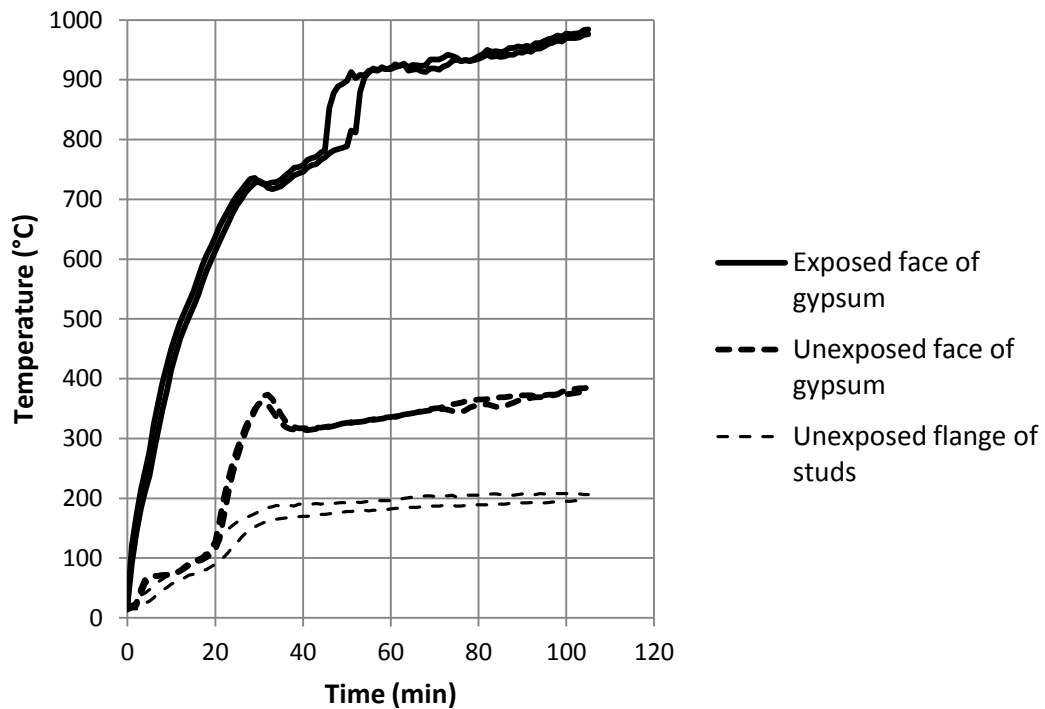


**Figure 6.8.** Temperature recordings for test T3F (12.5mm single-layer non-insulated Fireline gypsum)

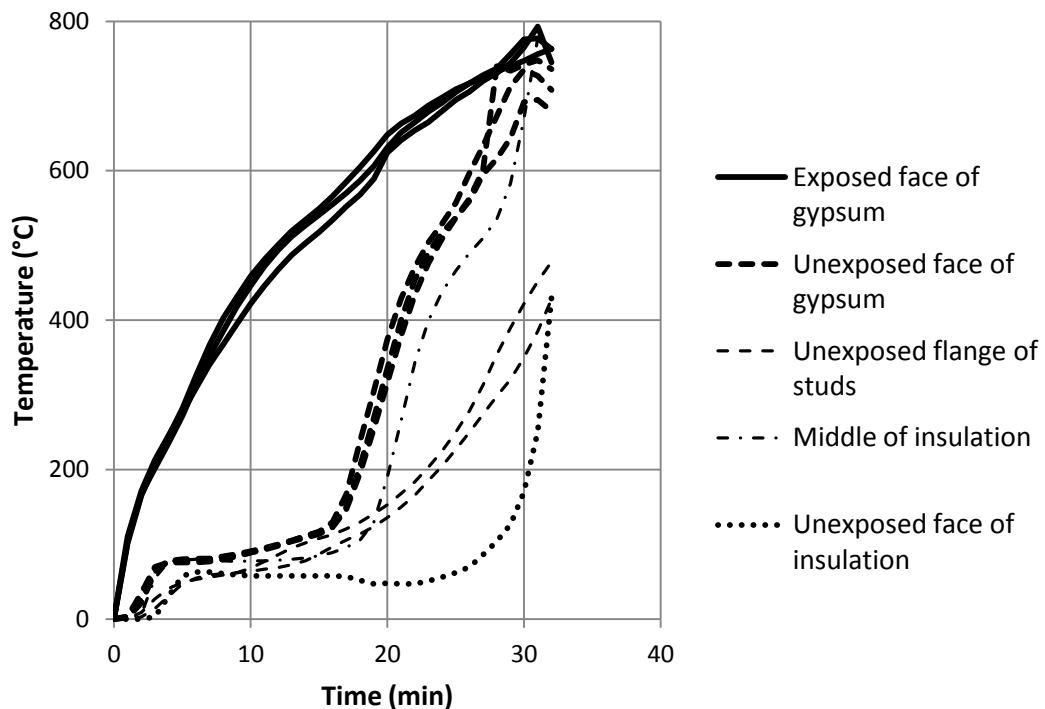


**Figure 6.9.** Temperature recordings for test T4W (12.5mm single-layer insulated Wallboard gypsum)

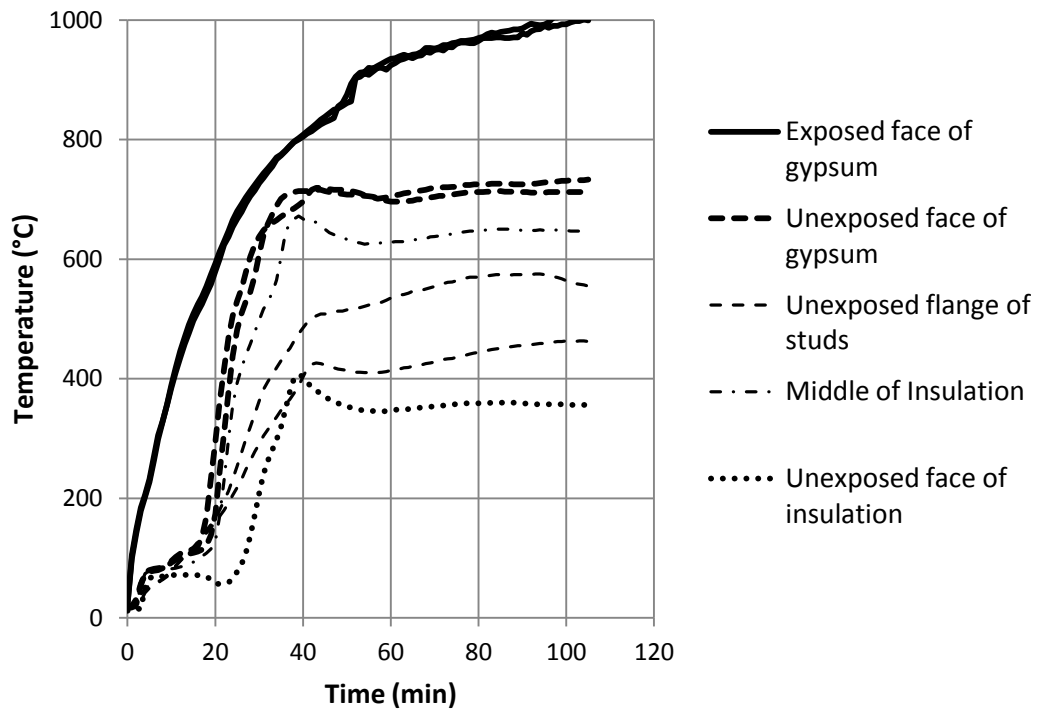


**Figure 6.10.** Temperature recordings for test T4F (12.5mm single-layer insulated Fireline gypsum)

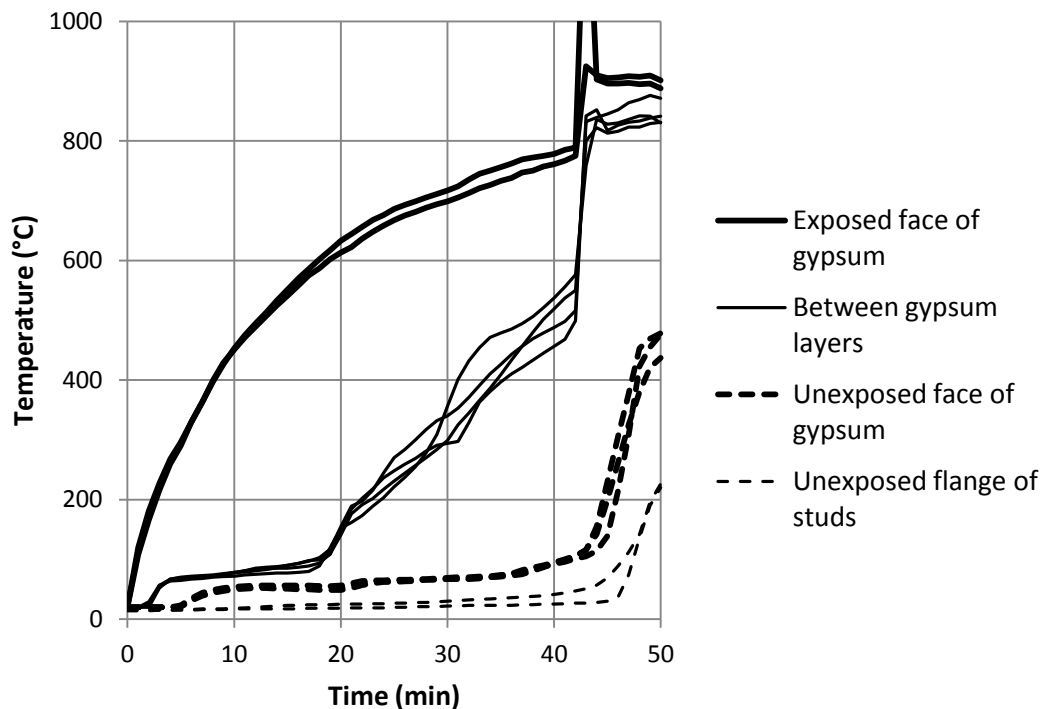


**Figure 6.11.** Temperature recordings for test T5W (25mm double-layer non-insulated Wallboard gypsum)

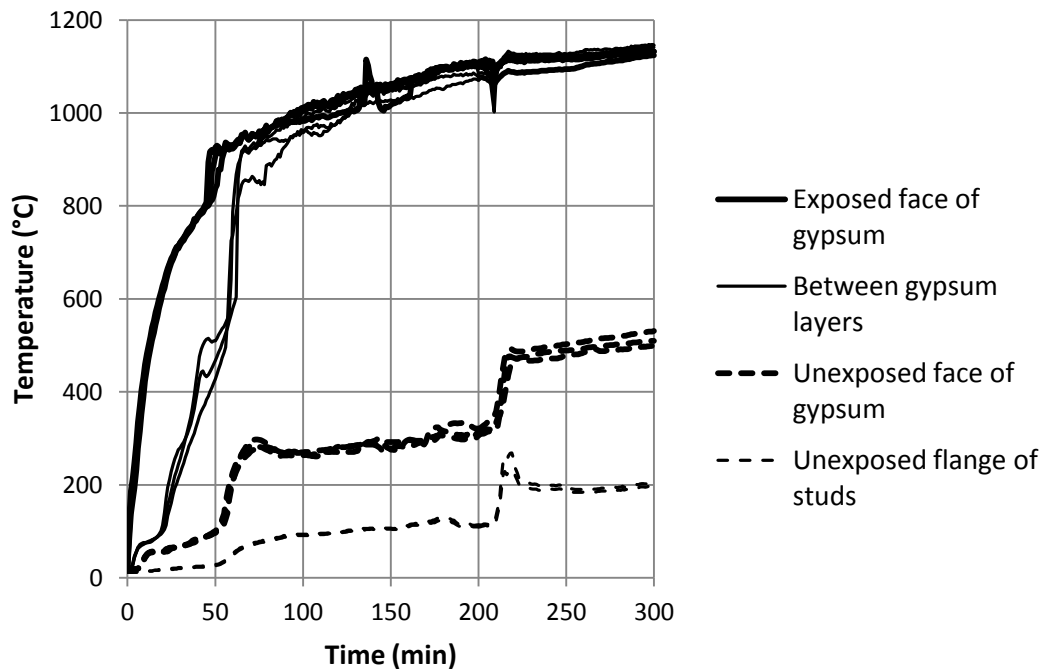


**Figure 6.12.** Temperature recordings for test T5F (25mm double-layer non-insulated Fireline gypsum)

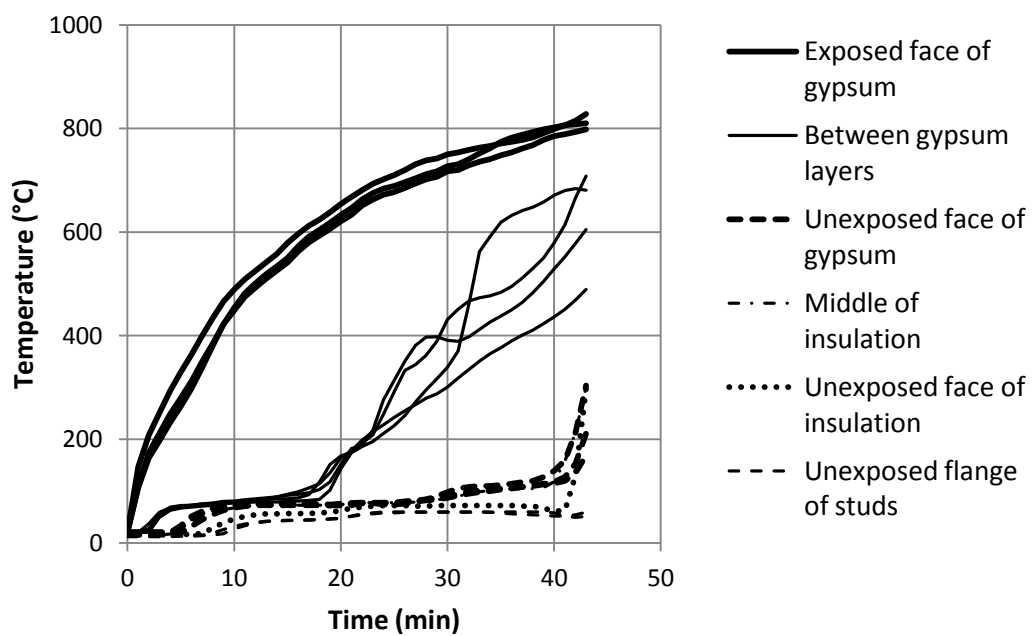


**Figure 6.13.** Temperature recordings for test T6W (25mm double-layer insulated Wallboard gypsum)

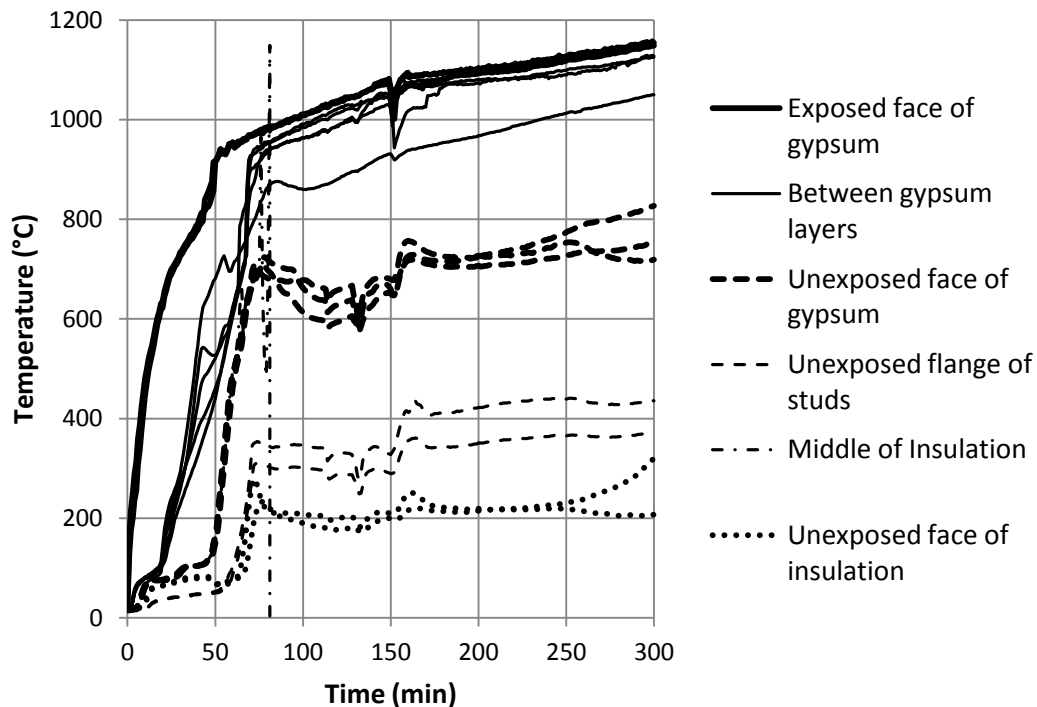


**Figure 6.14.** Temperature recordings for test T6F (25mm double-layer insulated Fireline gypsum)

The out-of-plane deflection of the walls were measured both at the mid-span of the gypsum boards using laser sensors, and at the flange of the steel studs using draw-wire transducers. The results are presented in Figures 6.15 to 6.17. As expected, the steel studs mainly bowed towards the furnace due to larger expansion on the exposed side, while the gypsum boards mostly bent out of the furnace due to larger shrinkage on the exposed side. The recorded deflections on the gypsum boards include the deflection of the studs as supports. Hence the net deflection of the board in each test can be calculated by deducting the average deflection of the studs from the recorded deflection on the board. This net deflection is compared to numerical results in CHAPTER 7.

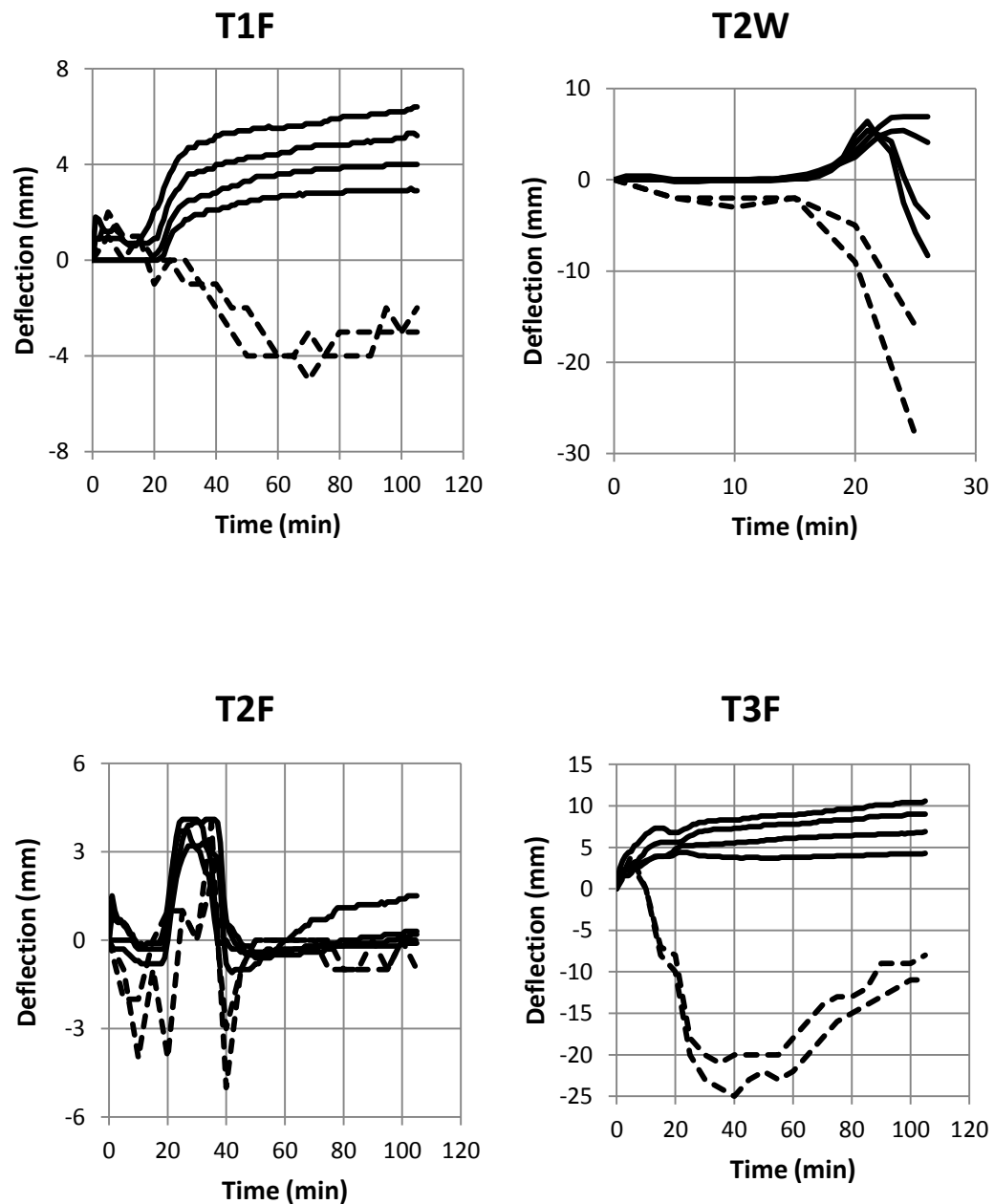


**Figure 6.15.** Deflection recordings of tests T1F, T2W, T2F and T3F - Solid lines: draw-wire transducers, dashed lines: laser sensors - Negative values indicate deflecting towards the furnace

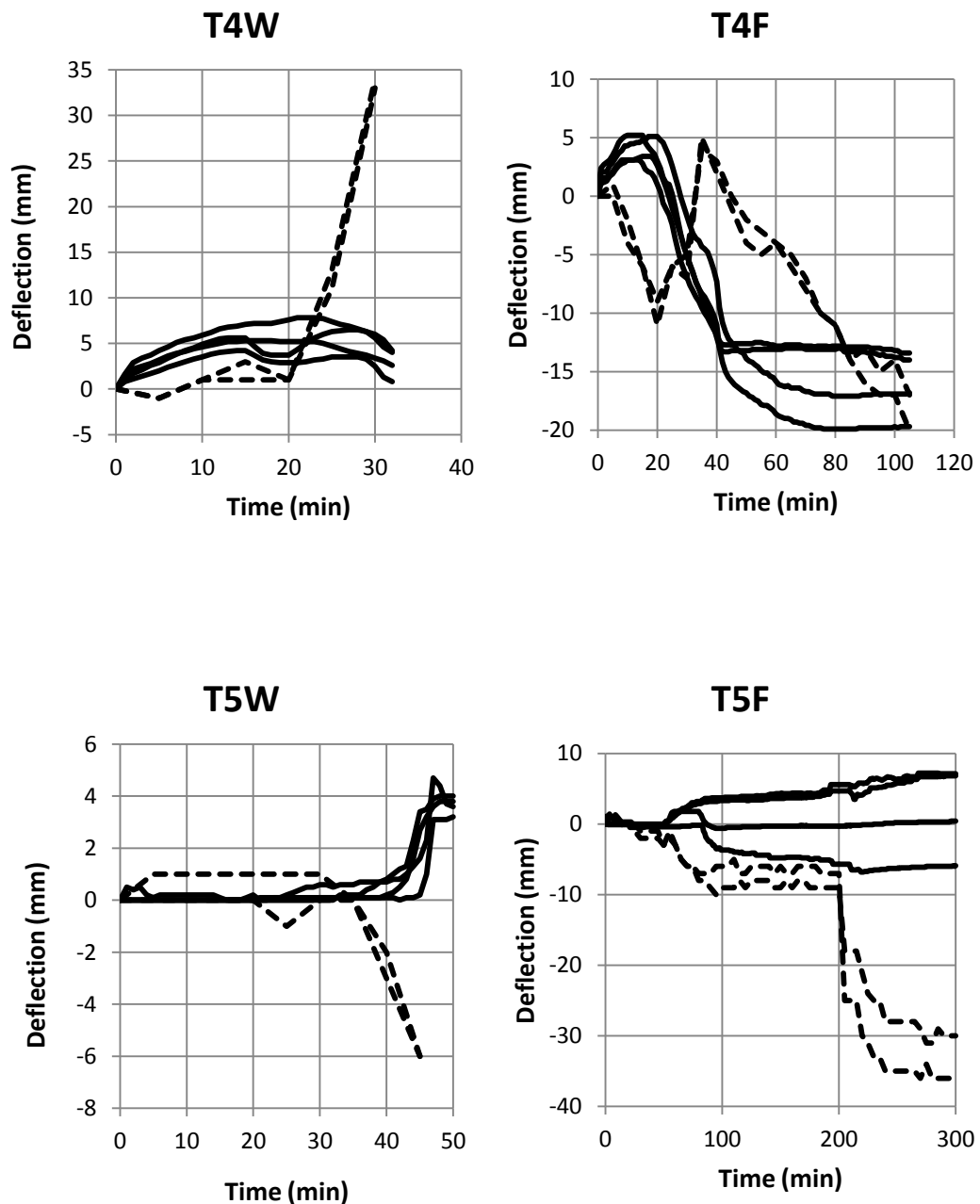


**Figure 6.16.** Deflection recordings of tests T4W, T4F, T5W and T5F - Solid lines: draw-wire transducers, dashed lines: laser sensors - Negative values indicate deflecting towards the furnace

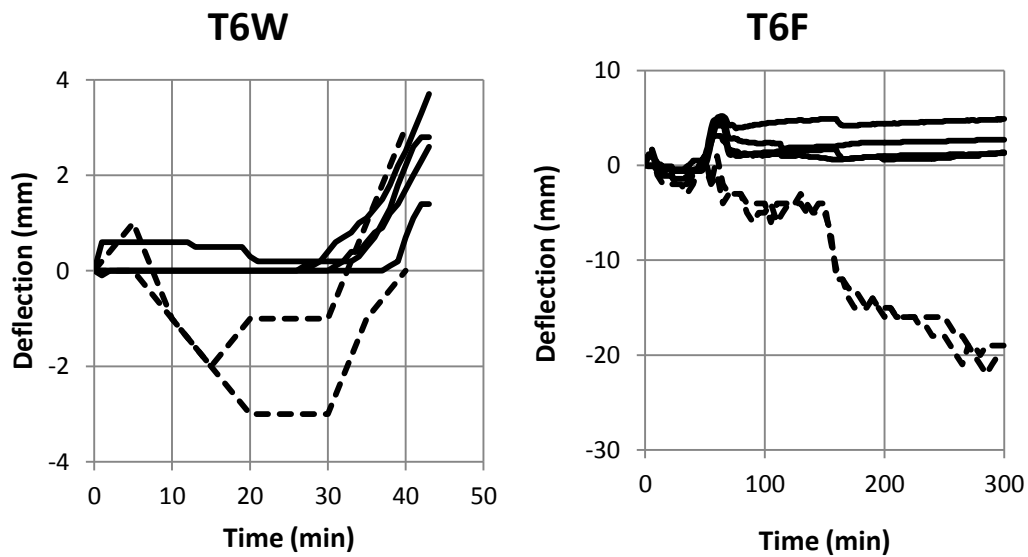


**Figure 6.17.** Deflection recordings of tests T6W and T6F - Solid lines: draw-wire transducers, dashed lines: laser sensors - Negative values indicate deflecting towards the furnace

#### 6.4 Canadian Full-Scale Fire Tests

The National Research Council of Canada has performed numerous full-scale fire tests on gypsum board wall assemblies to investigate the effects of various factors and components on fire resistance of the walls (Sultan and Lougheed, 2002, Bwalya et al., 2007). Four of these tests have been selected to be used for validation of the numerical analysis presented in CHAPTER 7; these are tests F-07 and F-09 from the first paper (Sultan and Lougheed, 2002), and tests UW-8V and UW-9V from the second paper (Bwalya et al., 2007). The set-up details of these tests are presented here.

The arrangement of tests F-07 and F-09 are very similar (see Figures 6.18 and 6.19). The wall assemblies are 3048mm high and 3658mm wide. The walls are made of 90mm steel studs with one layer of gypsum type X on the exposed side and two layers of gypsum type X on the unexposed side. The density of the boards is 9.85kg/m<sup>2</sup>. The cavity of the wall in test F-07 is left empty but filled with Glass Fibre Insulation (R12) in test F-09.

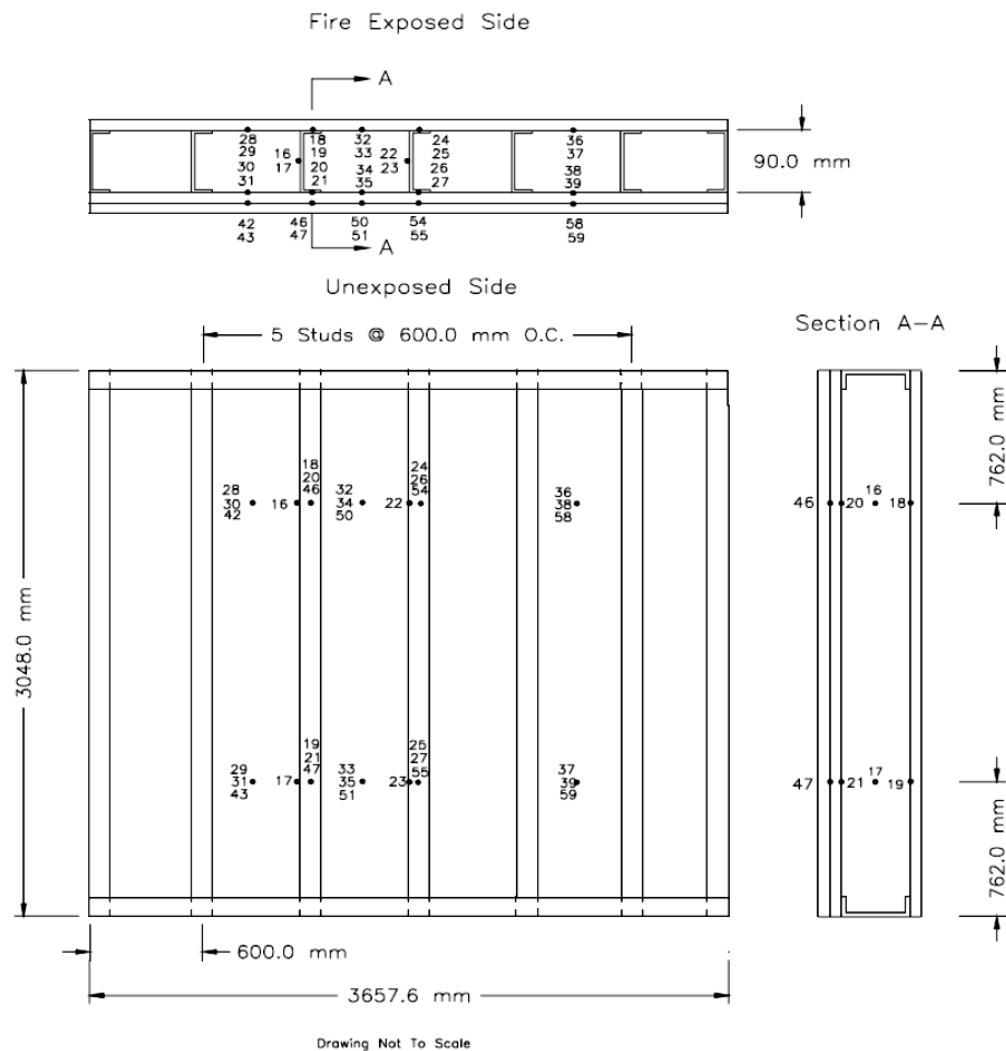


**Figure 6.18.** Test arrangement for full-scale wall assembly F-07 (Sultan and Lougheed, 2002)

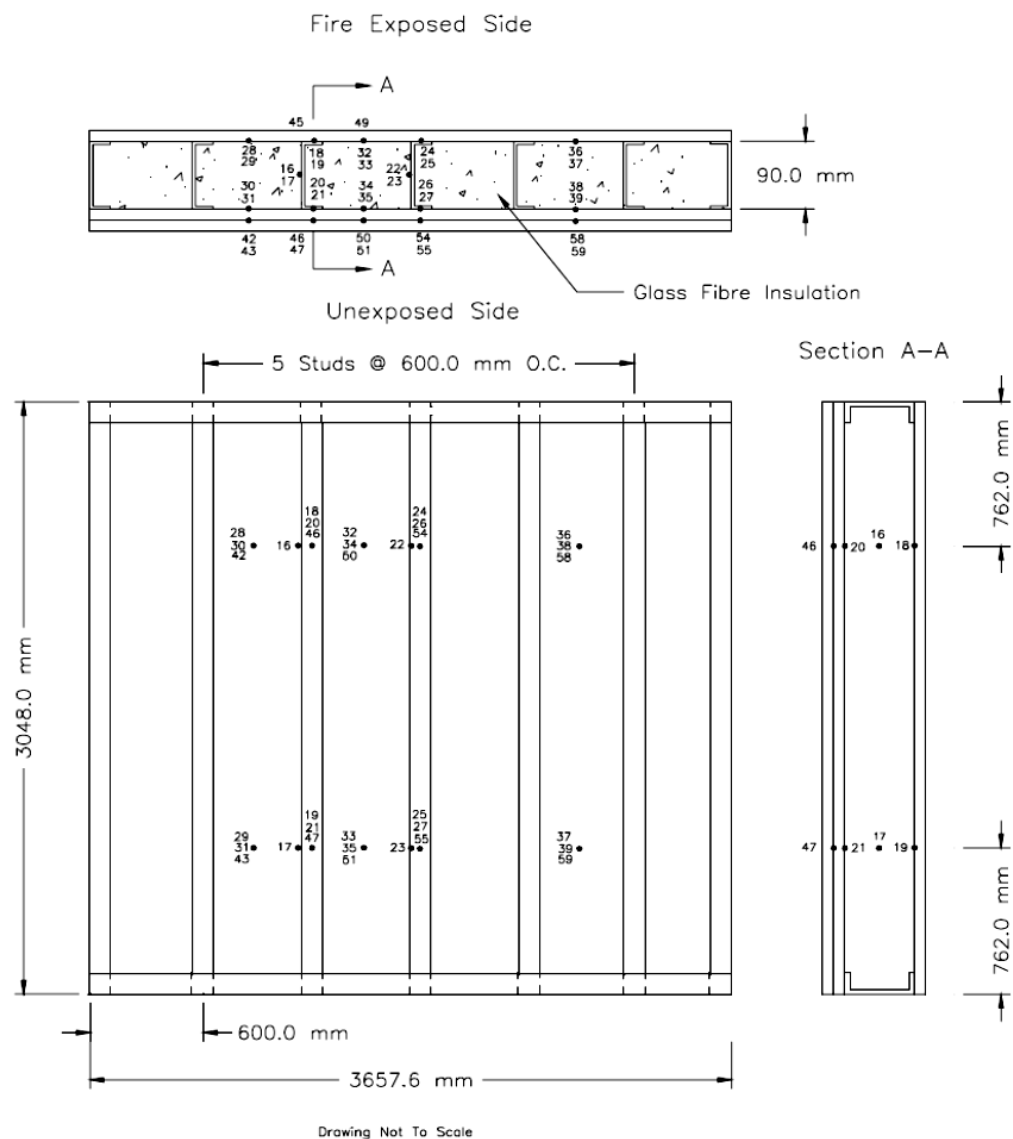


**Figure 6.19.** Test arrangement for full-scale wall assembly F-09 (Sultan and Lougheed, 2002)

Tests UW-8V and UW-9V are repeats of full-scale fire tests on assemblies with identical arrangements as shown in Figure 6.20. The wall assemblies are 3048mm high and 3658mm wide, and are made of 89mm deep wood studs clad with a single-layer of regular gypsum board on each side. The cavity of the walls is left empty. The density of the boards used is  $7.82\text{kg/m}^2$ .

A short study was performed by the author, while visiting the National Research Council of Canada, on video recordings of the exposed side of these assemblies taken from two small windows in the furnace. It was observed that the first discrete crack on the exposed board of tests UW-8V formed at around minute 14, and the first fall-off of the board occurred around minute 24 of the test. Figure 6.21 shows opening of wide vertical cracks on the gypsum boards after termination of test UW-8V. Although the picture depicts cracking on the unexposed panel, similar behaviour was observed on the exposed boards. In experiment UW-9V, the first crack opened around minute 16, and the first fall-off took place roughly 25 minutes into the fire test. As shown in Figure 6.22, temperature measurements at the back of the exposed board experience a sudden increase around the time of the fall-off.

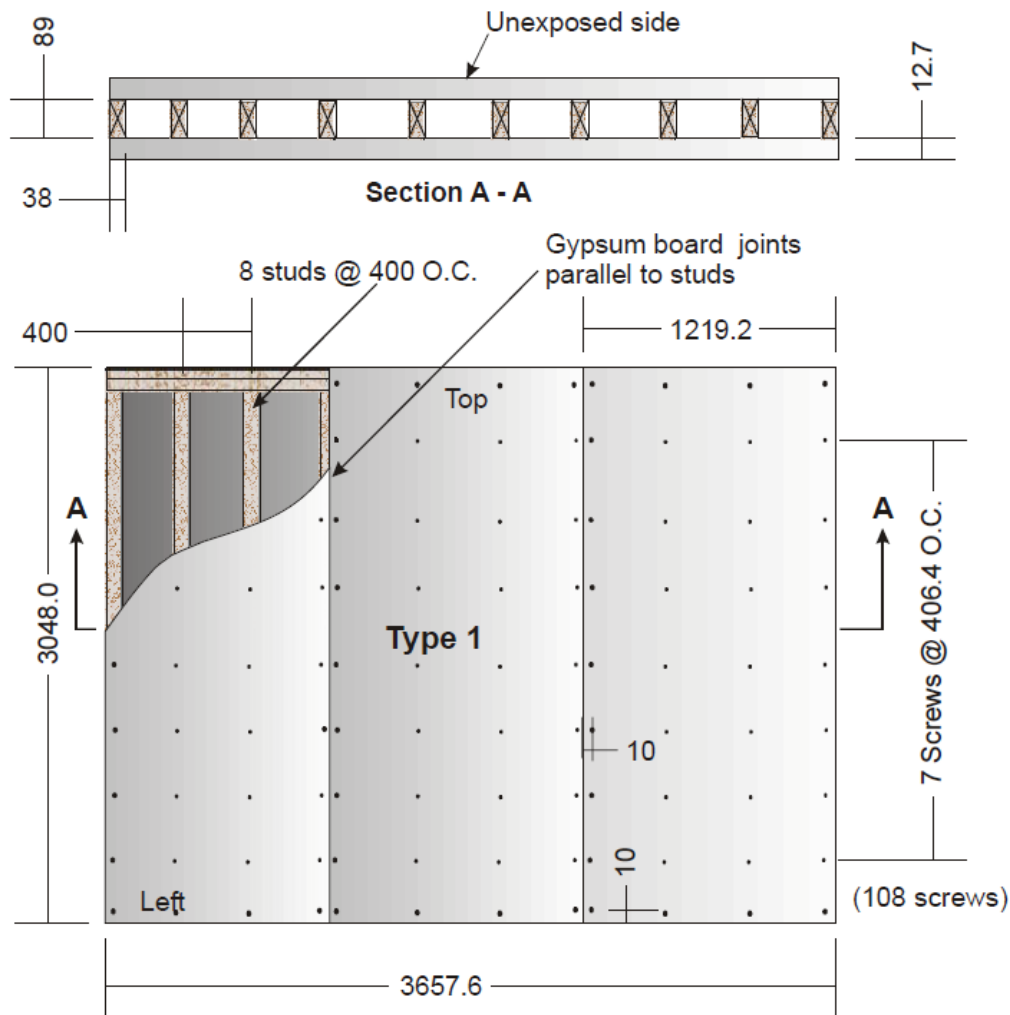


**Figure 6.20.** Test arrangement for full-scale wall assemblies UW-8V and UW-9V (Bwalya et al., 2007)



**Figure 6.21.** Wide vertical cracks on the unexposed gypsum board in test UW-8V

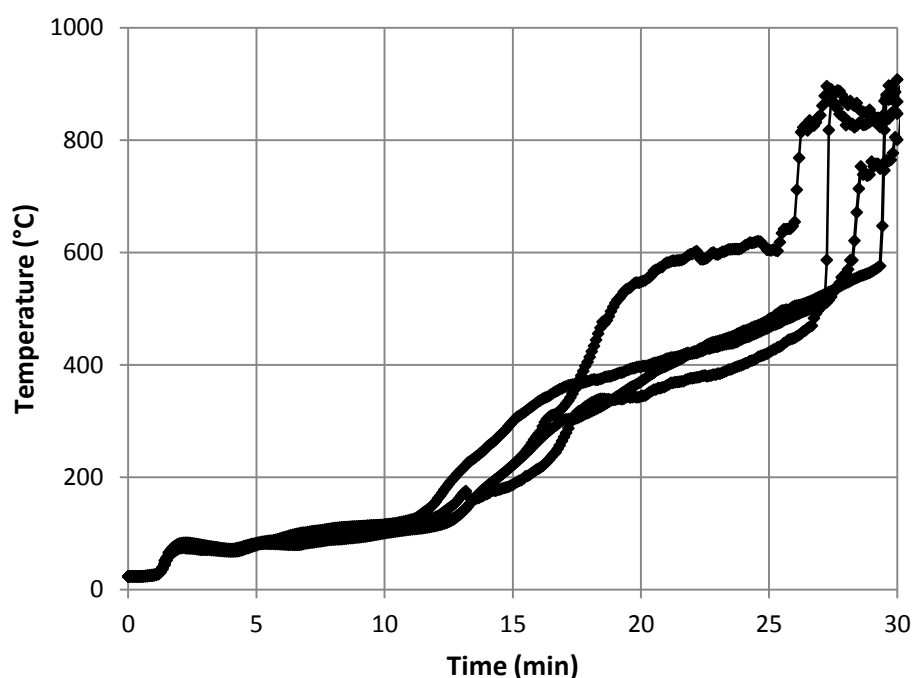


**Figure 6.22.** Temperature history on the back of the exposed board in test UW-9V.

## **6.5 Conclusions**

A large number of medium-scale fire tests have been performed on gypsum board wall assemblies. The assemblies included a wide range of arrangements with various boundary conditions for gypsum boards, different number of gypsum board layers, the two Fireline and Wallboard gypsum types and for insulated and non-insulated wall assemblies. Out-of-plane deflections of the walls and temperature history for various locations across the thickness of the walls have been recorded during the fire tests. The recorded data and observations of fall-off of gypsum in fire provide valuable information for the validation of the thermal and structural numerical study proposed in CHAPTER 7.

To widen the range of tests used for validation of numerical results, a limited number of Canadian tests have also been studied and the details of the layout of the wall assemblies have been included in this chapter.

## **CHAPTER 7. Finite Element Modelling of Structural Performance of Gypsum Boards in Fire**

### **7.1 Introduction**

Gypsum is mainly used as lining material in light-weight construction and its mechanical strength is rarely considered in structural performance of wall assemblies. Hence there have not been any studies, to the knowledge of the author, on numerical simulation of structural behaviour of gypsum in fire. Yet gypsum shrinks and loses its mechanical strength with temperature rise. The non-uniform shrinkage across the thickness of gypsum during a heating regime causes stresses along the gypsum panel, especially since the panel is restrained to its frame. When the tensile stresses exceed the mechanical strength of gypsum, cracks form in the gypsum board. Formation of discrete cracks leads to fall-off of gypsum and, in turn, greatly affects the fire resistance of the assembly. Thus, although the mechanical strength of gypsum can be ignored for the main load-bearing structure, structural performance of gypsum board affects its primary purpose of insulation, and therefore merits meticulous investigations.

Having extracted the mechanical properties of gypsum boards at high temperatures (in CHAPTER 5), this chapter presents the details and results of finite element modelling of structural performance of gypsum boards under fire conditions. Numerical simulations are conducted using the common finite element package, ABAQUS, and enable the prediction of the formation and opening of discrete cracks in gypsum boards. The results from numerical analysis are validated against the fire tests reported in CHAPTER 6.

## **7.2 Modelling Methodology**

Predicting cracks in gypsum requires first, a thermal analysis to predict the temperature developments in gypsum, and second, a structural analysis to predict the structural performance of gypsum at the elevated temperatures. Finite element procedures are now extensively employed both in thermal and structural analyses of different systems. Various computer packages are available which incorporate the finite element method. The adopted package for this study is ABAQUS/CAE version 6.10, which is a powerful engineering simulation programme and can be used to simulate complicated structural problems as well as problems in the heat transfer area.

As the pioneer in numerical simulation of structural behaviour of gypsum boards in fire, this study aims to utilize all simplifications possible to downsize the mathematical model of the physical problem without compromising the validity of the model. This will provide a basis that can later be elaborated to include further complexities. Hence, in this study:

- The simulation of the test wall assemblies only includes the gypsum board and not the steel frame. The interaction between the support steel frame and the gypsum board is applied as boundary conditions.

This approach will reduce the computational cost and complexity associated with the behaviour of the steel frame, e.g. buckling.

- In all simulations, gypsum boards, both the standard and the fibre reinforced types, are assumed to be homogenous and isotropic.
- The model incorporates a sequentially coupled thermal and structural analysis and therefore, the influence of the opening of the cracks on the temperature development across the board is ignored. This is justified on the basis of the limitations of the current research. Modelling the development of cracks in structures still represents a formidable challenge to computational mechanics researchers. Therefore, the structural simulation of this study aims to predict the formation of a discrete crack, and cannot deal with the performance of the board, whether thermally or structurally, beyond the opening of a discrete crack.

- The three-dimensional problem of the real case is reduced to a two-dimensional structural model.

Since the thickness of a gypsum board is much smaller than its other two dimensions, the deflection of the board can be rationally limited to the direction perpendicular to the board. Consider the gypsum board illustrated in Figure 7.1. If the board deflects towards the furnace, the screws will provide restraint to the steel frame; whereas, if the deflection of the board is out of the furnace, the restraints are provided by the steel frame itself. The latter practically results in a wide beam continued over its two spans, and can be modelled as a strip of this wide beam. Since the deflection of the board is mainly out of the furnace (due to shrinkage at higher temperatures), this approximation is considered acceptable. As a result, the model reduces to a two-dimensional beam, where the length of the beam is the horizontal dimension of the board, and its depth is the thickness of the board.

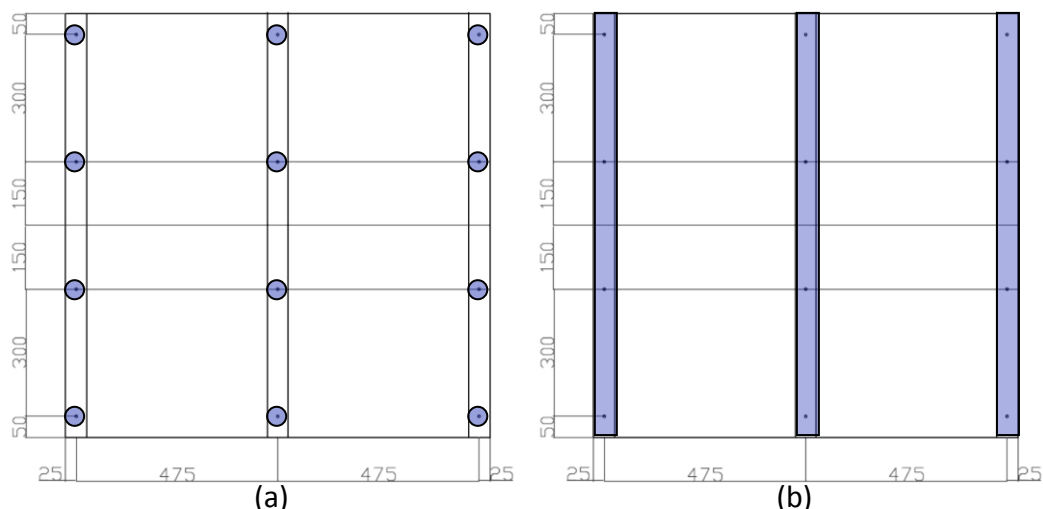


**Figure 7.1.** Boundary conditions for out-of-plane deflection of the gypsum board in (a) and out (b) of the furnace

- The thermal problem is reduced to a one-dimensional heat transfer analysis through the thickness of the board, i.e. temperatures are assumed to be uniform in the width direction of the board.

The heat of the furnace can be assumed to be uniform across the plane of the board. Therefore, away from the edges and the steel frame, heat transfer is only in the direction of the thickness of the board. The slight non-uniformity of temperature distribution close to the steel frame is not considered in the simulation.

Having chosen a sequentially coupled thermal-stress analysis, first a pure heat transfer problem is solved and then the temperature solution is read into a stress analysis as a predefined field. The following sections present the details of the thermal and structural models.

### **7.3 Thermal Analysis Using ABAQUS**

ABAQUS allows for a pure heat transfer analysis to be performed on various models. This is achieved via defining a transient “Heat transfer” step after the initial step in this study. The objective of this analysis is to obtain the temperatures of the board to be used in the structural analysis.

#### **7.3.1 Geometry**

The geometry of the model is defined as a 2D planar structure. Although the heat transfer model is practically a one-dimensional one, as explained in section 7.2, the two-dimensional model allows for the temperature solution to be directly read into the two-dimensional model for structural analysis. Figure 7.2 shows a typical 2D geometry used for simulation.



**Figure 7.2.** Geometry of the heat transfer model

### **7.3.2 Material Properties**

The main thermal properties of a material are its thermal conductivity, specific heat and density. ABAQUS allows for these properties to be defined as temperature-dependent data. The properties input in the model for gypsum boards are based on the ones extracted in CHAPTER 3.

### **7.3.3 Mesh and Element Type**

A standard heat transfer element type is chosen for heat transfer analysis. In the ABAQUS material library this element is denoted by DC2D4 and it is a 4-node linear heat transfer quadrilateral element.

Since heat transfer is only in the direction of the thickness, the number of elements in the other direction does not affect the simulation. To choose the optimum number of elements across the thickness, a sensitivity study has been performed for a 12.5mm layer of Fireline gypsum with the following different mesh sizes:

Case a: 4 elements through the thickness, mesh size: 3.125mm

Case b: 6 elements through the thickness, mesh size: 2.083mm

Case c: 10 elements through the thickness, mesh size: 1.25mm

Figure 7.3 shows the temperature of the exposed and unexposed surfaces of the gypsum board for the cases above. It is observed that the temperature predictions of both surfaces in Case b are slightly different from the predictions in Case a. However, increasing the number of elements to 10, in case c, hardly changes the results. Therefore, 6 seems to be the optimum number of elements through the thickness, corresponding to the mesh size of about 2mm.

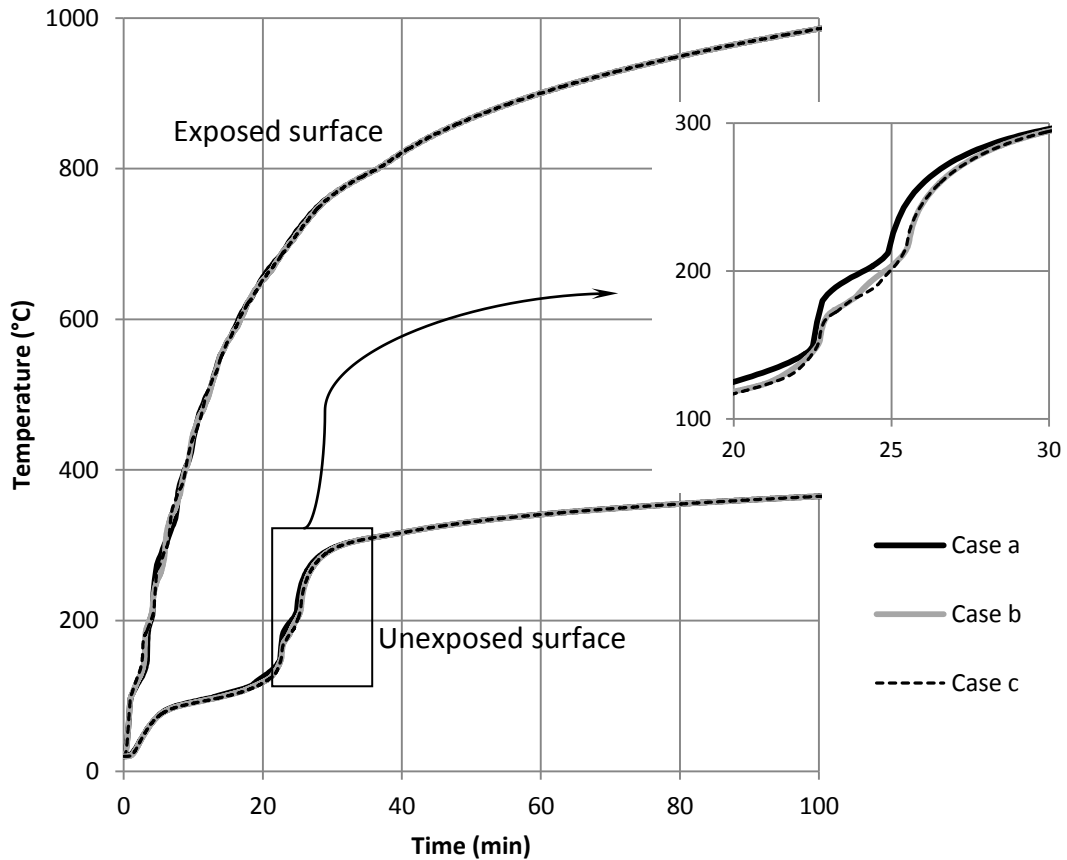


**Figure 7.3.** Temperature predictions on the exposed and unexposed surfaces of a 12.5mm layer of Fireline gypsum board using different number of elements through the thickness of the board

### 7.3.4 Initial and Boundary Conditions

The initial temperature of the boards is assumed to be uniform and equal to 20°C. Convection and radiation boundary conditions were defined for the top and bottom surfaces of the panel using ‘Interactions’. The interaction types used for convection and radiation boundary conditions are ‘Surface film condition’ and ‘Surface radiation to ambient’, respectively.

The furnace side of the board is exposed to the standard cellulosic fire test introduced in BS476 (1987), and the room side of the board is in interaction with a constant room temperature of 20°C. The effective emissivity at the exposed and unexposed surfaces is 0.7 and 0.25, respectively. The convection heat transfer

coefficients are assigned according to BS EN 1991-1-2 (2002), i.e.  $4 \text{ W/m}^2 \cdot ^\circ\text{C}$  for the unexposed surface and  $25 \text{ W/m}^2 \cdot ^\circ\text{C}$  for the exposed surface.

Where the unexposed surface of the board is facing the ISOVER APR insulation (in tests T2, T4 and T6), the temperature readings of the unexposed side are directly applied as temperature boundary condition in the model.

In double-layer tests, the thermal interaction between the two boards is defined using the “surface to surface” interaction available in ABAQUS. It is assumed that the two boards are in full contact and therefore, the thermal conductivity of the interaction is the same as that of the gypsum board and emissivity is equal to unity.

### **7.3.5 Validation of Numerical Results for Thermal Analysis**

The temperature predictions from the thermal analysis are compared with experimental measurements of the temperatures at the exposed and unexposed surfaces and between the two layers of gypsum in double-layer tests. This is to verify that the temperature solution used in the stress analysis is as close to the experiment as possible. Figures 7.4 to 7.13 illustrate that the numerical results closely predict the experiments. It should be noted that where gypsum boards are cracked widely or sections of the board falls off during heating, the temperature profiles are affected considerably. This effect is not included in the analysis; hence there is some noticeable difference between the analysis and test temperatures, especially in double-layer wall assemblies after the first fall-off of gypsum. This effect is more closely studied in the structural analysis of the gypsum later in this chapter.

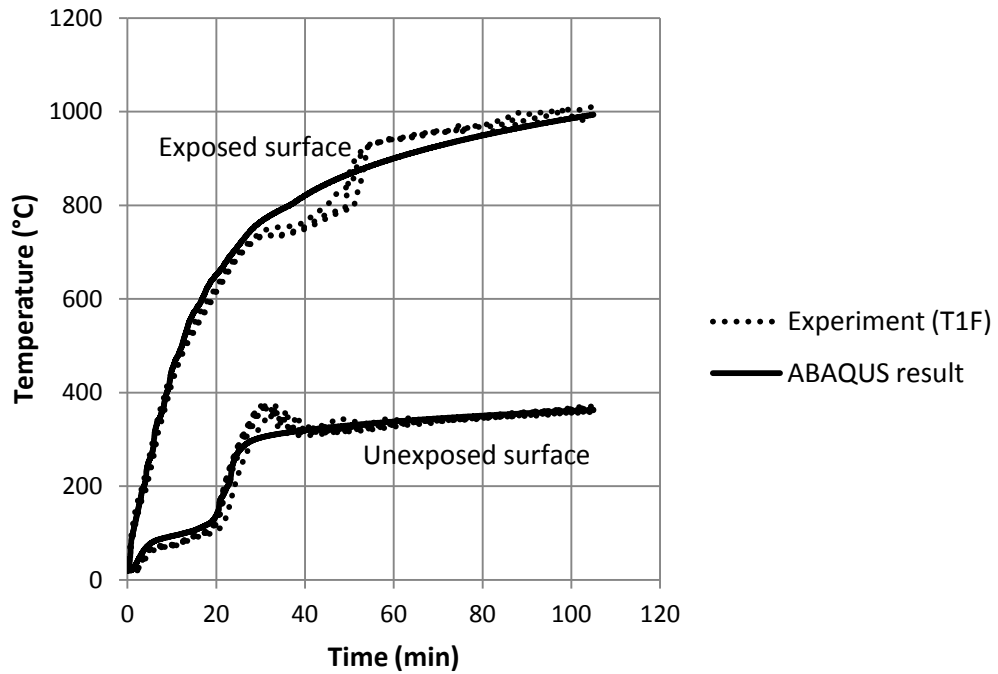


**Figure 7.4.** Temperature history for Test T1F (12.5mm single-layer non-insulated Fireline gypsum)

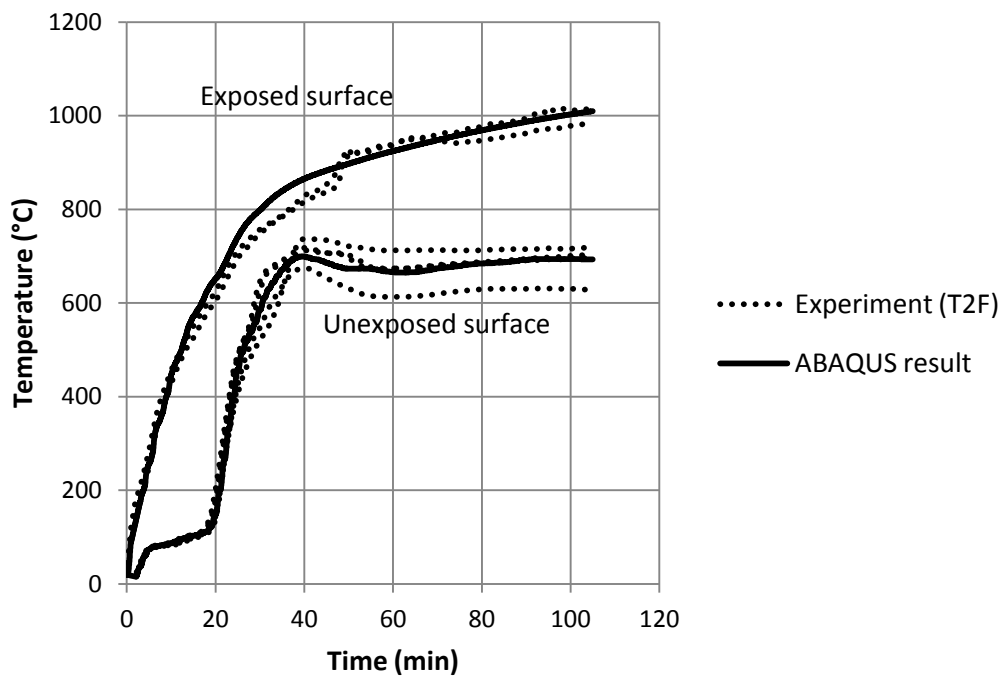


**Figure 7.5.** Temperature history for Test T2F (12.5mm single-layer insulated Fireline gypsum)

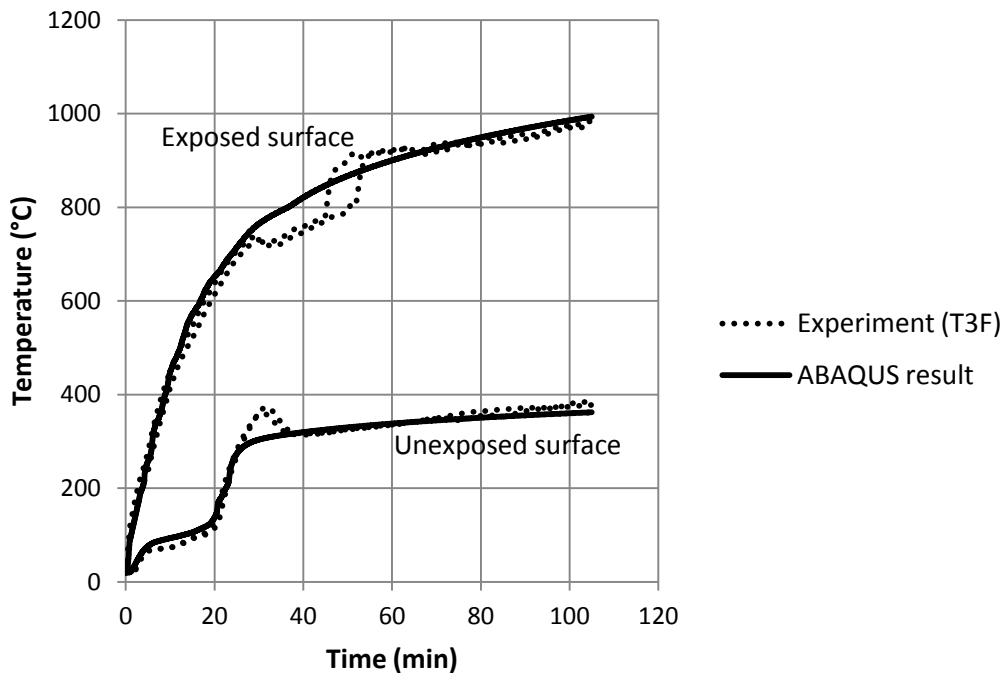


**Figure 7.6.** Temperature history for Test T3F (12.5mm single-layer non-insulated Fireline gypsum)

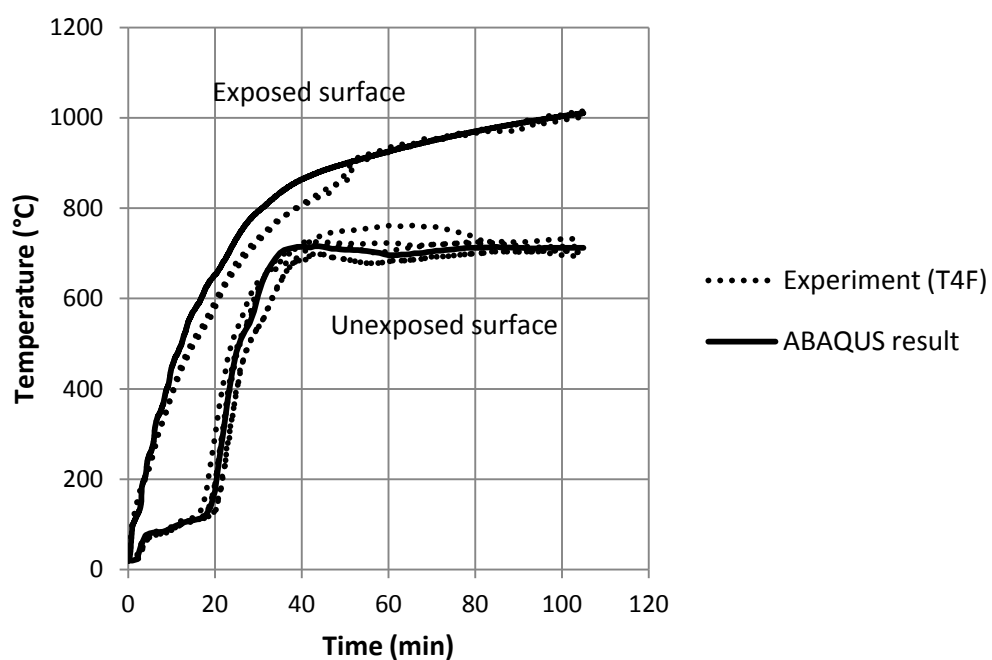


**Figure 7.7.** Temperature history for Test T4F (12.5mm single-layer insulated Fireline gypsum)

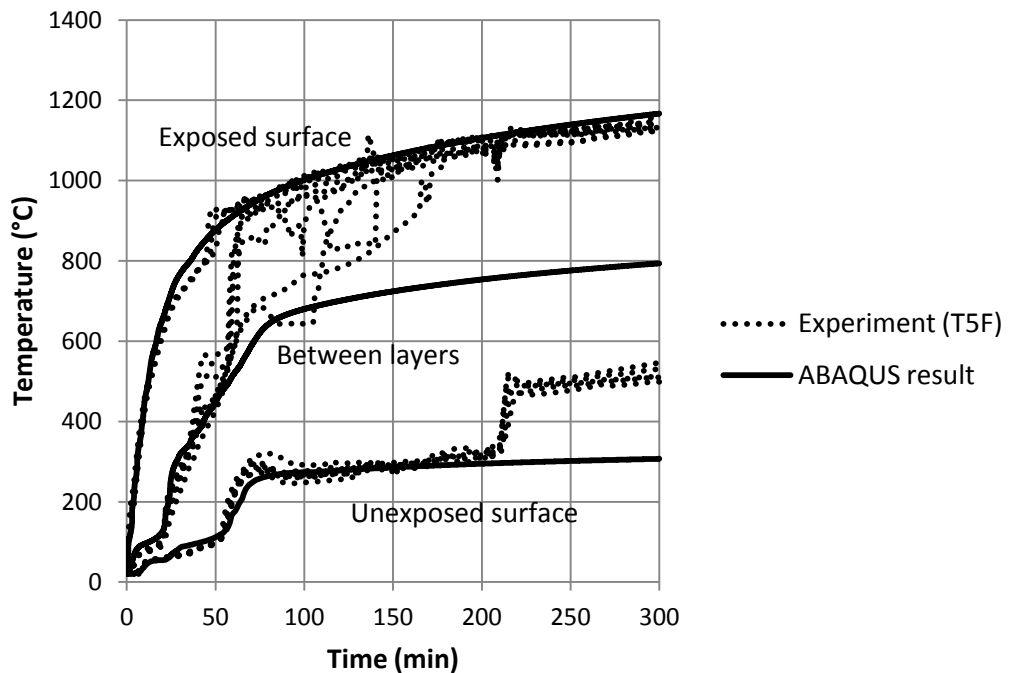


Figure 7.8. Temperature history for Test T5F (25mm double-layer non-insulated Fireline gypsum)

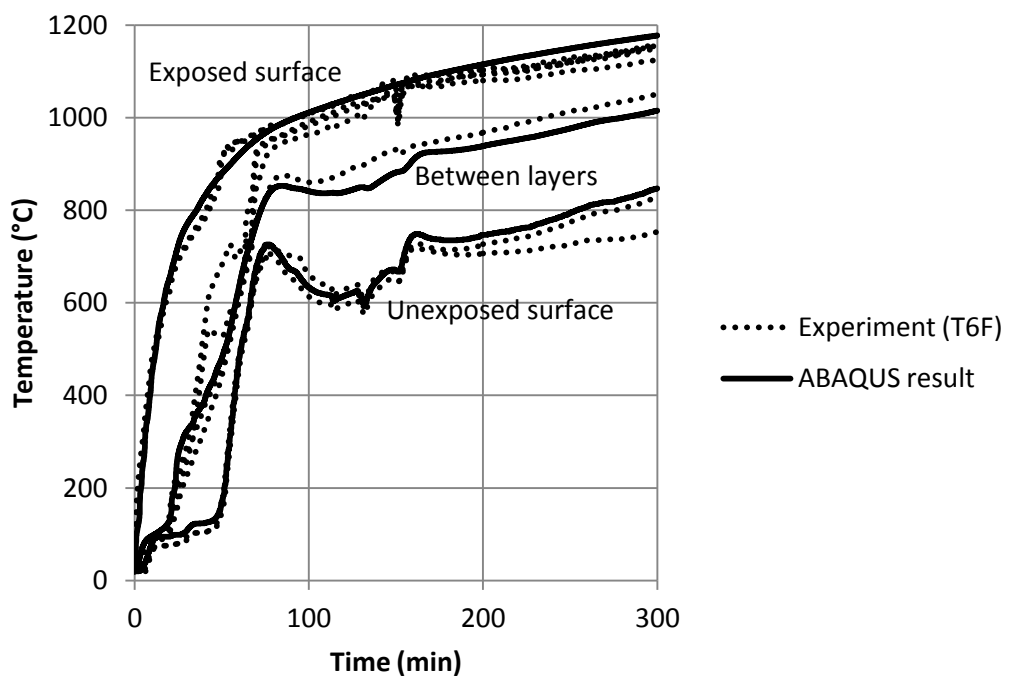
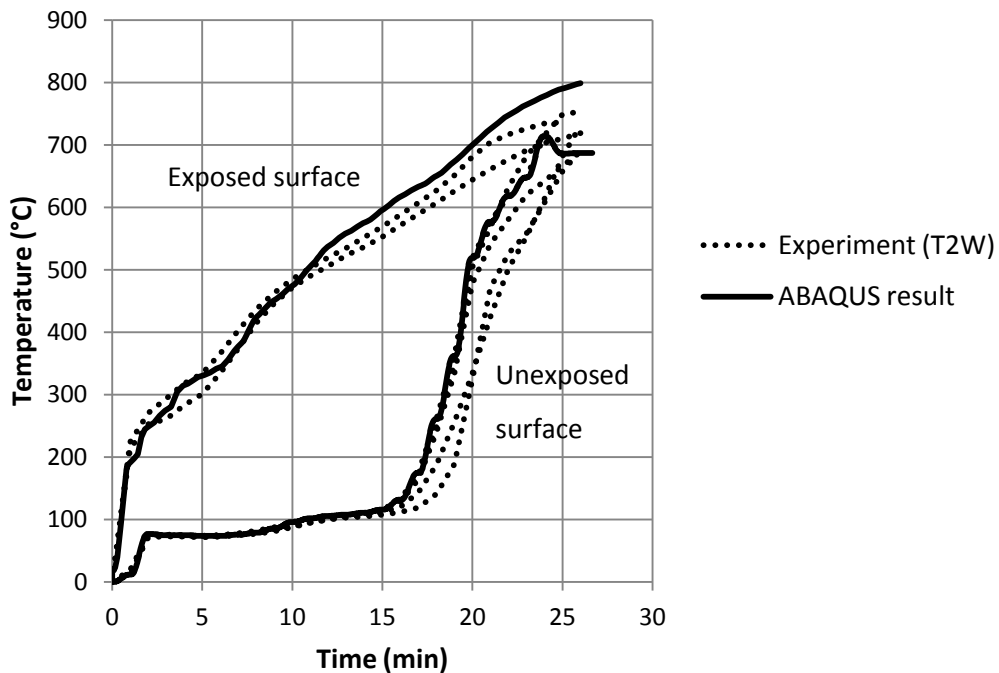
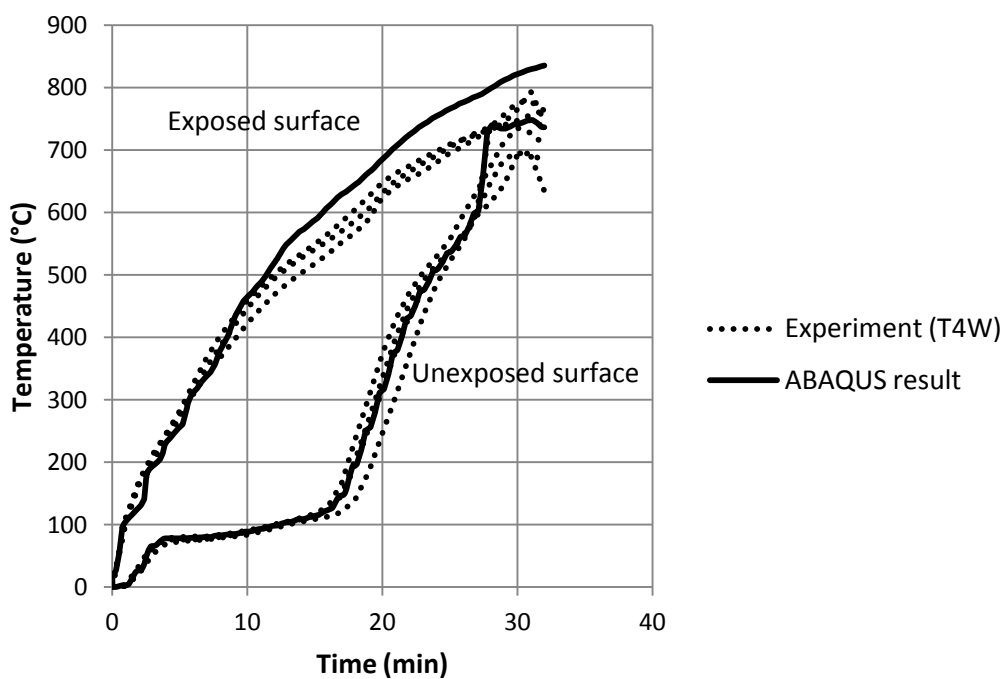


Figure 7.9. Temperature history for Test T6F (25mm double-layer insulated Fireline gypsum)



**Figure 7.10.** Temperature history for Test T2W (12.5mm single-layer insulated Wallboard gypsum)



**Figure 7.11.** Temperature history for Test T4W (12.5mm single-layer insulated Wallboard gypsum)

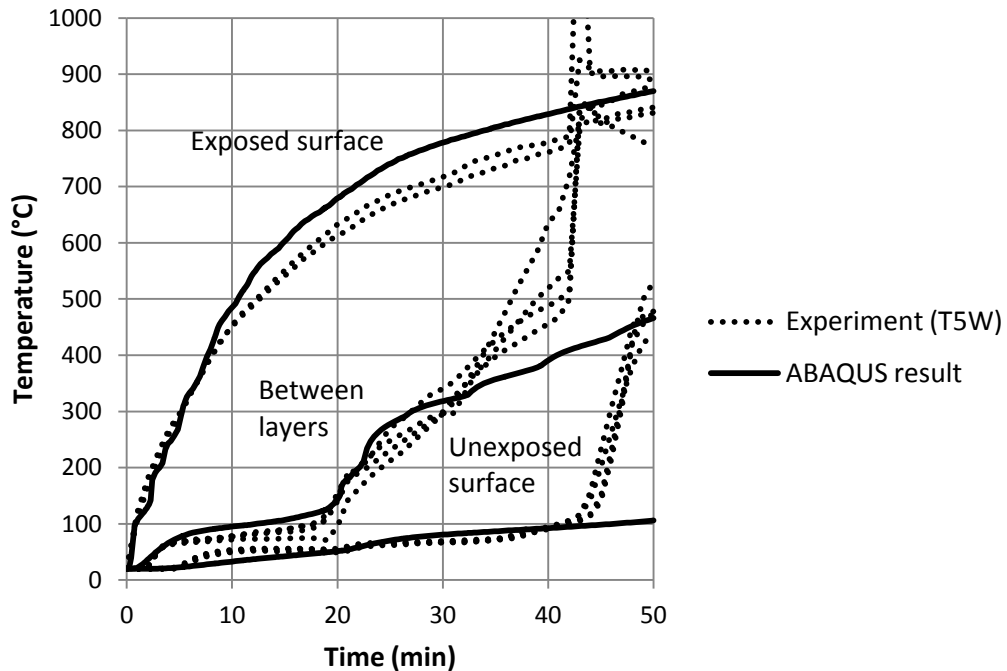


**Figure 7.12.** Temperature history for Test T5W (12.5mm double-layer non-insulated Wallboard gypsum)

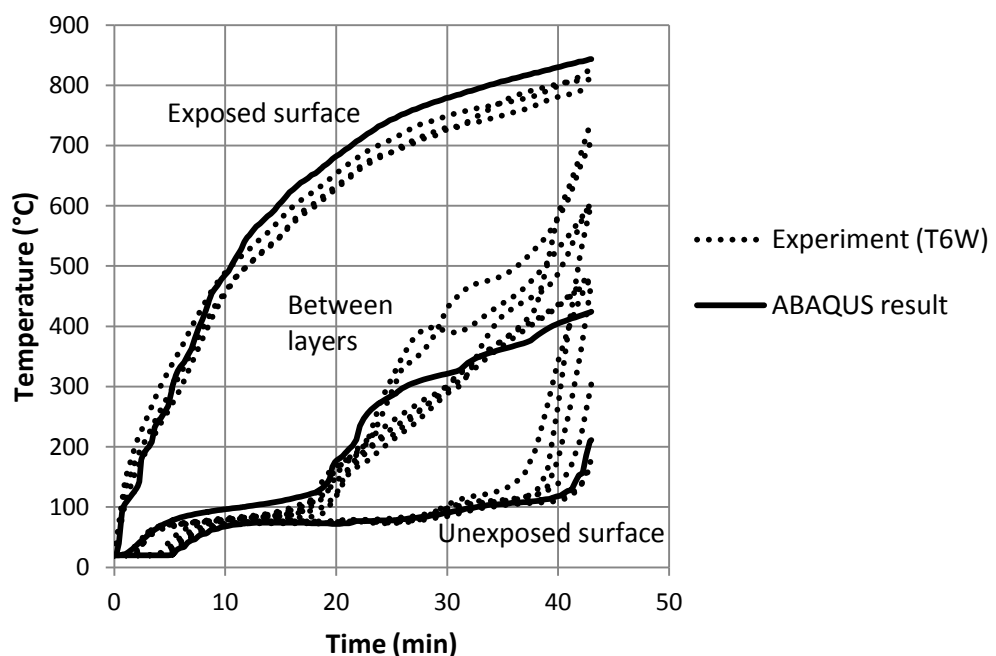


**Figure 7.13.** Temperature history for Test T6W (12.5mm double-layer insulated Wallboard gypsum)

## **7.4 Structural Analysis Using ABAQUS**

The structural analysis method used in ABAQUS for the purpose of this study is the “General Static” method. Geometric nonlinearity arising from large displacement effects was included in all cases.

This model uses the temperature output of the heat transfer model as input data. The objective of the simulation is to predict the opening of the first discrete crack that runs through the thickness of the board, and this is considered to give the closest indication of falling off of gypsum in fire. At present, it is not possible to predict multiple cracks and gypsum board falling-off. The following sections explain the features of the structural simulation.

### **7.4.1 Geometry**

The geometry of the model is defined as a 2D planar deformable structure, similar to the beam shown in Figure 7.2. Considering symmetry of the structure, the length of the beam in tests T1, T2, T5 and T6 is the width of one span, i.e. the distance between the centres of the adjacent studs (475mm). Similarly, in tests T3 and T4 the length of the beam is half of the span of the board, which equals 300mm. The thickness of the board in all cases is taken as 12.5mm. It should be noted that in double-layer panels, each layer of the gypsum board is analysed separately. Given the different temperature profile across each layer and different curvature of the two boards, separate analysis of each allows for a more accurate structural simulation.

### **7.4.2 Material Models**

It was demonstrated in CHAPTER 5 that the stress-strain relationship for Wallboard gypsum is a linear elastic one, whereas for Fireline gypsum, this relationship is better estimated by a bi-linear elastic-plastic relationship. It was also mentioned that the tensile and compressive behaviour of gypsum was assumed to be identical, although experimental observations confirmed that both gypsum board types were weaker in tension than in compression.

Elastic behaviour of gypsum can be simulated using the linear elasticity feature in mechanical properties of the material defined in ABAQUS. The modulus of elasticity of gypsum for all cases is defined as temperature-dependent and based on the values given in CHAPTER 5. Poisson's ratio is taken as 0.2.

ABAQUS does not have a material model for gypsum but a number of material models embedded in ABAQUS may be utilized for modelling plastic behaviour and failure of gypsum. The following material models have been tried and the most suitable one is selected for the purpose of this study.

#### **7.4.2.1 Classic Metal Plasticity**

Using the classic metal plasticity model in ABAQUS, the isotropic plastic hardening of gypsum can be defined identically in tension and compression. Failure of the material can be defined by introducing a sudden drop from the ultimate strength to a minimal stress value, as demonstrated in Figure 7.14. This material model can be applied to any element types with displacement degrees of freedom. The problem observed with this failure model was that failure would occur in compression, which is in contrast with experimental observations of brittle tensile failure of gypsum.

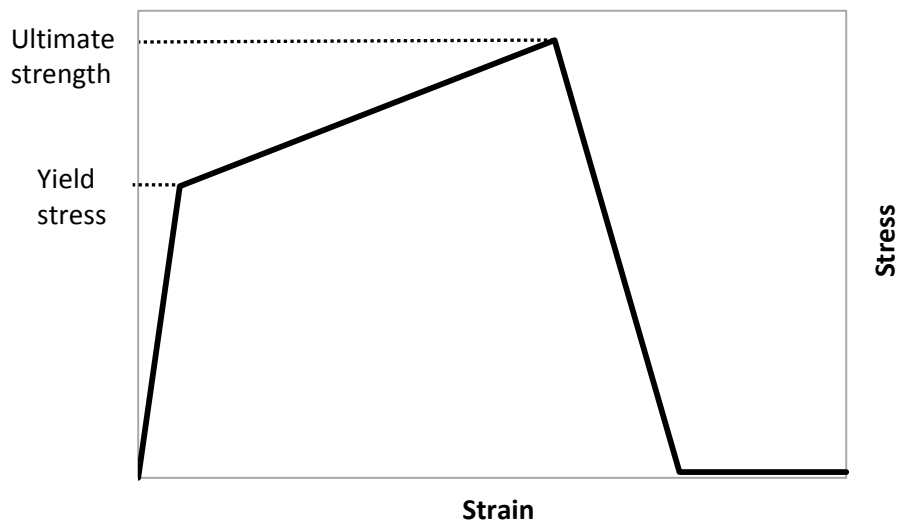


**Figure 7.14.** Defining failure in classic metal plasticity material model by introducing a sudden drop in the stress-strain relationship

#### **7.4.2.2 Cast Iron Plasticity**

Cast iron plasticity allows for definition of different plastic behaviour in tension and compression, and thereby avoiding the unexpected failure in compression. Again, failure can be defined by introducing a sudden drop in the stress-strain relationship as shown in Figure 7.14. The use of this material model is only limited to “Solid” element types and, given that the stiffness matrix is an unsymmetrical one, convergence problems are likely to stop the analysis. But the main problem observed with this model was that the analysis would halt soon after the first element had reached its ultimate strength. Since the objective of the structural analysis is to predict the complete opening of a crack, cast iron plasticity model is not suitable, and was therefore discarded.

#### **7.4.2.3 Concrete Smeared Cracking**

Concrete smeared cracking model is intended for materials like concrete, where cracking (in tension) is the most important aspect of the behaviour and dominates the modelling. Cracking occurs when the stress reaches a failure surface. After detection of a crack, the calculations are affected, because a damaged elasticity model is used and the stress and material stiffness associated with the integration point are affected by the crack. So the analysis continues with independent calculations at each integration point of the finite element model, but no individual macro cracks are tracked.

This model can be applied to a variety of element types, but comes with other limitations too. Plasticity in this material model can only be defined in compression. Therefore, the behaviour of gypsum in tension has to be modified to a linear one, which greatly compromises the accuracy of the analysis. It should also be noted that calculations can be highly unstable and convergence problems are very likely.

As a result, although this material model can simulate cracks and allows for the calculation to continue after the opening of a crack, it was tried but discarded too, mainly because it cannot track discrete cracks.

#### **7.4.2.4 Damage for Traction-Separation Laws**

The most suitable material model in ABAQUS that was tried for modelling gypsum boards is what referred to as “damage for traction-separation laws”. This damage model, used alongside the Extended Finite Element Method (XFEM) that was only added to ABAQUS in version 6.10, enables modelling discontinuities like cracks. The next section presents more details of this advanced modelling technique, which has been adopted in this study to simulate cracking in gypsum. The material behaviour before cracking is defined by the linear elasticity and classic metal plasticity models in ABAQUS.

#### **7.4.3 Extended Finite Element Method**

Extended Finite element Method (XFEM) is a relatively new modelling approach in fracture mechanics, first introduced by Belytschko and Black (1999), that makes modelling of cracks easier and accurate.

With the conventional finite element method, the surface of a crack has to be defined by the user and considerable mesh refinement is required in the vicinity of the tip of a stationary crack, so that the mesh matches the geometry of the discontinuity. Modelling a growing crack is even more demanding as it requires continuous updating of the mesh to conform to the geometry of the progressing crack.

Unlike the conventional finite element method, XFEM can be used to simulate the initiation and propagation of a discrete crack along an arbitrary, solution-dependant path, and alleviates the need for remeshing the crack surfaces, as crack propagation is not tied to the element boundaries in a mesh. Instead the discontinuity is modelled by defining a region with special enriched functions and additional degrees of freedom that allow for the displacement jump across a cracked element. More detailed information on the theories employed in this method can be found in ABAQUS 6.10 Documentations (ABAQUS, 2010) and papers by Remmers *et al* (2008) and Song *et al* (2006).

XFEM is a very attractive and effective way to simulate the initiation and propagation of discrete cracks and fits the purpose of this study. Currently (in ABAQUS 6.10), this technique is only available for first-order solid elements, and there are two distinct types of damage modelling within the XFEM framework: cohesive damage and linear elastic fracture mechanics. Since Fireline gypsum exhibits plastic behaviour in fire, the cohesive damage model has been chosen, which allows for both material and geometrical nonlinearity. This model uses traction-separation laws, and the damage properties are specified as part of the bulk material definition. The failure mechanism consists of two ingredients: a damage initiation criterion and a damage evolution law.

The process of degradation of the cohesive response at an enriched element begins when the stresses or the strains satisfy the specified crack initiation criteria. The criterion used for gypsum is the maximum principal stress, so that when the maximum principal tensile stress in an element reaches the ultimate strength of gypsum at the given temperature, a crack is formed. The direction of the crack is always orthogonal to the maximum principal stress direction. The enriched elements in this model do not undergo damage under pure compression.

The damage evolution law governs the rate at which the cohesive stiffness is degraded as soon as the initiation criterion is satisfied. The traction-separation damage evolution models that are available in ABAQUS are of two types: displacement-based or energy-based. Both options greatly alleviate the mesh dependency associated with strain localisation during material softening, and can be used to define a linear or nonlinear response with a failure mechanism as shown in Figure 7.15. When the crack initiation criterion is met (i.e. crack opening=0), the stresses decrease linearly or nonlinearly (Figure 7.15 (a) and (b) respectively) with the opening of the crack. However, if stress distributions in the structure compress the already opened crack, it will close through a linear route as depicted in Figure 7.15 by the arrows.

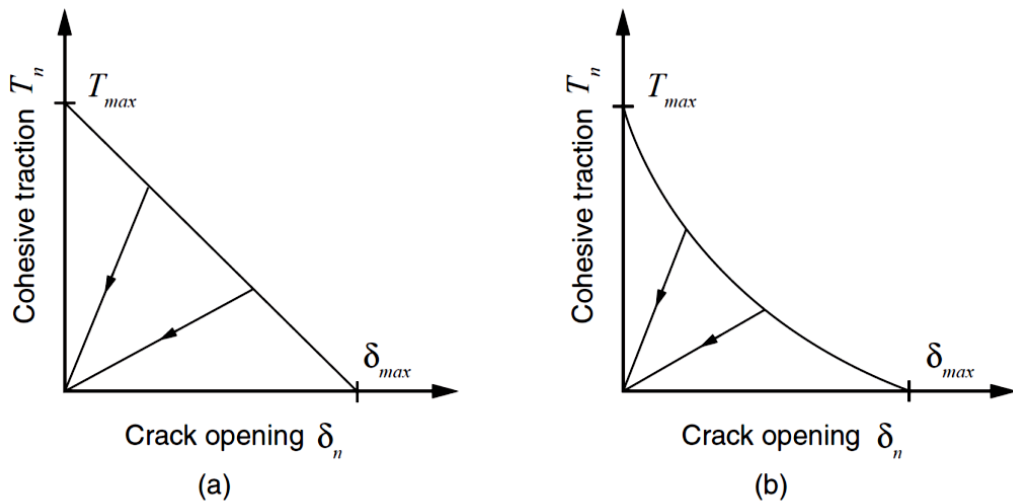


**Figure 7.15.** Typical linear (a) and nonlinear (b) traction-separation response

Since the energy performance of gypsum boards is not available at high temperatures, the displacement-based damage evolution model has been adopted. To define the softening part of the constitutive law as a stress-displacement relation, a characteristic length is introduced into the formulation, which in ABAQUS is related to the element size. The characteristic length is defined as the typical length of a line across an element for a first-order element. ABAQUS Documentation (ABAQUS, 2010) explains that “this definition of the characteristic length is used because the direction in which fracture occurs is not known in advance. Therefore, elements with large aspect ratios will have rather different behaviour depending on the direction in which they crack: some mesh sensitivity remains because of this effect, and elements that have aspect ratios close to unity are recommended.”

The displacement at which crack initiates ( $\delta_c$ ) can be calculated using the characteristic length ( $L_c$ ):  $\delta_c = L_c \varepsilon_u$ , where  $\varepsilon_u$  is the strain corresponding to the ultimate strength of gypsum. The displacement at failure ( $\delta_{max}$  in Figure 7.15), depends on factors such as the density of glass fibre reinforcement and the bond between the fibres and the gypsum substrate. This value should be estimated. For modelling concrete, ABAQUS advises that a reasonable starting point is to assume that the stress linearly reduces to zero at a total strain of about 10 times the strain

that causes the cracks to initiate. This is adopted for modelling gypsum. Therefore,  $\delta_{max}$  is specified to be 10 times  $\delta_c$  at any given temperature, and the traction-separation response is assumed to be linear. It should be noted that the numerical results are not sensitive to the value of  $\delta_{max}$ , and as shown in Figure 7.16, hardly any change is observed with half or twice the adopted value for  $\delta_{max}$ .

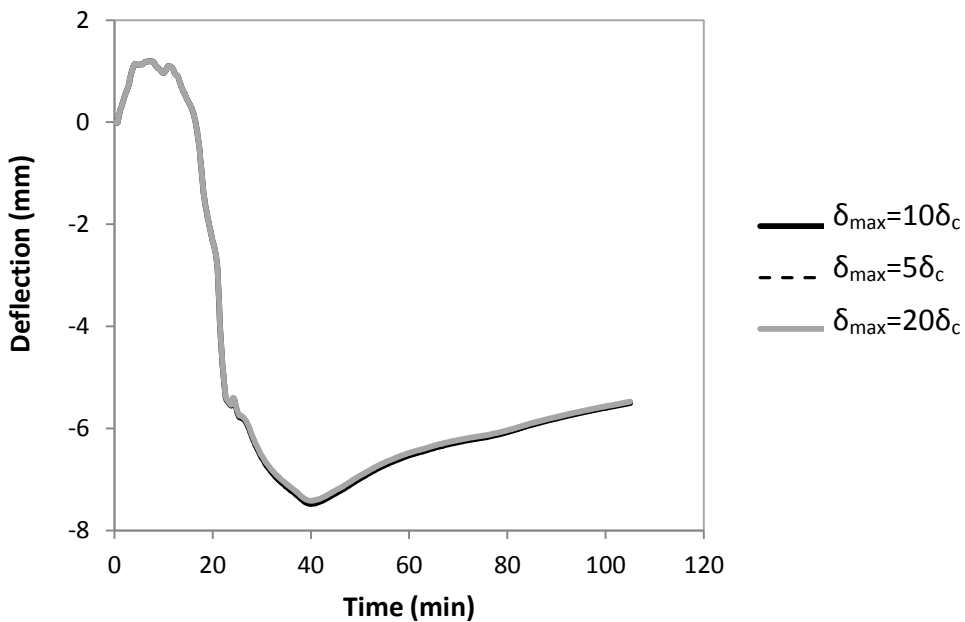


**Figure 7.16.** Sensitivity of the simulation results of the deflection at the mid-span of test T1F to different values of the displacement at failure ( $\delta_{max}$ )

The cohesive damage model in ABAQUS also allows for damage stabilization. Fracture makes the structural response nonlinear and non-smooth. In ABAQUS/Standard such stiffness degradations often lead to severe convergence difficulties. Using viscous regularization helps with the convergence of the Newton-Raphson method, which is used to solve the nonlinear equilibrium equations. This option is available in the definition of the material properties. A small value regularizes the analysis, helping with convergence while having a minimal effect on the response. A value of  $10^{-3}$  has been chosen for viscous regularization in all cases. To ensure that viscous regularization does not affect the response of the structure,

the total energy associated with viscous regularization can be checked against the total strain energy of the whole model. Figure 7.17 shows such a comparison for test T1F and confirms the suitability of the value chosen.

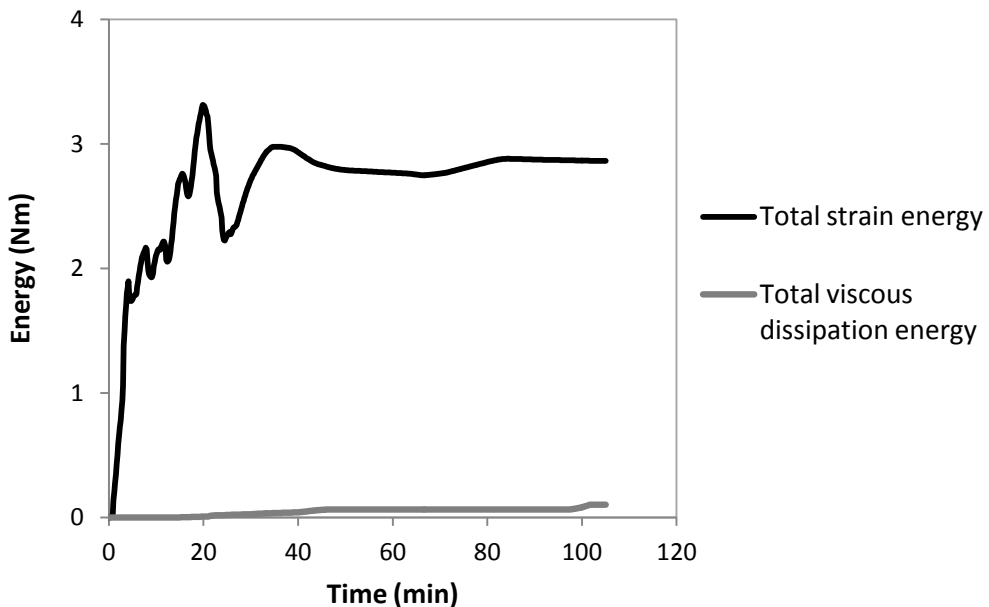


**Figure 7.17.** Comparison between the total strain energy and the total viscous dissipation energy in test T1F

To sum up, the material defined in ABAQUS to represent gypsum includes elastic and plastic behaviour as well as damage initiation and evolution models. The elastic and plastic stress-strain relationships of the two gypsum board types are based on those presented in CHAPTER 5.

#### **7.4.3.1 Current Limitations of the Numerical Analysis**

Although the cohesive damage model in ABAQUS and the extended finite element method of analysis provide the most suitable option amongst other material models explored for simulating cracks in gypsum, there are some limitations associated with this model that should be noted:

- The model is intended for single or a few non-interacting cracks in the structure. Therefore, it cannot simulate fall-off of gypsum. However, the model can simulate the opening of discrete cracks that will lead to falling off of gypsum.
- Multiple cracks can only happen if the crack initiation criterion is satisfied for multiple elements at the same increment. Then the program will simulate the propagation of all the cracks. But if at least one crack is propagating, no other cracks will initiate.
- An element cannot be cut by more than one crack.
- Cracks cannot turn more than 90 degrees in one increment.
- Cracks cannot branch.
- Once a crack initiates, it cannot be recovered and remains throughout the analysis, but it may open and close. The only available contact considered for crack surfaces is frictionless small-sliding contact.

Despite the limitations, the cohesive damage model and XFEM proves to be very effective for the purpose of this study, as will be demonstrated later in this chapter.

#### **7.4.3.2 Improving Convergence of Numerical Analysis**

Given the specified softening behaviour and stiffness degradation in the model, achieving convergence during numerical computations might prove difficult. There are a number of methods available that can be used to improve convergence behaviour of damage and fracture models (Wang et al., 2011):

- Viscous regularization, which is defined as part of the material properties, provides an artificial damping that causes the tangent stiffness matrix to be positive for sufficiently small time increments. As mentioned before, this parameter needs to be calibrated for different models, so that the energy associated with viscous regularization is very small compared to the total strain energy of the model and the response of the structure is not affected.

- Automatic stabilization is another option, defined as part of the analysis solution (so-called step in ABAQUS), that can be used to overcome localized instabilities where global solutions are not suitable. The preferred approach in ABAQUS is applying a varying damping factor that is based on the user-specified dissipated energy as a small fraction of the total strain energy. ABAQUS calculated the damping factor at each increment so that the dissipated energy does not exceed the fraction of the total strain energy specified.

It should be noted that in the simulations performed for this study there was no need for automatic stabilization.

- When extreme nonlinearities occur, such as in the case of modelling damage and fracture, the default solution controls in ABAQUS may not be adequate. Some of the analysis controls that can be set to aid in convergence are listed here:
  - Using smaller values for the minimum and maximum increment sizes will help avoiding premature cutbacks and large displacements in difficult analysis.
  - Selecting the unsymmetric matrix storage option instead of the solver default will also help convergence in cases where an unsymmetric system of equations is produced.
  - Time incrementation can be changed to the numerical scheme applicable to discontinuous analysis.
  - The maximum number of attempts before abandoning an increment is set to a default value of 5. This can be increased to 20 to accommodate the required cutbacks.

Solving a damage model usually requires applying all or some of the measures explained above. Adjusting the solution controls, such as the time incrementation features, has proved the most effective in modelling gypsum boards.

#### **7.4.4 Thermal Expansion**

In CHAPTER 5, dilatometer test results were presented for Fireline and Wallboard gypsum. It was observed that thermal expansion of gypsum is mainly negative, i.e. gypsum shrinks with temperature rise, and that shrinkage depends on the heating rate of gypsum.

In a standard fire test, the heating regime has a varying increase rate and only one side of the board is exposed to heat. Therefore, gypsum is heated at different rates through its thickness and at different times throughout the test. When gypsum is heated with a lower heating rate, it has the time to shrink more at any given temperature. But with a higher heating rate, the increase in shrinkage is delayed to a higher temperature. The fact that gypsum is heated more rapidly on the exposed side as compared to the unexposed side is actually favourable for the structural performance of the board. The stresses and the consequent deflections in gypsum are caused by the different shrinkage rates across the thickness of the board. The higher the shrinkage difference, the higher the stresses. But since the unexposed side is heated with a lower rate, it experiences higher shrinkage at any temperature. So the shrinkage difference of the two sides is less than the hypothetical case where the heating rate had no effect on shrinkage.

The experimental data for thermal shrinkage are only available for two constant heating rates of 5°C/min and 50°C/min. The numerical analysis performed using this data will not account for the favourable effect of shrinkage dependency on the heating rate. Therefore, it is speculated that using the shrinkage results from the higher heating rate (i.e. lower shrinkage results), will result in closer agreement between the numerical predictions of deflection and the experimental readings. As Figure 7.18 demonstrates, the speculation is confirmed and in all subsequent structural analyses, the average thermal shrinkage from dilatometer tests with heating rate of 50°C/min is used.

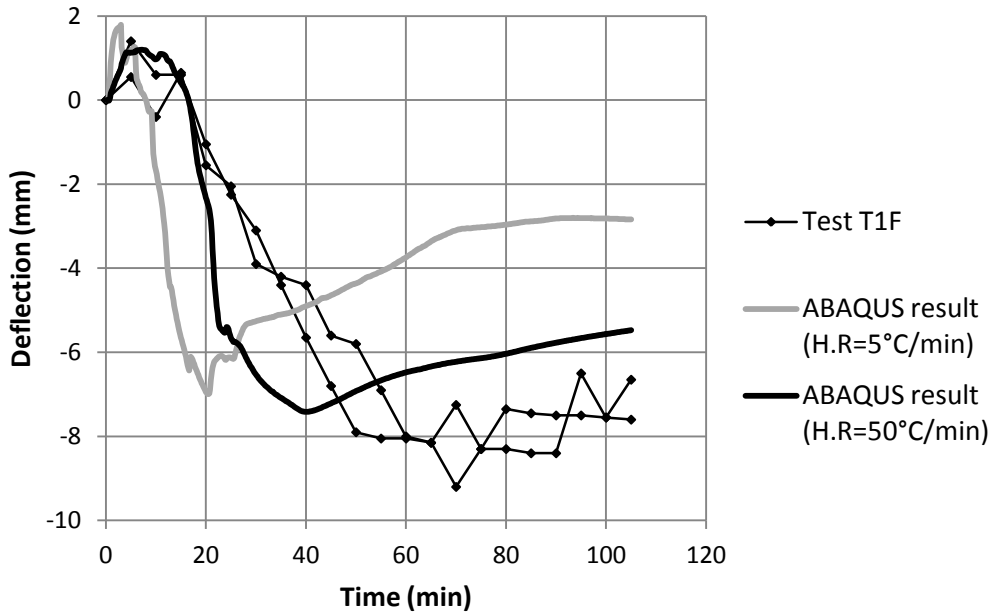


**Figure 7.18.** Comparison of numerical results for the mid-span deflection in test T1F, using thermal shrinkage data from dilatometer tests with different heating rates

#### 7.4.5 Mesh and Element Type

Since the physical problem has been reduced to a 2-dimensional numerical problem, the element type has to be either plane stress or plane strain. The dimension excluded from analysis is the height of the board which is greater compared to the other two dimensions. The strains associated with this length are therefore small compared to the cross-sectional strains. Hence, the element type is plane strain. The standard plane strain element for stress analysis in ABAQUS library is CPE4R, which is a 4-node bilinear plane strain quadrilateral element with hourglass control and reduced integration. The reduced integration option has been chosen to reduce the already costly computational volume.

The aspect ratio of the elements for the chosen analysis type is recommended to be close to one. To choose the optimum size of the elements, a sensitivity study has been performed for the 12.5mm layer of Fireline gypsum in test T1F with different mesh sizes:

Case d: 4 elements through the thickness, mesh size: 3.125mm

Total number of elements: 4x152

Case e: 6 elements through the thickness, mesh size: 2.083mm

Total number of elements: 6x228

Case f: 8 elements through the thickness, mesh size: 1.562mm

Total number of elements: 8x304

In all cases, assuming an aspect ratio of one for all the elements, the beam will have more than 150 elements in its longer dimension, which is more than enough for any moment analysis. Figure 7.19 shows the deflection of the mid-span for the three cases.

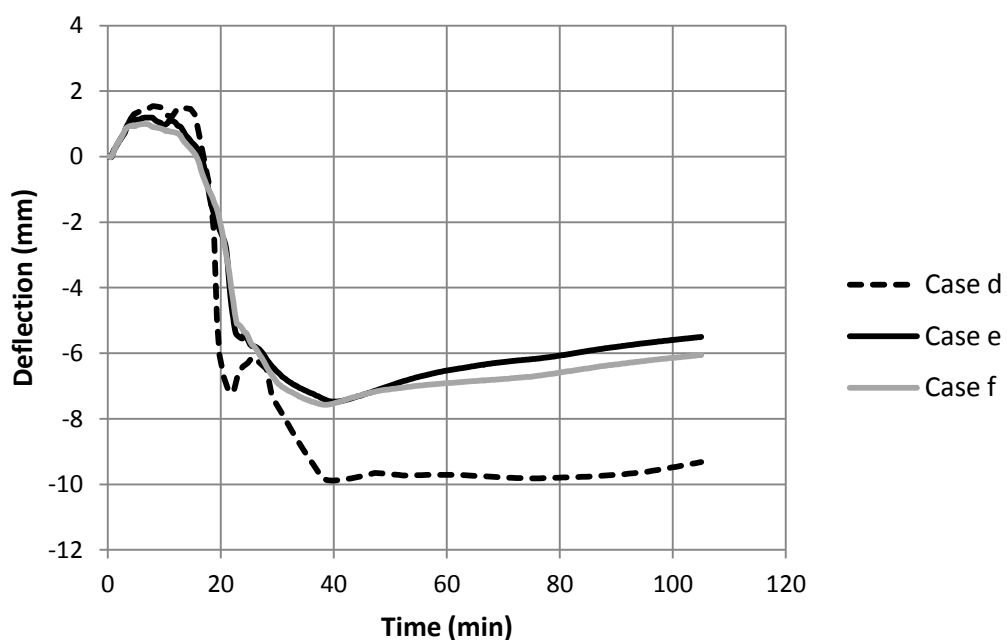


**Figure 7.19.** Deflection at the mid-span of Fireline gypsum board in test T1F, predicted by numerical analysis using different mesh sizes

It is observed that refining the mesh from Case d to Case e, affects the results greatly. However, further mesh refinement in Case f, with almost twice number of elements, produces only slightly different deflection predictions. Therefore, mesh size of about 2mm in Case e appears to be the optimum mesh size and has been adopted for all simulations.

#### 7.4.6 Predefined Fields and Boundary Conditions

The temperature solution from heat transfer analysis is assigned to the structural analysis as a predefined field. Since the mesh size and structure of both analyses is identical, compatible mesh option can be chosen to input the nodal temperatures of the integration points into the structural analysis.

Figure 7.20 shows a sketch of the support condition to the gypsum panels in tests T1, T2, T5 and T6, which is imposed by the studs and screws.

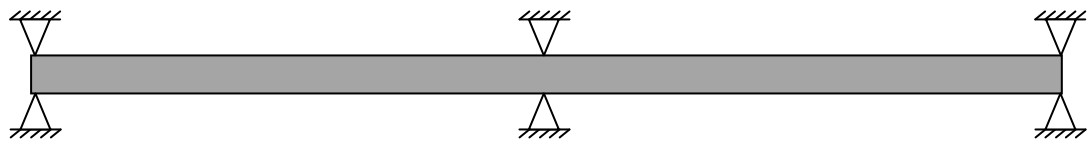


**Figure 7.20.** Support condition for the gypsum board in tests T1, T2, T5 and T6

Given the symmetry of the structure and loading, half of the beam is modelled in the simulation. The boundary conditions are defined at the positions highlighted in Figure 7.21 as follows: Displacement in direction 1 is restrained at node 1 and line 1. Displacement in direction 2 is restrained at nodes 1 and 2. This simulates total axial restraint in the member and rotational restraint at the symmetrical position in Figure 7.20. To avoid cracks forming at the corners due to the stress concentration, no enriched region is defined for the layer of elements closest to the left corner.



**Figure 7.21.** Boundary conditions, defined at the highlighted nodes and line on the half board in tests T1, T2, T5 and T6

The boundary conditions of tests T3 and T4 are sketched in Figure 7.22. Again symmetry reduces the numerical model to half of the board. Therefore, the boundary conditions can be defined at the highlighted positions in Figure 7.23: Displacement in direction 1 is restrained at line 1 (mid-span), and consequently the rotation is restrained too. All the nodes on line 2 are coupled to a reference node 1mm away from the board. Displacement in direction 2 at the reference node is restrained. Also applied to the reference node is a spring with linear stiffness. This spring simulates the stiffness that the stud imposes on the board, which can be fully rigid, semi-rigid or not rigid at all. The rigidity of this support is further discussed in the next section.



**Figure 7.22.** Schematic boundary conditions imposed on the gypsum board from the steel studs in tests T3 and T4



**Figure 7.23.** Boundary conditions, defined at the highlighted positions on the half board in tests T3 and T4

#### **7.4.7 Validation of Numerical Simulation Models – Fireline Gypsum**

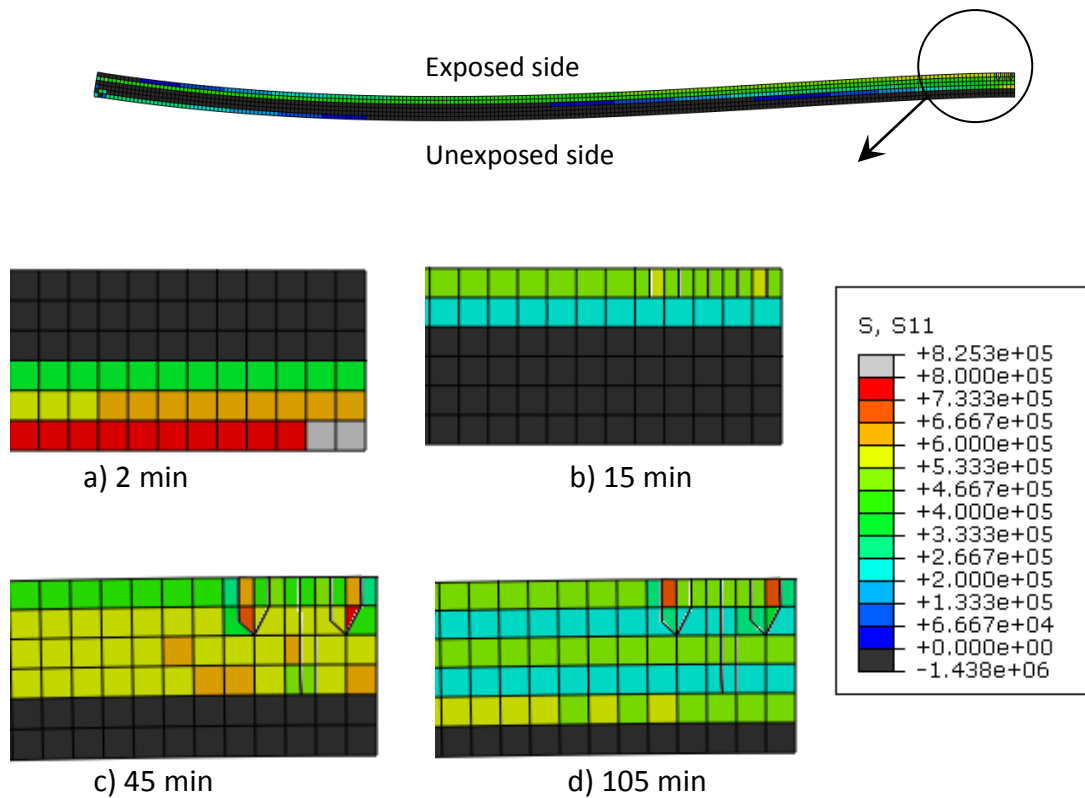
The six tests with different arrangements performed on Fireline gypsum boards, described in CHAPTER 6, are used to validate the results of the numerical analysis. The evaluation of the numerical results is achieved through comparing two parameters with the experimental results: the deflection at the mid-span of the boards, and the time at which the temperature at the unexposed side of the gypsum board experienced a sudden rise, compared with the simulation time when

the predicted cracks cut through the thickness of the board. Previous studies by Roy-Poirier and Sultan (2007) and Sultan (Sultan, 2010) suggest that soon after this sudden increase in temperature, the first section of the gypsum board falls off in fire.

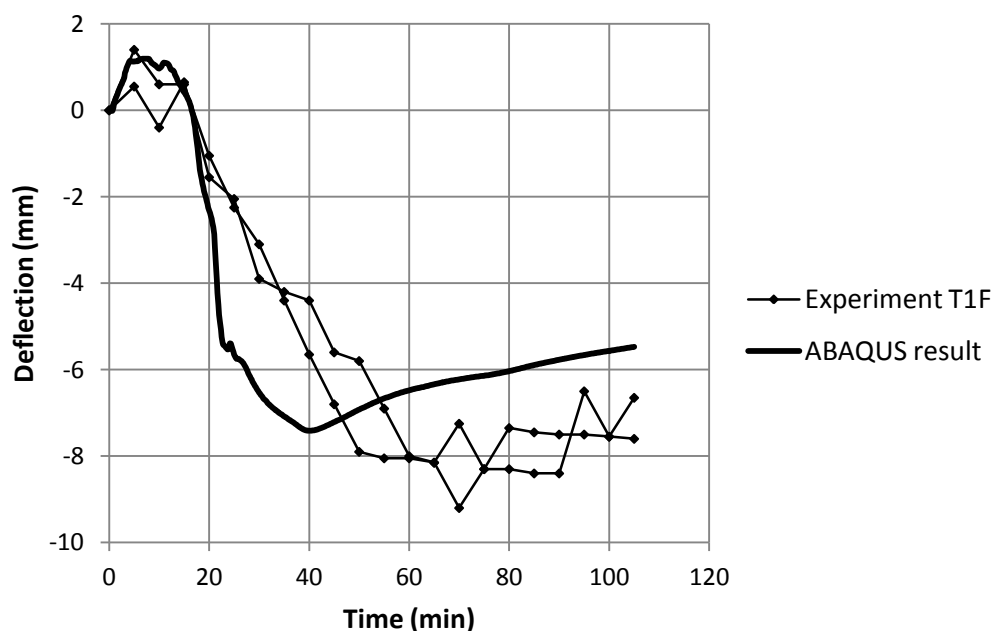
#### **7.4.7.1 Experiments T1F and T2F**

Figure 7.24 shows the simulated stress distributions in the longitudinal direction of the gypsum board (modelled as a beam) for test T1F at different times during heating. Gypsum slightly expands until about 200°C and then starts shrinking with further temperature rise. Therefore, for the first few minutes of the fire test, the exposed side of the gypsum board is expanding more than the unexposed side. Hence the unexposed side is confining the exposed side and the exposed side experiences compressive stresses (Figure 7.24.a). With further temperature increase, gypsum starts to shrink. Consequently, the situation reverses and the stresses on the unexposed side become compressive (Figure 7.24.b). As heating continues, the neutral axis of the beam moves lower, and the thickness of the compression strip reduces.

Accordingly, the deflection at the mid-span in the first few minutes of the test is towards the furnace. Gradually, as the gypsum board starts to shrink, the mid-span will deflect out of the furnace. The rate of deflection increase will reduce as the temperature of the unexposed side of the gypsum board catches up with the temperature of the exposed side, and the shrinkage difference between the two sides decreases. Figure 7.25 compares the experimental readings of the deflection at the two mid-span positions with numerical predictions. It is confirmed that the chosen analysis type, material model and the material properties used in the analysis provide results in very close agreement with the test measurements.



**Figure 7.24.** ABAQUS stress distribution results in the direction of the length of the beam for test T1F at different times during heating. Compressive stresses are shown in grey



**Figure 7.25.** Comparison between numerical and experimental results for the deflection at the mid-span of the gypsum board in test T1F

The temperature measurements on the unexposed side of the board in test T1F did not experience any sudden increase, suggesting that there was no gypsum fall-off in this test. This is in conformity with the ABAQUS results that do not show any complete cracks through the thickness of the board.

The ABAQUS simulation predicts cracks forming on the exposed side, close to the stud in the middle of the assembly. These cracks start about 15 minutes into the test, but they do not run through the thickness of the board when the specified test is completed. The stress distribution along the gypsum board on the exposed side, just before the cracks have started, is rather uniform, with the difference between the maximum and minimum stresses on the upper layer of the elements (excluding the first few elements above the pin support) being about 5%. This implies that, in fact, cracks might start anywhere along the beam to release the stress. However, since the analysis cannot simulate other cracks while one is progressing, ABAQUS does not predict any other cracks.

It should also be noted that the deformations close to the simple boundary (node 1 in Figure 7.21) increase considerably as the simulation progresses, but no cracks are predicted as there are already progressing cracks present elsewhere in the simulation (Figure 7.26). This suggests that the gypsum board might experience local cracks and detachment at the position of the screws along its vertical edge. This phenomenon will lead to the opening of the joints in wall assemblies and encourage falling off of gypsum soon after other cracks along the board cut through the thickness of gypsum.

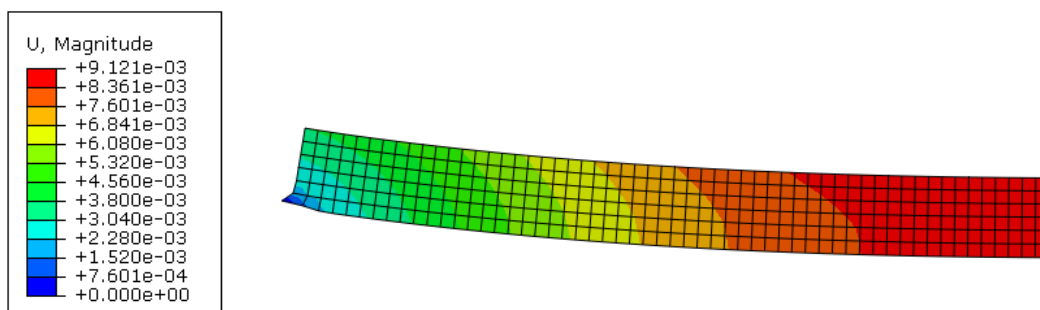


**Figure 7.26.** Large deformation of the board close to the edge in test T1F

The stress distribution and pattern of cracking in test T2F are very similar to those in test T1F. Again cracks are formed close to the middle stud but there is no crack through the thickness of the board during heating (Figure 7.27). This is in agreement with the test observations that there was no indication of gypsum falling.

The predicted deflection at the mid-span from the analysis is compared with the experimental results in Figure 7.28, and a good agreement is confirmed.

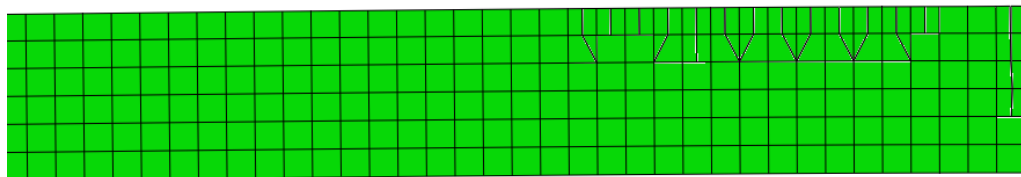


**Figure 7.27.** Crack pattern for test T2F as predicted by ABAQUS just before the test is terminated

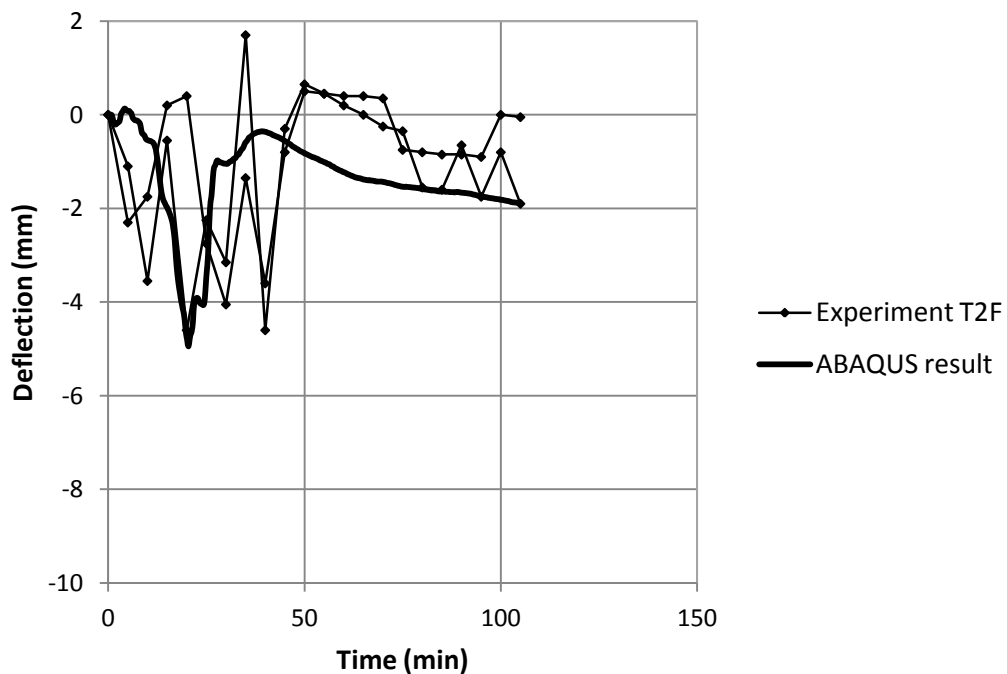


**Figure 7.28.** Comparison between numerical and experimental results for the deflection at the mid-span of the board in test T2F

#### 7.4.7.2 Experiments T3F and T4F

In tests T3 and T4, the gypsum board is slotted into the vertical studs with no screws, and therefore the studs provided no horizontal restraint for the board. However, they cause some rotational restraint at the two ends of the gypsum board, as shown in Figure 7.22. This bending rigidity is simulated by a spring as demonstrated in Figure 7.23. Assuming no rigidity for this spring, the predicted deflections at the mid-span of the board are much higher than the test results. On the other hand, considering full rigidity at the supports results in the predicted deflections to be much smaller than the experimental results (Figure 7.29). Therefore, the studs were considered to have provided semi-rigid supports for the gypsum board, and the rigidity of the spring in Figure 7.23 should be included in simulation.

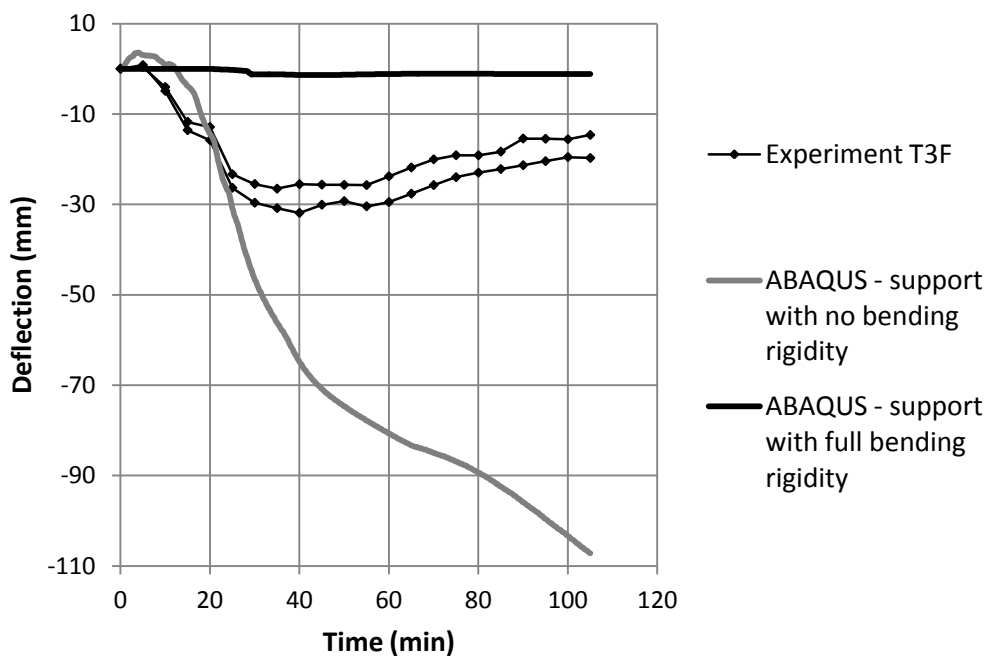


**Figure 7.29.** Comparison between numerical results for the deflection at the mid-span of the beam in test T3F, considering fully-rigid or pin supports and the experimental results

Consider the board and the studs as shown in Figure 7.30. The bending rigidity provided by the studs,  $R_s$ , can be expressed as:

$$R_s = \frac{M}{\theta}$$

where  $M$  and  $\theta$  are defined as:

$$M = F(L_1 - L_2)$$

$$\theta = \frac{\Delta_1 + \Delta_2}{L_1 - L_2}$$

$\Delta_1$  and  $\Delta_2$  are the deflections of the studs at  $L_1$  and  $L_2$  respectively, calculated from:

$$\Delta_1 = \frac{FL_1^3}{3E_1 I}$$

$$\Delta_2 = \frac{FL_2^3}{3E_2 I}$$

In which,  $I$  is the moment of inertia of the steel section and  $E_1$  and  $E_2$  are the elastic moduli of the steel sections which change with temperature. To calculate the elastic modulus of steel at elevated temperatures, Eurocode 3 (BSI, 2005b) suggests reduction factors to be applied to the elastic modulus of steel at 20°C. The elastic modulus of steel at 20°C,  $E_a$ , is taken as 210000N/mm<sup>2</sup> (BSI, 2005a). Hence  $E_1$  and  $E_2$  can be expressed in terms of the reduction factors  $K_{R1}$  and  $K_{R2}$ :

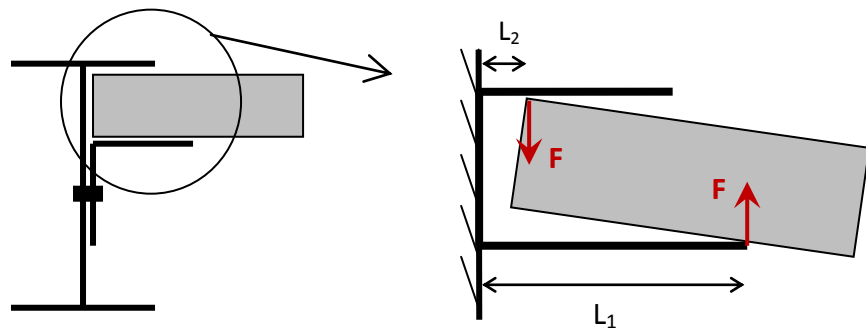
$$E_1 = K_{R1} E_a$$

$$E_2 = K_{R2} E_a$$

Therefore, the bending rigidity of the support can be expressed as:

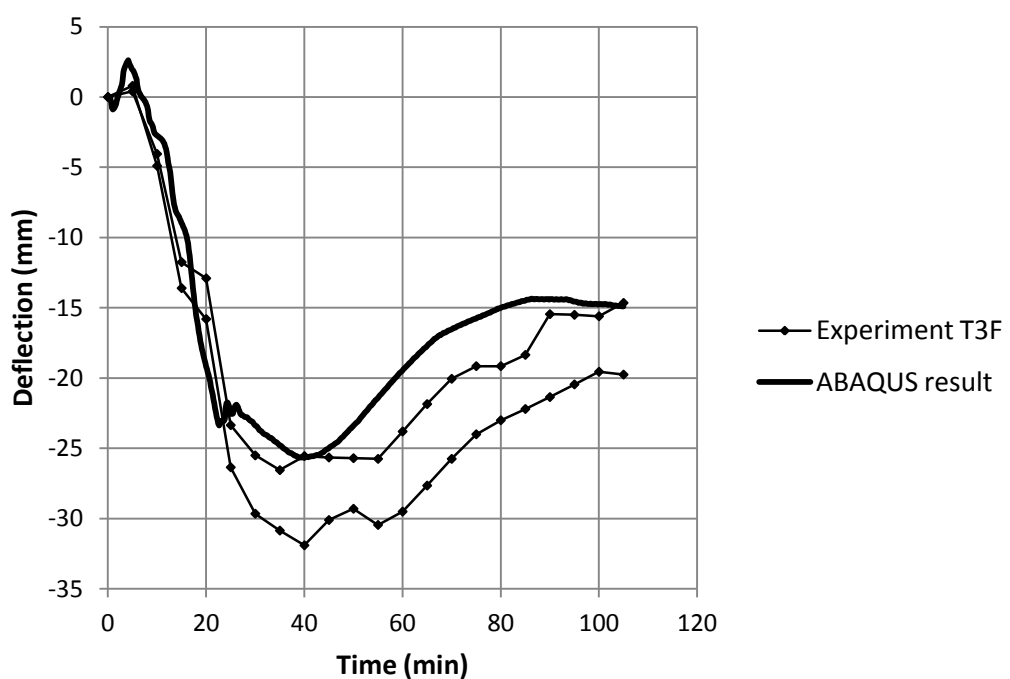
$$R_s = 3E_a I \frac{(L_1 - L_2)^2}{\left(\frac{L_1^3}{K_{R1}} + \frac{L_2^3}{K_{R2}}\right)} \quad (7.1)$$

$L_1$  is the length of the steel angle, which is 25mm, and  $L_2$  changes as the board shrinks with temperature. The variations in  $L_2$  do not affect the rigidity of the gypsum board considerably; hence taking an average value of about 3mm would suffice for the calculations.



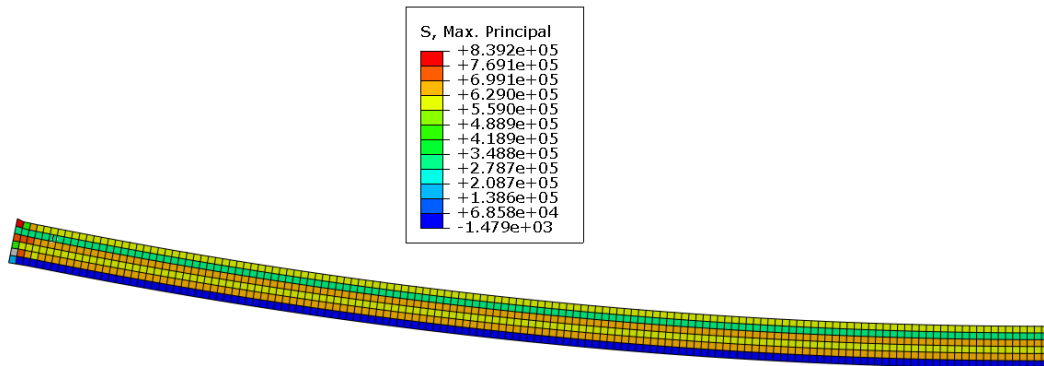
**Figure 7.30.** Schematic view of the semi-rigid support provided to the gypsum board by the studs in tests T3 and T4

Thus, the stiffness of the spring in Figure 7.23 can be calculated using Eq. (7.1) for different temperatures. The mid-span deflection results using the semi-rigid support model are demonstrated in Figure 7.31, which indicates that the numerical and experimental deflections are in very close agreement.



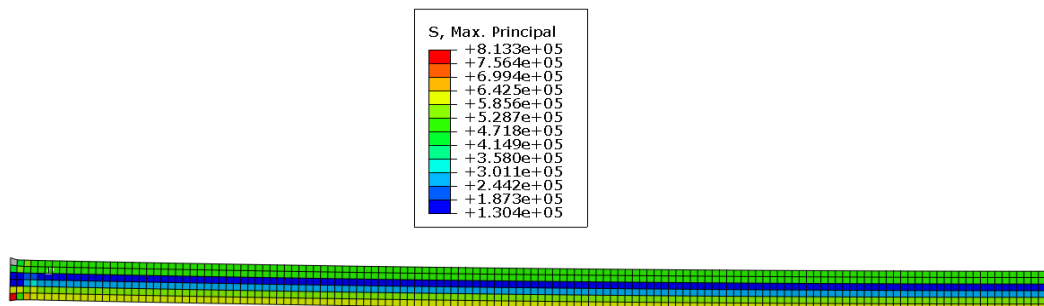
**Figure 7.31.** Comparison between numerical results of the deflection at the mid-span of the gypsum board in test T3F using the semi-rigid support model and the experimental results

Figure 7.32 shows the predicted stress distribution throughout the gypsum board on the deflected shape of the board. The ABAQUS model only predicts cracking in one element close to the support. The experimental observations confirm that there was no wide crack or fall-off of the gypsum board.



**Figure 7.32.** Distribution of the maximum principal stresses on the gypsum board in test T3F just before the test is terminated

The simulation and the experimental results of the cracking pattern in test T4F are very similar to those of test T3F. Figures 7.33 and 7.34 show the corresponding results. Again the agreement between the numerical and experimental results is very good.



**Figure 7.33.** Distribution of the maximum principal stresses on the gypsum board in test T4F just before the test is terminated

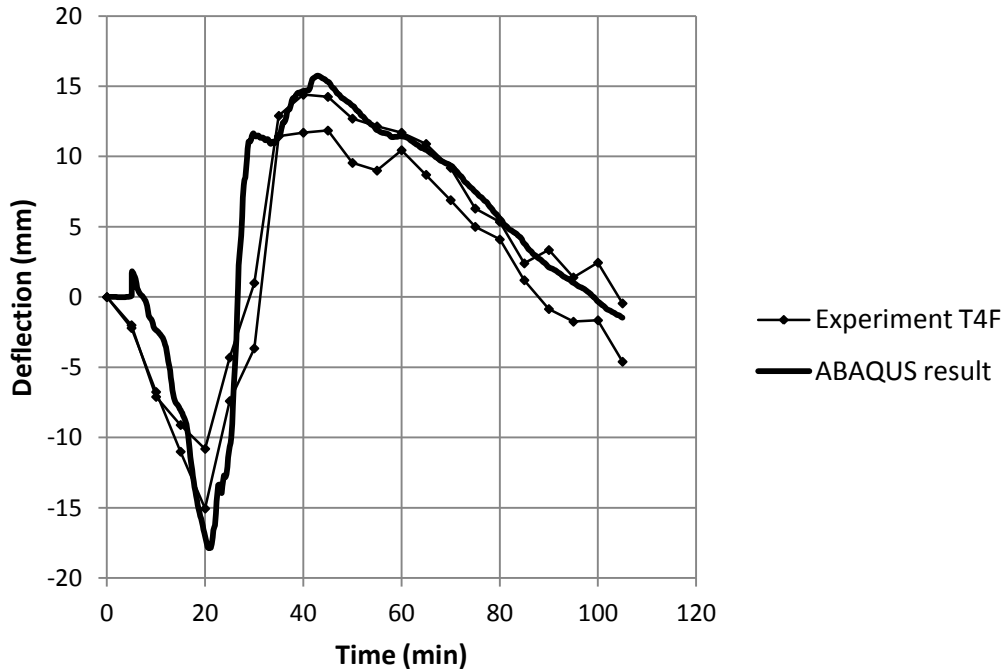


**Figure 7.34.** Comparison between numerical and experimental results of the deflection at the mid-span of the board in test T4F

#### 7.4.7.3 Experiments T5F and T6F

In tests T5 and T6, there are two layers of gypsum board installed. Each layer is simulated separately, and there is no structural interaction between the two layers. The recordings of mid-span deflection are only available for the unexposed board. Therefore, other measures have to be used to validate the simulation of the exposed board. Figure 7.35 shows that the temperature on the back of the exposed board (between the two layers) experiences a sudden increase of about 200°C within one or two minutes. This is observed between 56 to 61 minutes into the test for four thermocouples, and suggests that the exposed board has formed cracks that allow the heat to penetrate rapidly. The simulation results for the exposed board predicts that through-thickness cracks form near the middle stud at about minute 55 of the test. This time concurs with the experimental observations. Figure 7.36 shows the deflection shape of the board at different times of the simulation.

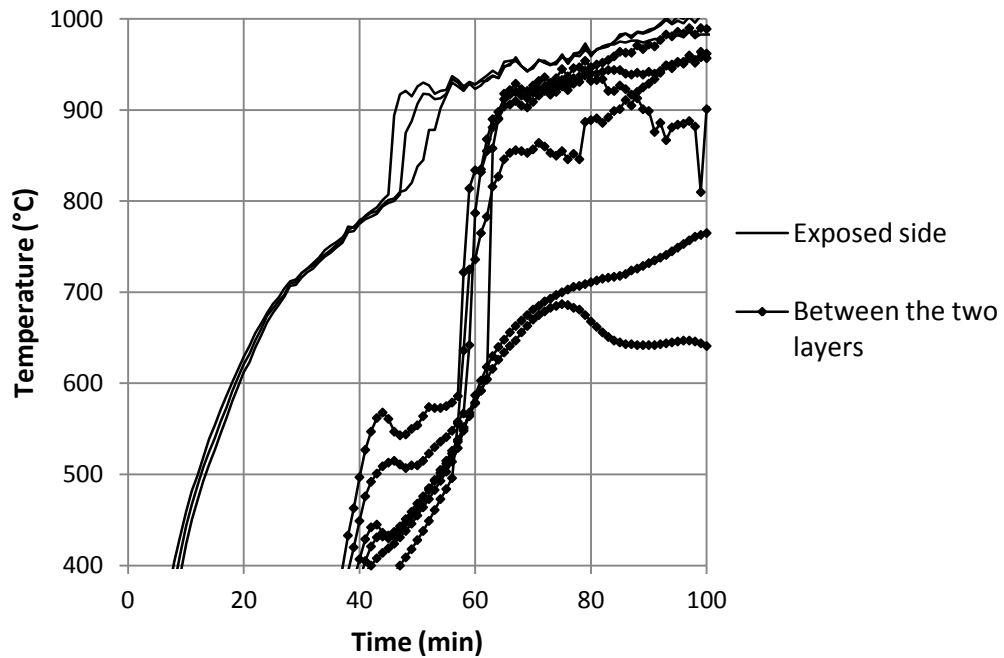


Figure 7.35. Temperature history for the exposed board in Test T5F

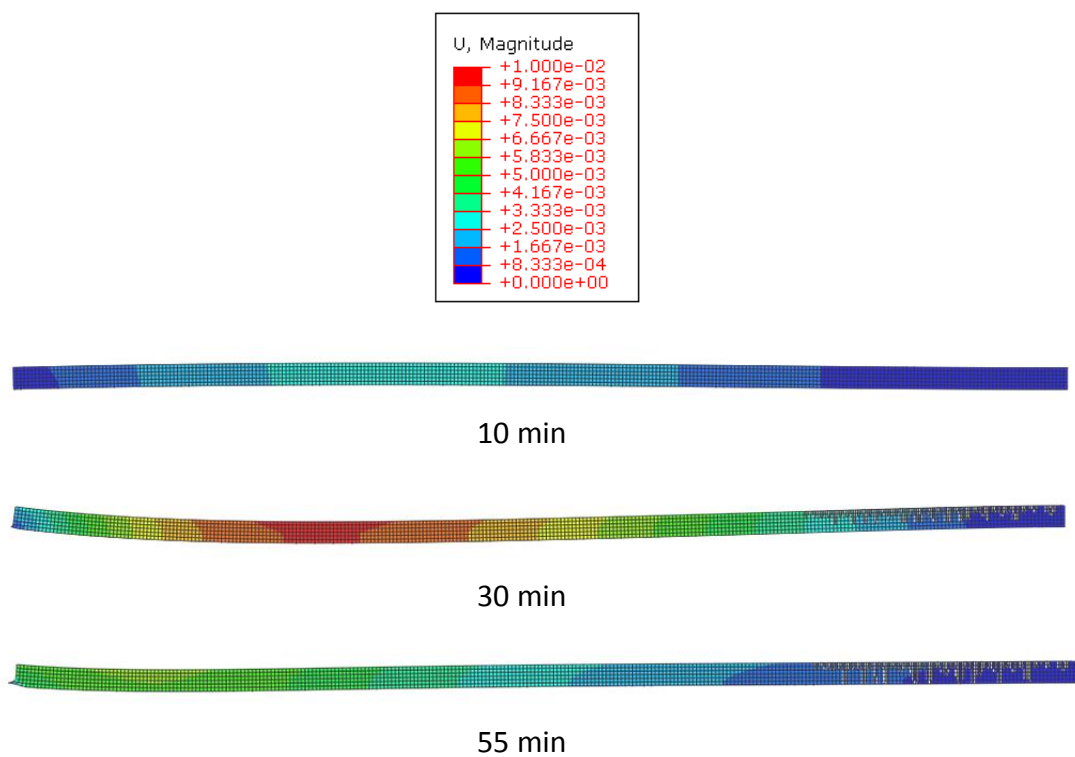
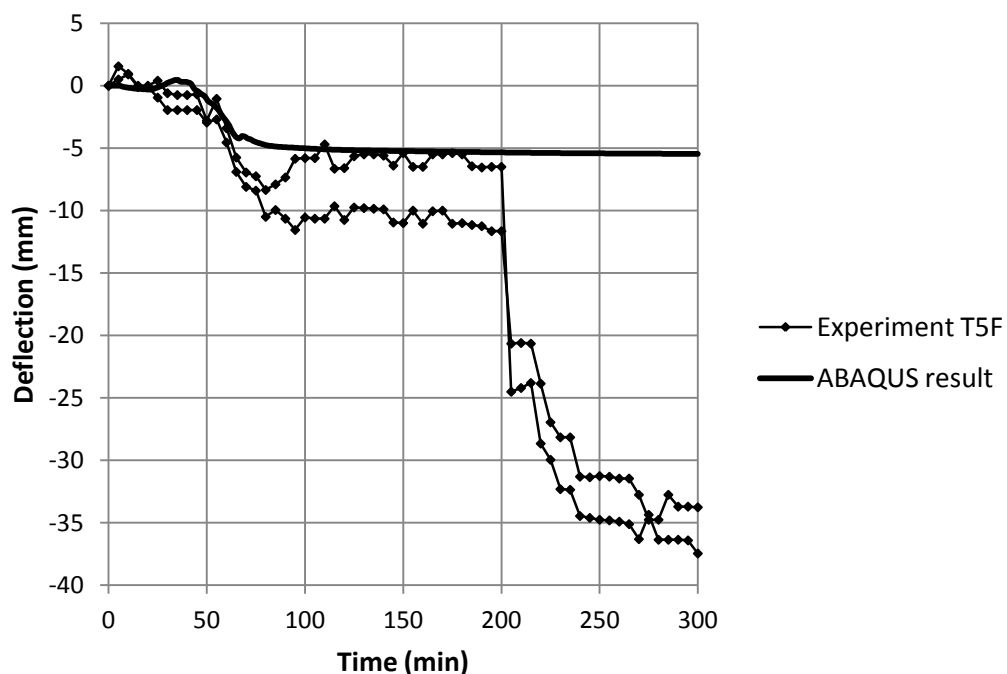


Figure 7.36. Deflection of the exposed gypsum board in test T5F at 10, 30 and 55 minutes

Figure 7.37 compares the predicted and recorded deflections at the mid-span of the unexposed board in test T5W. The numerical results agree well with the experiment results until about 200 minutes into the test, after which recordings of the deflection experience a sudden increase, but the numerical prediction stays relatively unchanged. The test report indicates that at 210 minutes, about half of the exposed board falls off in fire. At present, it is not possible to include gypsum board falling off in the simulations; hence it is not possible to simulate the observations after 200 minutes. Nevertheless, it is encouraging to see the ABAQUS model predicting the formation of the first through-thickness crack with good accuracy.



**Figure 7.37.** Comparison between numerical and experimental results of the deflection at the mid-span of the unexposed gypsum board in test T5F

The results for test T6F are very similar to those in test T5F. In this test, the sudden increase in temperature at the back of the exposed board (between the two layers) is observed between 63 to 68 minutes of the test (Figure 7.38); this is compared with the simulation time of 64 minutes when the through-thickness crack appeared (Figure 7.39).

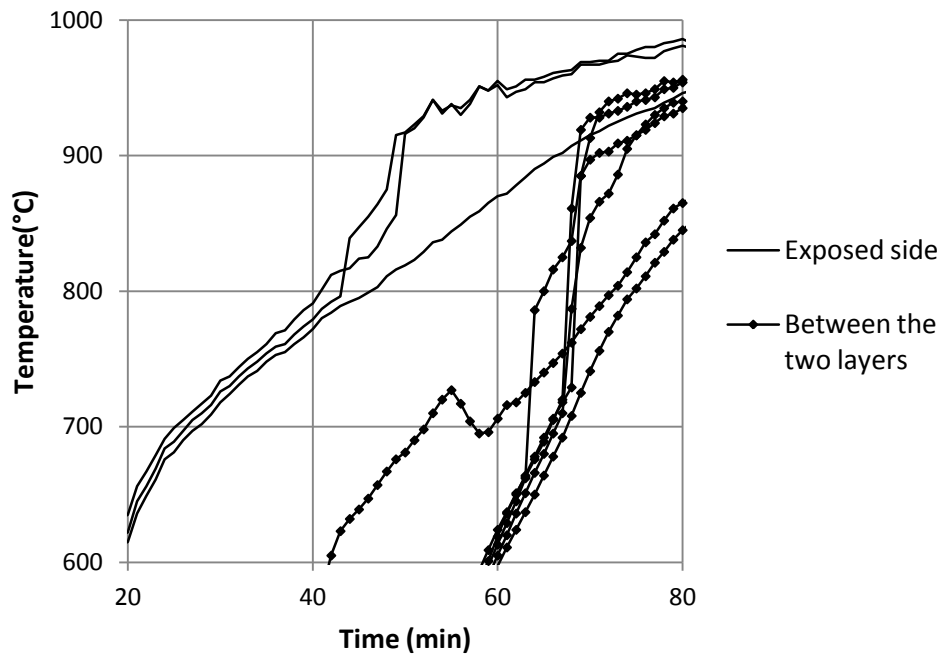


Figure 7.38. Temperature history for the exposed board in Test T6F.

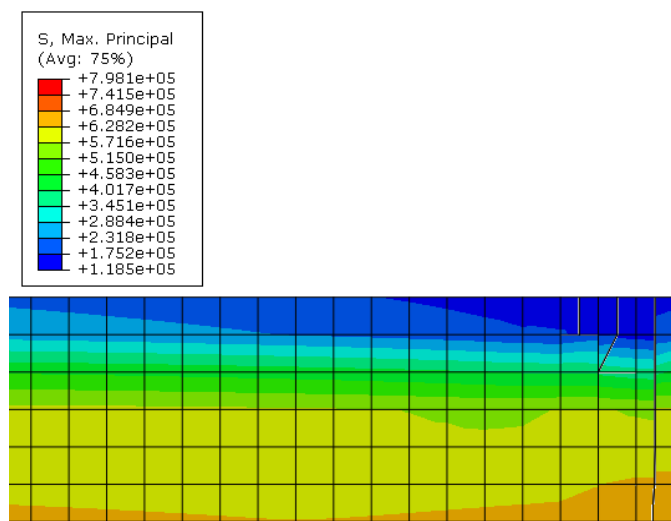
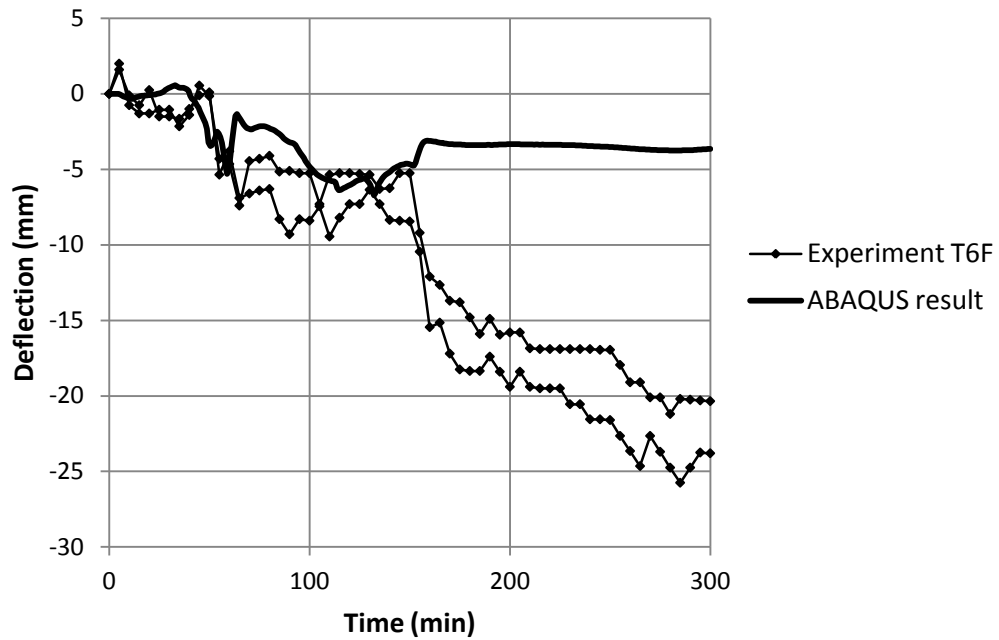


Figure 7.39. Distribution of maximum principal stresses on the exposed beam in test T6F just after the crack cuts through the thickness of the board.

Figure 7.40 compares the predicted and experimental deflections for the unexposed gypsum board in test T6F. Similar to test T5F, the numerical prediction of

deflection agrees well with the experimental measurements until about 170 minutes into test. The experimental report indicates observation of falling off of the entire exposed board at 180 minutes into the test.



**Figure 7.40.** Comparison between numerical and experimental results of the deflection at the mid-span of the unexposed board in test T6F.

#### 7.4.7.4 Summary

Tables 7.1 and 7.2 summarise the numerical and experimental results for all the six tested wall assemblies with Fireline gypsum board. It can be concluded that the numerical predictions of the deflection of the boards in single-layer tests are in very good agreement with the experimental recordings. The same applies to the deflection of the unexposed board in double-layer tests as long as the exposed board has not fallen off in fire. Complete cracks are numerically predicted to happen, for the exposed boards in double-layer tests, at times very close to the observation of the sudden temperature rise on the back of the exposed boards. For the double gypsum assemblies, the effects of through thickness crack in the exposed board are not felt in the unexposed board until gypsum fall-off. It is currently not possible to predict this event, but the behaviour of the unexposed board is well predicted until this event.

Single-layer experiments		T1F	T2F	T3F	T4F
Experimental results	Vertical crack observed on the exposed side of the board	None	None	None	None
	Sudden temperature rise observed on the unexposed side of the board	None	None	None	None
	First fall-off of the board	None	None	None	None
ABAQUS results	Complete opening of at least one crack	None	None	None	None
	Agreement between the deflection at the mid-span of the board with test results	Good	Good	Good	Good

**Table 7.1.** Comparison between experimental and numerical results for single-layer Fireline gypsum board wall assemblies.

Double-layer experiments		T5F	T6F
Experimental results	Vertical crack observed on the exposed board	160min	None
	Sudden temperature rise observed at the back of the exposed board	56-61min	63-68min
	First fall-off of the exposed board	210min	180min
ABAQUS results	Deflection shock on the unexposed board	200min	170min
	Complete opening of at least one crack	55min	64min
Agreement of the deflection of the unexposed board with test results		Good until 200min	Good until 170min

**Table 7.2.** Comparison between experimental and numerical results for double-layer Fireline gypsum board wall assemblies.

#### 7.4.8 Validation of Numerical Results for Stress Analysis – Wallboard Gypsum

Out of the 6 tests performed on Wallboard gypsum, tests T1W and T3W were discarded. As mentioned in CHAPTER 6, the draw wire transducers that were used for measuring the deflections of the boards applied too great a load on the boards that invalidated the tests. The four remaining experiments are used to validate the simulation results for Wallboard gypsum.

##### 7.4.8.1 Experiments T2W and T4W

Experimental observations of the exposed side of the Wallboard gypsum in test T2W indicate visible cracks at 20 minutes. The simulation results also show that just before 20 minutes into the tests, the cracks close to the middle stud developed through the thickness of the board (Figure 7.41). Soon after this point the numerical simulation halts, as the structure becomes unstable. The thermocouple readings on the unexposed side of the board show a sudden increase in temperature at 18-19 minutes into the test (Figure 7.42).

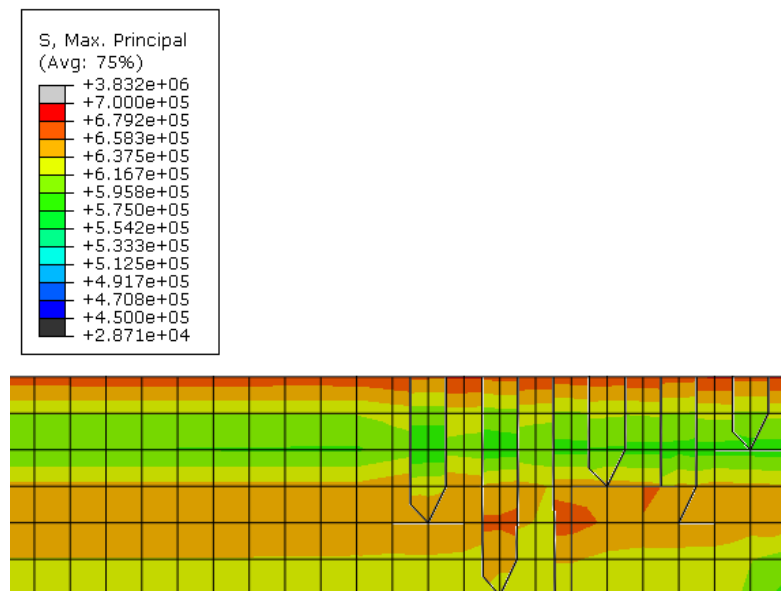


**Figure 7.41.** Distribution of maximum principal stresses on the beam in test T2W just after the cracks cut through the thickness of the board

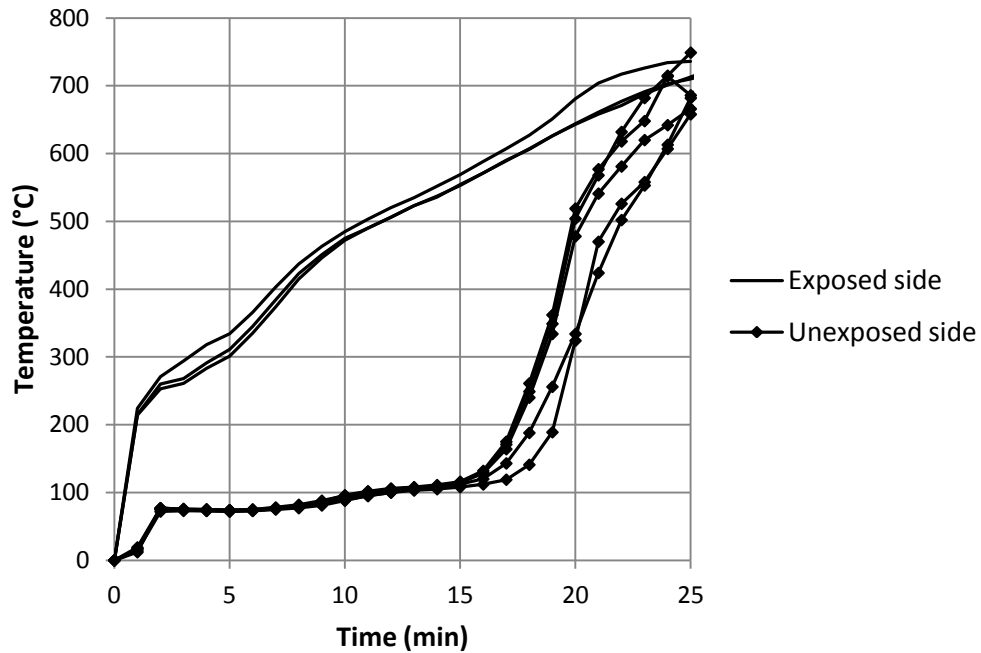
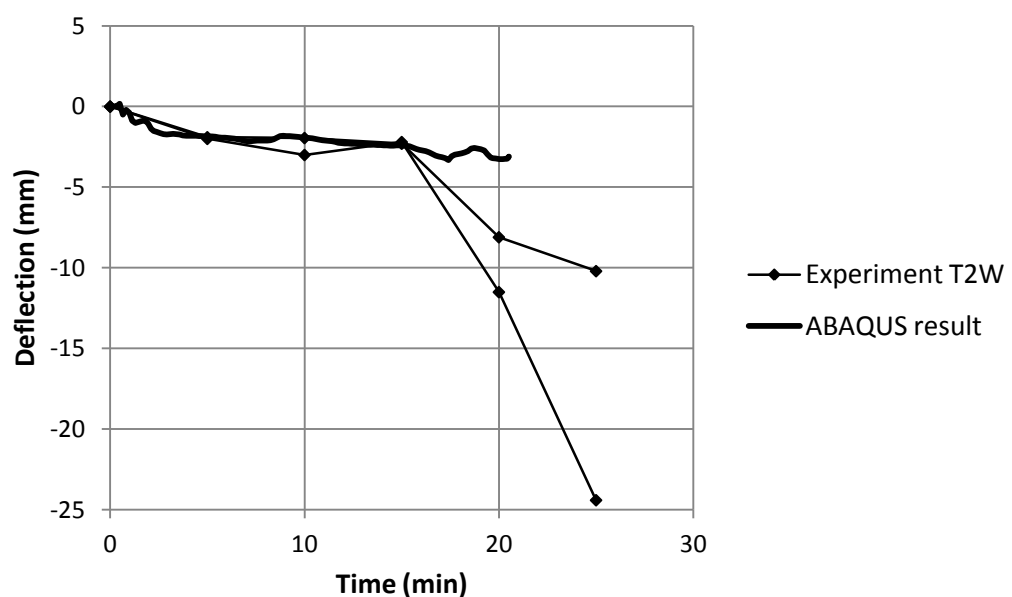


Figure 7.42. Temperature history for the Wallboard gypsum in Test T2W

The test observations also indicate that the centre stud buckles into the furnace before 25 minutes into the test (Figure 7.43). The recordings of the deflection of the flange of the stud also confirm possible torsional buckling, as the flange starts to move out of the furnace just after 20 minutes. Therefore, the deflection recordings of the board are affected after 20 minutes. Figure 7.44 compares the numerical and experimental results for the mid-span deflection of the board in test T2W. The numerical analysis accurately predicts the deflection before cracking. The effects of cracking and buckling of the steel stud increase the deflection of the test specimen measured at minutes 20 and 25.



**Figure 7.43.** Buckling of the middle stud into the furnace at 24 minutes in test T2W



**Figure 7.44.** Comparison between numerical and experimental results for the deflection at the mid-span of the gypsum board in test T2W

In test T4W, the stiffness of the spring boundary condition is defined using Eq. (5.1) as explained earlier. The simulation results show that a crack close to the studs develops through the thickness at about 16 minutes into the test (Figure 7.45). There are no reports of cracks during test. However, the temperature recordings on the unexposed surface of the board show a rapid temperature increase around minute 20, although this may have been caused by dehydration of the gypsum at about 100°C (Figure 7.46). At 27 to 29 minutes into the test, on the other hand, there is evidence of sharp temperature increase of more than 100°C per minute, which coincides with the report of falling off of a section of the board in fire at 30 minutes into the test just before the test is terminated.

Figure 7.47 compares the numerical and experimental deflections at the mid-span of the board. The analysis predicts the deflection well until about 16 minute of the test, when the simulation stops due to the opening of a complete crack. Nonetheless, the predicted deflections are very close to the test recordings before this time.

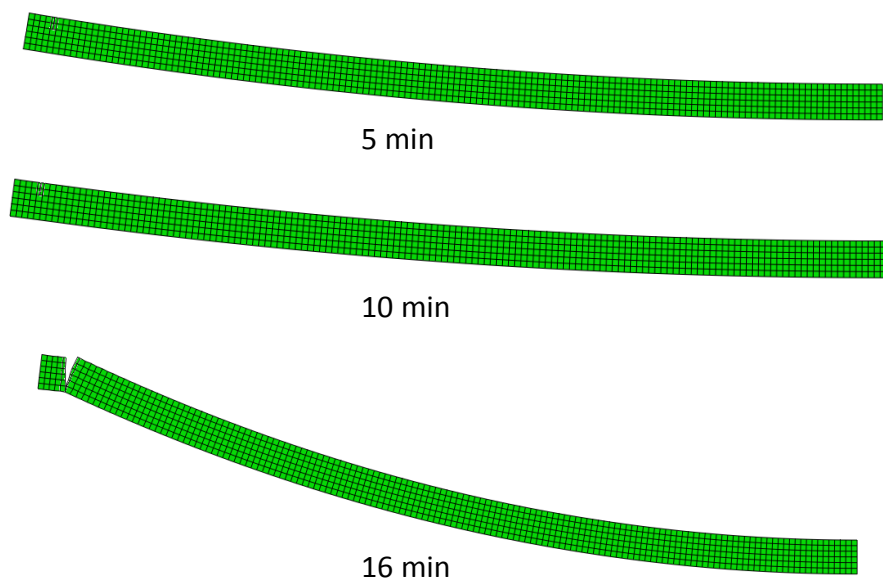


**Figure 7.45.** Deflection of the gypsum board in test T4W at 5, 10 and 16 minutes  
(deflections are 5 times magnified)

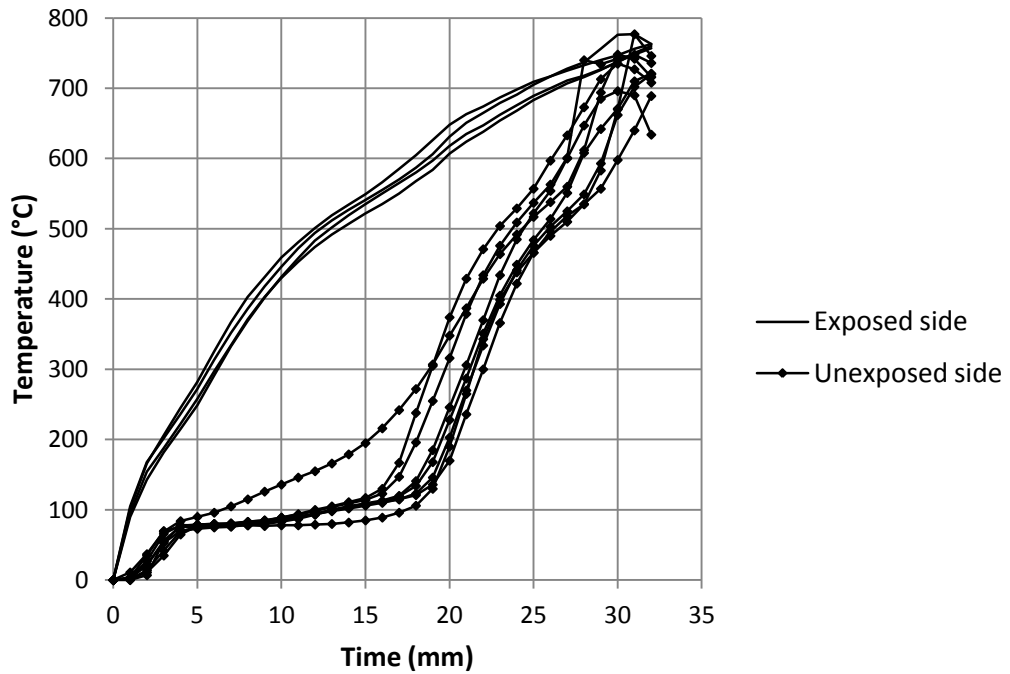


Figure 7.46. Temperature history for the Wallboard gypsum in Test T4W

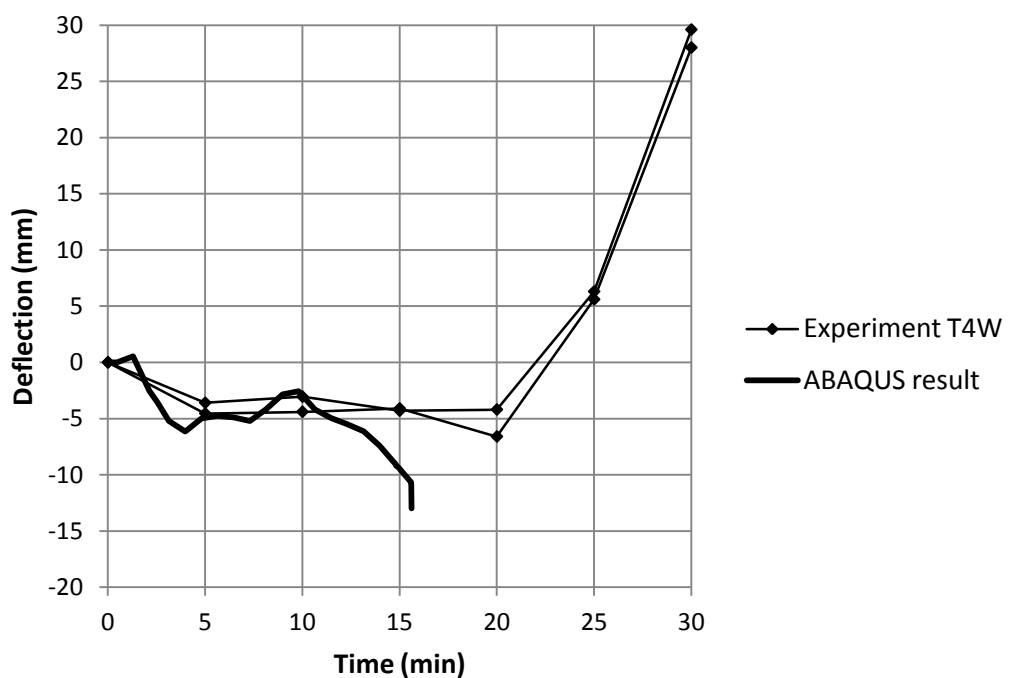
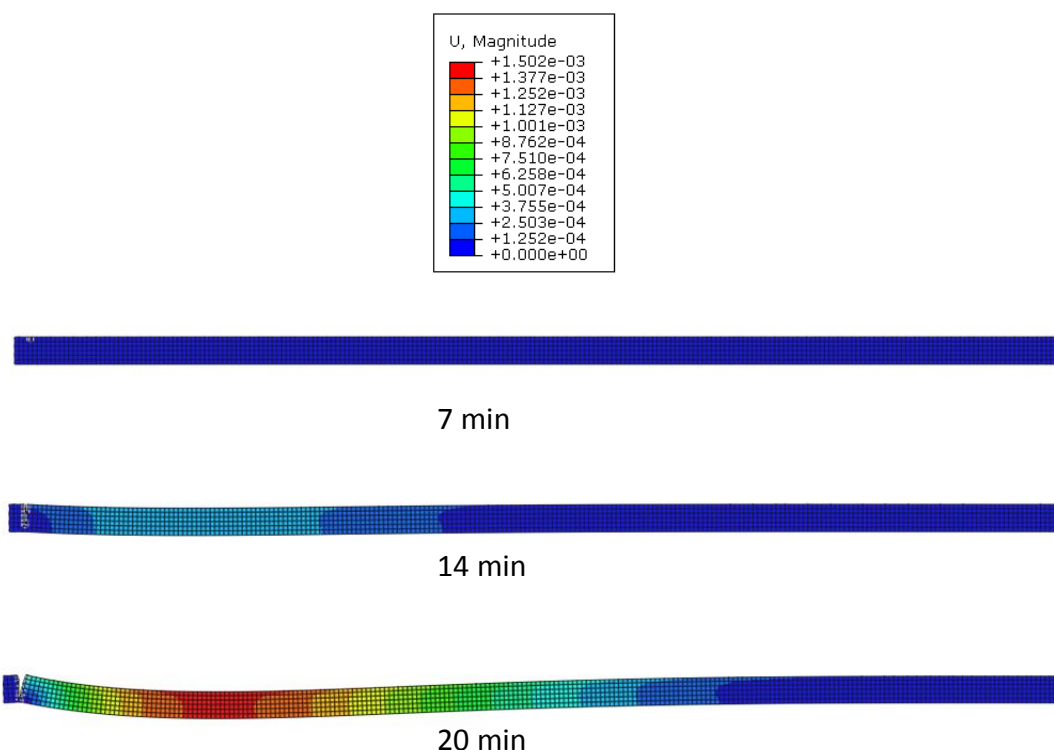


Figure 7.47. Comparison between numerical and experimental results for the deflection at the mid-span of the gypsum board in test T4W

#### 7.4.8.2 Experiments T5W and T6W

The experimental observations of the exposed board in test T5W report vertical cracks opening at 20 minute into the test. The simulation results for the exposed board also show a crack developing through the gypsum board thickness at about 20 minutes (Figure 7.48). The complete crack is close to the corner stud, however, soon after it completely progresses through the board thickness, numerous other cracks start opening all along the gypsum board (Figure 7.49). The limitation of the ABAQUS analysis does not allow other cracks forming until the first one is completed. Such results and the relatively uniform distribution of the maximum principal stress along the gypsum board suggest that cracks could, in fact, occur anywhere along the board tested in T5W.

The cracks do not seem to have a noticeable influence on the temperature of the backside of the exposed board. As shown in Figure 7.50, although the temperatures increase considerably from 100°C due to dehydration, the temperature increase per minute does not exceed 50°C.



**Figure 7.48.** Deflection of the exposed gypsum board in test T5W at 7, 14 and 20 minutes  
(deflections are 5 times magnified)



**Figure 7.49.** Cracks opening all along the gypsum board in test T5W soon after the first crack completes its progress through the thickness. (The image is presented out of scale to improve visual clarity of the cracks)

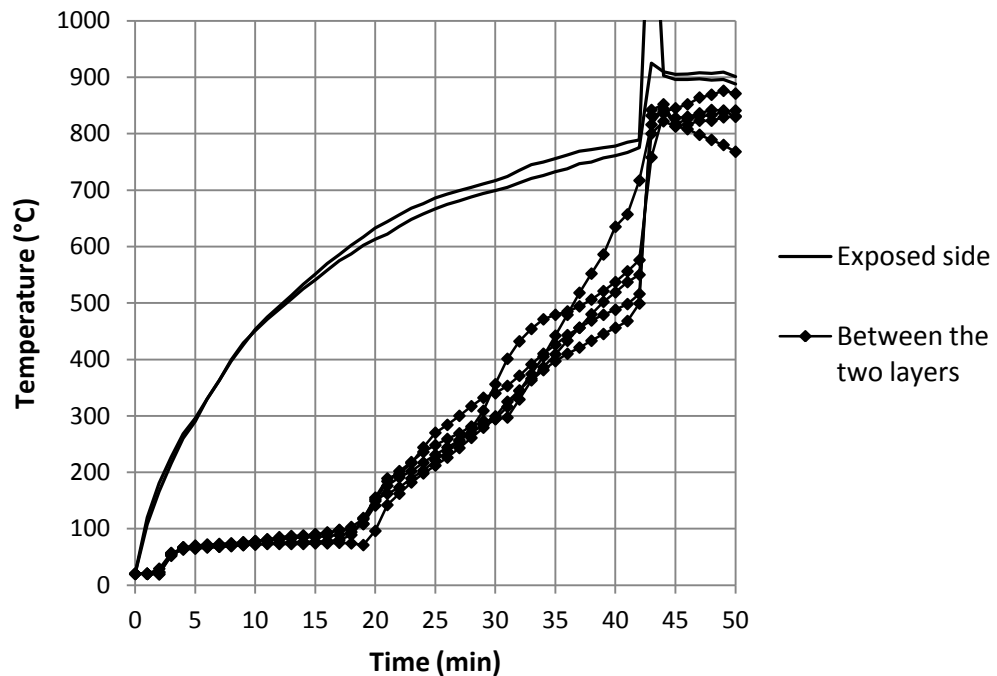


**Figure 7.50.** Temperature history between the two layers of the boards in test T5W

The first fall-off of the exposed board in test T5W is reported occurring at 40 minutes. The recorded temperature on the back of the exposed side experiences a sudden increase of more than 200°C at minute 42, which corresponds to the fall-off. The deflection of the unexposed board at mid-span is also affected by the temperature shock due to the fall-off (Figure 7.51). Again, the ABAQUS simulation results predict deflections very close to the experimental recordings before the fall-off of the exposed board.

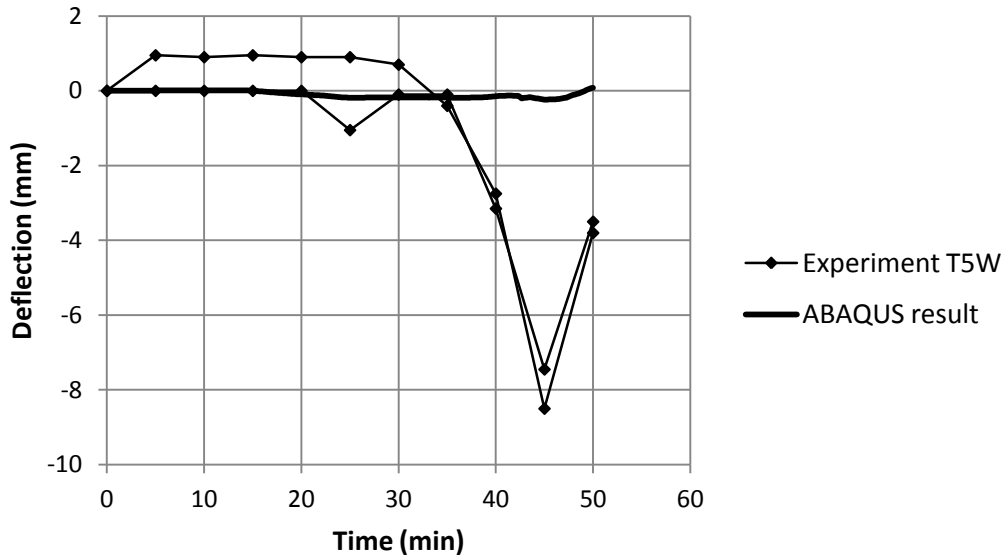


**Figure 7.51.** Comparison between numerical and experimental results for the deflection at the mid-span of the unexposed board in test T5W

In Test T6W, observations of the exposed board report opening of a horizontal crack in the board at 13 minute into the test. Vertical cracks reportedly open at 20 minute into the test. Since the simulation is reduced to a two-dimensional analysis, the horizontal cracks cannot be simulated. These cracks occur as a result of the restraints that the screws provide in the vertical span of the board between any two screws. Nevertheless, the ABAQUS analysis predicts opening of cracks close to the centre stud about 21 minutes into the test (Figure 7.52), which agrees satisfactorily with the experimental observations. Again, the influence of cracking on the temperatures at the back of the exposed side does not induce any temperature increase of more than 50°C (Figure 7.54).

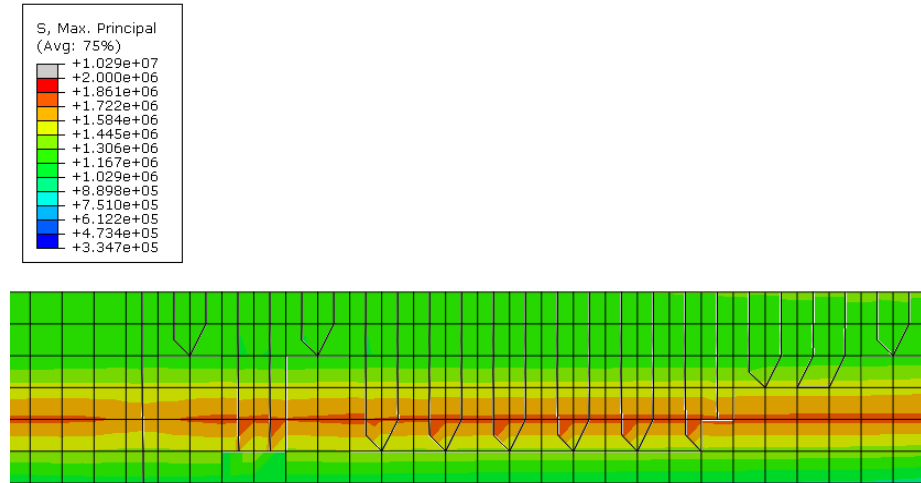


**Figure 7.52.** Distribution of maximum principal stresses on the exposed beam in test T6W just after a crack cuts through the thickness of the board

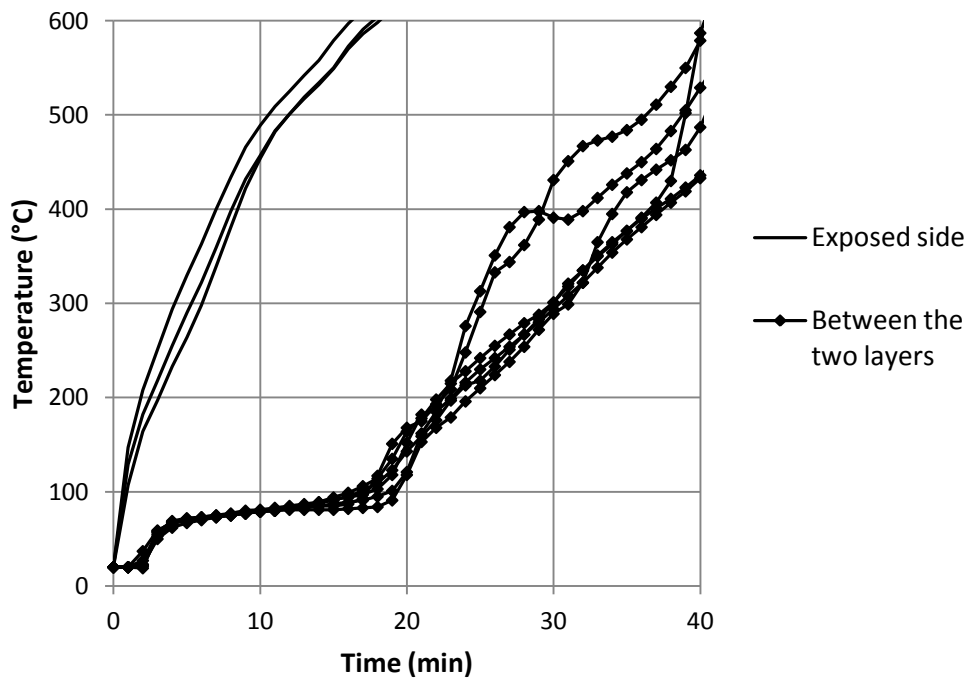


**Figure 7.53.** Temperature history between the two layers of the boards in test T5W

The deflection at the mid-span of the unexposed board recorded during test T6W is plotted against the numerical results in Figure 7.54. Good agreement is achieved once again.

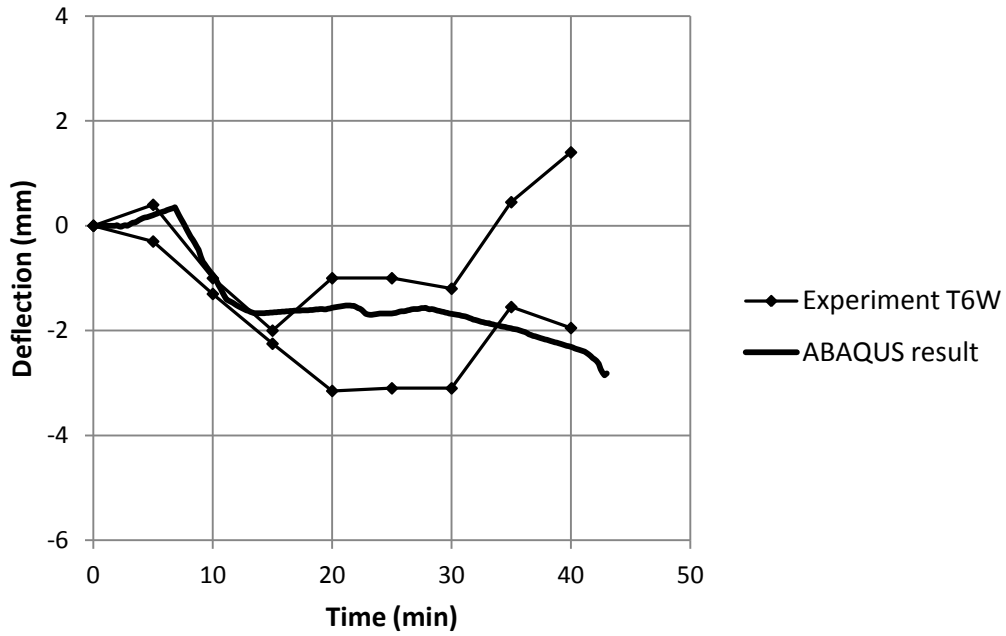


**Figure 7.54.** Comparison between numerical and experimental results for the deflection at the mid-span of the unexposed board in test T6W

#### 7.4.8.3 Summary

The numerical and experimental results for the four tested wall assemblies with Wallboard gypsum are summarised in Tables 7.3 and 7.4. Similar to Fireline gypsum boards, the recorded and predicted deflections of the boards are in very good agreement, until the exposed board in the double-layer experiments falls off in the fire test.

The numerical prediction of one complete crack through the gypsum board thickness coincides with the observation of cracks on the furnace side of the boards. But the temperature recordings on the back of the exposed side do not show rapid increase in some tests. However, in test T4W and T5W, where the exposed board falls off in fire, there is a sudden temperature increase at the same time at the back of the exposed board. In test T5W, this temperature shock affects the deflection recordings of the unexposed board, too. Although the ABAQUS simulation model is not able to predict gypsum board fall off and the subsequent

behaviour, its predictions of the first through-thickness crack and gypsum board deflections until falling off are in very good agreement with the test results.

Single-layer experiments		T2W	T4W
Experimental results	Vertical crack observed on the exposed side of the board	20min	None
	Sudden temperature rise observed on the unexposed side of the board	18-19min	27-29min
	First fall-off of the board	None	30min
ABAQUS results	Complete opening of at least one crack	20min	16min
	Agreement of the deflection of the unexposed board with test results	Good	Good

**Table 7.3.** Comparison between experimental and numerical results for single-layer Wallboard gypsum wall assemblies

Double-layer experiments		T5W	T6W
Experimental results	Vertical crack observed on the exposed board	20min	20min
	Sudden temperature rise observed at the back of the exposed board	40min	None
	First fall-off of the exposed board	40min	None
ABAQUS results	Deflection shock on the unexposed board	40min	None
	Complete opening of at least one crack	20min	21min
	Agreement of the deflection of the unexposed board with test results	Good until 40min	Good

**Table 7.4.** Comparison between experimental and numerical results for double-layer Wallboard gypsum wall assemblies

#### **7.4.9 Validation of Numerical Results for Stress Analysis – Canadian Tests**

The National Research Council of Canada has performed numerous fire tests on wall assemblies with different arrangements (Sultan, 2010, Sultan and Lougheed, 2002, Sultan et al., 1994a, Sultan et al., 1994b). Four of these tests have been selected to verify the validity of the numerical analysis for a diverse range of wall assemblies. Details of these tests (F-07, F-09, UW-8V and UW-9V) have been presented in CHAPTER 6.

Although the gypsum boards used in the Canadian tests are from various manufacturers and their properties might not be exactly the same as those of British Gypsum products, the two general categories of boards, namely fire-rated and regular, are expected to perform fairly similarly irrespective of their manufacturers. Therefore, the thermal and mechanical properties of Type X and Regular gypsum in the Canadian tests are simulated using the properties of British Gypsum Fireline and Wallboard gypsum, respectively. The temperature recordings at the back side of the exposed board in all the tests have been used as thermal boundary conditions for the heat transfer models. In test UW-8V, and its repeat UW-9V, the gypsum board is extended over three spans attached to wood studs. Hence the boundary conditions are defined for half of the board as sketched in Figure 7.55. Other features of the simulations are as explained earlier in this chapter.

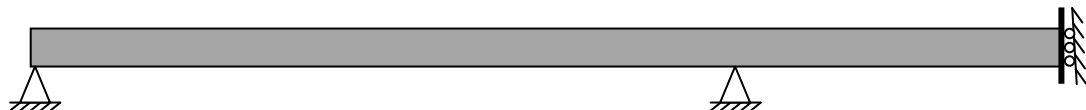


**Figure 7.55.** Schematic boundary conditions used for modelling Canadian test UW-8V.

In test F-07, one layer of fire-rated gypsum board is used on the exposed side. Sultan (2010) suggests that the first fall-off of gypsum in fire can be identified by the sudden increase of temperature at the back of the exposed layer of gypsum. In test F-07 the sudden increase is observed at 51 minute into the test, as shown in

Figure 7.56. The ABAQUS prediction of opening of the first complete crack is at minute 44 of the test (Figure 7.57). Considering the possible differences of the material properties, the predicted time is very close to the observation of the sudden increase in temperature.

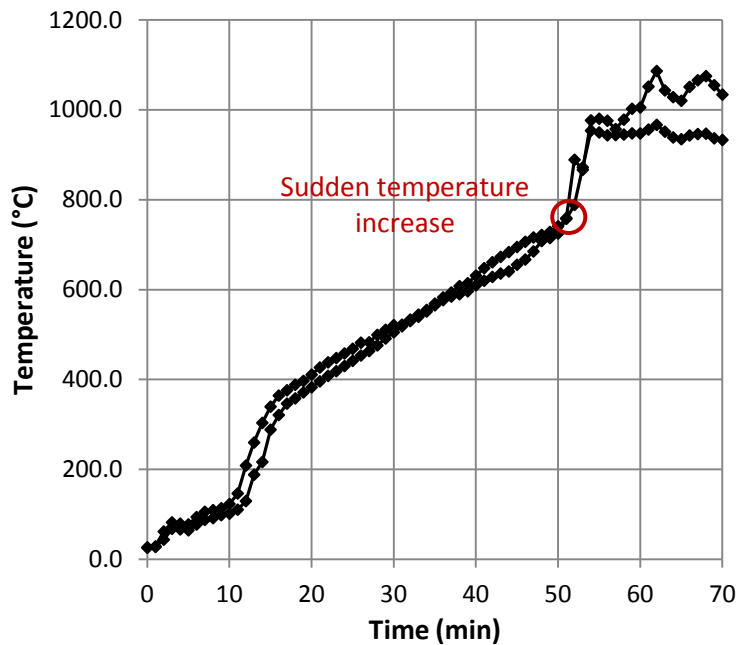


Figure 7.56. Temperature history on the back of the exposed board in test F-07

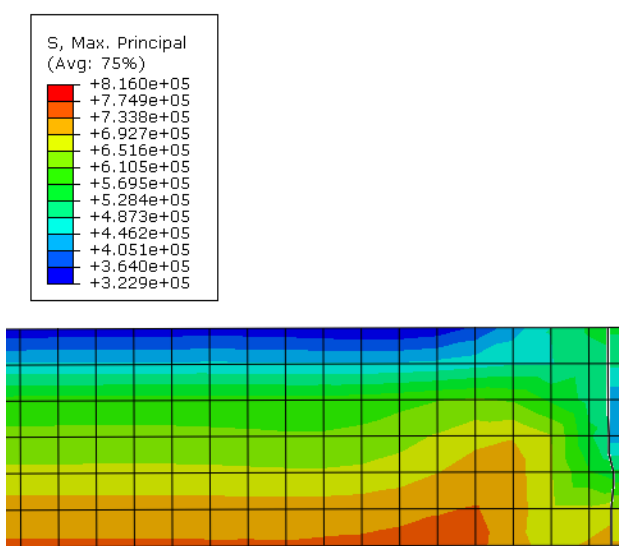
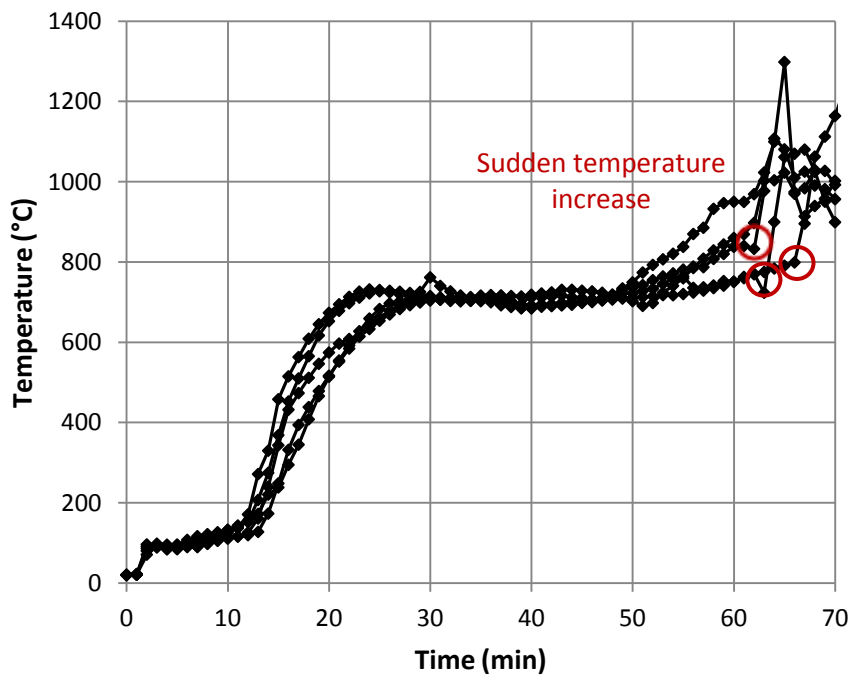
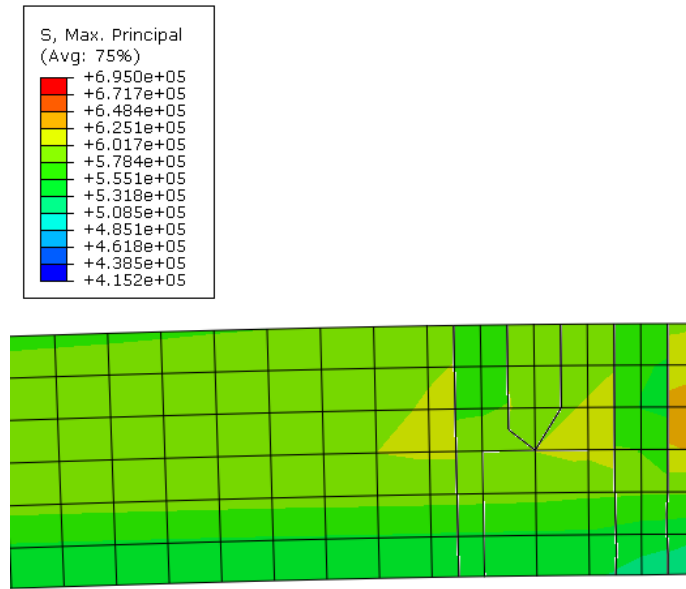


Figure 7.57. Distribution of maximum principal stresses on the exposed board in test F-07 just after a crack cuts through the thickness of the board

In test F-09, which is similar to F-07, there is one layer of fire-rated gypsum board on the exposed side of the assembly, and glass fibre insulation has been used to fill the cavity. The temperature recordings at the back of the exposed board experience a sudden increase at 62-66 minutes for the different thermocouples (Figure 7.58). The ABAQUS prediction of a through-thickness crack is at minute 61 of the test (Figure 7.59), which is very close to the time of the sudden temperature increase. It appears that the sudden increase in temperature for the fire-rated boards is very closely linked to the opening of discrete cracks, and the ABAQUS model is able to predict this time.



**Figure 7.58.** Temperature history on the back of the exposed board in test F-09



**Figure 7.59.** Distribution of maximum principal stresses on the exposed board in test F-09 just after cracks cut through the thickness of the board

Tests UW-8V and UW-9V both have similar arrangements, where there is one layer of regular gypsum board on the exposed side of the wall assembly. Video recordings of the tests show cracks to form at about minute 14 for both tests. The numerical results show cracks to go through the thickness, close to the middle boundary, at about minute 15 of the test (

Figure 7.60), which is in good agreement with the test observations. The first fall-off of the exposed board is observed at 24 and 25 minutes respectively in tests UW-8V and UW-9V. The fall-off times correspond to the temperature jump on the back of the exposed board, as shown in Figure 6.22 for test UW-8V.

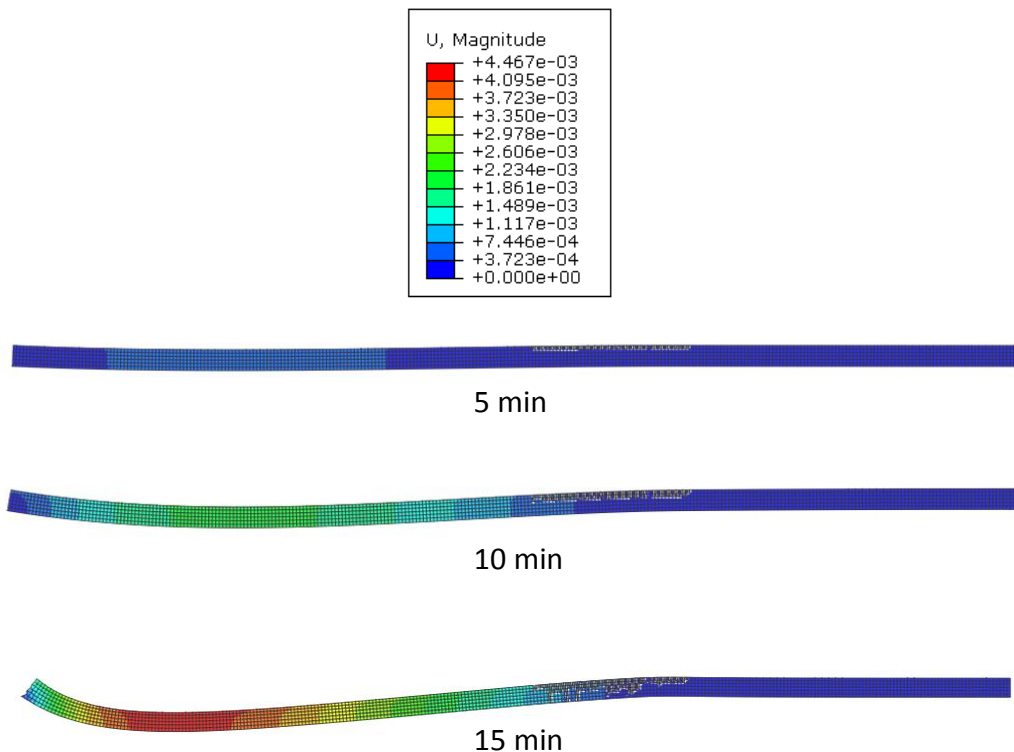


**Figure 7.60.** Deflection of the gypsum board in tests UW-8V and UW-9V at 5, 10 and 15 minutes (deflections are 5 times magnified)

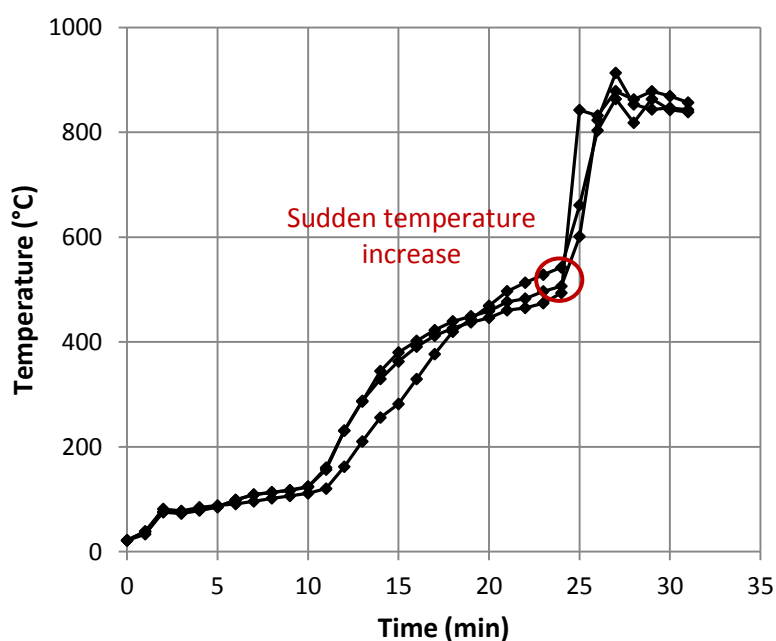


**Figure 7.61.** Temperature history on the back of the exposed board in test UW-8V

## 7.5 Conclusions

This chapter has presented a novel modelling methodology for simulation of structural performance of gypsum boards exposed to high temperatures. The model utilises the extended finite element method and the material mechanical properties of gypsum extracted in CHAPTER 5, to predict the formation of discrete cracks through the thickness of the gypsum boards. The model is verified by test results for a variety of test arrangements. Comparison of the predicted deflections of the board with test results satisfactorily validates the proposed numerical method.

The simulation of complete cracks in Fireline gypsum boards coincides with the observation of a sudden increase in temperature (more than 100°C per minute) on the backside of the exposed board. As a result of the sudden increase, the temperature on the unexposed side reaches the temperature of the exposed side of the board. This effect is not consistently observed in all Wallboard gypsum tests, but visual observations of crack opening in the fire tests match very well with the numerical predictions of cracks. Numerical simulations of a number of Canadian tests yield similar results for regular and fire-rated boards, which confirms the validity of the model for a wide range of boards and test arrangements.

The simulation results for fire-rated gypsum boards suggest that the opening of a discrete crack is closely linked to the sudden temperature increase at the back of the exposed board. Fall-off of the gypsum boards, however, is more complex and requires the cracks to form in a certain arrangement to allow falling off of a section of the board, which might take place much later in the test. At present, the ABAQUS model is unable to simulate this event.

The proposed numerical model is a promising technique for predicting cracks in gypsum boards. Especially for fire-rated gypsum boards, where the fire performance of the boards is of great importance, the prediction of cracks can facilitate including the effects of cracking and falling-off of gypsum on the fire resistance of the system.

## **CHAPTER 8. Critical Parameters in Structural Behaviour of Gypsum Boards in Fire**

### **8.1 Introduction**

Fall-off of gypsum in fire significantly affects the fire resistance of gypsum board assemblies. Gypsum fall-off is a result of structural failure and a sufficient number of discrete through-thickness cracks forming in gypsum. At present, it is still not possible to predict the time of gypsum fall-off and the numerical simulation method reported in Chapter 7 can only be used to identify the time of formation of the first crack. However, it is assumed that formation of the first through-thickness crack is related to eventual fall-off of gypsum. Hence, if the formation of the first through-thickness crack could be delayed, the fall-off of gypsum would occur later in a fire, and the fire resistance of the assembly would improve. It is then important to identify the detailing parameters in a gypsum board assembly that significantly affect formation of the first through-thickness crack in gypsum.

In CHAPTER 7, a finite element model (using extended features) was presented and validated for predicting the formation of through-thickness cracks in gypsum at high temperatures. Utilizing the aforementioned model, this chapter investigates the effects of various detailing parameters of gypsum board wall assemblies on the formation of the first crack in gypsum exposed to fire. The study provides invaluable recommendations on light-weight construction practice, which enables improvement of fire resistance of gypsum wall assemblies through making practical changes to their detailing.

## **8.2 Detailing Parameters in Gypsum Board Wall Assemblies**

The numerical model presented in CHAPTER 7, simulates gypsum board as a two-dimensional beam. Assuming that the beam is exposed to the standard fire curve, the parameters that can affect the failure of gypsum in such a model are the dimensions of the beam, its boundary conditions, the through-thickness temperature profile of the board and the properties of its material. Changing these details of a gypsum wall assembly can be implemented in the model by changing the above features in simulation. The following detailing parameters are considered in this study:

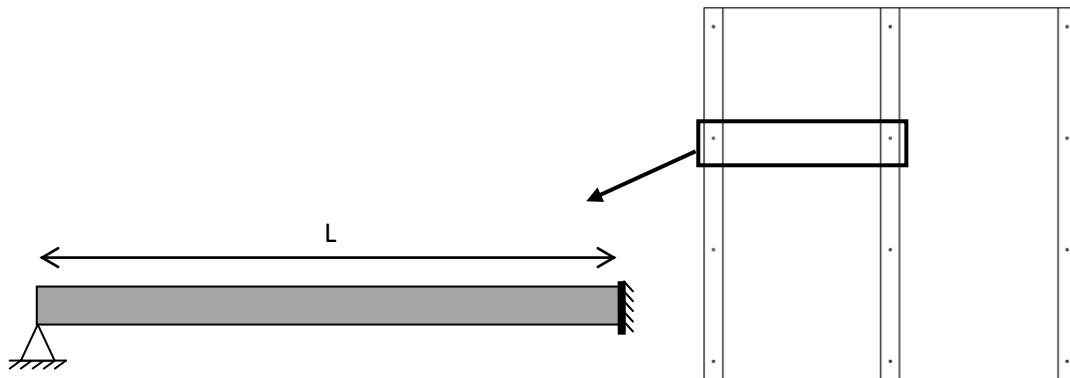
- The spacing of steel studs in the assembly - implemented by changing the length of the beam in the finite element model.
- The method of attachment of gypsum board to the studs - implemented by changing the boundary conditions of the beam in simulation.
- The number of gypsum board layers - implemented by changing the temperature profile of the beam in the model.
- The presence of insulation in the wall cavity - applied by changing the temperature profile of the beam in the structural model.
- Improved gypsum board material with less thermal shrinkage - applied by adapting the material properties in the structural model.

It should be pointed out that the temperature profiles are according to those measured in the tests reported in CHAPTER 6. Since the test arrangements (number of layers of gypsum, insulation) do not match gypsum assembly construction in real-life, the results of these numerical simulations should be understood as the effects of changing gypsum temperature profile through the thickness.

## **8.3 Stud Spacing**

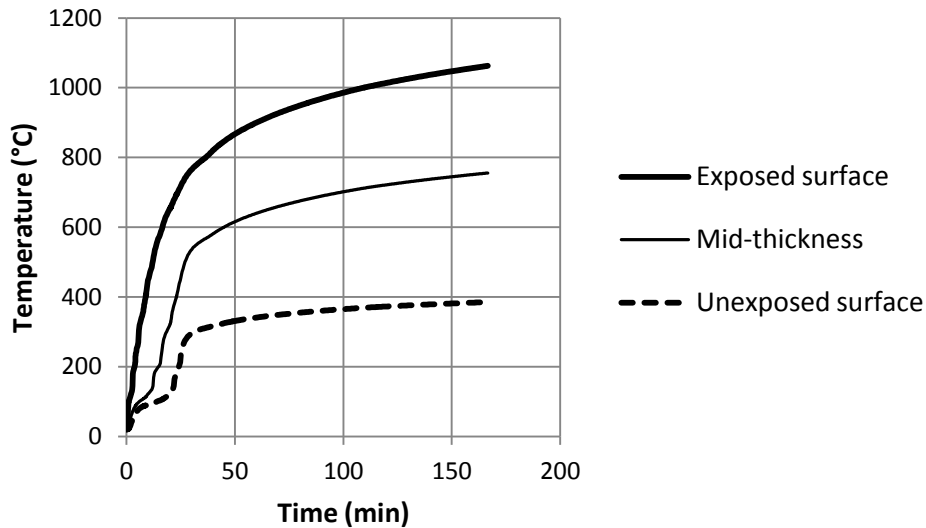
British Gypsum recommends that gypsum board wall assemblies are constructed by positioning the vertical studs at 600mm centres (British Gypsum, 2011). A gypsum board, therefore, is extended over two spans of studs. As explained in CHAPTER 7, the geometry of the numerical model to simulate the gypsum board can be defined

as depicted in Figure 8.1. The length of the beam in the model is the spacing of the studs. The fixed boundary represents the symmetry at the centre of the board over the middle stud. To investigate the effect of stud spacing on crack formation in gypsum, three cases have been studied: studs positioned at 400mm, 600mm and 800mm centres. The thickness of the board is 12.5mm, and the material model is defined as explained in CHAPTER 5.



**Figure 8.1.** Schematic gypsum board model for structural analysis

Using ABAQUS, first a heat transfer analysis is run on the model, assuming that the upper side of the beam is exposed to the standard fire curve and the lower side of the beam is facing ambient temperature of 20°C (Figure 8.2). The calculated gypsum temperatures are then input in the structural model to predict crack formation in the gypsum in fire.



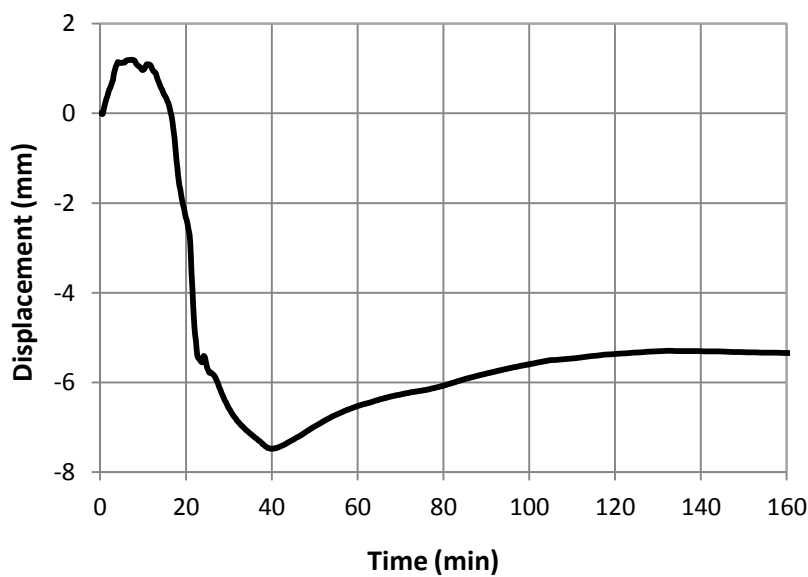
**Figure 8.2.** Temperature history calculated through thermal analysis in ABAQUS for a 12.5mm gypsum board exposed to standard fire on one side and ambient temperature on the other

Figure 8.3 shows the resulting gypsum board deformation at the centre of the beam. Initially, the gypsum board bends towards the furnace as a result of thermal expansion of gypsum at low temperatures. But, as the thermal expansion of gypsum becomes negative (shrinkage) at high temperatures, the board bends out of the furnace (downwards in Figure 8.1) and cracks start to form close to the fixed boundary. The simulation results show that the first crack cuts through the thickness of the gypsum board with a span of 400mm after 100 minutes of exposure to fire, while the opening of the first through-thickness crack in the 800mm long gypsum board is at minute 44 of fire exposure. In both cases, the cracks form close to the fixed boundary of the beam, starting from the exposed side and progressing to the unexposed side of the board. The difference in crack formation time is expected. Although the thermal strains in both cases are the same, they induce higher mechanical strains and stresses in the longer beam. Hence, the wider the spacing of the studs, the sooner the failure of gypsum in fire.

Therefore, the failure time of the 600mm long gypsum board is expected to be between 44 and 100 minutes of fire exposure. However, simulation of the gypsum

board with a span of 600mm does not show a complete through-thickness crack even after more than 150 minutes of fire exposure (Figure 8.4). This is due to the limitations of the numerical modelling and does not represent the physical scenario, as a slight change in the gypsum failure criteria would allow the numerical analysis to show failure of the board. If the maximum principal stresses that gypsum can sustain at 400°C -700°C is reduced by 10%, the simulation predicts a through-thickness crack after about 45 minutes of fire exposure. Some limitations of the numerical modelling method were presented in CHAPTER 7. Further discussions are included in the next chapter as part of conclusions and recommendations.

Given the problems of the numerical model, making definitive conclusions should be avoided. Nonetheless, the results suggest that decreasing the stud spacing from 600mm to 400mm delays the first crack formation time of gypsum appreciably, while increasing the stud spacing to 800mm does not significantly affect the crack formation time.



**Figure 8.3.** Simulation results for the deflection at the mid-span of gypsum board with 600mm span and 12.5mm thickness

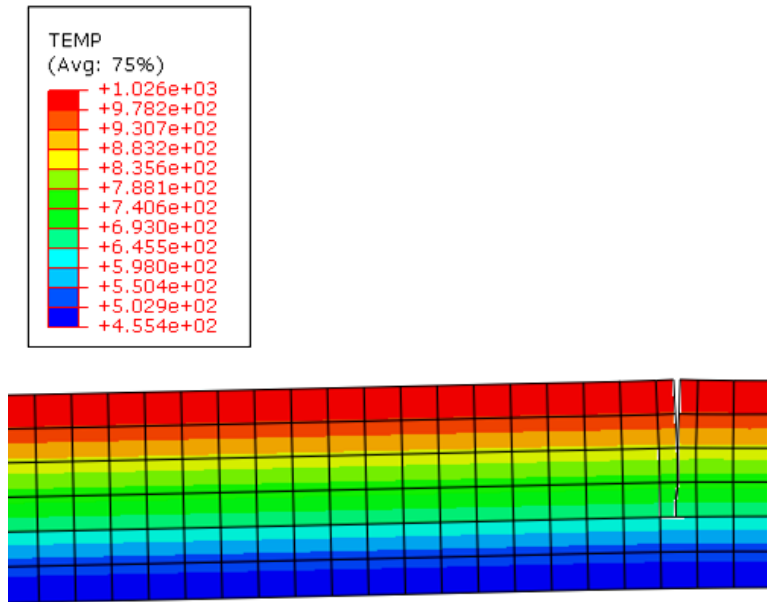


**Figure 8.4.** Incomplete formation of through-thickness cracks in gypsum board with 600mm span and 12.5mm thickness after 150 minutes of fire exposure

#### 8.4 Gypsum Board Attachment

In light-weight wall assemblies, gypsum boards are fixed to the studs by several screws usually centred at 300mm (in the vertical direction of the wall assembly shown in Figure 8.1). It is assumed that the vertical edge of a gypsum board is not rotationally restrained when there is only one screw connecting the gypsum to the stud. This was confirmed in CHAPTER 7, by comparing the experimental and numerical deflections of the board when the support was modelled by a pin boundary condition (the left boundary in Figure 8.1). However, if the edge of the gypsum board is fixed to the stud by two screws with a reasonable distance, the screws can provide some rotational fixity to the board (Figure 8.5). Representing this attachment by a fixed boundary condition and analysing the structural performance of the gypsum board in fire, shows that the through-thickness crack forms in the gypsum board after only 27 minutes of fire exposure. Expectedly, the crack opens close to the studs, since the tensile stresses are the maximum close to the fixed boundaries. Initially, it was thought that fixing the rotational boundary conditions of the gypsum might reduce the stresses in the board. However, the

numerical analysis results indicate that although fixed boundaries induce lower stresses close to the mid-span of the board, they cause higher tensile stresses on the exposed side of the gypsum close to the boundaries, where mechanical strength drops considerably. Therefore, the crack formation time of the board reduces by 40%. It can be concluded that one screw close to the edge of the gypsum board would increase its failure time, considering the parameters that were included in the analysis.

Two screws

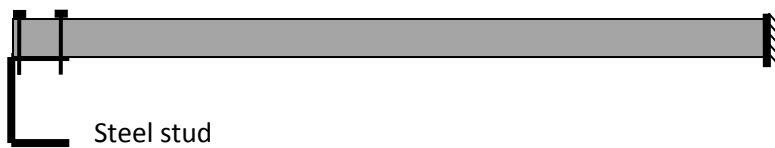


**Figure 8.5.** Schematic drawing of a gypsum board fixed to a steel stud by two screws at its edge

### 8.5 Number of Gypsum Board Layers

The light-weight framing in wall assemblies is often clad by one or two layers of gypsum board on either side. There is no doubt that installing a double-layer of gypsum board on either side of a wall assembly enhances its insulation capacity in fire condition, as long as the layers stay in place. However, it is important to study the effect of an extra layer of gypsum in structural failure time of the exposed board. Having two layers of gypsum changes the temperature profile of the exposed board. Figure 8.6 compares the temperature recordings of the exposed board in tests T1F (single-layer) and T5F (double-layer). The temperature increase of the unexposed face of the board after dehydration has a similar gradient in both cases until about 40 minutes into the test. However, the temperature of the unexposed face of the exposed board in the double-layer assembly continues to rise higher than 600°C, while that of the single-layer assembly does not reach 400°C after 100 minutes of fire exposure. The higher temperature on the unexposed side in the double-layer assembly has two contradicting effects on the structural performance of the board. On the one hand, it causes a higher loss of strength in

the gypsum; on the other hand, it increases shrinkage on the unexposed face, and consequently, decreases the thermal strain curvature along the board. The numerical results show that the through-thickness crack in the double-layer assembly forms after 55 minutes of fire exposure, which is a 20% improvement compared to the single-layer assembly. It appears that the favourable effect of a lower thermal gradient counteracts the negative influence of the loss in strength. An experimental study of gypsum board fall-off times in floor assemblies by Elewini et al. (2007) also yields similar results.

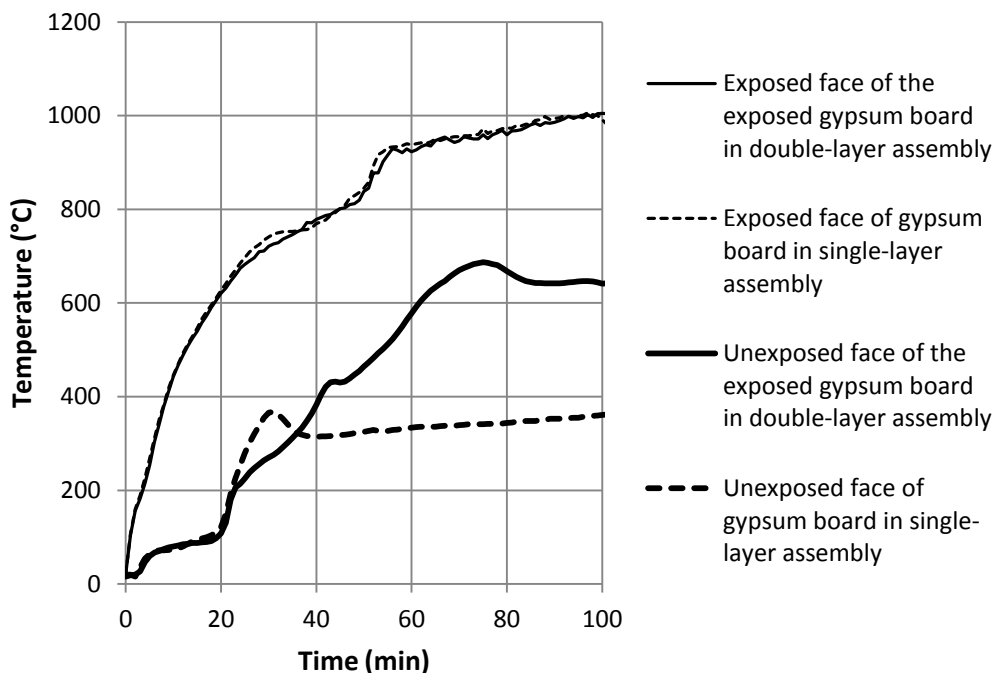


**Figure 8.6.** Temperature history for 12.5mm exposed gypsum board in single-layer and double-layer assembly

## 8.6 Use of Insulation in the Wall Cavity

According to normal insulation requirements of building construction, the cavity in a wall assembly is either left empty or filled with insulation material. During fire, the effect of insulation is observed as a significant increase in the temperature of the unexposed face of the exposed gypsum board. Figure 8.7 shows the recorded temperatures for tests T1F (non-insulated) and T2F (insulated). In the insulated test, the temperature of the unexposed face of gypsum after dehydration rises

significantly higher than that of the non-insulated test. 30 minutes into the test, the temperature of the unexposed side of the insulated gypsum exceeds 600°C. This steep temperature increase through the thickness of the board causes a rapid loss of strength in gypsum. The results of numerical simulation of the structural performance of the insulated board confirm an earlier failure time compared to the non-insulated gypsum. Through-thickness cracks appear after 26 minutes of fire exposure, which suggests an approximately 40% decline in the failure time of gypsum. Although higher temperatures on the back of the board reduce the thermal gradients, the sharp temperature increase reduces the mechanical strength of gypsum so rapidly that the loss of strength dominates the performance of gypsum, and hastens gypsum failure. Reassuringly, the experimental study by Elewini et al. (2007) suggests that gypsum board fall-off times in floor assemblies also reduce noticeably when insulations are used in the cavity, especially when glass fibre batts were used for insulation. The insulation used in this study (Isover APR) is of the same type.

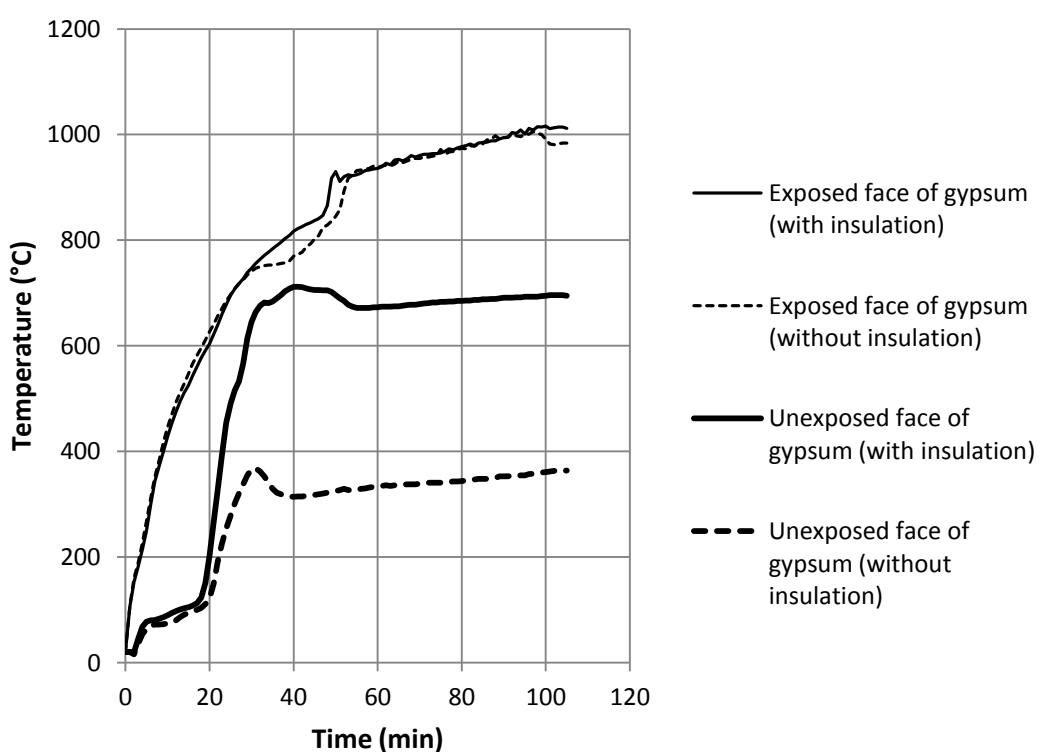
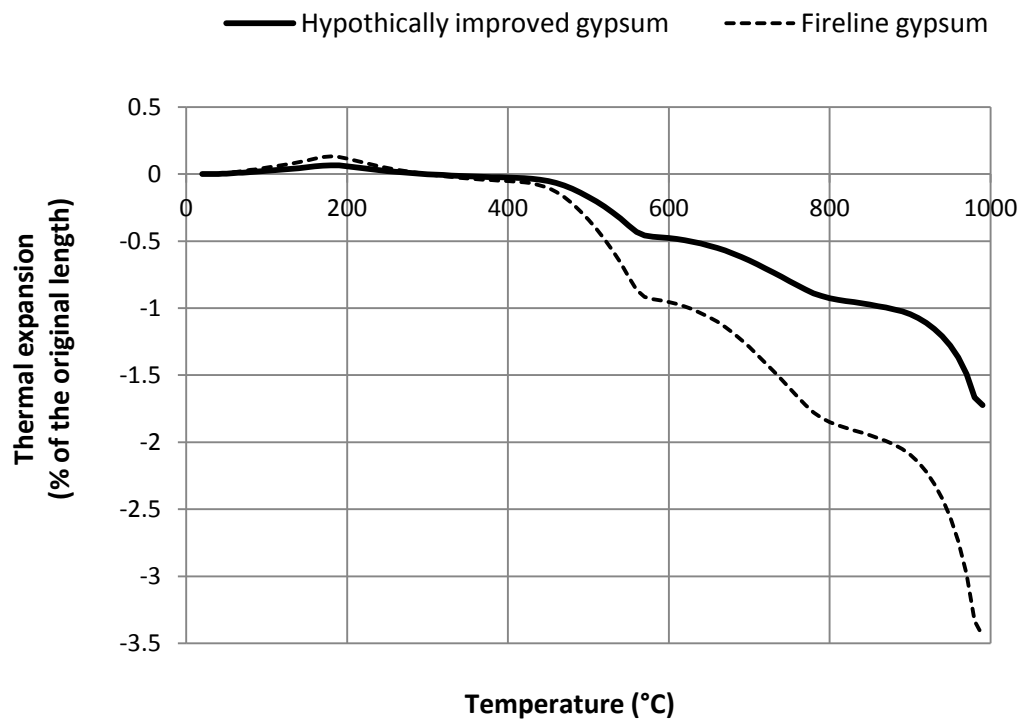


Figure 8.7. Temperature history for 12.5mm gypsum board with and without insulation

## 8.7 Thermal Shrinkage of Gypsum

Structural failure of gypsum boards in fire is primarily due to the shrinkage of gypsum at high temperatures. The non-uniform temperature across the thickness of the board means gypsum experiences different shrinkage rates across its thickness, which results in thermal strains along the board. Gypsum attachment to the studs restrains the board. Hence, the restrained thermal strains induce mechanical stresses, which, given the loss of strength of gypsum at high temperatures, lead to its failure. It is established in the literature that gypsum fall-off in fire significantly affects the fire resistance of the gypsum board assemblies. Thus, gypsum manufacturers are continuously seeking to improve the structural performance of their gypsum board products. It is therefore reasonable to investigate whether a gypsum product with lower shrinkage rates would demonstrate improved structural performance in fire conditions.



**Figure 8.8.** Thermal shrinkage of an improved gypsum board product (hypothetical) as compared to thermal shrinkage of Fireline gypsum board.

For this purpose, it was assumed that shrinkage of an improved gypsum product is half of the shrinkage of the Fireline gypsum board type. Figure 8.8 compares the thermal shrinkage of the hypothetically improved board with the average thermal shrinkage measured for Fireline gypsum.

Results of structural simulation of the hypothetically improved gypsum show through-thickness cracks occurring after 58 minutes of exposure to the standard fire. The failure time of the gypsum board with 50% lower shrinkage rates, is improved by just short of 30%. Lowering the shrinkage rates in gypsum boards to half their current values requires considerable research and investment by manufacturers. However, achieving such state improves the structural performance of gypsum by only about 30%. The results suggest that although shrinkage rates affect the time of structural failure of gypsum, the dominating factor appears to be the reduced mechanical strength of gypsum at high temperatures. The sudden loss of strength of gypsum boards at temperatures beyond 300°C is so influential that it dominates the structural performance of gypsum, even when no mechanical loads are applied. It is suggested that the priority of gypsum manufacturers in improving gypsum fire resistance be given to other issues, such as changing the stud spacing, than to reducing the shrinkage rate of gypsum.

## **8.8 Conclusions**

The structural performance of gypsum boards in wall assemblies is vastly influenced by the configuration and detailing of the assembly. Detailing factors such as the spacing of the vertical studs, the attachment of the boards to the stud, the number of gypsum board layers and the use of insulation in the wall cavity have been studied in this chapter. The numerical analysis method, presented and validated in CHAPTER 7, predicts the formation of through-thickness cracks in gypsum boards exposed to high temperatures. The time at which the first crack occurs is considered as an important indicator of structural failure of gypsum. The numerical method is applied to a number of different cases, and the crack formation times are compared for the different detailing parameters. Based on the numerical simulation, the following key findings can be drawn:

- Increasing the stud spacing from 600mm to 800mm slightly decreases the crack formation time of gypsum, while decreasing the stud spacing to 400mm substantially delays this time.
- Increased rotational stiffness by the support to the edge of gypsum boards, hastens the crack formation time of gypsum boards by 40%.
- Adding a second layer of gypsum can delay the crack formation time of the exposed board by 20%.
- Adding insulation can adversely affect the structural performance of gypsum boards. The use of 75mm thick glass fibre batt (Isover APR) at the back of 12.5mm Fireline gypsum reduces its failure time by about 40%.
- If the thermal shrinkage of gypsum is lowered by 50%, its crack formation time is increased by 30%. Such a return may not be worthwhile considering the difficulty of reducing the shrinkage rate by 50%.

# **CHAPTER 9. Conclusions and Recommendations for Future Research**

## **9.1 Summary and Conclusions**

Gypsum industries have long relied on numerous full-scale tests to evaluate fire resistance of gypsum board assemblies. However, fire test results can only be used for the products and arrangements tested, and cannot be extended to evaluate new materials and arrangements. This practice is, therefore, too expensive and time-consuming to be adopted for developing new products and systems. It is essential to understand gypsum behaviour at high temperatures, and develop analytical methods that can capture the thermal and structural performance of gypsum boards in fire conditions. This thesis has presented a methodology that facilitates the prediction of fire resistance of gypsum board assemblies, and involves a combination of theoretical, numerical and experimental approaches. The key contributions of this study can be categorised under three main themes:

- Thermal properties of gypsum
- Mechanical properties of gypsum
- Modelling structural failure of gypsum in fire

The following main conclusions are drawn under each of the above three categories.

### Thermal Properties of Gypsum

- The moisture content of gypsum has a great effect on its thermal properties and fire performance. This moisture content dissociates and evaporates at

elevated temperatures, and hence, the thermal properties of gypsum are temperature-dependent.

- Thermal conductivity and specific heat of gypsum are considered as the most influential parameters in conduction of heat through gypsum.
- The specific heat of gypsum is defined so that two peaks in the specific heat-temperature relationship account for the energy absorbed for the dissociation and evaporation of water, as well as moisture movement and possible re-condensation. The value of the peaks can be calculated using the correction factors proposed by Ang and Wang (2004).
- The existing publically accessible literature suggest that thermal conductivity of gypsum before evaporation of moisture is almost steady and equals its value at room temperature, which can be measured using common methods. Thermal conductivity drops considerably when water is driven off above 100°C. However, at high temperatures there are wide discrepancies in the values of thermal conductivity of gypsum reported in the literature.
- This study has developed a combined numerical and experimental approach to extract the thermal conductivity of gypsum at high temperatures. This approach treats gypsum as a porous material, and develops a theoretical model of thermal conductivity that accounts for the effects of radiation through voids. The thermal conductivity-temperature relationship of gypsum is defined as a function of two variables: reduction in thermal conductivity from its value at ambient temperature to that of dried gypsum to account for the effects of dehydration, and effective spherical void size. These two parameters can be determined through a hybrid experimental-numerical method. The proposed model employs a one-dimensional Finite Difference heat conduction program and high temperature test results on small samples of gypsum boards. Through a clearly defined trial and error procedure, the water evaporation related drop in thermal conductivity value and void size that give the best agreement between numerical prediction

and high temperature tests can be obtained to quantify the gypsum thermal conductivity-temperature relationship.

- One-dimensional Finite Difference formulations have been introduced for simulating conduction through gypsum panels. A computer program has been developed using the Finite Difference formulations and the results are validated against theoretical methods and an independent Finite element method. Validations confirm excellent efficiency of the Finite Difference method despite its relative simplicity. The computer program runs in the familiar environment of Microsoft Excel, which is easily accessible by the industry.
- Several small-scale high temperature tests have been performed on gypsum board samples. The results are used for calibration of the two parameters in the thermal conductivity-temperature relationship of two British Gypsum products, namely, Wallboard and Fireline gypsum. The high temperature test results verify the proposed methodology and its efficiency in extracting thermal conductivity of different gypsum products at high temperatures.
- The key data for the thermal conductivity of the two British Gypsum products are as follows. For Wallboard gypsum: ambient-temperature thermal conductivity = 0.19 W/m°C, dry gypsum thermal conductivity at 220°C = 0.1 W/m°C, effective void size = 0.12 mm; for Fireline gypsum: ambient-temperature thermal conductivity = 0.24 W/m°C, dry gypsum thermal conductivity at 220°C = 0.12 W/m°C, effective void size = 0.12 mm.

### Mechanical Properties of Gypsum

- Gypsum shrinks and loses its strength at high temperature. This leads to gypsum cracking and falling off in fire.
- The main temperature-dependent mechanical properties of gypsum addressed in this study are the coefficient of thermal expansion and shrinkage, mechanical strength and stress-strain relationships.

- Dilatometer tests have been performed on gypsum samples to measure their thermal shrinkage rates. The results show that gypsum expands slightly until about 200°C, and then shrinks considerably with further temperature rise.
- Three-point bending tests have been performed on gypsum samples at temperatures up to 800°C, and stress-strain relationship and mechanical strength of Wallboard and Fireline gypsum have been determined. The stress-strain relationship for Wallboard gypsum is linear, and it loses all its strength by about 500°C. The addition of glass fibres in Fireline gypsum improves the strength of the composite at high temperatures and causes nonlinear mechanical behaviour at temperatures above 300°C.
- The nonlinear stress-strain relationship for glass fibre reinforced gypsum at high temperatures can be represented by a bi-linear stress-strain relationship shape.
- Based on the three-point test results and analytical studies, a mechanical property model is proposed for the two types of gypsum (standard and fire-rated) that can be used in numerical modelling.
- A limited number of compression tests have also been performed, and the results indicate that the compression strength of gypsum is much greater than its tensile strength.

#### Modelling Structural Failure of Gypsum in Fire

- Gypsum fall-off in fire greatly influences the fire resistance of gypsum board assemblies. However, simulating this phenomenon is extremely complex, and no research work has yet been published that tackles this problem via analytical approaches. Falling-off of gypsum is a result of the formation of several discrete cracks in gypsum. Available structural simulation models can only be used to predict the opening of the first discrete crack in gypsum, which may be used as an indication of gypsum fall-off in fire.
- In this study the commercial Finite Element package, ABAQUS, has been used to model the structural behaviour of gypsum boards in fire. Several

material models embedded in ABAQUS have been examined for the purpose of this study, many of which fail to satisfactorily simulate the structural failure of gypsum in fire. However, using the built-in Extended Finite Element Method in ABAQUS, it is possible to successfully simulate structural behaviour of gypsum until formation of the first through-thickness crack. The cohesive material model in ABAQUS and its Traction-Separation Laws for fracture assessment allows for the opening of cracks in gypsum, and despite some limitations, can be used efficiently for modelling the structural behaviour of gypsum at high temperatures.

- This study is a pioneer in developing a two-dimensional Finite Element model (with extended features) that captures cracking of gypsum boards in fire. This model requires a heat transfer analysis that determines the temperature development through the gypsum board, followed by a structural analysis that includes the effects of thermal shrinkage and loss of strength in gypsum at high temperatures. The thermal and mechanical properties of gypsum used in the numerical analysis are those extracted as part of this research in CHAPTER 3 and CHAPTER 5, respectively.
- Several medium-scale fire tests have been performed on different gypsum wall assemblies. Out-of plane deflection of the walls and observations of cracks and gypsum fall-off have been recorded during the fire tests. The results are used for validation of the numerical analysis by ABAQUS. Numerical predictions of deflection match closely with experimental recordings of deflection before gypsum fall-off, and confirm the reliability of the numerical analysis. The numerical analysis also predicts the opening of discrete cracks in gypsum. However, it is unable to simulate gypsum fall-off.
- Opening of the first through-thickness crack can be considered as an indication of gypsum failure in fire. Although this phenomenon is not directly related to gypsum fall-off, it can be assumed that delaying the complete opening of through-thickness cracks in gypsum will delay gypsum fall-off and improve the fire resistance of gypsum assemblies.

- A number of studies have been carried out to investigate the effects of different detailing parameters on opening times of through-thickness cracks in gypsum wall assemblies. The studies use the configuration of the tests reported in CHAPTER 6, and do not match the real-life arrangements of gypsum wall assemblies. However, the results of the parametric study can provide guidelines on arrangements of gypsum boards for optimum structural performance in fire. The following points summarises the key findings of the parametric study:
  - Increasing the stud spacing from 600mm to 800mm slightly decreases the crack formation time of gypsum, while decreasing the stud spacing to 400mm substantially delays this time.
  - Increased rotational stiffness by the support to the edge of gypsum boards, hastens the crack formation time of gypsum boards by 40%.
  - Adding a second layer of gypsum can delay the crack formation time of the exposed board by 20%.
  - Adding insulation can adversely affect the structural performance of gypsum boards. The use of 75mm thick glass fibre batt (Isover APR) at the back of 12.5mm Fireline gypsum reduces its failure time by about 40%.
  - If the thermal shrinkage of gypsum is lowered by 50%, its crack formation time is increased by 30%. Such a return may not be worthwhile considering the difficulty of reducing the shrinkage rate by 50%.

## **9.2 Recommendations for Further Research**

The research work presented in this thesis proposes a method for extracting thermal properties of gypsum products at high temperatures. It also presents the first major attempt at measuring the mechanical properties of gypsum in fire and simulating its structural performance at high temperatures. Inevitably, many simplifications have been made in simulating the physical phenomena, and conclusions are drawn based on a limited number of experiments. Naturally, more

research needs to follow, so that a better understanding of the behaviour of gypsum boards in fire is achieved, and their fire performance is improved. Presented here are suggestions for a number of research studies that are directly related to the scope of this thesis:

- The one-dimensional Finite Difference program developed in this study uses the recorded temperatures on the exposed side of gypsum boards as boundary conditions to avoid the uncertainty associated with the heat transfer coefficient at the fire exposed side of gypsum. A study can be performed investigating the effects of varying values of heat transfer coefficient and their influence on heat transfer through gypsum boards. Heat transfer tests can be carried out on different gypsum board samples of vertical and horizontal configurations to provide the experimental data required.
- The thermal conductivity model proposed in this study assumes that the porous dried gypsum is made of spherical voids of a constant uniform size. Although its uniformity is a reasonable assumption and a different distribution might be considered too complex for the purpose it serves, the uniform void size can be assumed to vary at different temperatures to allow for other complex phenomena such as cracking or ablation at high temperatures.
- The stress-strain relationships of gypsum at high temperatures extracted in this study are based on a limited supply of experimental data. It is recommended that more three-point bending tests are performed on different gypsum samples and the stress-strain models are refined for use in numerical modelling.
- The stress-strain relationships extracted for gypsum in this study are based on three-point bending tests, and it is conservatively assumed that the mechanical properties of gypsum are identical in tension and compression. A more desirable test method is performing tensile and compressive tests on gypsum at high temperatures, which enables quantification of independent tensile and compressive mechanical properties for different

gypsum types. The recommended study requires availability of some high-tech facility for testing gypsum samples at high temperatures. It is also suggested to investigate the effect of different additives (and their quantities) in gypsum board composition on the mechanical properties of the composite.

- The material model used for simulation of the structural behaviour of gypsum in fire, has some limitations as mentioned in CHAPTER 7. In some cases numerical limitations can prevent the cracks progressing and cut through the thickness of gypsum boards. Further investigations are required to ensure realistic numerical results. For example, if at least one crack is progressing, ABAQUS is unable to simulate the opening of other cracks. This limitation can lead to a different stress distribution in the structure, which can be insignificant in some cases but crucial in others. Within the limits of the program and with the release of the new versions it might be possible to improve the prediction of through-thickness cracks. Practices such as several partitioning of the structure modelled, defining various cracks in different partitions, or forcing the cracks to form at different locations in gypsum are among those that could be utilised to enhance the prediction of the structural behaviour of gypsum.
- Further parametric study can be carried out on the detailing of wall assemblies with arrangements closer to their common use in building construction, where the cavity of the walls are also simulated in the analysis.
- The numerical model used in this study for simulation of the structural performance of gypsum in fire is a two-dimensional one, and the effects of the deflection of the steel studs in wall assemblies are considered by superimposing the recorded stud deflections on the deflection predictions of the gypsum board. This method can be improved by creating a three-dimensional model that includes the studs as well as the boards. Naturally, the complexity of the model and the associated computational cost is a challenge that needs careful considerations.

- The structural model proposed for simulation of cracks in gypsum has been tried for wall assemblies where the effects of gravity are negligible on the performance of gypsum boards. The same model can be extended to investigate the structural performance of loaded and non-loaded gypsum board floor assemblies.
- Further medium and full-scale fire tests can be performed on gypsum board assemblies with diligent recordings of gypsum cracking and falling off in fire. The study of the results can lead to experimental correlations between the formation of cracks and gypsum fall-off in fire.

## REFERENCES

- ABAQUS, 2010. Abaqus Analysis User's Manual, Version 6.10. Dassault Systèmes Simulia Corp.
- Ali Nageim, H., Durka, F., Morgan, W. and Williams, D. 2003. *Structural Mechanics: Loads, Analysis, Design and Materials*, London, Pearson Education LTD.
- Ali, M. A. and Singh, B. 1975. The Effect of Porosity on the Properties of Glass Fibre-Reinforced Gypsum Plaster. *Journal of Materials Science*, 10, 1920-1928.
- Andersson, L. and Jansson, B. 1987. *Analytical Fire Design with Gypsum; A Theoretical and Experimental Study*, Lund, Institute of Fire Safety Design.
- Ang, C. N. and Wang, Y. C. 2004. The Effect of Water Movement on Specific Heat of Gypsum Plasterboard in Heat Transfer Analysis Under Natural Fire Exposure. *Construction and Building Materials*, 18, 505-515.
- ASTM, 1988. ASTM E119-88, Standard Test Method for Fire Tests of Building Construction and Materials. Philadelphia: American Society for Testing and Materials
- Axeneko, O. and Thorpe, G. 1996. The Modelling of Dehydration and Stress Analysis of Gypsum Plasterboards Exposed to Fire. *Computational Materials Science*, 6, 281-294.
- Bakhtiary, S. B., Jafarpoor, F. and Firoozyar, F. 2000. Thermal and Mechanical Properties of Fire-Resistant Gypsum Plasters. *Asian Journal of Civil Engineering*, 1, 67-82.
- Belytschko, T. and Black, T. 1999. Elastic Crack Growth in Finite Elements with Minimal Remeshing. *International Journal for Numerical Methods in Engineering*, 45, 601-620.
- Bénichou, N. and Sultan, M. A. 2000. Fire Resistance Performance of Lightweight Wood-Framed Assemblies. *Fire Technology*, 36, 184-219.
- Bénichou, N. and Sultan, M. A. 2001. Thermal Properties of Components of Lightweight Wood-Framed Assemblies at Elevated Temperatures *Fire and Materials International Conference*. San Francisco.
- Bénichou, N. and Sultan, M. A. 2005. Thermal Properties of Lightweight-Framed Construction Components at Elevated Temperatures. *Fire and Materials*, 29, 165-179.
- British-Gypsum. 2009. *The WHITE book* [Online]. Available: [www.british-gypsum.com](http://www.british-gypsum.com) [Accessed 2010].
- British Gypsum. 2011. *The FIRE BOOK* [Online]. Available: [www.british-gypsum.com](http://www.british-gypsum.com) [Accessed 2011].

- BS476 1987. Fire tests on building materials and structures, Part 20: Method for determination of the fire resistance of elements of construction (general principles).
- BSI, 1987. BS 476-20: Fire tests on building materials and structures, Method for determination of the fire resistance of elements of construction (general principles). London: British Standards Institution
- BSI, 2002. BS EN 1991-1-2: Actions on structures, General actions - Actions on structures exposed to fire. London: British Standard Institution
- BSI, 2005a. BS EN 1993-1-1: Design of steel structures, General rules and rules for buildings. London: British Standard Institution
- BSI, 2005b. BS EN 1993-1-2: Design of steel structures, General rules - Structural fire design. London: British Standard Institution
- Burns, P. J. and Tien, C. L. 1979. Natural convection in porous media bounded by concentric spheres and horizontal cylinders *International Journal of heat and Mass Transfer*, 22, 929-939.
- Bwalya, A. 2005. Fire Resistance Tests of Non-Insulated Walls with Parallel and Perpendicular Orientation of Gypsum Board. Research Report No. 188, National Research Council of Canada
- Bwalya, A., Thomas, R. and Sultan, M. 2007. Impact of Board Orientation on the Fire Performance of Regular Gypsum Board Walls. *Fire and Materials, 10th International Conference*. San Francisco, USA.
- Carslaw, H. S. and Jaeger, J. C. 1959. *Conduction of Heat in Solids*, Oxford, Oxford University Press.
- Cooper, L. Y. 1997. The Thermal Response of Gypsum-Panel/Steel Stud Wall Systems Exposed to Fire Environments – A Simulation for the Use in Zone-Type Fire Models. NISTIR 6027, Building and Fire Research Laboratory
- Cramer, S. M., Friday, O. M., White, R. H. and Sriprukiat, G. 2003. Mechanical Properties of Gypsum Board at Elevated Temperatures. *Proceeding of the Fire and Materials 2003 Conference*. California, USA.
- Croft, D. R. and Lilley, D. G. 1977. *Heat Transfer Calculations Using Finite Difference Equations*, London, Applied Science Publishers.
- Dusinberre, G. M. 1962. *Heat-Transfer Calculations by Finite Differences*, Pennsylvania, International Textbook Co.
- Elbeyli, I. Y. and Pişkin, S. 2004. Thermal Dehydration Kinetics of Gypsum and Borogypsum under Non-isothermal Conditions. *Chinese Journal of Chemical Engineering*, 12, 302-305.
- Elewini, E., Sultan, M. A. and Hadjisophocleous, G. V. 2007. Gypsum Board Fall-Off in Floor Assemblies Exposed to a Standard Fire. *Fire and Materials, 10th International Conference*. San Francisco, USA.

- Frangi, A., Schleifer, V., Fontana, M. and Hugi, E. Year. Fire Performance of Gypsum Plasterboards. In: The Fifth International Conference on Structures in Fire (SiF08), 2008 Singapore. 619-631.
- G.N. Dulnev , D. P. V., V.I. Malrarev 1989. Thermal Conductivity of Moist Porous Materials. *Journal of Engineering Physics*, 56, 198-206.
- Gerlich, J. T. 1995. Design of Loadbearing Light Steel Frame Walls for Fire Resistance. Fire Engineering Research Report 95/3, School of Engineering, University of Canterbury
- Gerlich, J. T., Collier, P. C. R. and Buchanan, A. H. 1996. Design of Light Steel-framed Walls for Fire Resistance. *Fire and Materials*, 20, 79-96.
- Ghazi Wakili, K. and Hugi, E. 2009. Four Types of Gypsum Plaster Boards and their Thermophysical Properties Under Fire Condition. *Journal of Fire Sciences*, 27, 27-43.
- Ghazi Wakili, K., Hugi, E., Wullschleger, L. and Frank, T. 2007. Gypsum board in Fire - Modelling and Experimental Validation. *Fire Sciences*, 25, 267-282.
- Groves, A. W. 1958. *Gypsum and Anhydrite*, Overseas Geological Surveys, London, Mineral Resources Division, HerMajesty's Stationary Office.
- Hadjisophocleous, G. V. 1996. Extract from Report on Furnace Tests on Walls for Department of National Defence, Canada. National Fire Laboratory, National Research Council of Canada
- Harmathy, T. Z. 1988. Properties of Building Materials. *The SFPE Handbook of Fire Protection Engineering*. Boston: Society of Fire Protection Engineers/National Fire Protection Association.
- Holman, J. P. 2002. *Heat Transfer*, Boston ; London, McGraw-Hill.
- ISO, 1992. ISO 834 Fire Resistance Tests - Elements of Building Construction. Switzerland: International Organisation for Standardisation
- Jakob, M. 1949. *Heat Transfer*, London, Chapman and Hall.
- Jones, B. 2001. *Performance of Gypsum Plasterboard Assemblies Exposed to Real Building Fires*. University of Canterbury, New Zealand.
- Kodur, V. R., Bénichou, N. and Sultan, M. A. 2001. Behaviour of Load-Bearing Wood-Stud Shear Walls Exposed to Fire. *Interflam 2001, 9<sup>th</sup> International Fire Science & Engineering Conference*. Edinburgh, Scotland.
- Konig, J. and Walleij, L. 2000. Timber Frame Assemblies Exposed to Standard and Parametric Fires, Part 2: A Design Model for Standard Fire Exposure. Report I 0001001, Swedish Institute for Wood Technology Research
- Mehaffey, J. R., Cuerrier, p. and Carisse, G. A. 1994. A Model for Predicting Heat Transfer through Gypsum-Board/Wood-Stud Walls Exposed to Fire. *Fire and Materials*, 18, 297-305.
- Ozisik, M. N. 1985. *Heat Transfer: A Basic Approach*, New York; London, McGraw-Hill.

- Parrott, J. E. and Stuckes, A. D. 1975. *Thermal Conductivity of Solids*, London, Pion Limited.
- Remmers, J. J. C., de-Borst, R. and Needleman, A. 2008. The Simulation of Dynamic Crack Propagation Using the Cohesive Segments Method. *Journal of the Mechanics and Physics of Solids*, 56, 70-92.
- Roy-Poirier, A. and Sultan, M. A. 2007. Approaches for Determining Gypsum Board Fall-Off Temperature in Floor Assemblies Exposed to Standard Fires. Research Report No. 226, National Research Council of Canada
- Song, J. H., Areias, P. M. A. and Belytschko, T. 2006. A Method for Dynamic Crack and Shear Band Propagation with Phantom Nodes. *International Journal for Numerical Methods in Engineering*, 67, 868-893.
- Sultan, M. A. 1996. A Model for Predicting Heat Transfer through Non-Insulated Unloaded Steel-Stud Gypsum Board Wall Assemblies Exposed to Fire. *Fire Technology*, 32, 239-259.
- Sultan, M. A. 2008. Fall-Off of Gypsum Plasterboard in Fire. *The Fifth International Conference on Structures in Fire (SiF08)*. Singapore.
- Sultan, M. A. 2010. Comparison of Gypsum Board Fall-Off in Wall and Floor Assemblies Exposed to Furnace Heat. *The 12th International Fire Science and Engineering Conference (Interflam)*, 5-7 July 2010. New York: Wiley.
- Sultan, M. A. and Bénichou, N. 2003. Fire Resistance Performance of Lightweight Floor Assemblies. NRCC-46105, National Research Council Canada
- Sultan, M. A., Latour, J. C., Leroux, P., Monette, R. C., Seguin, Y. P. and Henrie, J. 2005. Results of Fire Resistance Tests on Full-Scale Floor Assemblies - Phase II. Research Report 184, Institute for Research in Construction, National Research Council of Canada
- Sultan, M. A. and Lougheed, G. D. 2002. Results of Fire Resistance Tests on Full-Scale Gypsum Board Wall Assemblies. Internal Report No. 833, Institute for Research in Construction, National Research Council of Canada
- Sultan, M. A., Lougheed, G. D., Denham, E. M. A., Monette, R. C. and Macburin, J. W. 1994a. Temperature Measurements in Full-Scale fire Resistance Tests on Non-Insulated Regular Gypsum Board Wall Assemblies. Internal Report No. 674, Institute for Research in Construction, National Research Council of Canada
- Sultan, M. A., Maclaurin, J. W., Denham, M. and Monette, R. C. 1994b. Temperature Measurements in Full-Scale Insulated and Non-Insulated (1x2) Gypsum Board Protected Wall Assemblies with Steel Studs. Internal Report No. 675, Institute for Research in Construction, National Research Council of Canada
- Sultan, M. A., Seguin, Y. P. and Leroux, P. 1998. Results of Fire Resistance Tests on Full-Scale Floor Assemblies. Internal Report No. 764, Institute for Research in Construction, National Research Council of Canada
- Tadeka, H. and Mehaffey, J. R. 1998. WALL2D: a Model for Predicting Heat Transfer through Wood-Stud Walls Exposed to Fire *Fire and Materials*, 22, 133-140.

- Takeda, H. 2003. A Model to Predict Fire Resistance of Non-Load bearing Wood-Stud Walls. *Fire and Materials*, 27, 19-39.
- Thomas, G. 2002. Thermal Properties of Gypsum Plasterboard at High Temperatures. *Fire and Materials*, 26, 37-45.
- Thomas, R., Sultan, M. and Latour, J. 2005. Impact of the Variability of Type X Gypsum Board. Fire Research NRCC-47635, National Council of Canada
- Wang, H. B. 1995. *Heat Transfer Analysis of Components of Construction Exposed to Fire*. PhD, University of Salford.
- Wang, H. W., Ji, H. W., Sun, Y. and Miao, H. 2011. Discussion on Convergence Issues in ABAQUS/Standard while Carrying Out Damage and Fracture Analysis. *Advanced Materials Research*, 189-193, 2247-2250.
- Wang, Y. C. 2002. *Steel and Composite Structures: Behaviour and design for fire safety*, London: New York, Spon Press.
- Weast, R. C., Lide, D. R., Astle, M. J. and Beyer, W. H. 1989. *CRC Handbook of Chemistry and Physics*, Florida, CRC Press.
- Wullschleger, L. and Wakili, K. G. 2008. Numerical Parameter Study of the Thermal Behaviour of a Gypsum Plasterboard at Fire Temperatures. *Fire and Materials*, 32, 103-119.
- Yu, F., Wei, G., Zhang, X. and Chen, K. 2006. Two Effective Thermal Conductivity Models for Porous Media with Hollow Spherical Agglomerates. *International Journal of Thermophysics*, 27, 293-303.
- Yuan, J. 2009. *Fire Protection Performance of Intumescent Coating under Realistic Fire Conditions*. PhD Thesis, University of Manchester.

## PUBLICATIONS

Rahmanian, I. and Wang, Y.C., "A Combined Experimental and Numerical Method for Extracting Temperature-Dependent Thermal Conductivity of Gypsum Boards". *Construction and Building Materials*, Volume 26, Issue 1, January 2012, Pages 707-722

Rahmanian, I., "Fire Resistance of Gypsum Board Based Systems". The 11<sup>th</sup> annual Young Researchers' Conference (YRC09), London, 18 March 2009

Rahmanian, I. and Wang, Y.C., "Thermal Conductivity of Gypsum at High Temperatures - A Combined Experimental and Numerical Approach". Proceedings of International Conference Application of Structural Fire Engineering Prague, 19-20 February 2009 - Also published in a revised form in *Acta Polytechnica*, Vol. 49, No.1/2009

## Appendix A. Small-Scale Heat Transfer Test Results

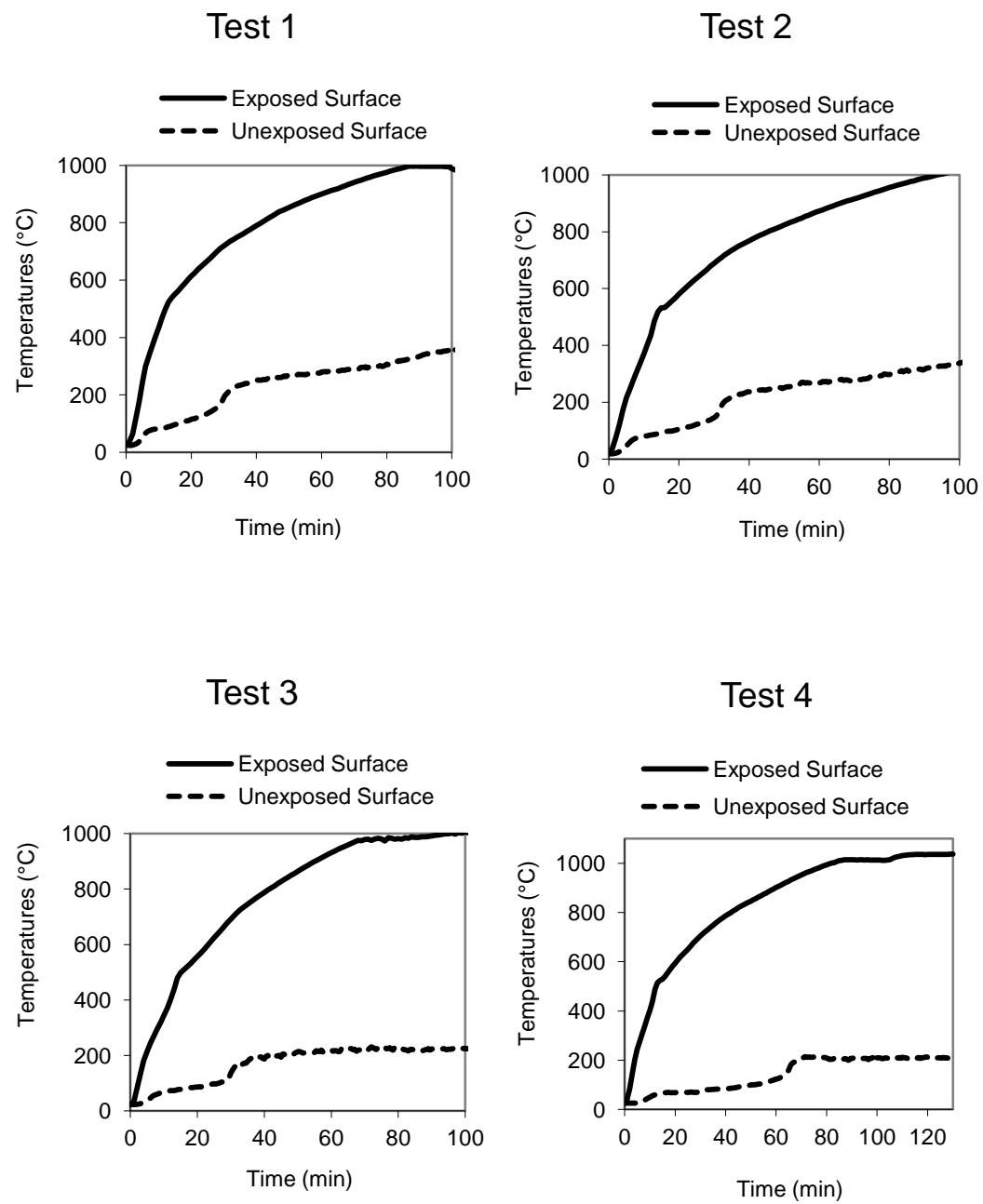


**Figure A.1.** Temperature recordings on the exposed and unexposed surfaces of gypsum panels in Tests 1 to 4

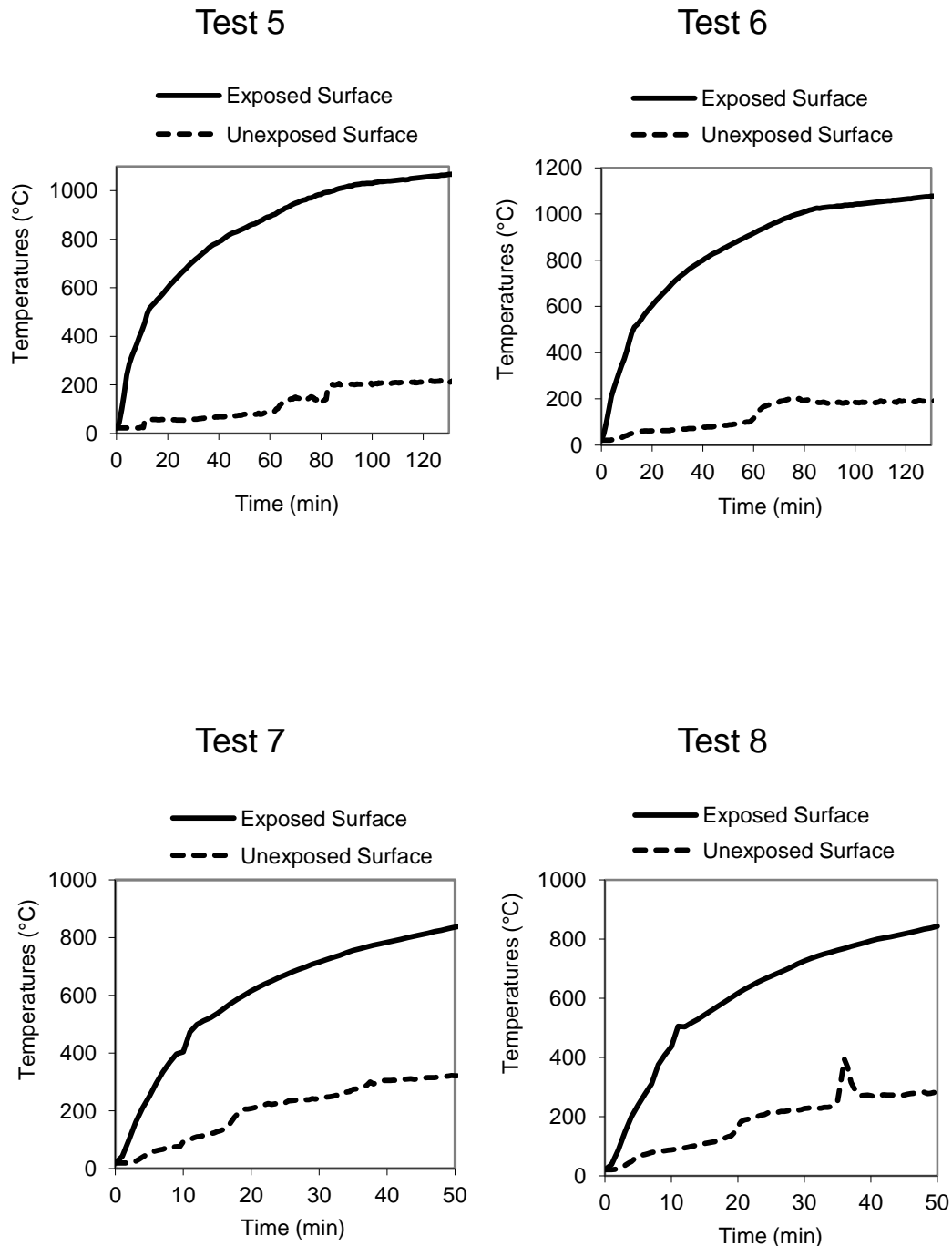


**Figure A.2.** Temperature recordings on the exposed and unexposed surfaces of gypsum panels in Tests 5 to 8

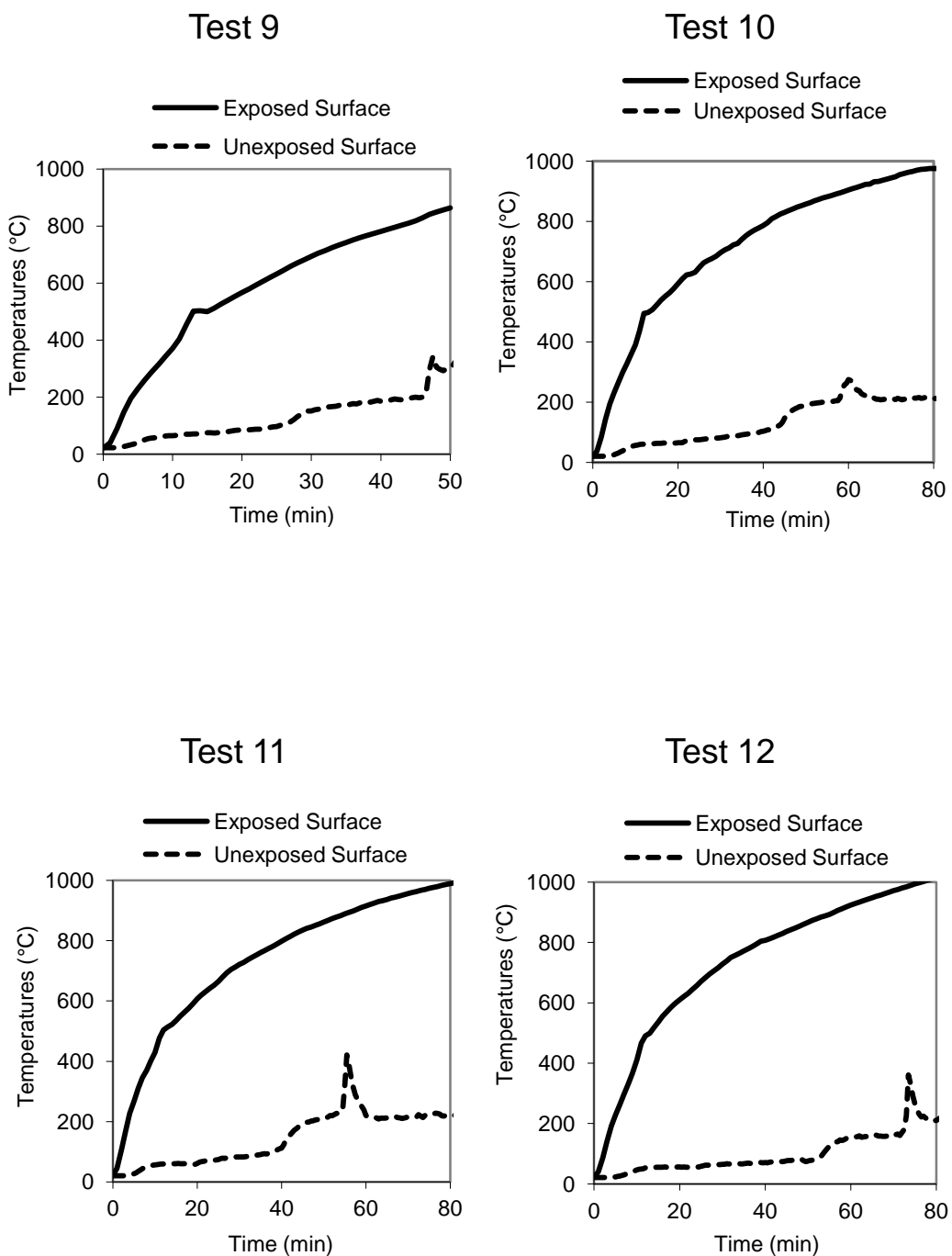


**Figure A.3.** Temperature recordings on the exposed and unexposed surfaces of gypsum panels in Tests 9 to 12

## **Appendix B.     Detailed Data of Mechanical Test Samples**

Sample ID	Weight (gr)	Length (mm)	Width (mm)	Height (mm)	Density (Kg/m <sup>3</sup> )
F1	2.3653	25.3	11.4	10.8	763
F2	2.1783	24.9	10.5	11.1	754
F3	2.3452	25.3	11.1	11.1	758
F4	2.4302	25.8	10.8	11.4	764
F5	2.322	24.7	11.1	11.4	739
F6	2.2818	24.4	11.1	11.3	745
E.L1	2.7587	25.9	11.0	11.6	837
E.L2	2.7445	25.6	11.5	10.9	858
W1	2.1373	25.1	11.4	10.7	695
W2	2.113	25.9	10.4	11.5	683
W3	2.1037	24.8	11.1	11.1	688
W4	2.141	25.1	11.3	10.8	699
W5	2.1384	25.3	11.5	11.1	665
W6	2.0775	24.4	11.5	11.0	677

**Table B.1.** Sample data for dilatometer tests

Test ID	Mass (gr)	Width (mm)	Depth (mm)	Density (Kg/m <sup>3</sup> )
20F1	302.5	98.84	13.26	770
20F2	297	98.88	13.43	746
80F1	296.3	99.07	13.21	755
80F2	299.4	98.74	13.06	774
180F1	297.1	98.87	13.10	765
180F2	297	98.92	13.13	762
300F1	296	98.97	13.15	758
300F2	300.1	98.83	13.13	771
400F1	293.7	98.67	12.96	766
400F2	295.2	98.80	13.15	758
500F1	291.9	98.91	13.10	751
500F2	293.5	99.11	13.08	755
600F1	286.4	98.69	12.95	747
600F2	282.2	98.94	12.68	750
700F1	306.6	98.95	13.16	785
700F2	281.7	98.78	12.68	750
800F1	281.9	98.90	12.78	743
800F2	299.1	98.98	13.22	762
20W1	266.8	98.90	12.93	695
20W2	276.2	98.73	13.24	704
80W1	277.3	98.81	13.46	695
80W2	276.1	98.70	13.25	704
180W1	268.6	98.75	13.10	692
180W2	275.1	98.68	13.43	692
300W1	268.5	100.19	12.30	727
300W2	255.6	100.35	11.65	729
400W1	262.4	100.02	12.00	729
400W2	257.6	100.31	11.50	744
500W1	271.8	100.32	12.27	736
500W2	260.8	99.91	11.87	733

**Table B.2.** Sample data for three-point bending tests

Sample ID	Mass (gr)	Height (mm)	Width (mm)	Length (mm)	Density (Kg/m <sup>3</sup> )
Sample 1 - 80°C	35.25	19.83	19.48	99.19	920
Sample 2 - 80°C	34.23	19.55	19.47	98.49	913
Sample 3 - 80°C	34.07	19.47	19.39	98.58	915
Sample 4 - 100°C	32.98	19.43	19.43	78.37	1115
Sample 5 - 100°C	32.11	19.59	19.38	98.67	857
Sample 6 - 100°C	34.85	19.97	19.87	101.13	868
Sample 7 - 120°C	31.19	19.99	19.97	98.02	797
Sample 8 - 120°C	30.97	19.57	19.60	98.65	818
Sample 9 - 120°C	33.08	20.06	19.93	100.92	820
Sample 10 - 160°C	32.24	19.95	19.98	100.58	804
Sample 11 - 160°C	31.72	19.96	20.01	100.82	787
Sample 12 - 160°C	30.1	19.76	19.71	98.86	782
Sample 13 - 180°C	32.09	19.96	20.04	100.75	796
Sample 14 - 180°C	29.96	19.52	19.47	98.81	798
Sample 15 - 180°C	29.07	19.45	19.26	98.51	788
Sample 16 - 40°C	34.6	19.53	19.51	98.51	922
Sample 17 - 40°C	37.91	20.20	20.00	100.82	931
Sample 18 - 40°C	37.32	20.15	20.01	100.78	918

**Table B.3.** Sample data for gypsum prism compression tests

## Appendix C. Observations of Medium-Scale Fire Tests

Time		Observations
hours	mins	All observations refer to the exposed face unless otherwise stated.
0	0	Test started.
0	04	No visible change.  <i>Unexposed face</i> Smoke issued from the head of the specimen.
0	15	Face papers blistered and charred.  <i>Unexposed face</i> Smoke issued from the head, base and both sides of the specimen.
0	26	Boards glowing white and 100% blistered.  <i>Unexposed face</i> Insulation tearing at both top corners and both sides.
0	27	<i>Unexposed face</i> The temperature rise of thermocouple no.34, positioned at mid-height on centre stud, exceeded 180 °C.
0	34	<i>Unexposed face</i> Gap forming at the top right corner of the specimen, extending approximately 30mm each way from the corner. Red glow visible.
0	38	No visible change.  <i>Unexposed face</i> Right stud bending at mid height.
0	48	<i>Unexposed face</i> Gap appeared at mid height between the right stud and the insulation; approximately 200mm in length.
0	55	<i>Unexposed face</i> Gap at the mid height of the specimen on the right hand side exceeded 6mm x 150mm (6mm gap gauge).
1	08	<i>Unexposed face</i> The gap at the top right hand corner had got slightly bigger.

**Table C.1.** Observation report for test T2F, part 1

Time		Observations
hours	mins	All observations refer to the exposed face unless otherwise stated.
1	11	No visible change.  <i>Unexposed face</i> No visible change.
1	18	No visible change.  <i>Unexposed face</i> No visible change.
1	30	No visible change.  <i>Unexposed face</i> The insulation on the left hand side at approximately 20mm height had burnt away; approximately 30mm.
1	45	No visible change.  <i>Unexposed face</i> No visible change.  <b>TEST TERMINATED</b> at the request of the laboratory.

**Table C.2.** Observation report for test T2F, part 2

Time		Observations <i>All observations refer to the exposed face unless otherwise stated.</i>
hours	mins	
0	0	Test started.
0	10	Plasterboard face paper peeling, approximately 25% of the paper peeled from the face.
0	15	Horizontal crack approx 1mm wide x 500mm long.  <i>Unexposed face</i> Smoking from above stud at top left hand corner.
0	20	Approximately 75% of paper peeled from face.  Horizontal crack approximately 2mm x 150mm.  2 vertical cracks approximately 1-2mm wide x 150mm long.  <i>Unexposed Face</i> Approximately 2mm wide dark patches around studs.
0	26	<i>Unexposed face</i> Smoking from top left above stud.
0	30	Horizontal crack opened to approximately 2-10mm.  Vertical crack opened to approximately 5-10mm.  Intersections between cracks creating a hole approximately 10mm x 15mm.  Approximately 90% of paper removed.  <i>Unexposed Face</i> Dark patches increased in size to approximately 10-30mm around studs.
0	40	Cracks widened to approximately 10mm along length.  First layer board fall at top left, approximately 50% of the first layer had fallen.  <i>Unexposed face</i> Dark patches increased in size to approximately 15x300mm.  Charring occurring at the stud edge and glowing.  Paper peeling.

Table C.3. Observation report for test T5W, part 1

Time		Observations
hours	mins	All observations refer to the exposed face unless otherwise stated.
0	44	<p><i>Unexposed face</i>            Upper right hand corner of specimen charred approximately 150mm x 350mm.</p> <p>The temperature rise of the standard five thermocouples exceeded 140°C.</p> <p>The temperature rise of thermocouple 34 located in the centre of the specimen at 650mm height exceeded 180 °C.</p> <p>Gap appeared in top right corner approximately 20mm in length.</p>
0	46	<p><i>Unexposed face</i>            Upper centre board charred and blackened around stud.</p> <p>Vertical cracks approximately 2mm wide and approximately half the board length between studs</p>
0	48	<p><i>Unexposed face</i>            Approximately 75% of paper removed from board face.</p>
0	49	<p>Approximately 75% of first layer board fallen.</p> <p><i>Unexposed face</i>            Gap at approximately 100mm from the head and 400mm from the left hand side exceeded 6mm x 150mm (visual).</p> <p>Gap at approximately 100mm from the head and 400mm from the left hand side exceeded 25mm (visual).</p>
0	50	<p><i>Unexposed face</i>            Board bowed.</p> <p>Approximately 250mm x 100mm section of board fallen.</p>
0	50	TEST TERMINATED at the request of the laboratory.

Table C.4. Observation report for test T5W, part 2